DISSERTATION

submitted
to the

Faculty of Mathematics and Physics
of
Charles University, Czech Republic

and

Combined Faculty for the Natural Sciences and Mathematics
of
Heidelberg University, Germany

for the degree of
Doctor of Natural Sciences

(Doppelpromotion)

Put forward by
Mgr. Martin Řehoř
Born in Moravská Třebová, Czech Republic

Oral examination: September 27, 2018

Diffuse interface models in theory of interacting continua

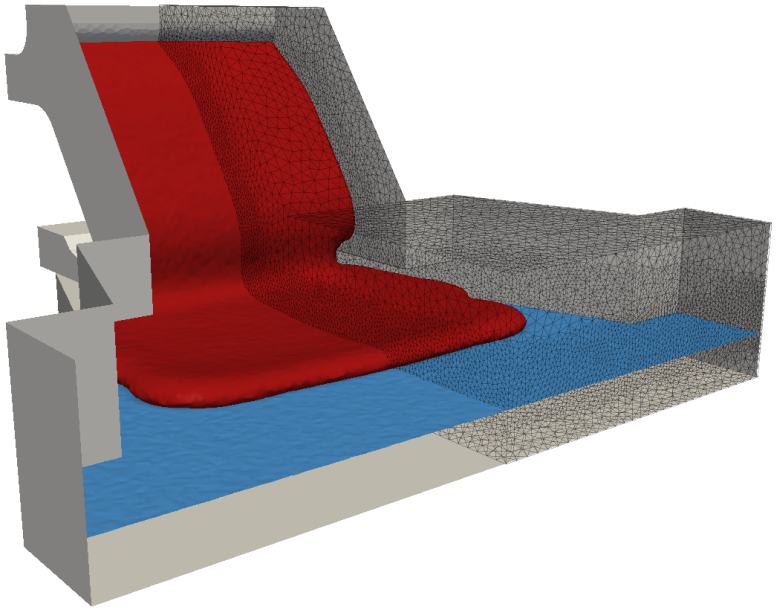

Advisors: { Mgr. Vít Průša, Ph.D.
Prof. Dr. Peter Bastian

To my beloved wife and children
Pavla, Zuzana and .....

Hereby, I would like to express my sincere gratitude to all the people who supported my efforts to work on this thesis.

First and foremost, I am grateful to both of my supervisors, Dr. Vít Průša and Prof. Peter Bastian, for their guidance during my doctoral studies. My great thanks go to my co-advisor, Prof. Josef Málek, for his enthusiasm and for the provided opportunity to work on interesting projects. Last but not least, I appreciate the possibility to take part in the *Bi–nationally Supervised Doctoral Thesis program* between Charles University and Heidelberg University. The excellent scientific background and hospitality that I met at both institutions, particularly at the Faculty of Mathematics and Physics in the former case and the Faculty of Mathematics and Computer Science in the latter case, made my work a pleasure.

I would also like to use this opportunity to thank my colleagues from both universities for the unique and friendly atmosphere they created both in and out of their workplaces. My special thanks belong to Michal Habera, Jaroslav Hron, Adam Janečka and Ondřej Souček who always carefully listened to my ideas and gave me an instanteneous feedback. Numerical solvers discussed in this document could not have been implemented without the invaluable help of Jan Blechta. The FEniCS Project has shown to be a handy tool for this particular work, thus my thanks go to all other developers involved in it. Most of all, I want to thank my family, especially my wife Pavla for her endless patience and unconditional support during my studies.

My thanks belong also to the following company and institutions for their material, financial and scientific support: Glass Service, a.s., Mathematical Institute of Charles University, Interdisciplinary Center for Scientific Computing at Heidelberg University and Heidelberg Graduate School MathComp. Moreover, I would like to acknowledge the support of following projects and grants: Project LL1202 in the programme ERC-CZ funded by the Ministry of Education, Youth and Sports of the Czech Republic (MŠMT ČR) and Large Infrastructures for Research, Experimental Development and Innovations project "IT4Innovations National Supercomputing Center – LM2015070" funded by MŠMT ČR.

Title: Diffuse interface models in theory of interacting continua

Author: Mgr. Martin Řehoř (rehor@karlin.mff.cuni.cz)

Institutes:

Mathematical Institute of Charles University
Interdisciplinary Center for Scientific Computing, Heidelberg University

Supervisors:

Mgr. Vít Průša, Ph.D. (prusv@karlin.mff.cuni.cz)
Mathematical Institute of Charles University

Prof. Dr. Peter Bastian (peter.bastian@iwr.uni-heidelberg.de)
Interdisciplinary Center for Scientific Computing, Heidelberg University

Abstract: We study physical systems composed of at least two immiscible fluids occupying different regions of space, the so-called phases. Flows of such multi-phase fluids are frequently met in industrial applications which rises the need for their numerical simulations. In particular, the research conducted herein is motivated by the need to model the float glass forming process. The systems of interest are in the present contribution mathematically described in the framework of the so-called diffuse interface models. The thesis consists of two parts.

In the modelling part, we first derive standard diffuse interface models and their generalized variants based on the concept of multi-component continuous medium and its careful thermodynamic analysis. We provide a critical assessment of assumptions that lead to different models for a given system. Our newly formulated class of generalized models of Cahn–Hilliard–Navier–Stokes–Fourier (CHNSF) type is applicable in a non-isothermal setting. Each model belonging to that class describes a mixture of separable, heat conducting Newtonian fluids that are either compressible or incompressible. The models capture capillary and thermal effects in thin interfacial regions where the fluids actually mix.

In the computational part, we focus on the development of an efficient and robust numerical solver for a specific isothermal model describing incompressible fluids. The proposed numerical scheme, which is based on the finite element method, partly decouples the system of governing equations on the level of time discetization. We carefully discuss the advanced design of the preconditioner for the computationally most demanding part of the scheme, given by the system of incompressible Navier–Stokes equations with variable coefficients. The numerical scheme has been implemented using the FEniCS computing platform. The code capable of running parallel 2D and 3D multi-phase flow simulations is available in the newly developed FEniCS-based library MUFLON.

Keywords: Diffuse interface models, multi-component systems, multi-phase flows, Cahn–Hilliard equations, Navier–Stokes–Fourier equations, preconditioning, float glass forming process.

Název práce: Modely s neostrým rozhraním v teorii směsí

Autor: Mgr. Martin Řehoř (rehor@karlin.mff.cuni.cz)

Školící pracoviště:

Matematický ústav Univerzity Karlovy
Interdisziplinäres Zentrum für Wissenschaftliches Rechnen, Universität Heidelberg

Vedoucí disertační práce:

Mgr. Vít Průša, Ph.D. (prusv@karlin.mff.cuni.cz)
Matematický ústav Univerzity Karlovy

Prof. Dr. Peter Bastian (peter.bastian@iwr.uni-heidelberg.de)
Interdisziplinäres Zentrum für Wissenschaftliches Rechnen, Universität Heidelberg

Abstrakt: V předložené práci se věnujeme studiu fyzikálních systémů sestávajících alespoň ze dvou nemísitelných tekutin, kde každá z nich vyplňuje jinou část prostoru a tvoří takzvanou fázi. S prouděním vícefázových tekutin se často setkáváme v průmyslových aplikacích, což přirozeným způsobem zvyšuje poptávku po numerických simulacích tohoto fyzikálního jevu. Výzkum prováděný v rámci předložené práce je motivován snahou modelovat proces výroby plochého plaveného skla. Studované systémy jsou matematicky popsány pomocí takzvaných modelů s neostrým rozhraním, přičemž práci samotnou lze tematicky rozdělit do dvou částí.

Ve fyzikálně zaměřené části práce nejprve odvodíme standardní modely s neostrým rozhraním a jejich zobecněné varianty. Zvolený postup se opírá o pojem vícesložkového kontinua a jeho důkladnou termodynamickou analýzu. Důležitou součástí odvození je kritické posouzení předpokladů, které svou podstatou vedou k odlišným modelům pro daný systém. Námi nově zformulovaná třída modelů typu Cahn–Hilliard–Navier–Stokes–Fourier (CHNSF) je využitelná při modelování neizotermálních procesů. Modely spadající do této třídy popisují směs separabilních, tepelně vodivých newtonských tekutin, které jsou buď stlačitelné nebo nestlačitelné. Jednotlivé modely zachycují kapilární a tepelné jevy uvnitř tenkého fázového rozhraní, kde fakticky dochází k mísení tekutin.

Ve výpočetní části práce se soustředíme na vývoj efektivního a zároveň robustního numerického řešiče pro vybraný izotermální model popisující nestlačitelné tekutiny. Navržené numerické schéma, založené na metodě konečných prvků, rozděluje na úrovni časové diskretizace systém řídících rovnic na menší podsystémy. Podstatnou část diskuze věnujeme návrhu moderní předpodmiňovací strategie pro výpočetně nejnáročnější podsystém, který koresponduje se systémem nestlačitelných rovnic typu Navier–Stokes s variabilními koeficienty. Numerické schéma je implementováno s využitím výpočetní platformy FEniCS. Vlastní zdrojový kód, zprostředkovávající možnost provádět simulace vícefázového proudění v paralelním módu ve 2D i 3D, je dostupný v nově vyvinuté knihovně MUFLON založené na FEniCS platformě.

Klíčová slova: Modely s neostrým rozhraním, vícesložkové systémy, vícefázové proudění, rovnice typu Cahn–Hilliard, rovnice typu Navier–Stokes–Fourier, předpodmínění, výroba plaveného skla.

Contents

List of Tables

List of Figures

List of Acronyms

Notation	Description	Page
ACNSF	Allen–Cahn–Navier–Stokes–Fourier	46
AMG	algebraic multigrid	112
CFD	computational fluid dynamics	3
CH	Cahn–Hilliard	8
CHNS	Cahn–Hilliard–Navier–Stokes	8
CHNSF	Cahn–Hilliard–Navier–Stokes–Fourier	10
DOF	degree of freedom	127
FC	fully-compressible	10
FEM	finite element method	10
FI	fully-incompressible	10
HPC	high performance computing	6
MAC	mass additivity constraint	17
NS	Navier–Stokes	8
NSF	Navier–Stokes–Fourier	51
ODE	ordinary differential equation	52
PCD	pressure convection–diffusion	104
PCDR	pressure convection–diffusion–reaction	112
PDE	partial differential equation	10
QI	quasi-incompressible	10
SPD	symmetric positive definite	53
VAC	volume additivity constraint	17

Nomenclature

Notation	Description	SI Units	Page
Latin letters			
a, b	constant coefficients given by shape of f	–	50
$\mathfrak{a}_i$	partial spin production	$\mathrm{J/m^3}$	29
$\boldsymbol{b}, \boldsymbol{b}_i$	averaged and partial specific body force	$\mathrm{N/kg}$	28
$\mathcal{B}_i$	continuous body associated with component i	–	15
$\boldsymbol{c}$	vector of first $(N-1)$ mass fractions	–	18
c_i	mass fraction of component i	–	16
$\mathrm{c_v}$	specific heat at constant volume	$\mathrm{J{\cdot}K^{-1}/kg}$	39
$\mathbb{D}$	symmetric part of velocity gradient	$\mathrm{s^{-1}}$	31
e, e_i	averaged and partial specific internal energy	$\mathrm{J/kg}$	30
$\mathfrak{e}_i$	partial energy production	$\mathrm{W/m^3}$	30
E, E_i	averaged and partial specific total energy	$\mathrm{J/kg}$	31
$\mathcal{E}$	total energy associated with Ω_t ($\mathcal{E} = \mathcal{E}_{\mathrm{kin}} + \Psi$)	J	94
f	potential function with double-well structure	–	47
$\boldsymbol{f}_{\mathrm{ca}}$	capillary force	$\mathrm{N/m^3}$	87
F	potential function with multi-well structure	$\mathrm{N \cdot m^{-1}}$	54
$\boldsymbol{g}$	vector of gravitational acceleration	$\mathrm{m \cdot s^{-2}}$	37
g_{a}	gravitational acceleration	$\mathrm{m \cdot s^{-2}}$	91
G	gravitational potential energy	$\mathrm{J/m^3}$	91
$\boldsymbol{h}_i$	partial entropy flux	$\mathrm{W{\cdot}K^{-1}/m^2}$	34
$\mathfrak{l}_i$	partial interaction force	$\mathrm{N/m^3}$	27
$\boldsymbol{\jmath}_i$	diffusive mass flux of component i	$\mathrm{kg{\cdot}s^{-1}/m^2}$	20
$\widetilde{\boldsymbol{j}}_i$	diffusive volume flux of component i	$\mathrm{m^3{\cdot}s^{-1}/m^2}$	20
$\boldsymbol{J}$	total diffusive mass flux	$\mathrm{kg{\cdot}s^{-1}/m^2}$	20
$\widetilde{\boldsymbol{J}}$	total diffusive volume flux	$\mathrm{m^3{\cdot}s^{-1}/m^2}$	20
ℓ_{ij}	$\boldsymbol{\Lambda}^{-1} = [\ell_{ij}]_{(N-1)\times(N-1)}$	$\mathrm{m \cdot N^{-1}}$	87
m	mean normal stress $\frac{1}{3}\operatorname{tr}\mathbb{T}$	Pa	40
$\mathrm{m}(\mathcal{P}_t)$	mass of the mixture associated with $\mathcal{P}_t$	kg	16
$\mathrm{m}_i(\mathcal{P}_t)$	mass of component i associated with $\mathcal{P}_t$	kg	16
$\mathbf{M}$	mobility matrix $[M_{ij}]_{(N-1)\times(N-1)}$	$\mathrm{m^3 \cdot s \cdot kg^{-1}}$	63
M_0	mobility coefficient	$\mathrm{m^3 \cdot s^{-1}}$	85
$\boldsymbol{n}$	outward unit normal to domain boundary	–	48
N	number of components/phases	–	15
$N_{t.s.}$	number of time steps	–	95

Notation	Description	SI Units	Page
$p, p_\mathrm{a}, \tilde{p}_\mathrm{a}$	augmented pressure	Pa	62
p_th	thermodynamic pressure	Pa	39
$\mathcal{P}_t$	arbitrary open subset of Ω_t	–	16
$\mathbb{P}_k, \mathbb{P}_k$	spaces of globally continuous scalar-valued and vector-valued piecewise polynomials of order not exceeding k	–	97
q, q_i	averaged and partial specific energy supply	$\mathrm{W/kg}$	31
$\boldsymbol{q}, \boldsymbol{q}_i$	averaged and partial energy flux	$\mathrm{W/m^2}$	31
$\boldsymbol{q}_e$	generalized energy flux	$\mathrm{W/m^2}$	32
$\boldsymbol{q}_\eta$	averaged entropy flux	$\mathrm{W{\cdot}K^{-1}/m^2}$	34
$\hat{r}_i$	relative difference $1 - \frac{\hat{\varrho}_i}{\hat{\varrho}_N}$	–	21
$\mathbb{R}$	set of real numbers	–	15
s, s_i	averaged and partial specific entropy supply	$\mathrm{W{\cdot}K^{-1}/kg}$	34
t	time	s	15
$\mathbb{T}, \mathbb{T}_i$	averaged and partial Cauchy stress tensor	Pa	28
$\boldsymbol{u}_i$	diffusion velocity of component i	$\mathrm{m \cdot s^{-1}}$	20
$\boldsymbol{v}, \boldsymbol{v}_i$	averaged and partial velocity	$\mathrm{m \cdot s^{-1}}$	20
$\mathrm{v}(\mathcal{P}_t)$	volume of the mixture associated with $\mathcal{P}_t$	$\mathrm{m^3}$	16
$\mathrm{v}_i(\mathcal{P}_t)$	volume of component i associated with $\mathcal{P}_t$	$\mathrm{m^3}$	16
$\boldsymbol{x}$	position vector in Ω_t	m	15
$\boldsymbol{X}_i$	position vector in $\boldsymbol{\kappa}_i^\mathrm{ref}(\mathcal{B}_i)$	m	19
Greek letters			
$\hat{\gamma}_i$	reciprocal value of material density $\hat{\varrho}_i$	$\mathrm{m^3 \cdot kg^{-1}}$	18
δ_{ij}	Kronecker delta	–	26
Δ_t	time step	s	95
ε	interface thickness	m	49
ϵ	interface thickness scaled by density	$\mathrm{m^4 \cdot kg^{-1}}$	50
η, η_i	averaged and partial specific entropy	$\mathrm{J{\cdot}K^{-1}/kg}$	34
κ	total thermal conductivity of mixture	$\mathrm{W \cdot m^{-1} \cdot K^{-1}}$	72
κ_i	thermal conductivity of component i	$\mathrm{W \cdot m^{-1} \cdot K^{-1}}$	72
$\boldsymbol{\kappa}_i^\mathrm{ref}, \boldsymbol{\kappa}_i^t$	mappings defining reference and current configurations of $\mathcal{B}_i$	–	15
$\boldsymbol{\Lambda}$	matrix of mixing surface energy coefficients $[\lambda_{ij}]_{(N-1)\times(N-1)}$	$\mathrm{J \cdot m^{-2}}$	53
μ_i, μ_i^c	specific chemical potential of component i	$\mathrm{J/kg}$	53
$\widetilde{\mu}_i, \widetilde{\mu}_i^\phi$	chemical potential of component i	$\mathrm{J/m^3}$	54
ν	total dynamic viscosity of mixture	$\mathrm{Pa \cdot s}$	72
ν_i	dynamic viscosity of component i	$\mathrm{Pa \cdot s}$	72
ξ, ξ_i	averaged and partial entropy production	$\mathrm{W{\cdot}K^{-1}/m^3}$	34
ϱ	total mixture density	$\mathrm{kg/m^3}$	16
ϱ_i	partial density of component i	$\mathrm{kg/m^3}$	16
$\hat{\varrho}_i$	material density of component i	$\mathrm{kg/m^3}$	16
$\boldsymbol{\Sigma}$	matrix of pairwise surface tensions $[\sigma_{ij}]_{N\times N}$	$\mathrm{N \cdot m^{-1}}$	83

Notation	**Description**	SI Units	**Page**
$\widetilde{\boldsymbol{\varsigma}}_i^c, \widetilde{\boldsymbol{\varsigma}}_i^\phi$	generalized surface energy of component i	$\mathrm{J} \cdot \mathrm{m}^{-2}$	53
ϑ	thermodynamic temperature	K	39
$\vartheta_{\mathrm{crit}}$	critical temperature for phase separation	K	46
$\hat{\vartheta}_{\mathrm{iso}}$	fixed temperature in isothermal setting	K	46
$\Theta_0, \Theta_1, \Theta_2$	toggle coefficients	–	38
$\tilde{\upsilon}$	total bulk viscosity of mixture	$\mathrm{Pa} \cdot \mathrm{s}$	72
$\tilde{\upsilon}_i$	bulk viscosity of component i	$\mathrm{Pa} \cdot \mathrm{s}$	72
$\boldsymbol{\phi}$	vector of first $(N-1)$ volume fractions	–	18
ϕ_i	volume fraction of component i	–	16
χ_i	combined chemical potential of component i	m^{-1}	87
$\boldsymbol{\chi}_i$	deformation function of component i	–	19
ψ	specific Helmholtz free energy	J/kg	39
$\widetilde{\psi}$	Helmholtz free energy density	J/m^3	51
Ψ	total free energy associated with Ω_t	J	50
Ω, Ω_t	domain occupied by a mixture (at time t)	–	15
$\partial\Omega$	(fixed) domain boundary	–	48
Superscripts			
δ	traceless part of a tensor	–	40
m	averaging/weighting by mass fractions	–	18
v	averaging/weighting by volume fractions	–	18

Chapter 1

Introduction

Suspensions, solutions and colloids are physical systems that can be generally denoted as *multi-component systems* or *mixtures*. Such physical systems are frequently met in many industrial applications ranging from production of wheat flour, through petroleum refining process, to disposal of nuclear waste. As a natural consequence, mathematical models have been developed to describe the behaviour of such mixtures.

Description and modelling of physical processes involving co-existence of multiple components and their mutual interaction has been a very challenging topic for decades and the problem has been tackled by variety of different modelling approaches. The standard approach, which is applied also in this thesis, is based on the rational treatment of multi-component systems as interacting continua. As such, it fits in to the classical framework of continuum thermodynamics and it is described in numerous publications; see, for example, Eckart (1940), Bowen (1976), Atkin and Craine (1976a,b), Truesdell (1984), Samohýl (1987), Rajagopal and Tao (1995) or Hutter and Jöhnk (2004).

The thesis is devoted to the study of physical systems that are composed of several chemically non-reacting components, each of them representing a uniform material that is physically distinct and separable from the other materials involved. In particular, we concentrate our study to flows of several *immiscible* fluids that occupy different regions of space in a fixed domain. (Think about oil and water in a container.)

The separate regions are often called *phases*, which is the term that brings us to the concept of *multi-phase flows*. From a broader perspective, a physical system described in the previous paragraph is generally referred to as a *multi-component fluid*. This term better characterizes the fact that our derivation of mathematical models describing multi-phase flows is based on the multi-component description of the underlying physical system. Even though there is a subtle difference between 'phase' and 'component', as each phase can be in fact comprised of several mixed material components (see Section 3.1.1), we shall use both terms interchangeably[1]. The fact that the fluids are immiscible is associated with the inherent presence of interfaces that are formed between them.

[1]In accordance with the idealization that each fluid involved in our considered physical system corresponds to exactly one component.

In principle, there are two major ways of representing the interfaces in mathematical models. First, in classical hydrodynamics, the interface separating two immiscible fluids is treated as being *sharp*, meaning that it is represented as a discontinuity of density and tangential velocity. The standard fluid equations are then posed in the bulk on both sides of the interface and jump conditions are prescribed across the surface of discontinuity. An alternative option is to replace the sharp interface by a narrow transition layer of finite thickness, so-called *diffuse* interface, across which the fluids are allowed to mix. Even though it may sound strange to allow for mixing of immiscible fluids, it is just a reflection of partial miscibility that real fluids always exhibit at the molecular level. The major advantage of this approach is the ability to describe critical phenomena like topological changes due to merging/splitting of individual phases or their interaction with walls in the computational domain.

Nice example of a three-component system of the above type can be identified in glass industry in the so-called *float glass forming process*. We shall describe this ingenious technology within the next section to motivate our research. After that, we shall briefly review the two modelling concepts that can be used to mathematically describe the process, with particular emphasis on the diffuse interface approach. Main objectives, research results and the outline of the thesis are advertised in the remainder of this introductory chapter.

1.1 Motivation: Float glass forming process

The float glass forming process, also known as the *Pilkington process* or simply the *float process*, is the standard industrial scale process for making flat glass. The technology was developed in the late 1950s and quickly became the universal method for producing high-quality flat glass. Nowadays, a modern float glass line produces in average of several hundred tonnes of glass each day and supplies it to a variety of different markets including automotive, architectural, and many other technical applications. An excellent historical overview of earlier techniques for making flat glass and the development of the float process is given in the survey by Pilkington (1969), who describes the process as follows:

> In the float process, a continuous ribbon of glass moves out of the melting furnace and floats along the surface of an enclosed bath of molten tin (Figure 1.1). The ribbon is held in a chemically controlled atmosphere at a high enough temperature for a long enough time for the irregularities to melt out and for the surfaces to become flat and parallel. Because the surface of the molten tin is dead flat, the glass also becomes flat.
>
> The ribbon is then cooled down while still advancing across the molten tin until the surfaces are hard enough for it to be taken out of the bath without the rollers marking the bottom surface; so a ribbon is produced with uniform thickness and bright fire polished surfaces without any need for grinding and polishing.

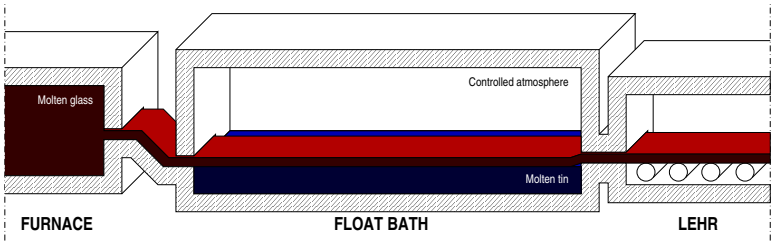

Figure 1.1: Schematic diagram of the float glass forming process.

The progressive growth in demand for high-quality flat glass pressures its manufactures to increase production. However, higher production rates in the float process lead to higher temperature and velocity gradients inside the tin bath. It is well known that the difficult operating conditions may induce formation of optical defects that cannot be corrected later, see Prieto et al. (2002). Moreover, high temperatures inside the tin bath (around 1000°C) make it complicated and costly to carry out detailed experiments that would help us to better understand these issues. Naturally, computational fluid dynamics (CFD) becomes a handy and powerful tool which provides us with the possibility to gain insight into the process and eventually optimize its various parts. This is typically done not only to meet customer's specific demands (for instance on the thickness of produced glass sheets), but generally to improve the overall performance of the manufacturing line (energy consumption savings, minimal contamination of the final product by impurities coming from the furnace, etc.).

The use of CFD techniques requires identification of a suitable mathematical model for the process. This is a challenging task as one has to deal with a multi-component system with free boundaries, for which it is necessary to incorporate the surface tension effects. From the point of view of numerical simulations, the problem is furthermore complicated by the presence of multiple length scales[2], large temperature/viscosity variations[3] and large density contrasts (see Table 1.1).

The whole process can be intuitively split into the three main stages as indicated in Figure 1.2. In the same figure, we show the visualization of the first stage of the process corresponding to the flow of the glass melt down an inclined plane (spout lip) and its impact on the tin bath. The second stage of the process is the stretching of the glass ribbon which is nicely illustrated in Figure 1.3. Finally, the third stage represents the cooling process of formed sheets of glass. The actual process of forming thus takes place in the first and the second stage respectively. The idea is to implement an iterative coupling (through the velocity and stress components) between the two stages that are otherwise modelled as separate processes. Such coupling should be effected along a transverse cross-section artificially made somewhere inside the tin bath, sufficiently far from the inlet.

[2]The typical industrial floats are about 60 m long and 4–8 m wide, while the equilibrium thickness of the glass ribbon is only about 7 mm.

[3]The glass suffers a gradual cooling from approximately 1050 °C to 600 °C, while its viscosity varies by several orders of magnitude along the float due to the significant dependence on the temperature.

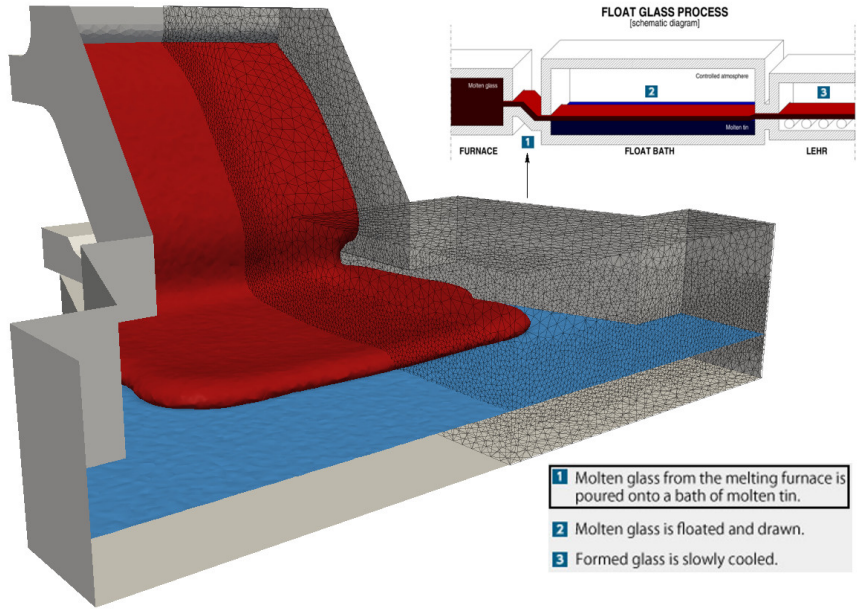

Figure 1.2: Inlet of molten glass in the float process.

The key physical mechanism in the second stage of the process is the temperature variation of the viscosity, which allows one to control—through the temperature distribution inside the tin bath—the thickness and solidification of the ribbon[4]. If we view the ribbon from the top, as in Figure 1.3, we can say that the longitudinal and transverse dimensions of the ribbon dominate its thickness. This suggests that one can try to model this part of the process by exploiting a variant of *thin film approximation*; see, for example, Narayanaswamy (1977, 1981), Popov (1982, 1983). On the other hand, no characteristic length scale can be identified in the proximity of the inlet, where we need to capture three-dimensional effects such as *wet back flow*. Therefore, a full mathematical model describing multi-component flows needs to be employed in this stage of the process.

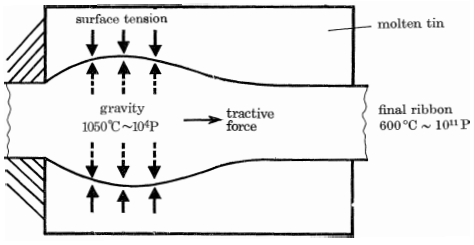

(a) Forces acting on the ribbon.

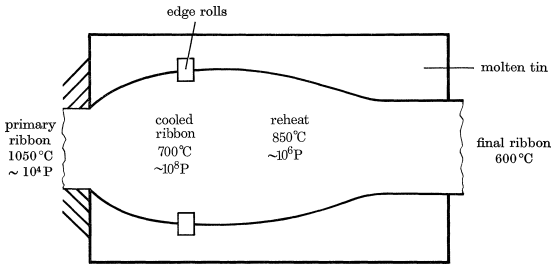

(b) Temperature/viscosity profile along the longitudinal axis of the bath.

Figure 1.3: Top-down view of glass ribbon stretching as part of the float process. [Both figures were reproduced from Pilkington (1969).]

[4]The thickness can be additionally controlled mechanically by adjusting the *lehr* speed and by using the so-called *edge rolls* (gearwheels placed close to the edges of the glass ribbon).

Fernández Oro et al. (2008) successfully used *volume-of-fluid* method with surface tensions incorporated via *continuum surface force* formulation to simulate the first stage of the float process[5]. Their approach was based on the following simplifying assumptions:

- The three immiscible components involved in the float process—the molten glass, the molten tin and the non-reactive protective atmosphere consisting of a mixture of nitrogen (approximately 94%) and hydrogen (approximately 6%)—are all treated as incompressible, viscous Newtonian fluids.
- The temperature variations in between the inlet and (artificial) outlet positions at the very beginning of the float process are neglected, so that the transport of molten glass is assumed to occur at a constant temperature.

The thesis is devoted to the development of a different class of models that are well suited to such types of simulations. Compared to the techniques used by Fernández Oro et al. (2008), where the interfaces were treated as being sharp, the models developed here are based on the aforementioned concept of diffuse interface. This approach allows not only for relatively easier implementation, but also for consistent incorporation of the surface tension effects and the thermal effects.

The applicability of a particular three-component diffuse interface model in the float process, under the above simplifying assumptions, was recently documented in Řehoř et al. (2017). Figure 1.4 shows the typical outcome of the transient simulation of the first stage of the float process. Even though the typical length scale characterizing the interface thickness is much larger in numerical

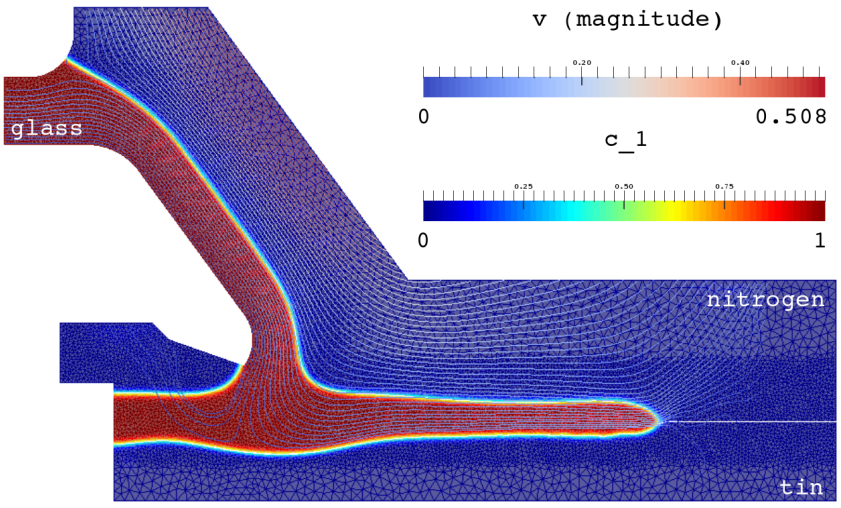

Figure 1.4: Diffuse interface approach applied in the float glass forming process to model the interaction of three immiscible fluids (glass/tin/nitrogen).

[5]To implement a physics-based interface tracking, the original volume-of-fluid method developed by Hirt and Nichols (1981) was combined with the continuum surface force approach suggested by Brackbill et al. (1992); see also Gueyffier et al. (1999).

simulations than in reality, let us point out that a very fine resolution of the computational mesh is needed to properly capture the interface dynamics. This inherently calls for the need to use high performance computing (HPC) platforms, ideally in combination with adaptive mesh refinement[6].

The model described in Řehoř et al. (2017) fits into a wider class of diffuse interface models that are developed and studied in the first, modelling part of the thesis (Chapters 2–4). In the second, computational part (Chapters 5–6), we shall identify the origin of computational issues previously encountered in simulations of glass/tin/nitrogen system, and we shall address possible improvements in the implementation of the model. Let us recall the main issues now.

Known computational issues

Table 1.1 captures density and viscosity values of individual components in the glass/tin/nitrogen system. Due to **high density contrast** between molten tin and nitrogen, which are both **low viscosity** fluids, we observe an occurrence of spurious velocity oscillations in the vicinity of the interface (see Figure 1.5a). Their presence in the simulation can eventually cause that the numerical solution blows up in finite time.

The most straightforward way of how to make the computations in the industrial setting feasible is to artificially increase the viscosity of the "problematic" components. As discussed in Řehoř et al. (2017), in some specific situations it might be sufficient to increase the viscosity of tin and nitrogen by three orders of magnitude without significantly affecting the expected outcome of the simulation (see Figure 1.5b). In the future, we would like to avoid this inconsistent approach by improving the applied numerical discretization, see Section 6.4.

In the typical industrial setting, one needs to handle large scale computations effectively (see Figure 1.6 for illustration of the typical problem size). It is well-known that the parallel **direct sparse solvers**, which were used in Řehoř et al. (2017) to resolve intermediate systems of algebraic equations, do not scale optimally on HPC platforms. To this end, we will develop an efficient and robust iterative solver which will result in computationally less costly simulations, see Section 5.4.

Material	Density $[\mathrm{kg/m^3}]$	Viscosity (realistic) $[\mathrm{Pa \cdot s}]$	Viscosity (modified) $[\mathrm{Pa \cdot s}]$
Glass	2 500	100	100
Tin	6 770	0.001	1.0
Nitrogen	1.225	18×10^{-5}	0.18

Table 1.1: Density and viscosity values for glass/tin/nitrogen system. Data taken from Fernández Oro et al. (2008).

[6]In this particular example we take the advantage of the fact that we are able to estimate the expected position of the interfaces, and we prepare the locally refined mesh *a priori*.

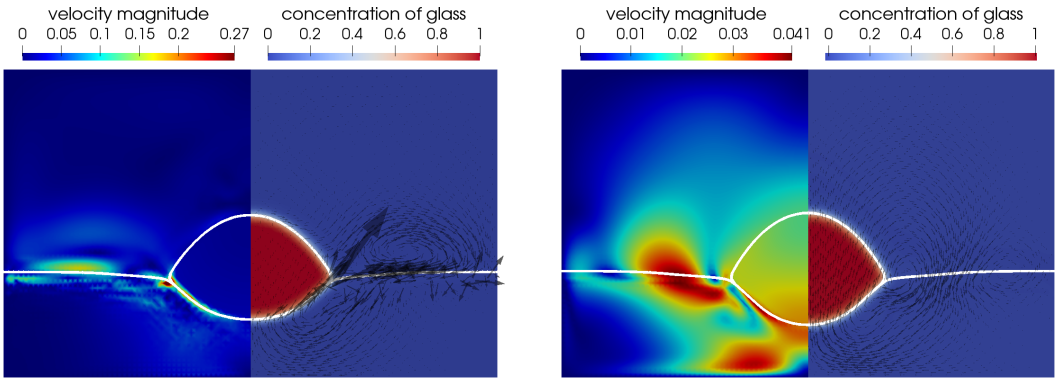

(a) Realistic viscosity values. (b) Modified viscosity values.

Figure 1.5: Glass droplet placed onto the tin bath for realistic and modified viscosity of the tin and the protective atmosphere surrounding the droplet.

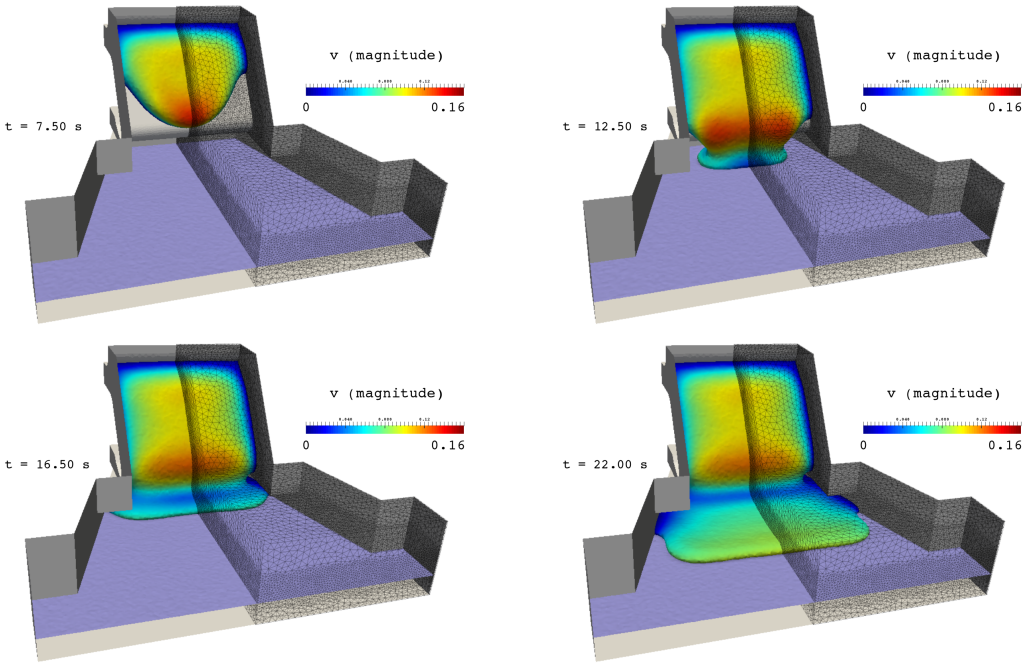

Figure 1.6: Snapshots capturing the glass flow over the spout lip and its impact onto the tin bath in 3D (simulation with modified viscosity values). The computation of 2 500 time steps took about 55 hours on 80 CPUs. Problem size: 3×10^5 degrees of freedom for the discrete Cahn-Hilliard system; 1.5×10^6 degrees of freedom for the discrete Navier-Stokes system.

1.2 A brief review of applied modelling concepts

The problem of proper description of the evolution of sharp interfaces is very challenging from the numerical point of view. The two main approaches of how to treat the moving interfaces in numerical simulations are *front tracking* and *front capturing* methods; see, for instance, the references given in Kim (2012).

In the front tracking methods, including the volume-of-fluid method mentioned in the previous section, the position of the interface is explicitly traced. (This is typically achieved with the aid of Lagrangian particles that are advected by the velocity field.) In the front capturing methods, the interface is implicitly captured by a contour of a particular scalar field.

The typical representative of the latter computational approach is the so-called level set method; see, for example, Osher and Sethian (1988) or Sussman et al. (1994). The scalar field that is used to capture the sharp interface is introduced as an artificial level set function. In order to avoid unwanted instabilities at the interface, it is necessary to consider an explicit smoothing of the flow discontinuities. This in turn leads to the interfacial layer of finite thickness in numerical simulations. From this point of view, the method could be seemingly identified with the idea to work with the concept of diffuse interface. Since the type of smoothing can substantially affect obtained solutions, it seems natural to consider a physically realistic scalar field instead of an artificial level set function with the aim to describe physical processes inside the interfacial layer in a thermodynamically consistent way[7]. Let us point out that this approach will allow us to naturally include surface tension effects into the model.

The diffuse interface models that are studied in this thesis are based on the description of mixing within the interfacial layers. Such mixing can be conveniently described in terms of mass or volume fractions, although it is equally possible to choose any other set of so-called *order parameters* that are appropriately related to partial densities of individual fluids. The thermodynamically consistent description is based on the postulate that the Helmholtz free energy density (at a fixed temperature) is determined not only by the actual composition of the mixture at a given point but also by its composition at neighboring points. This fundamental idea can be traced to van der Waals (1893). It was first constructively used by Cahn and Hilliard (1958) who proposed a model for the description of separation of components in binary mixtures.

In its original form, the now classic Cahn–Hilliard (CH) model does not take into account coupling between diffusion and mechanics, as the separation process is assumed to be governed exclusively by the diffusion. In this setting, the model describes solids and fluids equally well. Recall that we are interested in flows of several immiscible fluids. With respect to our target application described in the preceding section, we shall assume that flows of individual fluids can be described by the classical Navier–Stokes (NS) model. Nevertheless, the coupling of both models is highly non-trivial. In fact, there is a wide variety of competing models of the Cahn–Hilliard–Navier–Stokes (CHNS) type available in the literature nowadays.

Most of the recent works refer to the so-called "Model H", due to Hohenberg and Halperin (1977), as to the model that consistently couples fluid flow and CH diffusion for a conserved order parameter. Its thermodynamic consistency was established in Gurtin et al. (1996). The model has been successfully used to simulate two-component flows of incompressible fluids with matched densities;

[7]By the thermodynamic consistency of a model we mean its compatibility with the second law of thermodynamics.

see, for example, Chella and Viñals (1996). However, the last couple of requirements makes this model inapplicable in many interesting problems where the incompressible components have different densities (or where the fluids are compressible). As a consequence, numerous alternative generalizations of "Model H" have appeared in the literature. To name a few, let us mention the models developed by Boyer (2002), Ding et al. (2007) and Abels et al. (2012). These models were discussed and numerically compared by Aland and Voigt (2012). The thermodynamically consistent extension of "Model H" was provided by Lowengrub and Truskinovsky (1998). A comprehensive overview of possible generalizations of CH equations within the thermodynamic framework adopted in the thesis can be found in Heida et al. (2012b). For further references, the reader is kindly referred to the review papers by Anderson et al. (1998) and Kim (2012).

The majority of models mentioned above have been used to simulate flows in the *classical isothermal setting* with the temperature being fixed to a uniform constant value. Only a few exceptions can be found in the literature. For instance, Jasnow and Viñals (1996) modified "Model H" to study thermo-capillary flow with an externally imposed temperature gradient. A non-isothermal model for two-component fluids was studied in Sun et al. (2009), where a linearization of the internal energy balance was used in order to describe the evolution of the temperature. The thermodynamically consistent extension of "Model H" into a *general non-isothermal setting* with a variable temperature field has been recently analyzed by Eleuteri et al. (2015), see also Eleuteri et al. (2016). This extension, however, remains restricted to the special case of two different viscous incompressible fluids of equal density. A non-isothermal reformulation of the model proposed by Lowengrub and Truskinovsky (1998) appears in the recent interesting article due to Freistühler and Kotschote (2017).

1.3 Objectives

The thesis has the following two main objectives:

- Comprehensive thermodynamic analysis of diffuse interface models in a non-isothermal setting.

- Development and implementation of numerical solvers for simulations of physical systems described by diffuse interface models.

The expected outcome of the first objective is the explicitly formulated evolution equation for the temperature, which could be used in numerical simulations of some relevant non-isothermal problems. The second objective is motivated by the importance of modern CFD tools in industrial applications. The float glass forming process described in Section 1.1 was chosen as the target application for the development of efficient numerical solvers in the context of diffuse interface models.

1.4 Research results

When modelling a simultaneous flow of several immiscible fluids with the aid of diffuse interface approach, it is common practice to combine the CH equations (describing the separation of fluids) with the NS equations (describing the flow). The resulting mathematical model is thus represented by a system of *coupled* partial differential equations (PDEs) involving a single velocity field, shared by all fluids, as an unknown variable. The coupling of equations is not unique and the different models exhibit different levels of coupling. Loosely speaking, CH and NS equations can be either more coupled or less coupled depending on assumptions made on the material properties of individual fluids and especially on the particular choice of the averaged velocity field.

From the modelling point of view, the main novelty of the present work is twofold. Firstly, it comes with a unified consistent derivation of a wide class of existing diffuse interface models, including the variants with non-matching constant densities or compressible components. Secondly, it provides the extension of the models into a general non-isothermal setting. In this sense we reveal the class of Cahn–Hilliard–Navier–Stokes–Fourier (CHNSF) models with explicitly formulated evolution equation for the temperature.

Our derivation is based on the description of the multi-component systems on the level of individual components. We carefully elaborate the kinematical concept of mass-/volume-averaged velocity and we also discuss various choices of order parameters (mass/volume fractions, partial densities) suitable for modelling of fully-compressible (FC), quasi-incompressible (QI) and fully-incompressible (FI) mixtures; see diagram in Figure 1.7.

Currently, there is a number of well-developed numerical solvers designed to tackle the systems of PDEs corresponding to selected models of the above type. In the thesis we apply the finite element method (FEM) for the purpose of numerical discretization and we utilize the principles of automated scientific computing offered within the FEniCS Project. The automation of FEM facilitates the implementation of the specific solution approaches, which is a difficult task due to the complexity of the models. On top of the FEniCS computing platform we develop the MUlti-phase FLow simulatiON library MUFLON, see Section 5.3.1. The idea is to provide the scientific community with a tool for testing different diffuse interface models and their FEM-based discretizations.

The key result from the point of view of the development of efficient numerical solvers resides in the identification of the solution strategy that is applicable in computationally demanding simulations of industrial processes. In Řehoř et al. (2017), we have elaborated some practical issues concerning the implementation of the specific FI-CHNS model, in which the incompressible NS equations constitute numerically the most demanding subset of the system. In the thesis, we propose a fast iterative solver using modern mathematical methods with the application to incompressible NS equations with variable coefficients. We address the issues concerning feasibility of numerical simulations with real parameter values and we briefly discuss some methods with the capability to suppress numerical artifacts arising due to the presence of density contrasts in combination with low viscosity.

The following list summarizes the major contributions of this work:

- Theoretical extension of existing diffuse interface models into a general non-isothermal setting.
- Implementation of the framework for testing different discretization schemes for diffuse interface models using the FEniCS computing platform.
- Implementation of state-of-the-art preconditioning strategies for solving incompressible NS equations (with variable coefficients).
- Identification of the source of errors arising in numerical simulations of flows of multi-component systems described by diffuse interface models in critical regimes with density contrasts and low viscosities.

1.5 Outline

The thesis is organized as follows. In Chapter 2 we first briefly discuss fundamental concepts introduced in the theory of interacting continua for the mathematical description of mixtures. We formulate a basic set of assumptions with the help of which we will distinguish between compressible and incompressible mixtures. As a next step, we postulate balance equations for individual components of the mixture. At the same time, we adopt a certain type of model reduction in order to provide a transition from the general detailed description on the level of individual components towards a reduced description used in the context of diffuse interface models.

Chapter 3 is devoted to a thermodynamically consistent derivation of diffuse interface models. The models lead to a system of PDEs of CHNSF type. The derivation is based on the specification of constitutive assumptions for the specific Helmholtz free energy and the entropy production. Special attention is paid to models for two-component systems. We show that the derived binary models consistently reduce to their well-known isothermal counterparts, and we discuss under which conditions they retain the capability to properly describe single-component fluids.

Full specification of diffuse interface models describing isothermal flows of several immiscible incompressible fluids is discussed in Chapter 4. We accept a set of consistency/reduction conditions which bring us to the elaborated form of the Helmholtz free energy involving the state-of-the-art multi-well potential function, as well as to the particular choice of the mobility coefficients that characterize one of the dissipation mechanisms identified in the entropy production. In this way we derive the system of evolutionary equations for the FI-CHNS model, which is then suplemented by a set of boundary and initial conditions.

In Chapter 5 we discuss numerical discretization of FI-CHNS model. Using the techniques originally developed for binary and ternary systems, we propose an unconditionally stable scheme which leads to a computationally decoupled formulation of the problem. A single iteration of the resulting time-stepping algorithm requires solving a nonlinear system of algebraic equations corresponding to the CH part of the problem, followed by solving a saddle-point system of algebraic equations arising from the Oseen type linearization of the NS equations. A special attention is paid to efficient numerical solution strategies for the latter subproblem based on the application of appropriate preconditioning techniques.

Our implementation of the various discretization schemes is verified through a series of numerical experiments covered by Chapter 6. These experiments include code verification by the method of manufactured solutions and classical rising bubble benchmark. On top of that, we add two simplified problems characterized by the presence of a single interface between low viscosity components with a density contrast (for instance air/water interface). These two examples help to better understand the source of numerical errors that typically occur near such interfaces in the form of spurious velocity oscillations.

Finally, in Chapter 7 we summarize the results of the thesis and we discuss possible future directions for the follow-up research.

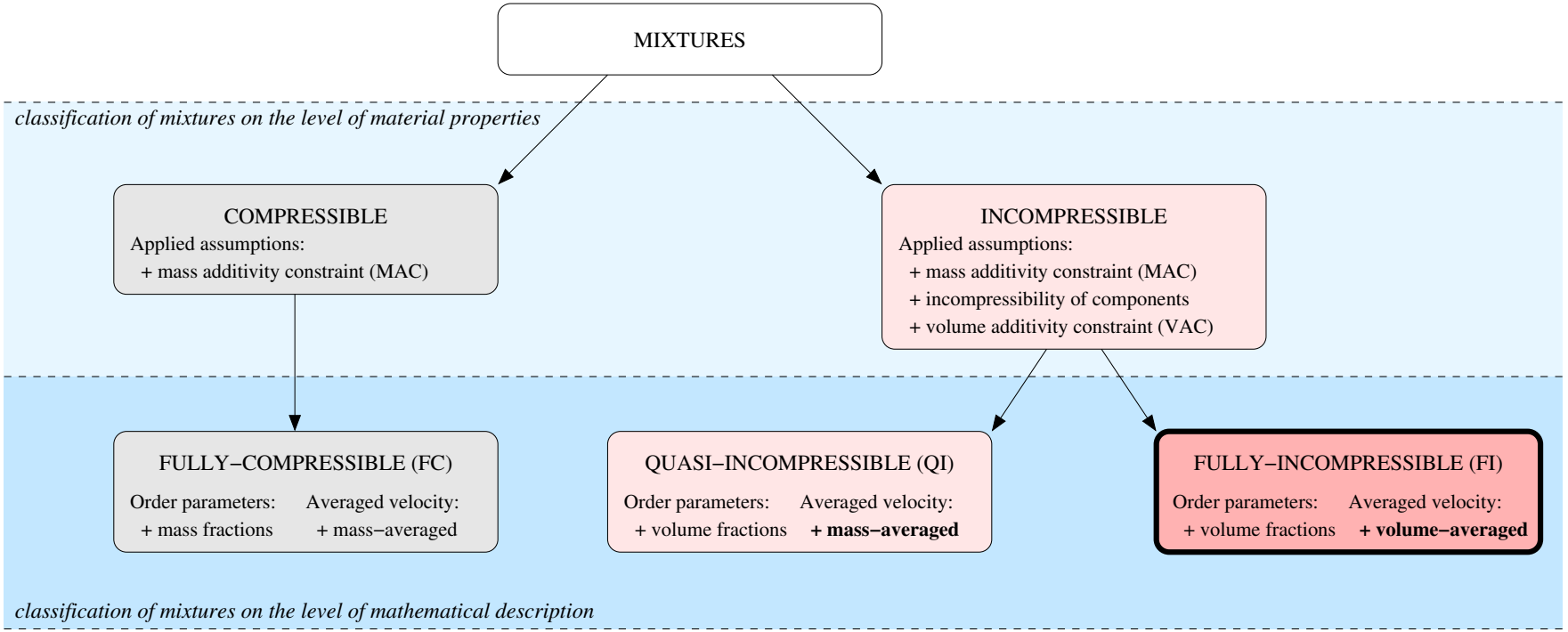

Figure 1.7: Two-level diagram for the classification of mixtures in the context of diffuse interface modelling; see Section 2.1 for the precise definition of applied assumptions and order parameters, and Definition 2.5 for the specification of the averaged velocity.

Chapter 2

Theory of Interacting Continua: Foundations

In this chapter we shall recall some of the basic concepts introduced within the *theory of interacting continua*, one of the frameworks developed to provide suitable description of mixtures[1]. Mathematical basis of the framework was laid down in the works by Truesdell (1957a,b), Truesdell and Toupin (1960).

The aim of the chapter is to introduce the key concepts particularly suitable for the description of flows of multi-component fluids, see Chapter 1. Recall that the fluid-like components are assumed to be immiscible and we aim to describe their mutual interaction in terms of diffuse interface models. There are multiple ways of deriving such type of models; see references given in Section 1.2. Our approach is based on the componentwise formulation of balance equations (balances of mass, linear and angular momentum, energy and entropy) which are accepted as basic postulates valid for "any" material.

This detailed description of our considered physical system is subsequently reduced as we are interested in developing a model where we distinguish only the individual partial densities of the components and otherwise we treat the mixture as a whole, that is, as a single homogenized continuous medium. In principle, the reduction is based on defining primitive mixture properties (such as mixture density, velocity, stress tensor, and so on) and on describing their evolution by balance equations derived from the aforementioned postulates. The reduced equations are therefore still universally valid for "any" material, meaning that they equally describe flows of the multi-component fluids composed either of oil and water, or those composed of molten tin and molten glass. The properties of the materials involved must be specified by appropriate constitutive relations the derivation of which is the subject of Chapter 3.

In the current chapter, we will at least distinguish between *compressible* and *incompressible* multi-component systems (regarding the material properties). As illustrated in the middle part of the diagram in Figure 1.7, we assume that a certain set of constraints can be applied for each such system. A formal definition of these constraints—in the form of fundamental assumptions—is given in Section 2.1.

[1]Occasionally, we will use the term *theory of mixtures*.

In Section 2.2 we introduce basic kinematic quantities for mixtures including the concept of *averaged velocity*. The diffuse interface models encountered in the literature are not consistent regarding the choice of this quantity. Some authors prefer to work with the mass-averaged velocity, others tend to use its volume-averaged counterpart. It is well known that the second one is divergence free, which is not generally true for the first one. From this point of view, the models based on the volume-averaged velocity might be more convenient for numerical treatment. On the other hand, the models based on the mass-averaged velocity are fully consistent with the componentwise description of the same system. In contrast to this, some additional levels of approximation usually must be accepted in the other case. Our objective here is to provide the derivation of the different diffuse interface models in a unified framework.

The cornerstone of this framework is laid in Section 2.3 where we formulate the reduced balance equations with respect to the two choices of the averaged velocity. Different form of these balance equations brings us to another possible classification of multi-component systems which is illustrated in the bottom part of Figure 1.7. In Section 2.4 we introduce basic thermodynamic quantities. Finally, Section 2.5 summarizes the evolution equations in the form appropriate for the subsequent derivation of the constitutive relations.

2.1 Fundamental assumptions

Let us consider a mixture consisting of N components. The theory of interacting continua is built on the *assumption of co-occupancy* which states that all components co-exist, in a homogenized sense, at each point of the domain occupied by the mixture in the observed space[2]. In the next paragraph, we will explain this concept using basic terms from continuum mechanics the detailed explanation of which can be found for example in Gurtin et al. (2010).

Let $\mathcal{B}_i$ denote the continuous body associated with the i-th component (for $i = 1, \dots, N$). It is an abstract set of material points that can be embedded into the classical Euclidean space $\mathbb{R}^3$. Let $\boldsymbol{\kappa}_i^{\mathrm{ref}}(\mathcal{B}_i)$ and $\boldsymbol{\kappa}_i^t(\mathcal{B}_i)$ denote an arbitrary reference configuration of the body and the current configuration of the body at time t respectively. The mappings $\boldsymbol{\kappa}_i^{\mathrm{ref}}$ and $\boldsymbol{\kappa}_i^t$ are linked through the deformation function which will be introduced in Section 2.2 to formally describe the motion of the continuous body. Following the above statement, one can say that the domain occupied by the mixture in the observed space at time t corresponds to the intersection of current configurations of all components. We will denote this domain by Ω_t for simplicity. In principle, the assumption of co-occupancy says that each point $\boldsymbol{x} \in \Omega_t$ can be seen as the position occupied by a material point, or particle, belonging to each component, see Figure 2.1.

Remark 2.1. Let us make some remarks on the notation used within the thesis. The usual summation convention is not used and summations are always shown

[2]The assumption of co-occupancy is of course just a mathematical abstraction that allows one to introduce the quantities associated with each component and use them, taking into account mutual interactions of the components, to describe properties of the mixture as a whole.

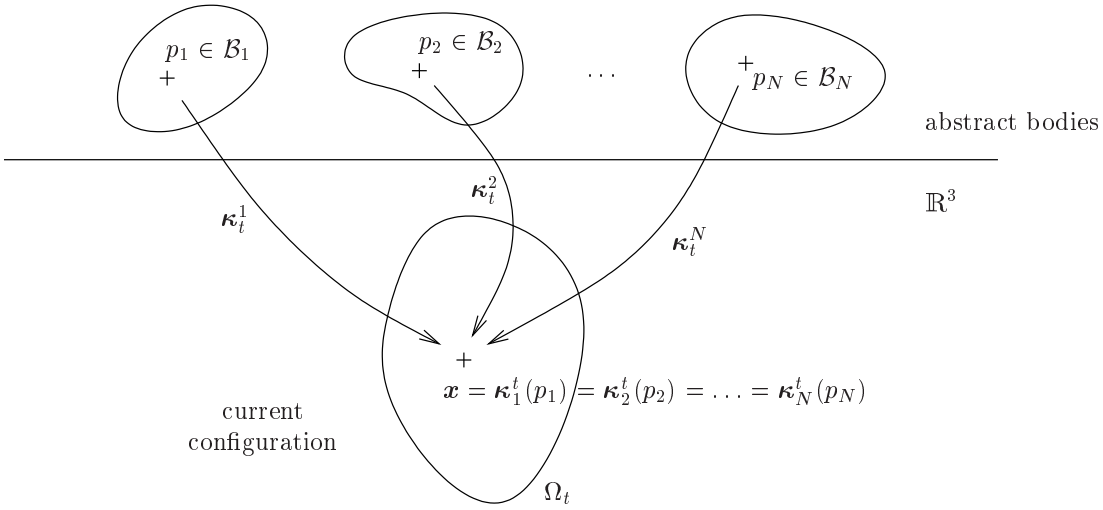

Figure 2.1: Assumption of co-occupancy.

explicitly. In order to avoid cumbersome statements of the type "for all times t in a given time interval", we shall simply write "for all t" having in mind that we are restricting ourselves to a time interval chosen for observations.

Let $\mathcal{P}_t \subset \Omega_t$ be an arbitrary open subset of the current configuration of the mixture. Let $\mathrm{m}(\mathcal{P}_t)$ and $\mathrm{v}(\mathcal{P}_t)$ denote the mass and the volume of the mixture as a whole associated with $\mathcal{P}_t$. Similarly, let $\mathrm{m}_i(\mathcal{P}_t)$ and $\mathrm{v}_i(\mathcal{P}_t)$ denote the mass and the volume of the i-th component associated with $\mathcal{P}_t$. Using these measures one can introduce three distinct notions of density. First, the density of the mixture as a whole is given by

$$\varrho = \frac{\mathrm{dm}}{\mathrm{dv}}, \tag{2.1a}$$

where 'dm' denotes the mass contained in an infinitesimal volume 'dv'; see Noll (1959) for the formalization thereof. On top of that we will distinguish between the partial density of the i-th component,

$$\varrho_i = \frac{\mathrm{dm}_i}{\mathrm{dv}}, \tag{2.1b}$$

and the material (true) density of the i-th component,

$$\hat{\varrho}_i = \frac{\mathrm{dm}_i}{\mathrm{dv}_i}. \tag{2.1c}$$

The latter corresponds to the density of the component before mixing. Last but not least, we introduce the mass fractions (concentrations) by

$$c_i = \frac{\mathrm{dm}_i}{\mathrm{dm}}, \tag{2.1d}$$

and the volume fractions (porosities) by

$$\phi_i = \frac{\mathrm{dv}_i}{\mathrm{dv}}. \tag{2.1e}$$

One can observe that

$$\varrho_i = \varrho c_i = \hat{\varrho}_i \phi_i. \tag{2.2}$$

Relations in (2.2) will be extensively used in subsequent discussion.

In order to understand the behaviour of the mixture as a whole it is natural to require that exactly N considered components contribute to the evolution of the system and there is no other component that would not be included among them. This leads us to the constraint relating the measures m, m_i in the following sense.

Assumption 1 (Mass additivity constraint)**.** *We assume that any mixture fulfills the* mass additivity constraint (MAC)*, that is*

$$\mathrm{m}(\mathcal{P}_t) = \sum_{i=1}^{N} \mathrm{m}_i(\mathcal{P}_t) \tag{2.3}$$

for any $\mathcal{P}_t \subset \Omega_t$*.*

The development of numerical simulations in the thesis is restricted exclusively to multi-component systems composed of incompressible fluids with constant material densities[3]. Such multi-component systems are in our terminology classified as incompressible mixtures.

Assumption 2 (Incompressibility of components)**.** *We assume that components of any incompressible mixture are mechanically and thermally incompressible in the sense that*

$$\hat{\varrho}_i \text{ are positive constants for } i = 1, \ldots, N. \tag{2.4}$$

When dealing with incompressible mixtures we will always assume that the volume of the mixture as a whole equals the sum of the volumes of individual components. (We say that the excess volume of mixing is zero.)

Assumption 3 (Volume additivity constraint)**.** *We assume that any incompressible mixture fulfills the* volume additivity constraint (VAC)*, that is*

$$\mathrm{v}(\mathcal{P}_t) = \sum_{i=1}^{N} \mathrm{v}_i(\mathcal{P}_t) \tag{2.5}$$

for any $\mathcal{P}_t \subset \Omega_t$*.*

[3]In principle, it would be possible to consider here the class of materials that are mechanically incompressible and thermally compressible or expansible. In such a case, the material densities would be treated as known positive functions of the temperature. This would introduce an unnecessary complexity into the governing equations with regard to practical applications of our interest. To illustrate this, in Appendix A we formulate balance of mass for mixtures formed by the components belonging to this class of materials.

Note that this is a severe restriction which is not true in general cases[4]. Nevertheless, this constraint will allow us to express the total density of the mixture as a linear function of volume fractions, which is the relation often used in the context of diffuse interface modelling.

Let us once again emphasize that all multi-component systems in the thesis are considered to obey Assumption 1 automatically. If no other assumptions can be applied, we shall refer to such systems as to compressible mixtures. On the other hand, Assumptions 2 and 3 characterize incompressible mixtures.

Consequences of mass additivity constraint

Since $\mathrm{m}(\mathcal{P}_t) = \int_{\mathcal{P}_t} \varrho \,\mathrm{dv}$ and $\mathrm{m}_i(\mathcal{P}_t) = \int_{\mathcal{P}_t} \varrho_i \,\mathrm{dv}$, see (2.1a) and (2.1b) respectively, from (2.3) it immediately follows that

$$\varrho = \sum_{i=1}^{N} \varrho_i. \tag{2.6}$$

With respect to the first equality in (2.2), we see that equation (2.6) is equivalent to the constraint

$$\sum_{i=1}^{N} c_i = 1. \tag{2.7}$$

Consequences of volume additivity constraint

Similarly as in the previous case, we observe that the statement (2.5), together with (2.1e), yields the identity

$$\sum_{i=1}^{N} \phi_i = 1. \tag{2.8}$$

Based on this constraint it is possible to find the expressions for the total density in terms of N material densities, or their reciprocal values

$$\hat{\gamma}_i \overset{\text{def}}{=} \frac{1}{\hat{\varrho}_i}, \tag{2.9}$$

and $(N-1)$ volume fractions, or mass fractions respectively. (In that respect, we shall omit the N-th component of the mixture without loss of generality.)

Lemma 2.2. *Let* Assumptions 1–3 *hold. Further, let* $\boldsymbol{\phi} = [\phi_1, \dots, \phi_{N-1}]^\top$ *and* $\boldsymbol{c} = [c_1, \dots, c_{N-1}]^\top$ *denote* $(N-1)$*-component vectors of volume fractions and mass fractions respectively. Then the total density* ϱ *can be expressed as*

$$\varrho^{\mathrm{v}}(\boldsymbol{\phi}) \overset{\text{def}}{=} \sum_{i=1}^{N-1} (\hat{\varrho}_i - \hat{\varrho}_N)\, \phi_i + \hat{\varrho}_N, \tag{2.10a}$$

$$\varrho^{\mathrm{m}}(\boldsymbol{c}) \overset{\text{def}}{=} \frac{1}{\sum_{i=1}^{N-1} (\hat{\gamma}_i - \hat{\gamma}_N)\, c_i + \hat{\gamma}_N}. \tag{2.10b}$$

[4]For example, a mixture of isopropyl alcohol and water exhibits excess volume of mixing which is negative.

PROOF. Using $\varrho_i = \hat{\varrho}_i \phi_i$ in (2.6), we get $\varrho = \sum_{i=1}^{N} \hat{\varrho}_i \phi_i$. Clearly, ϕ_N can be eliminated using the constraint (2.8). The resulting expression corresponds to (2.10a).

From (2.2) it follows that $\phi_i = \varrho \hat{\gamma}_i c_i$. Using this expression in (2.8), we get $\varrho \sum_{i=1}^{N} \hat{\gamma}_i c_i = 1$. If we use the constraint (2.7) to eliminate c_N, we obtain the expression for ϱ in the form (2.10b). □

2.2 Kinematics of mixtures

Let $\boldsymbol{\kappa}_i^{\mathrm{ref}}(\mathcal{B}_i)$ be a fixed but otherwise arbitrary reference configuration of the i-th component of the mixture. The *motion* of the body $\mathcal{B}_i$ is given by the mapping $\boldsymbol{\chi}_i$ that assigns to each particle $\boldsymbol{X}_i \in \boldsymbol{\kappa}_i^{\mathrm{ref}}(\mathcal{B}_i)$ and each time t a point $\boldsymbol{x} = \boldsymbol{\chi}_i(\boldsymbol{X}_i, t)$ in the current configuration of the mixture. The point $\boldsymbol{x}$ is referred as the *spatial point* occupied by $\boldsymbol{X}_i$ at time t.

Remark 2.3. The mapping $\boldsymbol{\chi}_i$, called the *deformation function* of the i-th component, is assumed to be invertible for each time t and smooth enough such that the corresponding derivatives are well defined in the classical sense.

We consider N particles $\boldsymbol{X}_1, \ldots, \boldsymbol{X}_N$, each of them associated with the corresponding component of the mixture. Due to the assumption of co-occupancy, these particles are allowed to occupy a single spatial point $\boldsymbol{x} \in \Omega_t$. The description of the motion of the mixture as a whole is thus given by N relations

$$\boldsymbol{x} = \boldsymbol{\chi}_i(\boldsymbol{X}_i, t). \tag{2.11}$$

Since we are primarily interested in the description of fluid mixtures, it is convenient to work with the *Eulerian description* of scalar, vector and tensor fields. In this respect we introduce *partial velocity* for each component through

$$\boldsymbol{v}_i(\boldsymbol{x}, t) \overset{\mathrm{def}}{=} \left. \frac{\partial \boldsymbol{\chi}_i(\boldsymbol{X}_i, t)}{\partial t} \right|_{\boldsymbol{X}_i = \boldsymbol{\chi}_i^{-1}(\boldsymbol{x}, t)}. \tag{2.12}$$

If g is any quantity represented as Eulerian scalar field, then its material time derivative following the i-th component is defined by

$$\frac{\mathrm{d}_i g(\boldsymbol{x}, t)}{\mathrm{d}t} \overset{\mathrm{def}}{=} \left. \frac{\mathrm{d} g(\boldsymbol{\chi}_i(\boldsymbol{X}_i, t), t)}{\mathrm{d}t} \right|_{\boldsymbol{X}_i = \boldsymbol{\chi}_i^{-1}(\boldsymbol{x}, t)} \tag{2.13}$$

It corresponds to the variation of the given quantity with respect to time at the material point $\boldsymbol{X}_i$ that at time t occupies the spatial position $\boldsymbol{x}$. Using the chain rule and (2.12), it follows from (2.13) that

$$\frac{\mathrm{d}_i g(\boldsymbol{x}, t)}{\mathrm{d}t} = \frac{\partial g(\boldsymbol{x}, t)}{\partial t} + \boldsymbol{v}_i(\boldsymbol{x}, t) \cdot \nabla g(\boldsymbol{x}, t). \tag{2.14}$$

The short form[5] of the above formula reads

$$\frac{\mathrm{d}_i g}{\mathrm{d}t} = \frac{\partial g}{\partial t} + \boldsymbol{v}_i \cdot \nabla g. \tag{2.15}$$

Obviously, the analogous definitions can be obtained for Eulerian vector fields and Eulerian tensor fields.

[5] We shall omit the arguments $(\boldsymbol{x}, t)$ whenever no confusion concerning variables can arise.

Remark 2.4. Similarly to the theory of single continuum, one can introduce the deformation gradient $\mathbb{F}_i$, the left and the right Cauchy-Green tensors $\mathbb{B}_i$, $\mathbb{C}_i$ and other deformation measures based on the relation (2.11). However, introduction of these quantities is not necessary for our purposes.

In the theory of mixtures, it is often convenient to introduce an averaged velocity associated with the mixture as a whole and work with it without the need to distinguish between individual partial velocities. This is the case also in the context of diffuse interface models. In what follows we shall work with *mass-averaged*[6] and *volume-averaged* velocity fields.

Definition 2.5 (Mass-averaged velocity, volume-averaged velocity)**.** *The* mass-averaged *velocity field is defined by*

$$\boldsymbol{v}^{\mathrm{m}} \stackrel{\mathrm{def}}{=} \sum_{i=1}^{N} c_i \boldsymbol{v}_i, \tag{2.16a}$$

while the volume-averaged *velocity field is defined by*

$$\boldsymbol{v}^{\mathrm{v}} \stackrel{\mathrm{def}}{=} \sum_{i=1}^{N} \phi_i \boldsymbol{v}_i. \tag{2.16b}$$

In the forthcoming manipulations with balance equations, we shall initially work with an arbitrary averaged velocity $\boldsymbol{v}$ without the need to precisely specify its structure. Afterwards, we shall examine consequences of the specific choice of the averaged velocity according to Definition 2.5.

Remark 2.6. The material time derivative associated with velocity $\boldsymbol{v}$ is defined by the formula (2.15) with $\boldsymbol{v}_i$ replaced by $\boldsymbol{v}$ and it is denoted simply by $\frac{\mathrm{d}}{\mathrm{d}t}$. If we need to emphasize that we are working explicitly with the mass-averaged or the volume-averaged velocity, we use the notation $\frac{\mathrm{d}^{\mathrm{m}}}{\mathrm{d}t}$ or $\frac{\mathrm{d}^{\mathrm{v}}}{\mathrm{d}t}$ respectively.

Definition 2.7 (Diffusion velocity, diffusive fluxes)**.** *Let $\boldsymbol{v}$ is an averaged velocity field associated with the current configuration of the mixture. The vector*

$$\boldsymbol{u}_i \stackrel{\mathrm{def}}{=} \boldsymbol{v}_i - \boldsymbol{v} \tag{2.17a}$$

is called the diffusion velocity *of the i-th component relative to $\boldsymbol{v}$. With this definition of $\boldsymbol{u}_i$ we further introduce the quantities*

$$\boldsymbol{\jmath}_i \stackrel{\mathrm{def}}{=} \varrho_i \boldsymbol{u}_i, \qquad\qquad \widetilde{\boldsymbol{\jmath}}_i \stackrel{\mathrm{def}}{=} \phi_i \boldsymbol{u}_i, \tag{2.17b}$$

that are referred to as the diffusive mass flux *and the* diffusive volume flux *of the i-th component respectively. The* total diffusive mass flux *and the* total diffusive volume flux *are then obtained as*

$$\boldsymbol{J} \stackrel{\mathrm{def}}{=} \sum_{i=1}^{N} \boldsymbol{\jmath}_i, \qquad\qquad \widetilde{\boldsymbol{J}} \stackrel{\mathrm{def}}{=} \sum_{i=1}^{N} \widetilde{\boldsymbol{\jmath}}_i. \tag{2.17c}$$

[6]The mass-averaged velocity is also known as *barycentric velocity*.

The quantities introduced in the above Definition 2.7 naturally depend on the choice of the averaged velocity. If we need to emphasize which averaged velocity is being used, we will equip these quantities with the corresponding superscript according to Definition 2.5. This notation is summarized in Table 2.1 at the end of the current section.

Taking into account (2.2) we observe that the fluxes in (2.17b) are related through simple formula

$$\widetilde{\boldsymbol{\jmath}}_i = \hat{\gamma}_i \boldsymbol{\jmath}_i. \tag{2.18}$$

Moreover, from the above definitions it follows that

$$\boldsymbol{J} = \sum_{i=1}^{N} \varrho_i \boldsymbol{u}_i = \sum_{i=1}^{N} \varrho_i \left(\boldsymbol{v}_i - \boldsymbol{v}\right) = \varrho \boldsymbol{v}^{\mathrm{m}} - \varrho \boldsymbol{v}, \tag{2.19a}$$

$$\widetilde{\boldsymbol{J}} = \sum_{i=1}^{N} \phi_i \boldsymbol{u}_i = \sum_{i=1}^{N} \phi_i \left(\boldsymbol{v}_i - \boldsymbol{v}\right) = \boldsymbol{v}^{\mathrm{v}} - \boldsymbol{v}, \tag{2.19b}$$

where we have used (2.6) in the last equality in (2.19a), and (2.8) in the last equality in (2.19b). We immediately see that

$$\boldsymbol{J}^{\mathrm{m}} = \sum_{i=1}^{N} \boldsymbol{\jmath}_i^{\mathrm{m}} = \boldsymbol{0}, \qquad\qquad \widetilde{\boldsymbol{J}}^{\mathrm{v}} = \sum_{i=1}^{N} \widetilde{\boldsymbol{\jmath}}_i^{\mathrm{v}} = \boldsymbol{0}, \tag{2.20}$$

while the remaining pair of total diffusive fluxes is given by

$$\boldsymbol{J}^{\mathrm{v}} = \varrho \left(\boldsymbol{v}^{\mathrm{m}} - \boldsymbol{v}^{\mathrm{v}}\right), \qquad\qquad \widetilde{\boldsymbol{J}}^{\mathrm{m}} = \boldsymbol{v}^{\mathrm{v}} - \boldsymbol{v}^{\mathrm{m}}. \tag{2.21}$$

Based on these relations we will demonstrate in the following paragraph that the difference of the averaged velocities introduced in Definition 2.5 is not identically zero in a general case.

In later discussions we will need the following expressions for $\widetilde{\boldsymbol{J}}^{\mathrm{m}}$ and $\boldsymbol{J}^{\mathrm{v}}$ in terms of $(N-1)$ diffusive volume fluxes. First, from the sequence of identities $\widetilde{\boldsymbol{J}}^{\mathrm{m}} = \widetilde{\boldsymbol{J}}^{\mathrm{m}} - \frac{1}{\hat{\varrho}_N}\boldsymbol{J}^{\mathrm{m}} = \sum_{i=1}^{N} \widetilde{\boldsymbol{\jmath}}_i^{\mathrm{m}} - \frac{1}{\hat{\varrho}_N}\sum_{i=1}^{N} \hat{\varrho}_i \widetilde{\boldsymbol{\jmath}}_i^{\mathrm{m}} = \sum_{i=1}^{N-1} \left(1 - \frac{\hat{\varrho}_i}{\hat{\varrho}_N}\right) \widetilde{\boldsymbol{\jmath}}_i^{\mathrm{m}}$ we observe that

$$\widetilde{\boldsymbol{J}}^{\mathrm{m}} = \sum_{i=1}^{N-1} \hat{r}_i \widetilde{\boldsymbol{\jmath}}_i^{\mathrm{m}}, \tag{2.22}$$

where we have introduced the shorthand notation

$$\hat{r}_i \overset{\mathrm{def}}{=} 1 - \frac{\hat{\varrho}_i}{\hat{\varrho}_N}, \quad i = 1, \ldots, N-1. \tag{2.23}$$

Second, from $\boldsymbol{J}^{\mathrm{v}} = \boldsymbol{J}^{\mathrm{v}} - \hat{\varrho}_N \widetilde{\boldsymbol{J}}^{\mathrm{v}} = \sum_{i=1}^{N} \hat{\varrho}_i \widetilde{\boldsymbol{\jmath}}_i^{\mathrm{v}} - \sum_{i=1}^{N} \hat{\varrho}_N \widetilde{\boldsymbol{\jmath}}_i^{\mathrm{v}}$ we obtain

$$\boldsymbol{J}^{\mathrm{v}} = \sum_{i=1}^{N-1} \left(\hat{\varrho}_i - \hat{\varrho}_N\right) \widetilde{\boldsymbol{\jmath}}_i^{\mathrm{v}}. \tag{2.24}$$

Both fluxes $\widetilde{\boldsymbol{J}}^{\mathrm{m}}$ and $\boldsymbol{J}^{\mathrm{v}}$ are therefore identically zero in the special case with matching material densities, but otherwise can attain non-zero values.

Table 2.1: Notation for diffusion related quantities with emphasized choice of the averaged velocity field, see Definitions 2.5 and 2.7.

$\boldsymbol{u}_i^{\mathrm{m}}$	diffusion velocity relative to **mass-averaged** velocity $\boldsymbol{v}^{\mathrm{m}}$
$\boldsymbol{u}_i^{\mathrm{v}}$	diffusion velocity relative to **volume-averaged** velocity $\boldsymbol{v}^{\mathrm{v}}$
$\boldsymbol{\jmath}_i^{\mathrm{m}}$	density weighted diffusion velocity relative to $\boldsymbol{v}^{\mathrm{m}}$
$\boldsymbol{\jmath}_i^{\mathrm{v}}$	density weighted diffusion velocity relative to $\boldsymbol{v}^{\mathrm{v}}$
$\boldsymbol{J}^{\mathrm{m}}$	sum of density weighted diffusion velocities relative to $\boldsymbol{v}^{\mathrm{m}}$
$\boldsymbol{J}^{\mathrm{v}}$	sum of density weighted diffusion velocities relative to $\boldsymbol{v}^{\mathrm{v}}$
$\widetilde{\boldsymbol{\jmath}}_i^{\mathrm{m}}$	volume fraction weighted diffusion velocity relative to $\boldsymbol{v}^{\mathrm{m}}$
$\widetilde{\boldsymbol{\jmath}}_i^{\mathrm{v}}$	volume fraction weighted diffusion velocity relative to $\boldsymbol{v}^{\mathrm{v}}$
$\widetilde{\boldsymbol{J}}^{\mathrm{m}}$	sum of volume fraction weighted diffusion velocities relative to $\boldsymbol{v}^{\mathrm{m}}$
$\widetilde{\boldsymbol{J}}^{\mathrm{v}}$	sum of volume fraction weighted diffusion velocities relative to $\boldsymbol{v}^{\mathrm{v}}$

2.3 Balance equations

Based on the assumption of co-occupancy we have observed that the motion of the mixture results from the motion of its individual components, see (2.11). By virtue of such an observation, we formulate balance equations for individual components, taking into account terms describing their mutual interaction, and we accept them as basic postulates.

The detailed description of the mixture on the level of individual components is however not required in many practical applications. In such a case, the mixture can be treated as a single homogenized continuous medium for which we formulate the governing equations in terms of averaged quantities[7]. The fact that we are dealing with the mixture is then captured by supplementary evolution equations for quantities describing the actual composition of the mixture, typically mass or volume fractions. The equivalence of the two approaches in a specific case of chemically non-reacting binary mixtures is discussed for example in Souček et al. (2014).

Depending on the level of description, it is possible to distinguish between several classes of mixture models; see for example the classification introduced in Hutter and Jöhnk (2004), where it is also possible to find the comprehensive exposition concerning balance equations and their general formulations. We formulate the equations in their local forms in the current configuration, and we directly employ several simplifying assumptions with regard to practical applications of our interest. (For example, we do not allow for mass exchange between the components, and each component is considered to form a non-polar continuum.) As already mentioned, diffuse interface models are based on the componentwise formulation of the balance of mass, while the balances for linear and angular

[7]According to the commonly accepted principle, see Truesdell (1984), the motion of the mixture is assumed to be governed by the same equations as is a single body. Such postulate, however, a priori determines the structure of primitive quantities associated with the mixture as a whole.

momentum, energy and entropy are considered for the mixture as a whole[8].

A certain type of *model reduction* must be applied in order to obtain the balance equations for the mixture as a whole from their counterparts postulated on the level of individual components. The reduction is based on the reformulation of these postulates in terms of the averaged velocity $\boldsymbol{v}$ and related diffusive fluxes $\boldsymbol{\jmath}_i$ or $\widetilde{\boldsymbol{\jmath}}_i$, see Definition 2.7. These "artificially" introduced fluxes are then included among the unknown fields for which we will need to derive appropriate constitutive relations, see Chapter 3. Tables 2.2–2.3 provide an overview of the balance equations in their general forms reflecting the choice of the averaged velocity according to Definition 2.5.

2.3.1 Balance of mass

Let us consider a mixture of chemically non-reacting components, which means that no transfer of mass between the components is allowed. Local form of the balance of mass for individual components reads

$$\frac{\partial \varrho_i}{\partial t} + \operatorname{div}(\varrho_i \boldsymbol{v}_i) = 0, \quad i = 1, \dots, N. \tag{2.25}$$

The quantity $\varrho_i \boldsymbol{v}_i$ represents the mass flux of the i-th component in the mixture.

Let $\boldsymbol{v}$ is an averaged velocity field as in Definition 2.7. We split the mass flux in two parts following the identity

$$\varrho_i \boldsymbol{v}_i = \varrho_i \boldsymbol{v} + \varrho_i(\boldsymbol{v}_i - \boldsymbol{v}), \tag{2.26}$$

where the first term on the right hand side can be interpreted as the advective mass flux of the i-th component (with respect to the mixture), while the second term coincides with $\boldsymbol{\jmath}_i$ introduced in (2.17b). Using the decomposition (2.26) we can now rewrite the equations in (2.25) to take the form

$$\frac{\partial \varrho_i}{\partial t} + \operatorname{div}(\varrho_i \boldsymbol{v}) = -\operatorname{div} \boldsymbol{\jmath}_i, \quad i = 1, \dots, N, \tag{2.27a}$$

or equivalently[9]

$$\frac{\mathrm{d}\varrho_i}{\mathrm{d}t} + \varrho_i \operatorname{div} \boldsymbol{v} = -\operatorname{div} \boldsymbol{\jmath}_i, \quad i = 1, \dots, N. \tag{2.27b}$$

In the previous paragraph we have just made the transition from the description of the mass balance in terms of ϱ_i and $\boldsymbol{v}_i$ towards the equivalent description in terms of ϱ_i, $\boldsymbol{v}$ and $\boldsymbol{\jmath}_i$. The latter description brings us to the reduced model in which each $\boldsymbol{\jmath}_i$ is treated as an unknown flux that needs to be specified by a constitutive relation. This is a natural consequence of the trade-off of N partial velocities for a single velocity field.

Equations in (2.27) describe the evolution of partial densities which uniquely determine composition of the mixture in a given point of current configuration.

[8] According to Hutter and Jöhnk (2004), such models are classified as *class I* mixture models.

[9] See Remark 2.6 for the exact meaning of the symbol $\frac{\mathrm{d}}{\mathrm{d}t}$.

In the context of diffuse interface models we usually work with a set of so-called *order parameters* (phase-field variables) that characterize the underlying physical system exactly in the above sense. The set of partial densities therefore becomes a natural candidate to take the role of order parameters. In principle, we can work with an arbitrary set of variables provided that we can relate them to partial densities. We will discuss other possible choices at the end of the current section.

In the next step we will replace one of the equations in (2.27b) with an alternative equation the form of which depends on whether we are dealing with compressible or incompressible multi-component systems.

Lemma 2.8 (Balance of mass for compressible mixtures)**.** *Let Assumption 1 holds. Then the system of equations*

$$\frac{\mathrm{d}\varrho_i}{\mathrm{d}t} + \varrho_i \operatorname{div} \boldsymbol{v} = -\operatorname{div} \boldsymbol{\jmath}_i, \quad i = 1, \dots, N-1, \tag{2.28a}$$

$$\frac{\mathrm{d}\varrho}{\mathrm{d}t} + \varrho \operatorname{div} \boldsymbol{v} = -\operatorname{div} \boldsymbol{J}, \tag{2.28b}$$

is equivalent to (2.27b).

Proof. By summing up N equations of (2.27b), one obtains the balance of mass for the mixture as a whole in the form (2.28b), see (2.6) and (2.17c). This equation then can be used to replace an arbitrary equation in (2.27b). □

Lemma 2.9 (Balance of mass for incompressible mixtures)**.** *Let Assumptions 1–3 hold. Then the system of equations*

$$\frac{\mathrm{d}\varrho_i}{\mathrm{d}t} + \varrho_i \operatorname{div} \boldsymbol{v} = -\operatorname{div} \boldsymbol{\jmath}_i, \quad i = 1, \dots, N-1, \tag{2.29a}$$

$$\operatorname{div} \boldsymbol{v} = -\operatorname{div} \widetilde{\boldsymbol{J}}, \tag{2.29b}$$

is equivalent to (2.27b).

Proof. We first show that constraint (2.29b) can be obtained from N equations of (2.27b). Using $\varrho_i = \hat{\varrho}_i \phi_i$ and $\boldsymbol{\jmath}_i = \hat{\varrho}_i \widetilde{\boldsymbol{\jmath}}_i$ in (2.27b), we get

$$\hat{\varrho}_i \frac{\mathrm{d}\phi_i}{\mathrm{d}t} + \phi_i \left(\frac{\mathrm{d}\hat{\varrho}_i}{\mathrm{d}t} + \hat{\varrho}_i \operatorname{div} \boldsymbol{v} \right) = -\operatorname{div} (\hat{\varrho}_i \widetilde{\boldsymbol{\jmath}}_i), \quad i = 1, \dots, N. \tag{2.30}$$

Since the material densities are assumed to be positive constants, their material derivatives vanish and we can divide the i-th equation by $\hat{\varrho}_i$. By summing up the resulting equations, applying the constraint (2.8) and using the notation introduced in Definition 2.7, we get the equation (2.29b).

Next, following Lemma 2.2 we know that the total density ϱ is given by

$$\varrho = \sum_{i=1}^{N-1} \left(1 - \frac{\hat{\varrho}_N}{\hat{\varrho}_i} \right) \varrho_i + \hat{\varrho}_N. \tag{2.31}$$

(This expression is obtained by using $\phi_i = \varrho_i/\hat{\varrho}_i$ in (2.10a).) Now, if $\varrho_1, \dots, \varrho_{N-1}$ solve (2.29a) and $\boldsymbol{v}$ fulfills the constraint (2.29b), we can show that ϱ satisfies the mass balance equation (2.28b). Indeed, we have

$$\begin{aligned}\frac{\mathrm{d}\varrho}{\mathrm{d}t} + \varrho \operatorname{div} \boldsymbol{v} &= \sum_{i=1}^{N-1} \left(1 - \frac{\hat{\varrho}_N}{\hat{\varrho}_i}\right) \left(\frac{\mathrm{d}\varrho_i}{\mathrm{d}t} + \varrho_i \operatorname{div} \boldsymbol{v}\right) + \hat{\varrho}_N \operatorname{div} \boldsymbol{v} \\ &= -\sum_{i=1}^{N-1} \left(1 - \frac{\hat{\varrho}_N}{\hat{\varrho}_i}\right) \operatorname{div} \boldsymbol{\jmath}_i + \hat{\varrho}_N \operatorname{div} \boldsymbol{v} = -\operatorname{div} \boldsymbol{J} + \hat{\varrho}_N \operatorname{div} \left(\boldsymbol{v} + \widetilde{\boldsymbol{J}}\right),\end{aligned}$$

and the last term vanishes in virtue of (2.29b). In this sense we have derived (2.28) from (2.29) and we already know that (2.28) is equivalent to (2.27b). □

Equations in (2.28) describe the evolution of $\varrho_1, \dots, \varrho_{N-1}$ and ϱ respectively. Once these quantities are known, the density ϱ_N can be recovered from (2.6). In this sense we still have the complete information about the actual composition of the mixture. On the other hand, the density ϱ for incompressible mixtures is given by (2.31) and it is not treated as an independent variable anymore. The complete characterization of the underlying system is in this case given by only $(N-1)$ partial densities that are required to satisfy the same equations as in the compressible case. However, there is one subtle difference. The velocity field in (2.29a) must obey the relation in (2.29b) which can be seen, by analogy with the theory of single continuum, as the constraint related to incompressibility[10] of the mixture as a whole.

It remains to discuss consequences associated with the choice of the averaged velocity field. Following the discussion at the end of Section 2.2, see (2.19)–(2.24), we know that $\boldsymbol{J}^{\mathrm{m}} = \widetilde{\boldsymbol{J}}^{\mathrm{v}} = \boldsymbol{0}$, but $\boldsymbol{J}^{\mathrm{v}}$ and $\widetilde{\boldsymbol{J}}^{\mathrm{m}}$ can generally attain non-zero values. Therefore, we observe that the total mass balance (2.28b) reduces to the classical form with zero right hand side if $\boldsymbol{v} = \boldsymbol{v}^{\mathrm{m}}$, but some diffusive mass flow appears on the right hand side if $\boldsymbol{v} = \boldsymbol{v}^{\mathrm{v}}$. At the same time, we see that the volume-averaged velocity field satisfies the classical incompressibility constraint

$$\operatorname{div} \boldsymbol{v}^{\mathrm{v}} = 0, \tag{2.32a}$$

while the mass-averaged velocity field is generally non-solenoidal as it obeys the relation

$$\operatorname{div} \boldsymbol{v}^{\mathrm{m}} = -\operatorname{div} \widetilde{\boldsymbol{J}}^{\mathrm{m}}. \tag{2.32b}$$

From this point of view, the mixture as a whole can be partly compressible even though its components are incompressible. This brings us to the concept of *quasi-incompressibility* as it was used by Lowengrub and Truskinovsky (1998).

Now we are ready to explain the origin of the classification introduced in the bottom part of Figure 1.7. When dealing with compressible mixtures we shall

[10] A single continuous body is considered to be incompressible if it obeys the constraint $\operatorname{div} \boldsymbol{v} = 0$. (So it can undergo only isochoric motions.) See, for example, Gurtin et al. (2010) for the detailed discussion of the concept of incompressibility.

work exclusively with the mass-averaged velocity and we shall talk about FC description. In case of incompressible mixtures we shall distinguish between QI and FI descriptions. The first one is obtained with non-solenoidal velocity $\boldsymbol{v}^{\mathrm{m}}$, the other one is obtained with solenoidal velocity $\boldsymbol{v}^{\mathrm{v}}$.

Table 2.2 provides an overview of the specific form of the mass balance equations with respect to two different definitions of the averaged velocity and three specific choices of order parameters (partial densities, mass fractions and volume fractions).

On the choice of order parameters

In the remainder of this section we want to restate (2.28a), and hence also (2.29a), in terms of general order parameters. As we have already mentioned, in order to do so, we need to supply a relation between the order parameters and partial densities.

Let $\boldsymbol{\varphi} = [\varphi_1, \dots, \varphi_{N-1}]^\top$ is a vector of $(N-1)$ order parameters. Suppose that $\varrho_1, \dots, \varrho_{N-1}$ are given functions of $\boldsymbol{\varphi}$ and possibly ϱ, that is $\varrho_i = \varrho_i(\boldsymbol{\varphi}, \varrho)$ for $i = 1, \dots, N-1$. Then, using the chain rule, it can be shown that (2.28a) is in fact equivalent to

$$\sum_{j=1}^{N-1} \frac{\partial \varrho_i}{\partial \varphi_j} \frac{\mathrm{d}\varphi_j}{\mathrm{d}t} + \left(\varrho_i - \varrho \frac{\partial \varrho_i}{\partial \varrho} \right) \operatorname{div} \boldsymbol{v} = -\operatorname{div} \boldsymbol{\jmath}_i + \frac{\partial \varrho_i}{\partial \varrho} \operatorname{div} \boldsymbol{J}, \ i = 1, \dots, N-1. \tag{2.33}$$

Let us briefly discuss several specific sets of order parameters:

- *Partial densities as order parameters.* Let $\varphi_i = \varrho_i$ for $i = 1, \dots, N-1$. Then $\varphi_i \in [0, \hat{\varrho}_i]$ and we have the simple relation $\varrho_i(\boldsymbol{\varphi}, \varrho) = \varphi_i$ which implies

  $$\frac{\partial \varrho_i}{\partial \varphi_j} = \delta_{ij}, \qquad \frac{\partial \varrho_i}{\partial \varrho} = 0,$$

  where δ_{ij} denotes the Kronecker delta. Not surprisingly, in this trivial case the equations in (2.33) take their original forms given by (2.28a).

- *Mass fractions as order parameters.* Let $\varphi_i = c_i$ for $i = 1, \dots, N-1$. Then $\varphi_i \in [0, 1]$ and in virtue of (2.2) we have $\varrho_i(\boldsymbol{\varphi}, \varrho) = \varrho\varphi_i$. The last relation yields

  $$\frac{\partial \varrho_i}{\partial \varphi_j} = \varrho\delta_{ij}, \qquad \frac{\partial \varrho_i}{\partial \varrho} = \varphi_i.$$

- *Volume fractions as order parameters.* Let $\varphi_i = \phi_i$ for $i = 1, \dots, N-1$. Then $\varphi_i \in [0, 1]$ and in virtue of (2.2) we have $\varrho_i(\boldsymbol{\varphi}, \varrho) = \hat{\varrho}_i\varphi_i$. The last relation yields

  $$\frac{\partial \varrho_i}{\partial \varphi_j} = \hat{\varrho}_i\delta_{ij}, \qquad \frac{\partial \varrho_i}{\partial \varrho} = 0.$$

- *Differences of volume fractions as order parameters.* Let $\varphi_i = \phi_i - \phi_N$ for $i = 1, \dots, N-1$ and let $\sum_{i=1}^{N} \phi_i = 1$ holds. Then $\varphi_i \in [-1, 1]$ and we have $\varrho_i(\boldsymbol{\varphi}, \varrho) = \hat{\varrho}_i \left(\varphi_i - \frac{1}{N} \sum_{j=1}^{N-1} \varphi_j + \frac{1}{N} \right)$. The last relation yields

$$\frac{\partial \varrho_i}{\partial \varphi_j} = \hat{\varrho}_i \left(\delta_{ij} - \frac{1}{N} \right), \qquad \frac{\partial \varrho_i}{\partial \varrho} = 0.$$

  Compared to previous choices, the equations in (2.33) are strongly coupled in this case.

Remark 2.10. Other admissible sets of order parameters for incompressible mixtures are discussed for example in Dong (2015). Note that the author formulates the mass balance equations (2.29) in different variables, namely $\bar{\varrho}_i = \varrho_i - \varrho_N$. Straightforward use of volume fractions as order parameters then leads to the coupled system of equations, unlike to our formulation.

2.3.2 Balance of linear momentum

Local form of the balance of linear momentum for individual components of a chemically non-reacting mixture is postulated as

$$\frac{\partial(\varrho_i \boldsymbol{v}_i)}{\partial t} + \operatorname{div}(\varrho_i \boldsymbol{v}_i \otimes \boldsymbol{v}_i) = \operatorname{div} \mathbb{T}_i + \varrho_i \boldsymbol{b}_i + \mathbf{l}_i, \quad i = 1, \dots, N, \tag{2.34}$$

where $\mathbb{T}_i$ denotes the Cauchy stress tensor, $\boldsymbol{b}_i$ is the specific external body force, and $\mathbf{l}_i$ is the internal body force due to the local interaction between the i-th component and other components[11]. We assume that no excess momentum in the mixture is produced by the interaction forces $\mathbf{l}_i$, which means that

$$\sum_{i=1}^{N} \mathbf{l}_i = \mathbf{0}. \tag{2.35}$$

Using definitions (2.17a) and (2.17b), the products on the left hand side of (2.34) can be rewritten as

$$\varrho_i \boldsymbol{v}_i = \varrho_i \boldsymbol{v} + \boldsymbol{\jmath}_i, \tag{2.36a}$$

$$\varrho_i \boldsymbol{v}_i \otimes \boldsymbol{v}_i = \varrho_i \boldsymbol{v} \otimes \boldsymbol{v} + \varrho_i \boldsymbol{u}_i \otimes \boldsymbol{u}_i + \boldsymbol{\jmath}_i \otimes \boldsymbol{v} + \boldsymbol{v} \otimes \boldsymbol{\jmath}_i. \tag{2.36b}$$

Substitution of these identities into (2.34) yields

$$\begin{aligned} \frac{\partial(\varrho_i \boldsymbol{v})}{\partial t} + \operatorname{div}(\varrho_i \boldsymbol{v} \otimes \boldsymbol{v}) = \operatorname{div}(\mathbb{T}_i - \varrho_i \boldsymbol{u}_i \otimes \boldsymbol{u}_i) + \varrho_i \boldsymbol{b}_i \\ + \mathbf{l}_i - \operatorname{div}(\boldsymbol{\jmath}_i \otimes \boldsymbol{v}) - \operatorname{div}(\boldsymbol{v} \otimes \boldsymbol{\jmath}_i) - \frac{\partial \boldsymbol{\jmath}_i}{\partial t}, \quad i = 1, \dots, N. \end{aligned} \tag{2.37}$$

[11] The internal body force $\mathbf{l}_i$ is also called the *interaction force* or the *momentum production*.

If we differentiate the products on the left hand side of (2.37) and if we make use of the mass balance (2.27a), we end up with the following form of (2.34), namely

$$\varrho_i \frac{\mathrm{d}\boldsymbol{v}}{\mathrm{d}t} = \operatorname{div}\left(\mathbb{T}_i - \varrho_i \boldsymbol{u}_i \otimes \boldsymbol{u}_i\right) + \varrho_i \boldsymbol{b}_i + \boldsymbol{\mathfrak{l}}_i - \left[(\operatorname{div}\boldsymbol{v})\,\mathbb{I} + \nabla \boldsymbol{v}\right]\boldsymbol{\jmath}_i - \frac{\mathrm{d}\boldsymbol{\jmath}_i}{\mathrm{d}t}, \quad i = 1, \ldots, N. \tag{2.38}$$

Now we are ready to formulate balance of linear momentum for the mixture as a whole. Summing up N equations in (2.38) with the use of (2.6), we get the equation

$$\varrho \frac{\mathrm{d}\boldsymbol{v}}{\mathrm{d}t} = \operatorname{div}\mathbb{T} + \varrho \boldsymbol{b} - \left[(\operatorname{div}\boldsymbol{v})\,\mathbb{I} + \nabla \boldsymbol{v}\right]\boldsymbol{J} - \frac{\mathrm{d}\boldsymbol{J}}{\mathrm{d}t}, \tag{2.39}$$

where we have introduced the averaged specific external body force, $\boldsymbol{b} \overset{\text{def}}{=} \sum_{i=1}^{N} c_i \boldsymbol{b}_i$, and the averaged stress tensor

$$\mathbb{T} \overset{\text{def}}{=} \mathbb{T}_{\mathrm{I}} - \sum_{i=1}^{N} \varrho_i \boldsymbol{u}_i \otimes \boldsymbol{u}_i, \qquad \mathbb{T}_{\mathrm{I}} \overset{\text{def}}{=} \sum_{i=1}^{N} \mathbb{T}_i. \tag{2.40}$$

Note that the definition of $\mathbb{T}$ includes diffusion velocities which depend on the choice of the averaged velocity, see Definition 2.7. Therefore, we will distinguish between $\mathbb{T}^{\mathrm{m}}$ and $\mathbb{T}^{\mathrm{v}}$ whenever needed.

Balance of linear momentum with mass-averaged velocity

The mass-averaged velocity field is usually privileged regarding the two facts. First, the total linear momentum is defined as the sum of partial moments $\varrho_i \boldsymbol{v}_i$ which corresponds to $\varrho \boldsymbol{v}^{\mathrm{m}}$. Second, equation (2.39) with $\boldsymbol{v} = \boldsymbol{v}^{\mathrm{m}}$ reduces to standard form

$$\varrho \frac{\mathrm{d}^{\mathrm{m}}\boldsymbol{v}^{\mathrm{m}}}{\mathrm{d}t} = \operatorname{div}\mathbb{T}^{\mathrm{m}} + \varrho \boldsymbol{b}, \tag{2.41}$$

which coincides with the balance of linear momentum for a single continuum.

Balance of linear momentum with volume-averaged velocity

Let Assumptions 1–3 hold and let $\boldsymbol{v} = \boldsymbol{v}^{\mathrm{v}}$. Then (2.39) becomes

$$\varrho \frac{\mathrm{d}^{\mathrm{v}}\boldsymbol{v}^{\mathrm{v}}}{\mathrm{d}t} + \left[\nabla \boldsymbol{v}^{\mathrm{v}}\right]\boldsymbol{J}^{\mathrm{v}} = \operatorname{div}\mathbb{T}^{\mathrm{v}} + \varrho \boldsymbol{b} - \frac{\mathrm{d}^{\mathrm{v}}\boldsymbol{J}^{\mathrm{v}}}{\mathrm{d}t}. \tag{2.42}$$

With the use of the total mass balance, see Table 2.2, the above equation can be manipulated to take the form

$$\frac{\partial(\varrho \boldsymbol{v}^{\mathrm{v}})}{\partial t} + \operatorname{div}\left(\boldsymbol{v}^{\mathrm{v}} \otimes (\varrho \boldsymbol{v}^{\mathrm{v}} + \boldsymbol{J}^{\mathrm{v}})\right) = \operatorname{div}\mathbb{T}^{\mathrm{v}} + \varrho \boldsymbol{b} - \frac{\mathrm{d}^{\mathrm{v}}\boldsymbol{J}^{\mathrm{v}}}{\mathrm{d}t}. \tag{2.43}$$

According to (2.21), we see that $\varrho \boldsymbol{v}^{\mathrm{v}} + \boldsymbol{J}^{\mathrm{v}}$ coincides with $\varrho \boldsymbol{v}^{\mathrm{m}}$. The left hand side of the previous equation thus corresponds to the time change of the quantity $\varrho \boldsymbol{v}^{\mathrm{v}}$

contained in a control volume (associated with the mixture) that is advected with velocity $\boldsymbol{v}^{\mathrm{m}}$. Upon rearranging the terms in (2.43), we can rewrite this equation in the form of the balance of $\varrho\boldsymbol{v}^{\mathrm{v}}$ with respect to $\boldsymbol{v}^{\mathrm{v}}$, namely

$$\frac{\partial(\varrho\boldsymbol{v}^{\mathrm{v}})}{\partial t} + \operatorname{div}(\varrho\boldsymbol{v}^{\mathrm{v}} \otimes \boldsymbol{v}^{\mathrm{v}}) = \operatorname{div}(\mathbb{T}^{\mathrm{v}} - \boldsymbol{v}^{\mathrm{v}} \otimes \boldsymbol{J}^{\mathrm{v}}) + \varrho\boldsymbol{b} - \frac{\mathrm{d}^{\mathrm{v}}\boldsymbol{J}^{\mathrm{v}}}{\mathrm{d}t}. \tag{2.44}$$

Remark 2.11. Note that Abels et al. (2012) in their derivation[12] of the diffuse interface model for incompressible two-phase flows assume that the inertia due to the motion of the fluid relative to the gross motion is negligible. In other words, they neglect the last term on the right hand side of (2.44).

2.3.3 Balance of angular momentum

Supposing that each component of the chemically non-reacting mixture can be treated as a non-polar continuum, local form of the balance of angular momentum for individual components reads[13]

$$\begin{aligned}\frac{\partial(\boldsymbol{x} \times \varrho_i\boldsymbol{v}_i)}{\partial t} + \operatorname{div}((\boldsymbol{x} \times \varrho_i\boldsymbol{v}_i) \otimes \boldsymbol{v}_i) \\ = \operatorname{div}(\boldsymbol{x} \times \mathbb{T}_i) + \boldsymbol{x} \times \varrho_i\boldsymbol{b}_i + \boldsymbol{x} \times \mathfrak{l}_i + \mathfrak{a}_i, \quad i = 1, \dots, N,\end{aligned} \tag{2.45}$$

where $\mathfrak{a}_i$ plays the same role as $\mathfrak{l}_i$ in (2.34). The angular momentum production caused by the local interaction of the i-th component with the other components is composed of the moment of the momentum production $\boldsymbol{x} \times \mathfrak{l}_i$ and the spin production[14] $\mathfrak{a}_i$. Just as (2.35) represents the fact that no excess linear momentum in the mixture is produced by the interaction forces, the production terms $\mathfrak{a}_i$ are subjected to similar condition, namely

$$\sum_{i=1}^{N} \mathfrak{a}_i = \boldsymbol{0}. \tag{2.46}$$

It can be shown, see Bowen (1976), that under this condition the sum of the partial stresses becomes a symmetric tensor even though $\mathbb{T}_i$ alone does not have to meet this requirement. Recalling the introduced notation for the averaged stress tensor (2.40), we have

$$\mathbb{T}_{\mathrm{I}} = \mathbb{T}_{\mathrm{I}}^{\top} \tag{2.47}$$

and it is clear that $\mathbb{T}$ is also symmetric regardless the choice of the averaged velocity field (because $\varrho_i\boldsymbol{u}_i \otimes \boldsymbol{u}_i$ is always symmetric).

[12] Abels et al. (2012) use the notation $\mathbf{T} \equiv \mathbb{T}^{\mathrm{v}}$ and $\tilde{\mathbf{T}} \equiv \mathbb{T}^{\mathrm{v}} - \boldsymbol{v}^{\mathrm{v}} \otimes \boldsymbol{J}^{\mathrm{v}}$.

[13] The quantity $\boldsymbol{x} \times \mathbb{T}_i$ is a linear transformation that assigns to each vector $\boldsymbol{u}$ the vector $\boldsymbol{x} \times (\mathbb{T}_i\boldsymbol{u})$.

[14] Here we use the terminology that was used also by Hutter and Jöhnk (2004). Other commonly used terms for the vector quantity $\mathfrak{a}_i$ are the *moment of momentum supply* or the *angular momentum supply*, see for example Bowen (1976) and Rajagopal and Tao (1995).

We conclude this section by accepting the condition for symmetry of the averaged stress tensor, that is

$$\mathbb{T} = \mathbb{T}^\top, \tag{2.48}$$

as the equivalent formulation of the balance of angular momentum for the mixture as a whole.

2.3.4 Balance of energy

Local form of the balance of energy for individual components of the mixture reads

$$\frac{\partial(\varrho_i E_i)}{\partial t} + \operatorname{div}(\varrho_i E_i \boldsymbol{v}_i) = \operatorname{div}\left(\mathbb{T}_i^\top \boldsymbol{v}_i - \boldsymbol{q}_i\right) + \boldsymbol{v}_i \cdot (\varrho_i \boldsymbol{b}_i) + \varrho_i q_i + \mathfrak{e}_i, \quad i = 1, \dots, N, \tag{2.49}$$

where E_i represents the specific energy for the i-th component and can be further decomposed into the sum of internal and kinetic energy, that is

$$E_i \overset{\text{def}}{=} e_i + \frac{1}{2}\left|\boldsymbol{v}_i\right|^2, \tag{2.50}$$

$\boldsymbol{q}_i$ denotes the energy flux, q_i is the specific external energy supply (radiation), and finally $\mathfrak{e}_i$ corresponds to the energy production caused by the interaction of the i-th component with other components.

In what follows, we assume that all components share a single temperature field. Such an assumption is in accordance with the chosen level of description. It allows us to work with a single equation representing the balance of energy for the mixture as a whole in the final reduced model. In analogy to conditions (2.35) and (2.46), we require that interaction between the components does not contribute to the sum of internal and kinetic energy of the mixture, that is

$$\sum_{i=1}^{N} \mathfrak{e}_i = 0. \tag{2.51}$$

Balance of the total energy for the mixture as a whole will be obtained as the sum of equations in (2.49). Let $\boldsymbol{v}$ is an averaged velocity as in the previous sections. By use of the definition of the diffusion velocity (2.17a), it follows from (2.50) that

$$\sum_{i=1}^{N} \varrho_i E_i = \sum_{i=1}^{N} \varrho_i e_i + \frac{1}{2}\sum_{i=1}^{N} \varrho_i \left|\boldsymbol{u}_i\right|^2 + \frac{1}{2}\varrho\left|\boldsymbol{v}\right|^2 + \boldsymbol{v}\cdot\boldsymbol{J}. \tag{2.52}$$

(Note that the last term on the right hand side vanishes if $\boldsymbol{v}$ is chosen as the mass-averaged velocity, see (2.20).) The standard definition of the specific internal energy for the mixture as a whole reads

$$e \overset{\text{def}}{=} e_{\mathrm{I}} + \frac{1}{2}\sum_{i=1}^{N} c_i \left|\boldsymbol{u}_i\right|^2, \qquad e_{\mathrm{I}} \overset{\text{def}}{=} \sum_{i=1}^{N} c_i e_i. \tag{2.53}$$

When balancing the total energy for the mixture, we use the notation

$$E \stackrel{\text{def}}{=} e + \frac{1}{2}\left|\boldsymbol{v}\right|^2, \tag{2.54}$$

even though the total energy of the mixture is given by $\sum_{i=1}^{N} \varrho_i E_i = \varrho E + \boldsymbol{v}\cdot\boldsymbol{J}$, see (2.52). Another identities that will be useful in the forthcoming algebraic manipulations read

$$\sum_{i=1}^{N} \mathbb{T}_i^\top \boldsymbol{v} = \mathbb{T}^\top \boldsymbol{v} + \sum_{i=1}^{N} \varrho_i \left(\boldsymbol{u}_i \cdot \boldsymbol{v}\right) \boldsymbol{u}_i, \tag{2.55}$$

which can be obtained from (2.40), and

$$\sum_{i=1}^{N} \varrho_i E_i \boldsymbol{u}_i = \sum_{i=1}^{N} \varrho_i \left(e_i + \frac{1}{2}\left|\boldsymbol{u}_i\right|^2\right) \boldsymbol{u}_i + \frac{1}{2}\left|\boldsymbol{v}\right|^2 \boldsymbol{J} + \sum_{i=1}^{N} \varrho_i \left(\boldsymbol{u}_i \cdot \boldsymbol{v}\right) \boldsymbol{u}_i, \tag{2.56}$$

which follows from (2.50) and definitions in (2.17). Last but not least, we introduce the averaged energy flux by

$$\boldsymbol{q} \stackrel{\text{def}}{=} \boldsymbol{q}_{\mathrm{I}} + \frac{1}{2}\sum_{i=1}^{N} \varrho_i \left|\boldsymbol{u}_i\right|^2 \boldsymbol{u}_i, \qquad \boldsymbol{q}_{\mathrm{I}} \stackrel{\text{def}}{=} \sum_{i=1}^{N} \left(\boldsymbol{q}_i - \mathbb{T}_i^\top \boldsymbol{u}_i + \varrho_i e_i \boldsymbol{u}_i\right), \tag{2.57}$$

and the averaged specific external energy supply by $q \stackrel{\text{def}}{=} \sum_{i=1}^{N} c_i q_i$.

With the above definitions[15] and identities we are ready to add up the equations in (2.49). In the first approach we get

$$\begin{aligned}\frac{\partial(\varrho E)}{\partial t} + \operatorname{div}\left(\varrho E \boldsymbol{v}\right) + \frac{\partial(\boldsymbol{v}\cdot\boldsymbol{J})}{\partial t} + \operatorname{div}\left[(\boldsymbol{v}\cdot\boldsymbol{J})\boldsymbol{v}\right] + \operatorname{div}\left(\frac{1}{2}\left|\boldsymbol{v}\right|^2 \boldsymbol{J}\right) \\ = \operatorname{div}\left(\mathbb{T}^\top \boldsymbol{v} - \boldsymbol{q}\right) + \sum_{i=1}^{N} \boldsymbol{\jmath}_i \cdot \boldsymbol{b}_i + \varrho \boldsymbol{v}\cdot\boldsymbol{b} + \varrho q.\end{aligned} \tag{2.58}$$

which can be further manipulated into the form

$$\begin{aligned}\frac{\partial(\varrho E)}{\partial t} + \operatorname{div}\left(\varrho E \boldsymbol{v}\right) = \operatorname{div}\left(\mathbb{T}^\top \boldsymbol{v} - \frac{1}{2}\left|\boldsymbol{v}\right|^2 \boldsymbol{J} - \boldsymbol{q}\right) + \sum_{i=1}^{N} \boldsymbol{\jmath}_i \cdot \boldsymbol{b}_i + \varrho q \\ + \varrho \boldsymbol{v}\cdot\boldsymbol{b} - \left(\operatorname{div}\boldsymbol{v}\right)\boldsymbol{v}\cdot\boldsymbol{J} - \frac{\mathrm{d}(\boldsymbol{v}\cdot\boldsymbol{J})}{\mathrm{d}t}.\end{aligned} \tag{2.59}$$

As a next step, we derive the evolution equation for the internal energy e. First of all, note that $\operatorname{div}\left(\mathbb{T}^\top \boldsymbol{v}\right) = \mathbb{T} : \nabla\boldsymbol{v} + \boldsymbol{v}\cdot\operatorname{div}\mathbb{T}$. Following the discussion in Section 2.3.3, we know that $\mathbb{T}$ is symmetric. Therefore, one can replace $\nabla\boldsymbol{v}$ in the previous formula by its symmetric part $\mathbb{D} \stackrel{\text{def}}{=} \frac{1}{2}\left(\nabla\boldsymbol{v} + \nabla\boldsymbol{v}^\top\right)$. Similarly, we

[15] Note that $\boldsymbol{q}$, e and E depend on the particular choice of the averaged velocity. To emphasize which of the two velocities (2.16) is being used, we will mark those quantities in Table 2.3 by the corresponding superscript (following the notation introduced in Table 2.1).

manipulate the second term under the divergence on the right hand side of (2.59) by noting that $\operatorname{div}\left(\frac{1}{2}\left|\boldsymbol{v}\right|^2\boldsymbol{J}\right) = \frac{1}{2}\left|\boldsymbol{v}\right|^2\operatorname{div}\boldsymbol{J} + \boldsymbol{v}\cdot[\nabla\boldsymbol{v}]\boldsymbol{J}$. Straightforward application of decomposition (2.54) in equation (2.59), followed by the use of (2.28b), yields

$$\begin{aligned}\varrho\frac{\mathrm{d}e}{\mathrm{d}t} - e\operatorname{div}\boldsymbol{J} = \mathbb{T}:\mathbb{D} - \operatorname{div}\boldsymbol{q} + \sum_{i=1}^{N}\boldsymbol{\jmath}_i\cdot\boldsymbol{b}_i + \varrho q \\ - \boldsymbol{v}\cdot\left(\varrho\frac{\mathrm{d}\boldsymbol{v}}{\mathrm{d}t} - \operatorname{div}\mathbb{T} - \varrho\boldsymbol{b} + \left[(\operatorname{div}\boldsymbol{v})\,\mathbb{I} + \nabla\boldsymbol{v}\right]\boldsymbol{J} + \frac{\mathrm{d}\boldsymbol{J}}{\mathrm{d}t}\right) - \boldsymbol{J}\cdot\frac{\mathrm{d}\boldsymbol{v}}{\mathrm{d}t}. \quad (2.60)\end{aligned}$$

The terms inside round brackets vanish by virtue of the balance of linear momentum (2.39). The remaining step is to reuse the same equation also in the last term on the right hand side of (2.60). In doing so, we arrive at

$$\begin{aligned}\varrho\frac{\mathrm{d}e}{\mathrm{d}t} - e\operatorname{div}\boldsymbol{J} = \mathbb{T}:\left(\mathbb{D} + \nabla_{\mathrm{sym}}\left(\varrho^{-1}\boldsymbol{J}\right)\right) - \operatorname{div}\boldsymbol{q}_e \\ + \sum_{i=1}^{N}\boldsymbol{\jmath}_i\cdot(\boldsymbol{b}_i - \boldsymbol{b}) + \varrho q + \varrho^{-1}\boldsymbol{J}\cdot\left(\left[(\operatorname{div}\boldsymbol{v})\,\mathbb{I} + \nabla\boldsymbol{v}\right]\boldsymbol{J} + \frac{\mathrm{d}\boldsymbol{J}}{\mathrm{d}t}\right), \quad (2.61)\end{aligned}$$

where we have introduced the generalized energy flux

$$\boldsymbol{q}_e \overset{\mathrm{def}}{=} \boldsymbol{q} + \varrho^{-1}\mathbb{T}\boldsymbol{J}, \quad (2.62)$$

and $\nabla_{\mathrm{sym}}\left(\varrho^{-1}\boldsymbol{J}\right)$ denotes symmetric part of $\nabla(\varrho^{-1}\boldsymbol{J})$.

Remark 2.12. Note that the last product on the right hand side in (2.61) can be further manipulated to obtain

$$\begin{aligned}\varrho\frac{\mathrm{d}e}{\mathrm{d}t} - e\operatorname{div}\boldsymbol{J} = \left(\mathbb{T} + \varrho^{-1}\boldsymbol{J}\otimes\boldsymbol{J}\right):\left(\mathbb{D} + \nabla_{\mathrm{sym}}\left(\varrho^{-1}\boldsymbol{J}\right)\right) - \operatorname{div}\widetilde{\boldsymbol{q}}_e \\ + \sum_{i=1}^{N}\boldsymbol{\jmath}_i\cdot(\boldsymbol{b}_i - \boldsymbol{b}) + \varrho q + \frac{1}{2\varrho}\left|\boldsymbol{J}\right|^2\operatorname{div}\boldsymbol{v} + \frac{\mathrm{d}}{\mathrm{d}t}\left(\frac{1}{2\varrho}\left|\boldsymbol{J}\right|^2\right), \quad (2.63)\end{aligned}$$

with the generalized energy flux

$$\widetilde{\boldsymbol{q}}_e \overset{\mathrm{def}}{=} \boldsymbol{q} + \varrho^{-1}\mathbb{T}\boldsymbol{J} + \frac{1}{2\varrho^2}\left|\boldsymbol{J}\right|^2\boldsymbol{J}. \quad (2.64)$$

Very often, certain approximations are made in the formulation of the balance of energy for a mixture. Typically, one can neglect all terms that are second and higher order in diffusion velocities. In this sense we have $\mathbb{T}\equiv\mathbb{T}_{\mathrm{I}}$, $e\equiv e_{\mathrm{I}}$ and also $\boldsymbol{q}_e \equiv \boldsymbol{q}_{\mathrm{I}} + \varrho^{-1}\mathbb{T}_{\mathrm{I}}\boldsymbol{J}$. If we additionally neglect time and space derivatives of these terms, we end up with the equation which formally matches (2.61) without the last term on the right hand side, that is

$$\varrho\frac{\mathrm{d}e}{\mathrm{d}t} - e\operatorname{div}\boldsymbol{J} = \mathbb{T}:\left(\mathbb{D} + \nabla_{\mathrm{sym}}\left(\varrho^{-1}\boldsymbol{J}\right)\right) - \operatorname{div}\boldsymbol{q}_e + \sum_{i=1}^{N}\boldsymbol{\jmath}_i\cdot(\boldsymbol{b}_i - \boldsymbol{b}) + \varrho q. \quad (2.65)$$

Balance of energy with mass-averaged velocity

The equation for the balance of the sum of internal and kinetic energy (2.59) reduces to

$$\varrho \frac{\mathrm{d}^{\mathrm{m}} E^{\mathrm{m}}}{\mathrm{d}t} = \operatorname{div}\left(\mathbb{T}^{\mathrm{m}} \boldsymbol{v}^{\mathrm{m}} - \boldsymbol{q}^{\mathrm{m}}\right) + \varrho \boldsymbol{v}^{\mathrm{m}} \cdot \boldsymbol{b} + \sum_{i=1}^{N} \boldsymbol{\jmath}_i^{\mathrm{m}} \cdot \boldsymbol{b}_i + \varrho q. \tag{2.66}$$

Except the penultimate term, equation (2.66) is identical to the usual energy equation in the theory of single continuum. If we assume $\boldsymbol{b}_1 = \ldots = \boldsymbol{b}_N = \boldsymbol{b}$, then this term becomes $\boldsymbol{J}^{\mathrm{m}} \cdot \boldsymbol{b}$ which is equal to zero, see (2.20).

The evolution equation for the internal energy takes the standard form as well, namely

$$\varrho \frac{\mathrm{d}^{\mathrm{m}} e^{\mathrm{m}}}{\mathrm{d}t} = \mathbb{T}^{\mathrm{m}} : \mathbb{D}^{\mathrm{m}} - \operatorname{div} \boldsymbol{q}_e^{\mathrm{m}} + \sum_{i=1}^{N} \boldsymbol{\jmath}_i^{\mathrm{m}} \cdot (\boldsymbol{b}_i - \boldsymbol{b}) + \varrho q. \tag{2.67}$$

According to (2.62) we see that $\boldsymbol{q}_e^{\mathrm{m}} = \boldsymbol{q}^{\mathrm{m}}$ in this case.

Balance of energy with volume-averaged velocity

Let Assumptions 1–3 hold and let $\boldsymbol{v} = \boldsymbol{v}^{\mathrm{v}}$. The corresponding form of the balance of total energy E^{v} can be obtained by reusing the balance of linear momentum (2.42) in the last term in the equation

$$\frac{\mathrm{d}^{\mathrm{v}}(\varrho E^{\mathrm{v}})}{\mathrm{d}t} = \operatorname{div}\left(\mathbb{T}^{\mathrm{v}} \boldsymbol{v}^{\mathrm{v}} - \frac{1}{2} \left|\boldsymbol{v}^{\mathrm{v}}\right|^2 \boldsymbol{J}^{\mathrm{v}} - \boldsymbol{q}^{\mathrm{v}}\right) + \varrho \boldsymbol{v}^{\mathrm{v}} \cdot \boldsymbol{b} + \sum_{i=1}^{N} \boldsymbol{\jmath}_i^{\mathrm{v}} \cdot \boldsymbol{b}_i + \varrho q - \frac{\mathrm{d}^{\mathrm{v}}(\boldsymbol{v}^{\mathrm{v}} \cdot \boldsymbol{J}^{\mathrm{v}})}{\mathrm{d}t}, \tag{2.68}$$

but we will not do it here.

The only term that vanishes in equation (2.61) is the one with the divergence of velocity. The resulting equation reads

$$\varrho \frac{\mathrm{d}^{\mathrm{v}} e^{\mathrm{v}}}{\mathrm{d}t} - e^{\mathrm{v}} \operatorname{div} \boldsymbol{J}^{\mathrm{v}} = \mathbb{T}^{\mathrm{v}} : \left(\mathbb{D}^{\mathrm{v}} + \nabla_{\mathrm{sym}}\left(\varrho^{-1} \boldsymbol{J}^{\mathrm{v}}\right)\right) - \operatorname{div} \boldsymbol{q}_e^{\mathrm{v}} + \sum_{i=1}^{N} \boldsymbol{\jmath}_i^{\mathrm{v}} \cdot (\boldsymbol{b}_i - \boldsymbol{b}) + \varrho q + \varrho^{-1} \boldsymbol{J}^{\mathrm{v}} \cdot \left(\left[\nabla \boldsymbol{v}^{\mathrm{v}}\right] \boldsymbol{J}^{\mathrm{v}} + \frac{\mathrm{d}^{\mathrm{v}} \boldsymbol{J}^{\mathrm{v}}}{\mathrm{d}t}\right). \tag{2.69}$$

Note that the left hand side in this case corresponds to $\frac{\mathrm{d}^{\mathrm{v}}}{\mathrm{d}t}(\varrho e^{\mathrm{v}})$.

Remark 2.13. It is a common practice, see for example Gurtin et al. (1996), Abels et al. (2012) and Dong (2014a), to neglect not only the inertia—as we have already commented in Remark 2.11—but also the kinetic energy due to the motion of the components relative to the bulk motion. It means that, in addition to $\frac{\mathrm{d}^{\mathrm{v}} \boldsymbol{J}}{\mathrm{d}t}$, one neglects also the last term in (2.68). It is easy to verify that in such a case the balance of internal energy reads

$$\varrho \frac{\mathrm{d}^{\mathrm{v}} e^{\mathrm{v}}}{\mathrm{d}t} - e^{\mathrm{v}} \operatorname{div} \boldsymbol{J}^{\mathrm{v}} = \mathbb{T}^{\mathrm{v}} : \mathbb{D}^{\mathrm{v}} - \operatorname{div} \boldsymbol{q}_e^{\mathrm{v}} + \sum_{i=1}^{N} \boldsymbol{\jmath}_i^{\mathrm{v}} \cdot \boldsymbol{b}_i + \varrho q. \tag{2.70}$$

(Let us remark that $\boldsymbol{q}_e^{\mathrm{v}} = \boldsymbol{q}^{\mathrm{v}}$ in this case.) The penultimate term corresponds to rate of work of the external body forces due to diffusion effects. In many practical situations it seems relevant to neglect this term as well.

2.3.5 Balance of entropy

The procedure is merely the same as in the above sections. Local form of the evolution of the entropy for individual components reads

$$\frac{\partial(\varrho_i \eta_i)}{\partial t} + \operatorname{div}(\varrho_i \eta_i \boldsymbol{v}_i) = -\operatorname{div} \boldsymbol{h}_i + \varrho_i s_i + \xi_i, \quad i = 1, \dots, N, \tag{2.71}$$

where η_i is the specific entropy, $\boldsymbol{h}_i$ is the entropy flux, s_i denotes the specific external entropy supply and finally ξ_i is the entropy production term. The mixture entropy production term is defined simply by $\xi \stackrel{\mathrm{def}}{=} \sum_{i=1}^{N} \xi_i$. The second law of thermodynamics requires that this term is non-negative, that is $\xi \geq 0$.

Introducing an averaged velocity $\boldsymbol{v}$, taking the sum of N equations in (2.71) and using the balance of mass (2.28b), one obtains the evolution equation for the total specific entropy $\eta \stackrel{\mathrm{def}}{=} \sum_{i=1}^{N} c_i \eta_i$. This equation reads

$$\varrho \frac{\mathrm{d}\eta}{\mathrm{d}t} - \eta \operatorname{div} \boldsymbol{J} = -\operatorname{div} \boldsymbol{q}_\eta + \varrho s + \xi, \tag{2.72}$$

provided that we define the averaged entropy flux

$$\boldsymbol{q}_\eta \stackrel{\mathrm{def}}{=} \sum_{i=1}^{N} (\boldsymbol{h}_i + \varrho_i \eta_i \boldsymbol{u}_i), \tag{2.73}$$

together with the averaged specific external entropy supply $s \stackrel{\mathrm{def}}{=} \sum_{i=1}^{N} c_i s_i$.

Balance of entropy with mass-averaged velocity

With the choice $\boldsymbol{v} = \boldsymbol{v}^{\mathrm{m}}$ we can write equation (2.72) in the standard form

$$\varrho \frac{\mathrm{d}^{\mathrm{m}}\eta}{\mathrm{d}t} = -\operatorname{div} \boldsymbol{q}_\eta^{\mathrm{m}} + \varrho s + \xi. \tag{2.74}$$

Balance of entropy with volume-averaged velocity

The entropy balance with $\boldsymbol{v} = \boldsymbol{v}^{\mathrm{v}}$ reads

$$\varrho \frac{\mathrm{d}^{\mathrm{v}}\eta}{\mathrm{d}t} - \eta \operatorname{div} \boldsymbol{J}^{\mathrm{v}} = -\operatorname{div} \boldsymbol{q}_\eta^{\mathrm{v}} + \varrho s + \xi. \tag{2.75}$$

The left hand side in this case corresponds to $\frac{\mathrm{d}^{\mathrm{v}}}{\mathrm{d}t}(\varrho\eta)$.

Table 2.2: Balance of mass for the N-component system formulated in terms of different sets of order parameters for two different choices of the averaged velocity (according to Definition 2.5). The balance equations are presented in the general form appropriate for both type of mixtures (compressible and incompressible, see Figure 1.7).

Order parameter*	Mass-averaged velocity	Volume-averaged velocity
φ_i	$\displaystyle\sum_{\beta=1}^{N-1} \frac{\partial \varrho_i}{\partial \varphi_\beta} \frac{\mathrm{d}^{\mathrm{m}} \varphi_\beta}{\mathrm{d}t} + \left(\varrho_i - \varrho \frac{\partial \varrho_i}{\partial \varrho} \right) \operatorname{div} \boldsymbol{v}^{\mathrm{m}} = - \operatorname{div} \boldsymbol{\jmath}_i^{\mathrm{m}}$	$\displaystyle\sum_{\beta=1}^{N-1} \frac{\partial \varrho_i}{\partial \varphi_\beta} \frac{\mathrm{d}^{\mathrm{v}} \varphi_\beta}{\mathrm{d}t} + \left(\varrho_i - \varrho \frac{\partial \varrho_i}{\partial \varrho} \right) \operatorname{div} \boldsymbol{v}^{\mathrm{v}} = - \operatorname{div} \boldsymbol{\jmath}_i^{\mathrm{v}} + \frac{\partial \varrho_i}{\partial \varrho} \operatorname{div} \boldsymbol{J}^{\mathrm{v}}$
$\varphi_i = \varrho_i$	$\displaystyle\frac{\mathrm{d}^{\mathrm{m}} \varrho_i}{\mathrm{d}t} + \varrho_i \operatorname{div} \boldsymbol{v}^{\mathrm{m}} = - \operatorname{div} \boldsymbol{\jmath}_i^{\mathrm{m}}$	$\displaystyle\frac{\mathrm{d}^{\mathrm{v}} \varrho_i}{\mathrm{d}t} + \varrho_i \operatorname{div} \boldsymbol{v}^{\mathrm{v}} = - \operatorname{div} \boldsymbol{\jmath}_i^{\mathrm{v}}$
$\varphi_i = c_i$	$\displaystyle\varrho \frac{\mathrm{d}^{\mathrm{m}} c_i}{\mathrm{d}t} = - \operatorname{div} \boldsymbol{\jmath}_i^{\mathrm{m}}$	$\displaystyle\varrho \frac{\mathrm{d}^{\mathrm{v}} c_i}{\mathrm{d}t} = - \operatorname{div} \boldsymbol{\jmath}_i^{\mathrm{v}} + c_i \operatorname{div} \boldsymbol{J}^{\mathrm{v}}$
$\varphi_i = \phi_i$	$\displaystyle\frac{\mathrm{d}^{\mathrm{m}} \phi_i}{\mathrm{d}t} + \phi_i \operatorname{div} \boldsymbol{v}^{\mathrm{m}} = - \operatorname{div} \widetilde{\boldsymbol{\jmath}}_i^{\mathrm{m}}$	$\displaystyle\frac{\mathrm{d}^{\mathrm{v}} \phi_i}{\mathrm{d}t} + \phi_i \operatorname{div} \boldsymbol{v}^{\mathrm{v}} = - \operatorname{div} \widetilde{\boldsymbol{\jmath}}_i^{\mathrm{v}}$
Total mass balance†	$\displaystyle\frac{\mathrm{d}^{\mathrm{m}} \varrho}{\mathrm{d}t} + \varrho \operatorname{div} \boldsymbol{v}^{\mathrm{m}} = 0$	$\displaystyle\frac{\mathrm{d}^{\mathrm{v}} \varrho}{\mathrm{d}t} + \varrho \operatorname{div} \boldsymbol{v}^{\mathrm{v}} = - \operatorname{div} \boldsymbol{J}^{\mathrm{v}}$
Incompress. constraint‡	$\displaystyle\operatorname{div} \boldsymbol{v}^{\mathrm{m}} = - \sum_{i=1}^{N-1} \hat{r}_i \operatorname{div} \widetilde{\boldsymbol{\jmath}}_i^{\mathrm{m}}$	$\displaystyle\operatorname{div} \boldsymbol{v}^{\mathrm{v}} = 0$

* Balance equations for individual constituents are considered for $i = 1, \ldots, N-1$. (The equations for the case with $\varphi_i = \phi_i$ are obtained provided that material densities are constants, see Assumption 2.)

† Balance of mass for the mixture as a whole. This equation is redundant from the individual mass balances in the case of incompressible mixtures.

‡ The constraint applies only for incompressible mixtures. The constants $\hat{r}_i$, given by relative differences $1 - \frac{\hat{\varrho}_i}{\hat{\varrho}_N}$, have been introduced in (2.23).

Table 2.3: General form of the balance equations for the mixture as a whole formulated for two different choices of the averaged velocity (according to Definition 2.5).

Balance	Mass-averaged velocity	Volume-averaged velocity*
Linear momentum	$\varrho\frac{\mathrm{d}^{\mathrm{m}}\boldsymbol{v}^{\mathrm{m}}}{\mathrm{d}t} = \operatorname{div}\mathbb{T}^{\mathrm{m}} + \varrho\boldsymbol{b}$	$\varrho\frac{\mathrm{d}^{\mathrm{v}}\boldsymbol{v}^{\mathrm{v}}}{\mathrm{d}t} = \operatorname{div}\mathbb{T}^{\mathrm{v}} + \varrho\boldsymbol{b} - \left[(\operatorname{div}\boldsymbol{v}^{\mathrm{v}})\,\mathbb{I} + \nabla\boldsymbol{v}^{\mathrm{v}}\right]\boldsymbol{J}^{\mathrm{v}} - \frac{\mathrm{d}^{\mathrm{v}}\boldsymbol{J}^{\mathrm{v}}}{\mathrm{d}t}$
Angular momentum	$\mathbb{T}^{\mathrm{m}} = (\mathbb{T}^{\mathrm{m}})^{\top}$	$\mathbb{T}^{\mathrm{v}} = (\mathbb{T}^{\mathrm{v}})^{\top}$
Total energy	$\varrho\frac{\mathrm{d}^{\mathrm{m}}E^{\mathrm{m}}}{\mathrm{d}t} = \operatorname{div}\left((\mathbb{T}^{\mathrm{m}})^{\top}\boldsymbol{v}^{\mathrm{m}} - \boldsymbol{q}^{\mathrm{m}}\right) + \varrho\boldsymbol{v}^{\mathrm{m}}\cdot\boldsymbol{b} + \sum_{i=1}^{N}\boldsymbol{\jmath}_i^{\mathrm{m}}\cdot\boldsymbol{b}_i + \varrho q$	$\varrho\frac{\mathrm{d}^{\mathrm{v}}E^{\mathrm{v}}}{\mathrm{d}t} = \operatorname{div}\left((\mathbb{T}^{\mathrm{v}})^{\top}\boldsymbol{v}^{\mathrm{v}} - \frac{1}{2}\lvert\boldsymbol{v}^{\mathrm{v}}\rvert^2\boldsymbol{J}^{\mathrm{v}} - \boldsymbol{q}^{\mathrm{v}}\right) + E^{\mathrm{v}}\operatorname{div}\boldsymbol{J}^{\mathrm{v}} + \sum_{i=1}^{N}\boldsymbol{\jmath}_i^{\mathrm{v}}\cdot\boldsymbol{b}_i + \varrho q + \boldsymbol{v}^{\mathrm{v}}\cdot(\varrho\boldsymbol{b} - (\operatorname{div}\boldsymbol{v}^{\mathrm{v}})\,\boldsymbol{J}^{\mathrm{v}}) - \frac{\mathrm{d}^{\mathrm{v}}(\boldsymbol{v}^{\mathrm{v}}\cdot\boldsymbol{J}^{\mathrm{v}})}{\mathrm{d}t}$
Internal energy†	$\varrho\frac{\mathrm{d}^{\mathrm{m}}e^{\mathrm{m}}}{\mathrm{d}t} = \mathbb{T}^{\mathrm{m}} : \mathbb{D}^{\mathrm{m}} - \operatorname{div}\boldsymbol{q}_e^{\mathrm{m}} + \varrho q + \sum_{i=1}^{N}\boldsymbol{\jmath}_i^{\mathrm{m}}\cdot(\boldsymbol{b}_i - \boldsymbol{b})$	$\varrho\frac{\mathrm{d}^{\mathrm{v}}e^{\mathrm{v}}}{\mathrm{d}t} = \mathbb{T}^{\mathrm{v}} : \left(\mathbb{D}^{\mathrm{v}} + \nabla_{\mathrm{sym}}\left(\varrho^{-1}\boldsymbol{J}^{\mathrm{v}}\right)\right) + e^{\mathrm{v}}\operatorname{div}\boldsymbol{J}^{\mathrm{v}} - \operatorname{div}\boldsymbol{q}_e^{\mathrm{v}} + \varrho q + \sum_{i=1}^{N}\boldsymbol{\jmath}_i^{\mathrm{v}}\cdot(\boldsymbol{b}_i - \boldsymbol{b}) + \varrho^{-1}\boldsymbol{J}^{\mathrm{v}}\cdot\left(\left[(\operatorname{div}\boldsymbol{v}^{\mathrm{v}})\,\mathbb{I} + \nabla\boldsymbol{v}^{\mathrm{v}}\right]\boldsymbol{J}^{\mathrm{v}} + \frac{\mathrm{d}^{\mathrm{v}}\boldsymbol{J}^{\mathrm{v}}}{\mathrm{d}t}\right)$
Entropy	$\varrho\frac{\mathrm{d}^{\mathrm{m}}\eta}{\mathrm{d}t} = -\operatorname{div}\boldsymbol{q}_\eta^{\mathrm{m}} + \varrho s + \xi$	$\varrho\frac{\mathrm{d}^{\mathrm{v}}\eta}{\mathrm{d}t} = \eta\operatorname{div}\boldsymbol{J}^{\mathrm{v}} - \operatorname{div}\boldsymbol{q}_\eta^{\mathrm{v}} + \varrho s + \xi$

* For incompressible mixtures we have the constraint $\operatorname{div}\boldsymbol{v}^{\mathrm{v}} = 0$ and $\boldsymbol{J}^{\mathrm{v}}$ is in that case given by (2.24), that is $\boldsymbol{J}^{\mathrm{v}} = \sum_{i=1}^{N-1}(\hat{\varrho}_i - \hat{\varrho}_N)\,\widetilde{\boldsymbol{\jmath}}_i^{\mathrm{v}}$.
† The (generalized) energy fluxes are given by $\boldsymbol{q}_e^{\mathrm{m}} = \boldsymbol{q}^{\mathrm{m}}$ and $\boldsymbol{q}_e^{\mathrm{v}} = \boldsymbol{q}^{\mathrm{v}} + \varrho^{-1}\mathbb{T}^{\mathrm{v}}\boldsymbol{J}^{\mathrm{v}}$, see (2.62).

2.3.6 Derived evolution equations

In the subsequent derivations, we will need evolution equations for ∇c_i and $\nabla \phi_i$, which can be obtained as a direct consequence of the corresponding balance equations for c_i and ϕ_i respectively.

Let $\boldsymbol{v}$ is a general averaged velocity and let $\boldsymbol{\varphi}$ is a vector of order parameters satisfying (2.33). The choice $\boldsymbol{\varphi} = \boldsymbol{c}$ leads to the relation $\varrho_i = \varrho\varphi_i$ and the balance equations in (2.33) reduce to the simple form

$$\varrho \frac{\mathrm{d}c_i}{\mathrm{d}t} = -\operatorname{div} \boldsymbol{\jmath}_i + c_i \operatorname{div} \boldsymbol{J}, \quad i = 1, \ldots, N-1. \tag{2.76}$$

From the definition of the material time derivative it follows that

$$\frac{\mathrm{d}\nabla c_i}{\mathrm{d}t} = \frac{\partial \nabla c_i}{\partial t} + \left[\nabla^{(2)} c_i\right] \boldsymbol{v}. \tag{2.77}$$

Application of the gradient to the i-th equation in (2.76) yields

$$(\nabla \varrho) \frac{\mathrm{d}c_i}{\mathrm{d}t} + \varrho \frac{\partial \nabla c_i}{\partial t} + \varrho\, \nabla(\boldsymbol{v} \cdot \nabla c_i) = -\nabla(\operatorname{div} \boldsymbol{\jmath}_i - c_i \operatorname{div} \boldsymbol{J}). \tag{2.78}$$

In the next step we first solve (2.77) for $\partial_t (\nabla c_i)$, we use the result in the second term on the left hand side of the previous equation and, at the same time, we use the identity $\nabla(\boldsymbol{v} \cdot \nabla c_i) = \left[\nabla \boldsymbol{v}^\top\right] \nabla c_i + \left[\nabla^{(2)} c_i\right] \boldsymbol{v}$ to reformulate the third term. After that, we reuse (2.76) to substitute into the first term and rearrange the terms. The resulting equation reads

$$\varrho \frac{\mathrm{d}\nabla c_i}{\mathrm{d}t} = -\varrho \left[\nabla \boldsymbol{v}^\top\right] \nabla c_i - \nabla(\operatorname{div} \boldsymbol{\jmath}_i - c_i \operatorname{div} \boldsymbol{J}) + (\operatorname{div} \boldsymbol{\jmath}_i - c_i \operatorname{div} \boldsymbol{J}) \frac{\nabla \varrho}{\varrho}. \tag{2.79}$$

Finally, we put together the last two terms on the right hand side and we divide the equation by ϱ. The evolution of the quantity ∇c_i is therefore given by

$$\frac{\mathrm{d}\nabla c_i}{\mathrm{d}t} = -\left[\nabla \boldsymbol{v}^\top\right] \nabla c_i - \nabla\left(\frac{1}{\varrho} (\operatorname{div} \boldsymbol{\jmath}_i - c_i \operatorname{div} \boldsymbol{J})\right). \tag{2.80}$$

Let Assumption 2 holds. By repeating the above procedure with (2.30) instead of (2.76), we derive the evolution equation for $\nabla \phi_i$, namely

$$\frac{\mathrm{d}\nabla \phi_i}{\mathrm{d}t} = -\left[\nabla \boldsymbol{v}^\top\right] \nabla \phi_i - \nabla(\phi_i \operatorname{div} \boldsymbol{v} + \operatorname{div} \widetilde{\boldsymbol{\jmath}}_i). \tag{2.81}$$

2.3.7 Simplifying assumptions

In the remainder of the thesis we shall suppose that the gravitational force is the only external body force acting on the system. Therefore, we assume that

$$\boldsymbol{b}_1 = \ldots = \boldsymbol{b}_N = \boldsymbol{b} = \boldsymbol{g}, \tag{2.82}$$

where $\boldsymbol{g}$ denotes the vector of gravitational acceleration. On top of that, we shall assume the absence of external energy and entropy supplies, which means that we put

$$q = 0, \qquad s = 0 \tag{2.83}$$

in the relevant balance equations.

Looking at Table 2.3, we can observe that the structure of balance equations is more complicated in the case with volume-averaged velocity. Keep in mind that the discussed equations have been obtained as a result of the model reduction, which should be understood as being the fundamental level of approximation in our description of multi-component systems. In order to proceed to the derivation of diffuse interface models using FI description, we will need to accept some additional levels of approximation.

In Section 2.5.3, we discuss three such approximation levels, each of them being based on omission of some particular terms in the equations. For this purpose we introduce auxiliary coefficients Θ_0, Θ_1 and Θ_2 to appear in front of the discussed terms, see (2.95). These so-called *toggle coefficients* are allowed to attain the values of either one or zero depending on the chosen level of approximation as discussed in Summary 7.

2.4 Preliminary thermodynamic considerations

Extending the classical concepts from equilibrium thermodynamics (see Callen (1985)) to non-equilibrium setting, we assume that the specific entropy η introduced in Section 2.3.5 is a differentiable function of the specific internal energy e and other state variables; see also de Groot and Mazur (1984). The models of our primary interest are expected to properly describe dynamics of the interfaces formed between the immiscible components of the mixture, taking into account capillary effects. As we have already mentioned in Chapter 1, van der Waals (1893) in his study of the nature of capillarity used density gradients to model the surface energy of the interfaces. Based on this idea, we include gradients of some density-related quantities among the state variables mentioned above. In particular, inspired by the work of Heida et al. (2012b), we shall assume that

$$\eta = \eta\left(e, \varrho, \varphi_1, \dots, \varphi_{N-1}, \nabla\varphi_1, \dots, \nabla\varphi_{N-1}\right), \tag{2.84}$$

where $\boldsymbol{\varphi} = [\varphi_1, \dots, \varphi_{N-1}]^\top$ is the vector of order parameters representing either mass or volume fractions. Note that we have directly applied the constraint $\sum_{i=1}^{N} \varphi_i = 1$, see (2.7) and (2.8) respectively, to exclude φ_N and $\nabla\varphi_N$ from the set of independent state variables.

From this point of view, we do not include balance of entropy among governing equations for a given model. Nevertheless, the presented form of the entropy balance will be used for identification of the entropy producing processes, which is the crucial step in thermodynamically consistent derivation of constitutive relations for the Cauchy stress tensor, the energy flux and the diffusive fluxes.

Remark 2.14. For convenience reasons, let us introduce the shorthand notation for expressions of the type (2.84), which in that particular case reads

$$\eta = \eta\left(e, \varrho, \boldsymbol{\varphi}, \nabla\boldsymbol{\varphi}\right).$$

Here, the gradient should be understood to be applied componentwise.

We further assume that η is an increasing function with respect to e, thus it can be inverted to obtain the specific internal energy as a differentiable function of the specific entropy and other state variables. In particular, we have

$$e = e\left(\eta, \varrho, \boldsymbol{\varphi}, \nabla\boldsymbol{\varphi}\right). \tag{2.85}$$

The thermodynamic temperature ϑ and the thermodynamic pressure p_{th} are defined through partial derivatives of e, namely

$$\vartheta \stackrel{\mathrm{def}}{=} \frac{\partial e}{\partial \eta}, \qquad\qquad p_{\mathrm{th}} \stackrel{\mathrm{def}}{=} \varrho^2 \frac{\partial e}{\partial \varrho}. \tag{2.86}$$

(Due to the above monotonicity assumption, we see that ϑ is strictly positive.)

The definitions in (2.86) allow us to introduce other thermodynamic potentials using the Legendre transformation. The convenient potential for our needs is the specific Helmholtz free energy ψ, which is defined by

$$\psi \stackrel{\mathrm{def}}{=} e - \vartheta\eta. \tag{2.87}$$

Provided that the first formula in (2.86) allows for inversion, we may express the entropy in terms of the temperature (and other state variables), which in turn yields

$$\psi = \psi\left(\vartheta, \varrho, \boldsymbol{\varphi}, \nabla\boldsymbol{\varphi}\right). \tag{2.88}$$

By application of the chain rule on (2.87), it can be shown that

$$\eta = -\frac{\partial \psi}{\partial \vartheta}, \qquad\qquad p_{\mathrm{th}} = \varrho^2 \frac{\partial \psi}{\partial \varrho}. \tag{2.89}$$

When deriving the evolution equation for the temperature, we find it convenient to work with the specific heat at constant volume $\mathrm{c_v}$, which can be introduced through[16]

$$\mathrm{c_v} \stackrel{\mathrm{def}}{=} -\vartheta \frac{\partial^2 \psi}{\partial \vartheta^2}. \tag{2.90}$$

The derivation of diffuse interface models in Chapter 3 is based on the precise specification of ψ in (2.88), although in theory we could work with (2.85) instead. The former option is however more convenient from the practical point of view, because the temperature—unlike the entropy—is directly measurable. Moreover, our objective is the inclusion of the evolution equation for ϑ in a system of PDEs representing the relevant model in a general non-isothermal setting.

Finally, let us mention that we put $\boldsymbol{\varphi} = \boldsymbol{c}$ in (2.88) whenever we are dealing with compressible mixtures. On the other hand, we prefer to work with $\boldsymbol{\varphi} = \boldsymbol{\phi}$ in case of incompressible mixtures. Our choice is motivated by the fact that ϱ can be expressed as a linear function in terms of $\boldsymbol{\phi}$, see (2.10a), which will become advantageous later in numerical simulations. Moreover, the density does not explicitly appear in the evolution equations for volume fractions, see Table 2.2.

[16]The definition (2.90) is tantamount to

$$\mathrm{c_v}(\vartheta, \varrho, \boldsymbol{\varphi}, \nabla\boldsymbol{\varphi}) = \frac{\partial}{\partial \vartheta}\left[e(\eta, \varrho, \boldsymbol{\varphi}, \nabla\boldsymbol{\varphi})|_{\eta=\eta(\vartheta,\varrho,\boldsymbol{\varphi},\nabla\boldsymbol{\varphi})} \right].$$

2.5 Summary: Governing equations

We consider a mixture of N chemically non-reacting fluids, that are referred to as components of the mixture. We distinguish between compressible and incompressible mixtures; see Figure 1.7 and fundamental assumptions in Section 2.1.

For each component we have postulated balances of mass, linear momentum, angular momentum, energy and entropy. These equations have been reformulated in terms of an averaged velocity $\boldsymbol{v}$ and related diffusive fluxes, $\boldsymbol{\jmath}_i$ or $\widetilde{\boldsymbol{\jmath}}_i$, associated with individual components, see Definition 2.7. Balance equations for the mixture as a whole have been obtained by adding up their reformulated componentwise counterparts, and by introducing relevant averaged quantities including the Cauchy stress tensor $\mathbb{T}$ and the energy flux $\boldsymbol{q}_e$, see (2.40) and (2.62) respectively.

The approach explained above has brought us to a reduced model in which the diffusive fluxes, the Cauchy stress tensor and the energy flux are treated as unknown fields that must be specified by constitutive relations. Tables 2.2–2.3 offer an overview of the balance equations in their general forms.

Final forms of governing and complementary equations, presented below with respect to three different descriptions according to the classification in Figure 1.7, are obtained by appealing to simplifying assumptions discussed in Section 2.3.7. The governing equations are formulated for the unknowns $\boldsymbol{\phi}$ or $\boldsymbol{c}$, $\boldsymbol{v}$, e, and possibly ϱ. On the other hand, the specific entropy η is assumed to be a given function of e and other state variables, see (2.84). For practical purposes we shall however work with a constitutive assumption for the Helmholtz free energy ψ, see (2.88), and we shall replace the equation for e with the corresponding equation for the temperature ϑ. These ideas have been briefly discussed in Section 2.4.

A couple of remarks on the notation follows. First, since each of the aforementioned descriptions is associated with the specific choice of the velocity field, we shall omit the superscripts 'm' and 'v', that have been used to differentiate between the averaged quantities so far. Second, we do not include the balance of angular momentum explicitly into the forthcoming recapitulation of the governing equations. As mentioned in Section 2.3.3, its equivalent formulation

$$\mathbb{T} = \mathbb{T}^\top \tag{2.91}$$

is assumed to hold in all three cases listed below. Moreover, in the balance of internal energy we shall consider the standard decomposition of the stress tensor into its spherical and traceless (deviatoric) parts, that is

$$\mathbb{T} = m\mathbb{I} + \mathbb{T}^\delta, \qquad\qquad m \stackrel{\text{def}}{=} \frac{1}{3}\operatorname{tr}\mathbb{T}, \tag{2.92}$$

where m is known as the mean normal stress. We will use this kind of decomposition also for other tensors quite frequently in the next chapter[17].

Finally, let us remark that m plays a role of Lagrange multiplier enforcing the constraint (2.29b) in the case of incompressible mixtures. In this sense it becomes

[17]The traceless part of a general tensor $\mathbb{A}$ is defined by $\mathbb{A}^\delta \stackrel{\text{def}}{=} \mathbb{A} - \frac{1}{3}(\operatorname{tr}\mathbb{A})\,\mathbb{I}$.

an unknown field that must be obtained as part of the solution of governing equations, thus only $\mathbb{T}^\delta$ can be specified by a constitutive relation in this case.

2.5.1 Fully-compressible description

Summary 1: Basic characteristics of FC description

- Properties of the components: mass additive (Assumption 1).
- Velocity field: mass-averaged (Definition 2.5).
- Order parameters: vector of mass fractions $\boldsymbol{c} = [c_1, \dots, c_{N-1}]^\top$.
- Total density: independent unknown variable.

Summary 2: FC description of the model

- Governing equations:

$$\varrho \frac{\mathrm{d}c_i}{\mathrm{d}t} = -\operatorname{div} \boldsymbol{\jmath}_i, \quad i = 1, \dots, N-1, \tag{2.93a}$$

$$\frac{\mathrm{d}\varrho}{\mathrm{d}t} = -\varrho \operatorname{div} \boldsymbol{v}, \tag{2.93b}$$

$$\varrho \frac{\mathrm{d}\boldsymbol{v}}{\mathrm{d}t} = \operatorname{div} \mathbb{T} + \varrho \boldsymbol{g}, \tag{2.93c}$$

$$\varrho \frac{\mathrm{d}e}{\mathrm{d}t} = \mathbb{T}^\delta : \mathbb{D}^\delta + m \operatorname{div} \boldsymbol{v} - \operatorname{div} \boldsymbol{q}_e. \tag{2.93d}$$

- Unknown fields: $\boldsymbol{c}, \varrho, \boldsymbol{v}, e$.
- Fields requiring constitutive relations: $\mathbb{T} = m\mathbb{I} + \mathbb{T}^\delta, \boldsymbol{q}_e, \boldsymbol{\jmath}_i$.
- Complementary fields: $c_N = 1 - \sum_{i=1}^{N-1} c_i$, $\boldsymbol{\jmath}_N = -\sum_{i=1}^{N-1} \boldsymbol{\jmath}_i$.
- Complementary equations:

$$\frac{\mathrm{d}\nabla c_i}{\mathrm{d}t} = -\left[\nabla \boldsymbol{v}^\top\right] \nabla c_i - \nabla\left(\frac{1}{\varrho} \operatorname{div} \boldsymbol{\jmath}_i\right), \quad i = 1, \dots, N-1. \tag{2.93e}$$

- Balance of entropy:

$$\varrho \frac{\mathrm{d}\eta}{\mathrm{d}t} = -\operatorname{div} \boldsymbol{q}_\eta + \xi. \tag{2.93f}$$

2.5.2 Quasi-incompressible description

Summary 3: Basic characteristics of QI description

- Properties of the components: mass additive, constant material densities, volume additive (Assumptions 1–3).
- Velocity field: mass-averaged (Definition 2.5).
- Order parameters: vector of volume fractions $\boldsymbol{\phi} = [\phi_1, \dots, \phi_{N-1}]^\top$.
- Total density: given by $\varrho = \sum_{i=1}^{N-1} (\hat{\varrho}_i - \hat{\varrho}_N)\, \phi_i + \hat{\varrho}_N$ (Lemma 2.2).

Summary 4: QI description of the model

- Governing equations (with $\mathbb{T} = m\mathbb{I} + \mathbb{T}^\delta$):

$$\frac{\mathrm{d}\phi_i}{\mathrm{d}t} = -\phi_i \operatorname{div} \boldsymbol{v} - \operatorname{div} \widetilde{\boldsymbol{j}}_i, \quad i = 1, \dots, N-1, \tag{2.94a}$$

$$\operatorname{div} \boldsymbol{v} = -\sum_{i=1}^{N-1} \hat{r}_i \operatorname{div} \widetilde{\boldsymbol{j}}_i, \tag{2.94b}$$

$$\varrho \frac{\mathrm{d}\boldsymbol{v}}{\mathrm{d}t} = \operatorname{div} \mathbb{T} + \varrho \boldsymbol{g}, \tag{2.94c}$$

$$\varrho \frac{\mathrm{d}e}{\mathrm{d}t} = \mathbb{T}^\delta : \mathbb{D}^\delta + m \operatorname{div} \boldsymbol{v} - \operatorname{div} \boldsymbol{q}_e, \tag{2.94d}$$

- Unknown fields: $\boldsymbol{\phi}, m, \boldsymbol{v}, e$.
- Fields requiring constitutive relations: $\mathbb{T}^\delta, \boldsymbol{q}_e, \widetilde{\boldsymbol{j}}_i$.
- Complementary fields: $\phi_N = 1 - \sum_{i=1}^{N-1} \phi_i$, $\widetilde{\boldsymbol{j}}_N = -\frac{1}{\hat{\varrho}_N} \sum_{i=1}^{N-1} \hat{\varrho}_i \widetilde{\boldsymbol{j}}_i$.
- Complementary equations:

$$\frac{\mathrm{d}\varrho}{\mathrm{d}t} = -\varrho \operatorname{div} \boldsymbol{v}, \tag{2.94e}$$

$$\frac{\mathrm{d}\nabla\phi_i}{\mathrm{d}t} = -\left[\nabla \boldsymbol{v}^\top\right] \nabla\phi_i - \nabla(\phi_i \operatorname{div} \boldsymbol{v} + \operatorname{div} \widetilde{\boldsymbol{j}}_i), \quad i = 1, \dots, N-1. \tag{2.94f}$$

- Balance of entropy:

$$\varrho \frac{\mathrm{d}\eta}{\mathrm{d}t} = -\operatorname{div} \boldsymbol{q}_\eta + \xi. \tag{2.94g}$$

2.5.3 Fully-incompressible description

Summary 5: Basic characteristics of FI description

- Properties of the components: mass additive, constant material densities, volume additive (Assumptions 1–3).
- Velocity field: volume-averaged (Definition 2.5).
- Order parameters: vector of volume fractions $\boldsymbol{\phi} = [\phi_1, \dots, \phi_{N-1}]^\top$.
- Total density: given by $\varrho = \sum_{i=1}^{N-1} (\hat{\varrho}_i - \hat{\varrho}_N)\, \phi_i + \hat{\varrho}_N$ (Lemma 2.2).

Summary 6: FI description of the model

- Governing equations (with $\mathbb{T} = m\mathbb{I} + \mathbb{T}^\delta$ and $\boldsymbol{J} = \sum_{i=1}^{N-1} (\hat{\varrho}_i - \hat{\varrho}_N)\, \widetilde{\boldsymbol{\jmath}}_i$):

$$\frac{\mathrm{d}\phi_i}{\mathrm{d}t} = -\operatorname{div} \widetilde{\boldsymbol{\jmath}}_i, \quad i = 1, \dots, N-1, \tag{2.95a}$$

$$\operatorname{div} \boldsymbol{v} = 0, \tag{2.95b}$$

$$\varrho \frac{\mathrm{d}\boldsymbol{v}}{\mathrm{d}t} + \Theta_2 \left[\nabla \boldsymbol{v}\right] \boldsymbol{J} = \operatorname{div} \mathbb{T} + \varrho \boldsymbol{g} - \Theta_0 \frac{\mathrm{d}\boldsymbol{J}}{\mathrm{d}t}, \tag{2.95c}$$

$$\begin{aligned} \varrho \frac{\mathrm{d}e}{\mathrm{d}t} - \Theta_2\, e \operatorname{div} \boldsymbol{J} = \mathbb{T}^\delta : \left(\mathbb{D} + \Theta_1\, \nabla_{\mathrm{sym}} \left(\varrho^{-1} \boldsymbol{J}\right)\right)^\delta - \operatorname{div} \boldsymbol{q}_e \\ + \Theta_1 m \operatorname{div} \left(\varrho^{-1} \boldsymbol{J}\right) + \Theta_1 \varrho^{-1} \boldsymbol{J} \cdot \left(\left[\nabla \boldsymbol{v}\right] \boldsymbol{J} + \Theta_0 \frac{\mathrm{d}\boldsymbol{J}}{\mathrm{d}t} \right). \end{aligned} \tag{2.95d}$$

- Unknown fields: $\boldsymbol{\phi}, m, \boldsymbol{v}, e$.
- Fields requiring constitutive relations: $\mathbb{T}^\delta, \boldsymbol{q}_e, \widetilde{\boldsymbol{\jmath}}_i$.
- Complementary fields: $\phi_N = 1 - \sum_{i=1}^{N-1} \phi_i$, $\widetilde{\boldsymbol{\jmath}}_N = -\sum_{i=1}^{N-1} \widetilde{\boldsymbol{\jmath}}_i$.
- Complementary equations:

$$\frac{\mathrm{d}\varrho}{\mathrm{d}t} = -\Theta_2 \operatorname{div} \boldsymbol{J}, \tag{2.95e}$$

$$\frac{\mathrm{d}\nabla\phi_i}{\mathrm{d}t} = -\left[\nabla \boldsymbol{v}^\top\right] \nabla\phi_i - \nabla(\operatorname{div} \widetilde{\boldsymbol{\jmath}}_i), \quad i = 1, \dots, N-1. \tag{2.95f}$$

- Balance of entropy:

$$\varrho \frac{\mathrm{d}\eta}{\mathrm{d}t} - \Theta_2 \eta \operatorname{div} \boldsymbol{J} = -\operatorname{div} \boldsymbol{q}_\eta + \xi. \tag{2.95g}$$

Summary 7: Additional levels of approximation for FI description

0. The term that brings additional complexity into the balance of linear momentum (2.42) is the material time derivative of $\boldsymbol{J}$. To cope with this term in the forthcoming derivations, one would need to identify evolution equations for diffusive fluxes $\widetilde{\boldsymbol{j}}_i$. These equations would contain the interaction terms $\mathbf{I}_i$, which in turn must be specified by appealing to some constitutive relations, see Souček et al. (2014). Such detailed approach is not covered within the thesis. Instead, we accept *ad hoc* assumption that the term $\frac{\mathrm{d}\boldsymbol{J}}{\mathrm{d}t}$ in (2.95d) simply vanishes[a]. Hereafter, we always put

$$\Theta_0 = 0. \tag{2.96a}$$

   In this sense the model is *not consistent* from the perspective of the transition from the componentwise formulation of the balance equations towards the current level of description with the equations formulated for the mixture as a whole.

1. Similar complication arises in balance of total energy (2.68), where the additional complexity appears due to the material time derivative of the term $\boldsymbol{v}\cdot\boldsymbol{J}$. If we accept another *ad hoc* assumptions that have been commented in Remark 2.13, we end up with governing equations (2.95) in which

$$\Theta_1 = \Theta_0 = 0. \tag{2.96b}$$

   Models based on this type of approximations were previously derived by Abels et al. (2012) and Dong (2014a), but they were applied only in the classical isothermal setting. Our primary objective here is to provide a variant of the model appropriate for computer simulations of multi-component flows in the extended non-isothermal setting.

2. Another possible level of approximation is to neglect the "correction" term (multiplied by Θ_2) on the left hand side of (2.95c); for its precise meaning see the discussion below (2.42). In such a case we put

$$\Theta_2 = \Theta_1 = \Theta_0 = 0. \tag{2.96c}$$

   As noted by Dong (2014a), this term represents the effect of the momentum flux associated with the mass transport at the scale of the diffuse interface layer. We should therefore neglect also the right hand side of (2.95e) together with related terms in (2.95d) and (2.95g). (If the previous approximations were *ad hoc*, then this one is AD HOC.)

[a] One possible interpretation of this approximation step is the requirement that the interplay between the interaction forces and partial stresses is such that $\frac{\mathrm{d}\boldsymbol{J}}{\mathrm{d}t} = \mathbf{0}$ is always satisfied. However, it is not a physically based argument. The other possible interpretation has been commented in Remark 2.11.

Chapter 3

Diffuse Interface Models

Our objective in this chapter is to propose a mathematical model suitable for the description of flows of N immiscible fluids, taking into account capillary effects at the interfaces between them, as well as the thermal effects. Diffuse interface models represent one particular class of mathematical models with such capabilities.

The standard approach to the derivation of diffuse interface models is based on the choice of an appropriate *ansatz* for the free energy of the considered system. A promising candidate must ensure separation of the components into their pure states and, at the same time, allow for their partial mixing within a thin interfacial regions.

In Section 3.1 we first discuss the standard form of such an *ansatz* for two-component (binary) systems at a constant temperature. Then, we discuss its possible extensions that can be used in the general non-isothermal setting with variable temperature field. The proposed function is then accepted as the constitutive assumption and it is extensively used in subsequent manipulation with the governing equations formulated in the preceding chapter. The purpose of the manipulation is twofold. The first aim is the identification of entropy producing processes in the model, which is crucial for the proposal of constitutive relations defining the Cauchy stress tensor, the energy flux and the diffusive fluxes respectively. These relations are obtained directly from a thermodynamically consistent constitutive assumption on the structure of the entropy production. The second aim is a consistent derivation of the temperature equation. Both procedures are described in detail in Sections 3.2–3.4, covering the three cases that have been summarized in Section 2.5.

The combination of the derived constitutive relations and the particular form of the balance equations eventually leads to a system of PDEs of CHNSF type. In order to apply the models, we need to specify all material parameters such as viscosity and thermal conductivity for the individual components, as well as parameters characterizing the properties of the continua in the interfacial region in between the individual components. Concerning the viscosity and the thermal conductivity at the interfacial mixed region, we opt for a certain type of interpolation that facilitates smooth transition of viscosity/conductivity from one pure component in the other. This is briefly discussed in Section 3.5. Other parame-

ters characterizing the interface, such as surface tension, are treated as genuine physical quantities. The entire specification of the free energy *ansatz* is a complicated matter, especially for general N-component systems with $N \geq 3$. In Section 3.6 we discuss at least the special case of binary fluids ($N = 2$). We also demonstrate how the generalized models developed within the current chapter reduce to some existing binary models which are available in the mathematical literature.

Remark 3.1. Another class of diffuse interface models, based on the approach outlined in Chapter 2, can be obtained if we replace diffusion effects in the model by reaction effects. This can be achieved by considering zero diffusive fluxes and non-zero reaction terms in the equations describing balance of mass. The corresponding governing equations in combination with suggested constitutive assumption yield a system of PDEs of Allen–Cahn–Navier–Stokes–Fourier (AC-NSF) type, see Heida et al. (2012a). The derivation of the temperature equation, and the corresponding classification of relevant diffuse interface models, may be discussed in future research.

3.1 Constitutive assumptions

At this point we shall continue our discussion initiated in Section 2.4. Before that, we shall briefly discuss the so-called phase separation process in binary systems. The main purpose of this little detour is to motivate our later choice of the function representing the specific Helmholtz free energy for incompressible multi-component systems, recall (2.88).

3.1.1 Motivation: Phase separation in binary systems

Description of phase separation

A model which describes the phenomenon of phase separation in binary systems was proposed by Cahn and Hilliard (1958). Imagine a mixture that exists in a state of isothermal equilibrium at a high temperature, for example a molten iron-nickel alloy. The phase separation is a process during which the mixture separates into its two components, or more precisely, a process during which we observe formation of a structure with two distinct phases[1]. It typically occurs if the mixture is quenched to a uniform fixed temperature $\hat{\vartheta}_{\text{iso}}$ below a critical temperature ϑ_{crit}.

Remark 3.2. Note that the observed phases are not necessarily occupied by the pure components. Each such phase can be created by a homogenized material which contains—regarding its detailed chemical composition—contributions from both components, although one of them predominates.

The derivation of the CH model is based on a free energy, usually called

[1]The term *phase* here refers to a region of space occupied by a material that is chemically uniform, physically distinct and separable from other materials.

Ginzburg–Landau energy, of the form

$$\mathcal{F}_{\mathrm{GL}}(\hat{\vartheta}_{\mathrm{iso}};\varphi_1) \stackrel{\mathrm{def}}{=} \int_\Omega \left(\frac{A(\hat{\vartheta}_{\mathrm{iso}})}{2} \left|\nabla\varphi_1\right|^2 + B(\hat{\vartheta}_{\mathrm{iso}}) f(\hat{\vartheta}_{\mathrm{iso}};\varphi_1) \right) \mathrm{d}\boldsymbol{x}. \tag{3.1}$$

Here, Ω is a fixed spatial domain occupied by the mixture and coefficients $A(\hat{\vartheta}_{\mathrm{iso}})$ and $B(\hat{\vartheta}_{\mathrm{iso}})$ are assumed to be positive. Recall that $\hat{\vartheta}_{\mathrm{iso}}$ is a fixed parameter, therefore we use semicolon to separate it from other variables. In particular, the only variable in the current case is a single order parameter $\varphi_1 = \varphi_1(\boldsymbol{x},t)$ which describes the composition of the mixture. We assume that $\varphi_1(\boldsymbol{x},t) \in [0,1]$ is a concentration of the first component (iron), while the corresponding concentration of the second component (nickel) is given by $\varphi_2(\boldsymbol{x},t) = 1 - \varphi_1(\boldsymbol{x},t) \in [0,1]$. It immediately follows that regions of pure iron and pure nickel are characterized by $\varphi_1 = 1$ and $\varphi_1 = 0$ respectively. We shall refer to them as to the pure phases.

The function $f : (0,\vartheta_{\mathrm{crit}}) \times \mathbb{R} \to \mathbb{R}$ in (3.1) represents a potential function with two distinct minima—one for each of the two observed phases—which are often called *wells*. A microscopically motivated double-well potential in our notation takes the form

$$f_{\log}(\hat{\vartheta}_{\mathrm{iso}};\varphi_1) = \hat{\vartheta}_{\mathrm{iso}} \left[(\varphi_1 \ln \varphi_1 + (1-\varphi_1) \ln (1-\varphi_1) \right] + 2\varphi_1(1-\varphi_1)\vartheta_{\mathrm{crit}}, \tag{3.2}$$

cf. Cahn and Hilliard (1958) and Cahn (1959). Figure 3.1a illustrates $f_{\log}$ for $\vartheta_{\mathrm{crit}} = 1$ and different values of $\hat{\vartheta}_{\mathrm{iso}}$. The minima of this function are located at the two points corresponding to $\varphi_1 = \frac{1}{2} \pm \beta_0(\hat{\vartheta}_{\mathrm{iso}})$, where $\beta_0(\hat{\vartheta}_{\mathrm{iso}})$ is the positive root of

$$\frac{\vartheta_{\mathrm{crit}}}{\hat{\vartheta}_{\mathrm{iso}}} = \frac{1}{4\beta} \ln \left(\frac{1+2\beta}{1-2\beta} \right), \tag{3.3}$$

cf. Copetti and Elliott (1992). The curve plotted in Figure 3.1b represents the right hand side of (3.3) and its intersection with an arbitrary horizontal line corresponding to $\vartheta_{\mathrm{crit}}/\hat{\vartheta}_{\mathrm{iso}} = \textit{const.} > 1$ determines the roots in question. We immediately see that the minima asymptotically approach the pure phases as $\hat{\vartheta}_{\mathrm{iso}}/\vartheta_{\mathrm{crit}} \to 0_+$.

The considered closed physical system evolves towards its equilibrium state characterized by φ_1 that minimizes the Ginzburg–Landau energy (3.1) subject to the conservative condition $\frac{\mathrm{d}}{\mathrm{d}t} \int_\Omega \varphi_1 \mathrm{d}\boldsymbol{x} = 0$. The first term on the right hand side of (3.1) is significant whenever φ_1 varies rapidly in space. Hence, its minimization gives rise to interfacial regions and accounts for capillary effects. The second term corresponds to the bulk free energy away from the interfaces. Its minimization penalizes values of φ_1 away from $\frac{1}{2} \pm \beta_0(\hat{\vartheta}_{\mathrm{iso}})$. Based on our previous observations, we can conclude that the considered mixture separates into its (almost) pure components if the quench is deep, that is, if $\hat{\vartheta}_{\mathrm{iso}} \ll \vartheta_{\mathrm{crit}}$.

The corresponding evolution equation describing the phase separation process reads

$$\frac{\partial\varphi_1}{\partial t} = \mathrm{div} \Big(M(\hat{\vartheta}_{\mathrm{iso}};\varphi_1) \, \nabla \Big(B(\hat{\vartheta}_{\mathrm{iso}}) f'(\hat{\vartheta}_{\mathrm{iso}};\varphi_1) - A(\hat{\vartheta}_{\mathrm{iso}}) \Delta\varphi_1 \Big) \Big). \tag{3.4}$$

Here, $M(\hat{\vartheta}_{\mathrm{iso}};\varphi_1) \geq 0$ ($M(\hat{\vartheta}_{\mathrm{iso}};\varphi_1) \not\equiv 0$) denotes the so-called mobility function, and by f' we denote the derivative of f with respect to φ_1. This fourth-order nonlinear PDE is known as the Cahn-Hilliard equation. Its various derivations were recently reviewed in Lee et al. (2014).

Obviously, the Cahn-Hilliard equation (3.4) can be restated in the form of two second-order equations

$$\frac{\partial \varphi_1}{\partial t} = \operatorname{div}\Big(M(\hat{\vartheta}_{\mathrm{iso}};\varphi_1)\,\nabla\mu_1\Big), \tag{3.5a}$$

$$\mu_1 = B(\hat{\vartheta}_{\mathrm{iso}})f'(\hat{\vartheta}_{\mathrm{iso}};\varphi_1) - A(\hat{\vartheta}_{\mathrm{iso}})\Delta\varphi_1. \tag{3.5b}$$

Here, μ_1 denotes the so-called generalized chemical potential. (This quantity will be formally introduced later in the current chapter.) In the standard case, the Cahn-Hilliard equation is supplemented with the homogeneous Neumann boundary conditions

$$\nabla\varphi_1 \cdot \boldsymbol{n} = 0 \qquad \text{on } \partial\Omega, \tag{3.6a}$$

$$\nabla\mu_1 \cdot \boldsymbol{n} = 0 \qquad \text{on } \partial\Omega, \tag{3.6b}$$

where $\boldsymbol{n}$ denotes the outward unit normal vector to the domain boundary $\partial\Omega$. The first condition is a natural condition associated with the variational problem of minimizing the Ginzburg–Landau energy (3.1). Due to this condition the interfaces remain perpendicular to the domain boundary. The second condition enforces zero flux across the domain boundary. In particular, this boundary condition implies

$$\frac{\mathrm{d}}{\mathrm{d}t}\int_\Omega \varphi_1 \mathrm{d}\boldsymbol{x} = \int_\Omega \frac{\partial\varphi_1}{\partial t}\mathrm{d}\boldsymbol{x} = \int_\Omega \operatorname{div}\Big(M(\hat{\vartheta}_{\mathrm{iso}};\varphi_1)\,\nabla\mu_1\Big)\mathrm{d}\boldsymbol{x} = \int_{\partial\Omega} M(\hat{\vartheta}_{\mathrm{iso}};\varphi_1)\,\nabla\mu_1\cdot\boldsymbol{n}\,\mathrm{d}\boldsymbol{s} = 0. \tag{3.7}$$

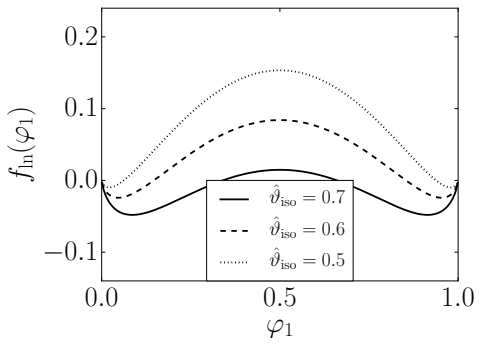

(a) The logarithmic potential $f_{\log}$ for $\vartheta_{\mathrm{crit}} = 1$ and various values of $\hat{\vartheta}_{\mathrm{iso}}$.

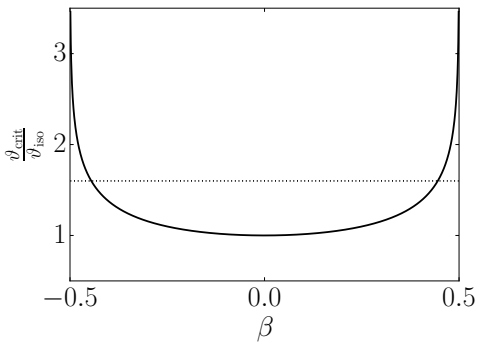

(b) Roots of (3.3) determining the minima of the logarithmic potential $f_{\log}$.

Figure 3.1: Thermodynamically consistent double-well potential.

Approximations of the logarithmic potential

The logarithmic potential (3.2) is often approximated by a quartic polynomial of the form

$$f_{\mathrm{pol}}(\hat{\vartheta}_{\mathrm{iso}};\varphi_1) = \left(\varphi_1 - \frac{1}{2} + \beta_0(\hat{\vartheta}_{\mathrm{iso}})\right)^2 \left(\varphi_1 - \frac{1}{2} - \beta_0(\hat{\vartheta}_{\mathrm{iso}})\right)^2, \tag{3.8}$$

which retains the double-well structure with the two minima at $\frac{1}{2} \pm \beta_0(\hat{\vartheta}_{\mathrm{iso}})$, taking into account their dependency on $\vartheta_{\mathrm{crit}}/\hat{\vartheta}_{\mathrm{iso}}$ via (3.3). The Cahn-Hilliard equation with this form of the potential function was extensively studied in the past from the analytical and numerical points of view; see for example Novick-Cohen and Segel (1984), Elliott (1989), Copetti and Elliott (1990).

Remark 3.3. Note that approximation of (3.2) by a quartic polynomial is relevant especially if $\hat{\vartheta}_{\mathrm{iso}} \approx \vartheta_{\mathrm{crit}}$. In cases with $\hat{\vartheta}_{\mathrm{iso}} \ll \vartheta_{\mathrm{crit}}$ it is more appropriate to use an approximation in the form of the non-smooth double-obstacle potential which was introduced by Oono and Puri (1988), see also Blowey and Elliott (1991). The setting with this type of potential function becomes more complicated, when compared to the smooth polynomial approximation, due to its non-differentiability. As a consequence, some special treatment of the double-obstacle potential is required in the applied numerical methods. For detailed information we refer to the recent work by Bosch (2016) and references therein.

Recall that the aim of the thesis is to propose models for description of flows of multi-component systems that are already found in their separate states with a multi-phase structure involving only pure phases and mixed interfaces. In principle, we are not interested in the description of the phase separation itself, but a relevant choice of the free energy will help us to keep the required structure.

Assumption 4 (Multi-phase structure)**.** *We assume that the multi-component system of our interest keeps its multi-phase structure* regardless the temperature variations. *Except mixed interfacial regions, the multi-phase structure involves only* pure phases *in the sense of spatial regions occupied by the pure components.*

Let us emphasize that the temperature variations are supposed to occur on moderate scales sufficiently below the critical temperature $\vartheta_{\mathrm{crit}}$. Following the above assumption, we simply put $\beta_0(\hat{\vartheta}_{\mathrm{iso}}) = \frac{1}{2}$ in (3.8), which brings us to the classical double-well potential in the form of the fourth-order polynomial function

$$f(\varphi_1) = \varphi_1^2 \left(1 - \varphi_1\right)^2. \tag{3.9}$$

Now we are ready to associate the coefficients A, B in (3.1) with the two positive parameters, ε and σ_{12}, where the fist one represents the approximate interface thickness and the second one denotes the surface tension between the components. Note that the surface tension is the physical quantity which generally depends on the temperature, see for example Adam (1941), while ε is a numerical parameter

that is considered to be fixed in the applications. It can be shown that[2]

$$A(\hat{\vartheta}_{\mathrm{iso}}) = a\sigma_{12}(\hat{\vartheta}_{\mathrm{iso}})\varepsilon, \qquad B(\hat{\vartheta}_{\mathrm{iso}}) = b\sigma_{12}(\hat{\vartheta}_{\mathrm{iso}})\varepsilon^{-1}, \tag{3.10a}$$

where a and b are positive constants given by the shape of the potential function. In particular, the fourth-order polynomial potential (3.9) yields

$$a = \frac{\max_{[0,1]}\sqrt{f}}{\int_0^1 \sqrt{f}} = \frac{3}{2}, \qquad b = \frac{1}{2\max_{[0,1]}\sqrt{f}\int_0^1 \sqrt{f}} = 12. \tag{3.10b}$$

Transition to Helmholtz free energy

The total free energy Ψ of our considered system at time t is given by integrating the specific Helmholtz free energy multiplied by the total density, namely

$$\Psi(t) = \int_\Omega \varrho\psi(\vartheta, \varrho, \varphi_1, \nabla\varphi_1)\mathrm{d}\boldsymbol{x}. \tag{3.11}$$

Let us fix the temperature to a uniform temperature $\hat{\vartheta}_{\mathrm{iso}}$ as above. By comparing the integrands in (3.1) and (3.11) we obtain the relation

$$\psi(\hat{\vartheta}_{\mathrm{iso}}; \varrho, \varphi_1, \nabla\varphi_1) = \frac{1}{\varrho}\left(\frac{A(\hat{\vartheta}_{\mathrm{iso}})}{2}\left|\nabla\varphi_1\right|^2 + B(\hat{\vartheta}_{\mathrm{iso}})f(\hat{\vartheta}_{\mathrm{iso}}; \varphi_1)\right), \tag{3.12}$$

which gives us the basic idea about the structure of the constitutive assumption for the specific Helmholtz free energy. Our further objective is to generalize the above relation to allow for temperature variations, both spatial and temporal.

3.1.2 Non-isothermal extension of double-well potential

Compressible binary systems

In case of compressible binary systems we accept the constitutive assumption of the form

$$\psi(\vartheta, \varrho, c_1, \nabla c_1) = \frac{1}{2}\epsilon\sigma_{12}(\vartheta)\left|\nabla c_1\right|^2 + \psi_{\mathrm{th}}(\vartheta, \varrho, c_1), \tag{3.13}$$

which mimics the *ansatz* used in (Lowengrub and Truskinovsky, 1998, Eq. (3.31)). The first term on the right hand side of (3.13) generalizes the corresponding term in (3.12) by taking into account the temperature-dependent surface tension, together with a constant parameter ϵ representing the typical length scale for the interface thickness divided by a characteristic density, cf. (3.10a). Note that the explicit presence of the variable density ϱ is suppressed in this term, so that the thermodynamic pressure p_{th} is given by

$$p_{\mathrm{th}} = \varrho^2\frac{\partial\psi_{\mathrm{th}}}{\partial\varrho}, \tag{3.14}$$

[2]The expressions for coefficients A, B can be obtained by analyzing the one-dimensional equilibrium profile with a single interface on the whole real axis, see (Boyer and Minjeaud, 2014, Appendix A).

cf. (2.89). The function ψ_{th} is assumed to reduce to a standard form—applicable in the context of the Navier–Stokes–Fourier (NSF) equations—if only one component is present in our considered physical system. (We will not discuss the detailed structure of ψ_{th} as the study of compressible models is not of our primary interest in this thesis.)

Incompressible binary systems

In case of incompressible binary systems we suggest to work with the constitutive assumption of the form

$$\psi(\vartheta, \varrho, \phi_1, \nabla\phi_1) = \frac{1}{\varrho}\,\widetilde{\psi}(\vartheta, \phi_1, \nabla\phi_1). \tag{3.15}$$

Recall that the density ϱ is in this case given by $\varrho(\phi_1) = (\hat{\varrho}_1 - \hat{\varrho}_2)\phi_1 + \hat{\varrho}_2$, see Lemma 2.2. It remains to specify the Helmholtz free energy density $\widetilde{\psi}$. In the classical isothermal setting, with a fixed uniform temperature $\hat{\vartheta}_{\mathrm{iso}}$, we shall require that $\widetilde{\psi}$ reduces to

$$\widetilde{\psi}(\hat{\vartheta}_{\mathrm{iso}}; \phi_1, \nabla\phi_1) = \frac{a\varepsilon}{2}\sigma_{12}(\hat{\vartheta}_{\mathrm{iso}})\,|\nabla\phi_1|^2 + \frac{b}{\varepsilon}\sigma_{12}(\hat{\vartheta}_{\mathrm{iso}})f(\phi_1), \tag{3.16}$$

with f given by (3.9) and a, b given by (3.10b). Recall that this particular choice of the double-well potential is consistent with the Assumption 4. The corresponding generalization to the non-isothermal setting with variable temperature field reads

$$\widetilde{\psi}(\vartheta, \phi_1, \nabla\phi_1) = \frac{a\varepsilon}{2}\sigma_{12}(\vartheta)\,|\nabla\phi_1|^2 + \widetilde{\psi}_0(\vartheta, \phi_1). \tag{3.17}$$

The function $\widetilde{\psi}_0$ in the above relation must not violate the Assumption 4. It means that the separation of the system into pure components—characterized by $\phi_1 = 0$ and $\phi_1 = 1$—must remain the most stable state irrespective of the actual value of the temperature. Note that it does not necessarily mean that $\widetilde{\psi}_0$ must have its local minima at $\phi_1 = 0$ and $\phi_1 = 1$. It must be convex at these points, namely

$$\left.\frac{\partial^2\widetilde{\psi}_0}{\partial\phi_1^2}\right|_{\phi_1=0} > 0, \qquad \left.\frac{\partial^2\widetilde{\psi}_0}{\partial\phi_1^2}\right|_{\phi_1=1} > 0, \tag{3.18a}$$

and any other admissible state satisfying VAC must be energetically less convenient[3]. Another restriction on the choice of $\widetilde{\psi}_0$ arises from the definition of the specific heat at constant volume $\mathrm{c_v}$, see (2.90), which can be rewritten in the current notation as

$$\mathrm{c_v} = -\frac{\vartheta}{\varrho}\frac{\partial^2\widetilde{\psi}}{\partial\vartheta^2} = -\frac{\vartheta}{\varrho}\left(\frac{a\varepsilon}{2}\frac{\mathrm{d}^2\sigma_{12}}{\mathrm{d}\vartheta^2}\,|\nabla\phi_1|^2 + \frac{\partial^2\widetilde{\psi}_0}{\partial\vartheta^2}\right).$$

[3]In Figure 3.2b, we observe that each plot representing the free energy density $\widetilde{\psi}_0$, for our specific choice (3.19) at a fixed value of ϑ, lies above the double tangent which represents the energy value in the state with two pure components as it goes through the pair of points $[1, \widetilde{\psi}_1(\vartheta)]$ and $[0, \widetilde{\psi}_2(\vartheta)]$.

Clearly, it is natural to assume that the value of c_v in the pure phases coincides with the specific heat of individual components. This is guaranteed by requiring

$$\left.\frac{\partial^2\widetilde{\psi}_0}{\partial\vartheta^2}\right|_{\phi_1=1} = -\frac{\hat{\varrho}_1}{\vartheta}\,\hat{c}_{v,1}, \qquad \left.\frac{\partial^2\widetilde{\psi}_0}{\partial\vartheta^2}\right|_{\phi_1=0} = -\frac{\hat{\varrho}_2}{\vartheta}\,\hat{c}_{v,2}, \tag{3.18b}$$

where $\hat{c}_{v,1}$ and $\hat{c}_{v,2}$ are assumed to be constants for simplicity. Last but not least, we must ensure that (3.17) reduces to (3.16), meaning that $\widetilde{\psi}_0$ must satisfy

$$\widetilde{\psi}_0\Big|_{\vartheta=\hat{\vartheta}_{iso}} = \frac{b}{\varepsilon}\sigma_{12}(\hat{\vartheta}_{iso})f(\phi_1). \tag{3.18c}$$

We suggest to work with $\widetilde{\psi}_0$ in the form

$$\widetilde{\psi}_0(\vartheta,\phi_1) = \frac{b}{\varepsilon}\sigma_{12}(\hat{\vartheta}_{iso})f(\phi_1) + (\widetilde{\psi}_1(\vartheta) - \widetilde{\psi}_2(\vartheta))\phi_1 + \widetilde{\psi}_2(\vartheta), \tag{3.19}$$

where $\widetilde{\psi}_1$ and $\widetilde{\psi}_2$ represent free energy densities in the bulk of the domains occupied by the pure components. Note that $\widetilde{\psi}_0$ in the above form automatically satisfies (3.18a). With respect to (3.18b), we see that $\widetilde{\psi}_i$ (for $i \in \{1,2\}$) must be a solution of the second-order ordinary differential equation (ODE)

$$\frac{\mathrm{d}^2\widetilde{\psi}_i}{\mathrm{d}\vartheta^2} = -\frac{\hat{\varrho}_i}{\vartheta}\hat{c}_{v,i}. \tag{3.20}$$

We choose the solution satisfying the initial conditions

$$\widetilde{\psi}_i\Big|_{\vartheta=\hat{\vartheta}_{iso}} = 0, \qquad \left.\frac{\mathrm{d}\widetilde{\psi}_i}{\mathrm{d}\vartheta}\right|_{\vartheta=\hat{\vartheta}_{iso}} = 0, \tag{3.21}$$

where the first one implies (3.18c), while the second one fixes the entropy of the pure components. It immediately follows that

$$\widetilde{\psi}_i(\vartheta) = -\hat{\varrho}_i\hat{c}_{v,i}\left[\ln\left(\frac{\vartheta}{\hat{\vartheta}_{iso}}\right) - \frac{\vartheta-\hat{\vartheta}_{iso}}{\vartheta}\right]\vartheta, \tag{3.22}$$

see Figure 3.2a.

Remark 3.4. Both conditions in (3.21) are admissible from the point of view of the classical thermodynamics, which is primarily concerned with changes in thermodynamic quantities—like the Helmholtz free energy or the entropy—and not their absolute values.

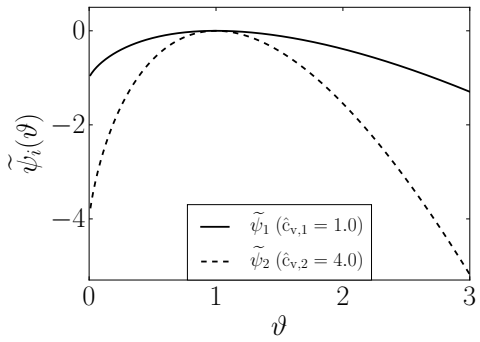

(a) The Helmholtz free energy density (3.22) for individual components with matching densities $\hat{\varrho}_1 = \hat{\varrho}_2 = 1$, but different values of the specific heat at constant volume.

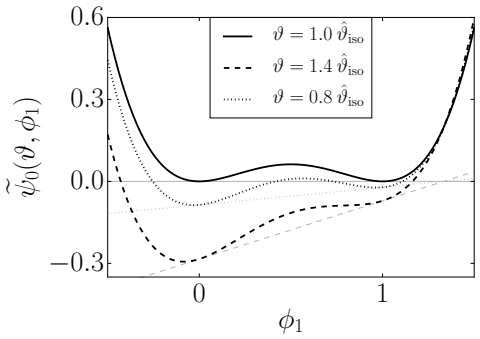

(b) The extended double-well potential (3.19) with $\widetilde{\psi}_1, \widetilde{\psi}_2$ depicted in (a) and $\varepsilon = \sigma_{12} = b = 1$. The full line corresponds to the double-well potential (3.9) which is often used in the isothermal setting.

Figure 3.2: Non-isothermal extension of the polynomial double-well potential for an incompressible system consisting of two components with $\hat{c}_{v,1} = 1$ and $\hat{c}_{v,2} = 4$. The reference temperature is set to $\hat{\vartheta}_{iso} = 1$.

3.1.3 Constitutive assumption for compressible systems

We assume that the specific Helmholtz free energy ψ, for a multi-component system consisting of N compressible components, is a given function of the form

$$\psi\left(\vartheta, \varrho, \boldsymbol{c}, \nabla \boldsymbol{c}\right) = \frac{\epsilon}{4} \sum_{i,j=1}^{N-1} \lambda_{ij}(\vartheta)\, \nabla c_i \cdot \nabla c_j + \psi_{\text{th}}(\vartheta, \varrho, \boldsymbol{c}), \tag{3.23}$$

which is required to reduce to (3.13) if $N = 2$. Here, λ_{ij} are temperature-dependent entries of a symmetric positive definite (SPD) matrix $\boldsymbol{\Lambda} \in \mathbb{R}^{(N-1)\times(N-1)}$. These so-called mixing surface energy coefficients are related to pairwise surface tensions. The required properties of the matrix $\boldsymbol{\Lambda}$ are important from both physical and mathematical point of view. We defer further discussion about the admissible choice of $\boldsymbol{\Lambda}$ to Chapter 4.

In addition to thermodynamic quantities introduced in Section 2.4, we define

$$\mu_i^c \stackrel{\text{def}}{=} \frac{\partial \psi}{\partial c_i}, \qquad\qquad \widetilde{\boldsymbol{\varsigma}}_i^c \stackrel{\text{def}}{=} \varrho \frac{\partial \psi}{\partial \nabla c_i}, \tag{3.24}$$

where μ_i^c is the specific chemical potential of the i-th component, while $\widetilde{\boldsymbol{\varsigma}}_i^c$ may be interpreted as the generalized surface energy associated with the variation of the mass fraction of the i-th component.

3.1.4 Constitutive assumption for incompressible systems

We assume that the specific Helmholtz free energy ψ, for multi-component systems consisting of N incompressible components, is a given function of the form

$$\psi(\vartheta, \varrho, \boldsymbol{\phi}, \nabla\boldsymbol{\phi}) = \frac{1}{\varrho}\widetilde{\psi}\,(\vartheta, \boldsymbol{\phi}, \nabla\boldsymbol{\phi})\,, \tag{3.25}$$

with $\varrho = \varrho(\boldsymbol{\phi})$ given by (2.10a). Similarly as in the previous case of compressible systems, the Helmholtz free energy density $\widetilde{\psi}$ is assumed to take the form

$$\widetilde{\psi}(\vartheta, \boldsymbol{\phi}, \nabla\boldsymbol{\phi}) = \frac{a\varepsilon}{4}\sum_{i,j=1}^{N-1}\lambda_{ij}(\vartheta)\,\nabla\phi_i\cdot\nabla\phi_j + \widetilde{\psi}_0(\vartheta, \boldsymbol{\phi}), \tag{3.26}$$

and it is required to reduce to (3.17) if $N = 2$. Based on the non-isothermal extension of the double-well potential, which has been proposed in Section 3.1.2, we further suggest to work with

$$\widetilde{\psi}_0(\vartheta, \boldsymbol{\phi}) = \frac{b}{\varepsilon}F(\boldsymbol{\phi}) + \sum_{i=1}^{N-1}(\widetilde{\psi}_i(\vartheta) - \widetilde{\psi}_N(\vartheta))\phi_i + \widetilde{\psi}_N(\vartheta). \tag{3.27}$$

Here, F is a potential function with multi-well structure which appropriately extends the double-well potential (3.9), and $\widetilde{\psi}_i$ corresponds to the Helmholtz free energy density of the i-th component given by (3.22). It is straightforward to verify that the specific heat at constant volume $\mathrm{c_v}$, see (2.90), reduces to

$$\mathrm{c_v}(\boldsymbol{\phi}) = \frac{1}{\varrho(\boldsymbol{\phi})}\left(\sum_{i=1}^{N-1}(\hat{\varrho}_i\hat{\mathrm{c}}_{\mathrm{v},i} - \hat{\varrho}_N\hat{\mathrm{c}}_{\mathrm{v},N})\phi_i + \hat{\varrho}_N\hat{\mathrm{c}}_{\mathrm{v},N}\right), \tag{3.28}$$

provided that $\widetilde{\psi}_i$ are given by (3.22) and λ_{ij} in (3.26) are independent of the temperature. It is worth noting that the previous formula is of the same structure as the analogous relation for the total density (2.10a). The precise specification of λ_{ij} and F will be discussed in Section 4.1.

In contrast to compressible multi-component systems, the density ϱ in (3.25) is not a classical state variable and the thermodynamic pressure p_{th} loses its original meaning. Indeed, by virtue of (2.89) we obtain the formal relation

$$p_{\mathrm{th}} = -\widetilde{\psi}, \tag{3.29}$$

which will be used in the forthcoming derivations. We also define

$$\widetilde{\mu}_i^{\,\phi} \stackrel{\mathrm{def}}{=} \frac{\partial\widetilde{\psi}}{\partial\phi_i}, \qquad\qquad \widetilde{\boldsymbol{\varsigma}}_i^{\,\phi} \stackrel{\mathrm{def}}{=} \frac{\partial\widetilde{\psi}}{\partial\nabla\phi_i}, \tag{3.30}$$

where $\widetilde{\mu}_i^{\,\phi}$ denotes the chemical potential of the i-th component and $\widetilde{\boldsymbol{\varsigma}}_i^{\,\phi}$ is the generalized surface energy associated with the variation of the volume fraction of the i-th component.

3.2 Fully-compressible model

3.2.1 Identification of the entropy production

Applying the material time derivative to $\psi = \psi(\vartheta, \varrho, \boldsymbol{c}, \nabla \boldsymbol{c})$, see (3.23), we get

$$\frac{\mathrm{d}\psi}{\mathrm{d}t} = -\eta \frac{\mathrm{d}\vartheta}{\mathrm{d}t} + \frac{p_{\mathrm{th}}}{\varrho^2}\frac{\mathrm{d}\varrho}{\mathrm{d}t} + \sum_{i=1}^{N-1}\left(\mu_i^c \frac{\mathrm{d}c_i}{\mathrm{d}t} + \frac{1}{\varrho}\widetilde{\boldsymbol{\varsigma}}_i^c \cdot \frac{\mathrm{d}\nabla c_i}{\mathrm{d}t}\right), \tag{3.31}$$

where we have used the notation introduced in (2.89) and (3.24). Similarly, we apply the material time derivative to (2.87) and substitute the result to the left hand side of (3.31). Doing so, we arrive to the identity

$$\frac{\mathrm{d}e}{\mathrm{d}t} - \vartheta \frac{\mathrm{d}\eta}{\mathrm{d}t} = \frac{p_{\mathrm{th}}}{\varrho^2}\frac{\mathrm{d}\varrho}{\mathrm{d}t} + \sum_{i=1}^{N-1}\left(\mu_i^c \frac{\mathrm{d}c_i}{\mathrm{d}t} + \frac{1}{\varrho}\widetilde{\boldsymbol{\varsigma}}_i^c \cdot \frac{\mathrm{d}\nabla c_i}{\mathrm{d}t}\right). \tag{3.32}$$

Next, we multiply (3.32) by ϱ, rearrange the terms and substitute from the system of equations (2.93). We obtain the evolution equation for the entropy in the form

$$\begin{aligned}\varrho\vartheta \frac{\mathrm{d}\eta}{\mathrm{d}t} = \mathbb{T}^\delta : \mathbb{D}^\delta + (m + p_{\mathrm{th}}) \operatorname{div} \boldsymbol{v} - \operatorname{div} \boldsymbol{q}_e + \sum_{i=1}^{N-1} \mu_i^c \operatorname{div} \boldsymbol{\jmath}_i \\ + \sum_{i=1}^{N-1} \widetilde{\boldsymbol{\varsigma}}_i^c \cdot \left(\left[\nabla \boldsymbol{v}^\top\right] \nabla c_i + \nabla\left(\frac{1}{\varrho}\operatorname{div} \boldsymbol{\jmath}_i\right)\right).\end{aligned} \tag{3.33}$$

The objective is to identify the entropy flux $\boldsymbol{q}_\eta$ and the entropy production term ξ in this equation, cf. (2.93f). The summation on the second line in (3.33) can be rewritten using the identities $\widetilde{\boldsymbol{\varsigma}}_i^c \cdot \left[\nabla \boldsymbol{v}^\top\right] \nabla c_i = (\widetilde{\boldsymbol{\varsigma}}_i^c \otimes \nabla c_i) : \nabla \boldsymbol{v}^\top$ and

$$\widetilde{\boldsymbol{\varsigma}}_i^c \cdot \nabla\left(\frac{1}{\varrho}\operatorname{div} \boldsymbol{\jmath}_i\right) = \operatorname{div}\left(\frac{1}{\varrho}(\operatorname{div} \boldsymbol{\jmath}_i)\,\widetilde{\boldsymbol{\varsigma}}_i^c\right) - \frac{1}{\varrho}(\operatorname{div} \boldsymbol{\jmath}_i)\operatorname{div} \widetilde{\boldsymbol{\varsigma}}_i^c.$$

Motivated by these manipulations we introduce the notation

$$\mu_i \stackrel{\mathrm{def}}{=} \mu_i^c - \frac{1}{\varrho}\operatorname{div} \widetilde{\boldsymbol{\varsigma}}_i^c, \tag{3.34}$$

for the specific generalized chemical potential of the i-th component, and

$$\mathbb{T}_{\mathrm{DI}} \stackrel{\mathrm{def}}{=} \sum_{i=1}^{N-1} \widetilde{\boldsymbol{\varsigma}}_i^c \otimes \nabla c_i, \tag{3.35}$$

for the complementary stress tensor which represents the contribution to stress coming from the diffuse interface. Note that $\mathbb{T}_{\mathrm{DI}}$ is symmetric due to our particular choice of the constitutive assumption (3.23) with the symmetric matrix $\boldsymbol{\Lambda} = [\lambda_{ij}]_{(N-1)\times(N-1)}$. In what follows, we use the decomposition $\mathbb{T}_{\mathrm{DI}} = m_{\mathrm{DI}}\mathbb{I} + \mathbb{T}_{\mathrm{DI}}^\delta$

with the spherical part given by $m_{\mathrm{DI}} = \frac{1}{3}\sum_{i=1}^{N-1} \widetilde{\boldsymbol{\varsigma}}_i^c \cdot \nabla c_i$. With the above definitions we can rewrite (3.33) as

$$\varrho\vartheta\frac{\mathrm{d}\eta}{\mathrm{d}t} = \left(\mathbb{T} + \mathbb{T}_{\mathrm{DI}}\right)^{\delta} : \mathbb{D}^{\delta} + \left(m + m_{\mathrm{DI}} + p_{\mathrm{th}}\right)\operatorname{div}\boldsymbol{v} + \sum_{i=1}^{N-1}\mu_i \operatorname{div}\boldsymbol{\jmath}_i - \operatorname{div}\left(\boldsymbol{q}_e - \frac{1}{\varrho}\sum_{i=1}^{N-1}\left(\operatorname{div}\boldsymbol{\jmath}_i\right)\widetilde{\boldsymbol{\varsigma}}_i^c\right). \quad (3.36)$$

The straightforward use of the formula $\mu_i \operatorname{div}\boldsymbol{\jmath}_i = \operatorname{div}\left(\mu_i\boldsymbol{\jmath}_i\right) - \boldsymbol{\jmath}_i \cdot \nabla\mu_i$ yields

$$\varrho\vartheta\frac{\mathrm{d}\eta}{\mathrm{d}t} = \left(\mathbb{T} + \mathbb{T}_{\mathrm{DI}}\right)^{\delta} : \mathbb{D}^{\delta} + \left(m + m_{\mathrm{DI}} + p_{\mathrm{th}}\right)\operatorname{div}\boldsymbol{v} - \sum_{i=1}^{N-1}\boldsymbol{\jmath}_i \cdot \nabla\mu_i - \operatorname{div}\left(\boldsymbol{q}_e + \boldsymbol{q}_{\mathrm{DI}}\right), \quad (3.37)$$

where we have introduced the complementary energy flux

$$\boldsymbol{q}_{\mathrm{DI}} \overset{\mathrm{def}}{=} -\sum_{i=1}^{N-1}\left(\mu_i\boldsymbol{\jmath}_i + \frac{1}{\varrho}\left(\operatorname{div}\boldsymbol{\jmath}_i\right)\widetilde{\boldsymbol{\varsigma}}_i^c\right). \quad (3.38)$$

In the final step, we first divide equation (3.37) by ϑ and then we use the identity $\frac{1}{\vartheta}\operatorname{div}\left(\boldsymbol{q}_e + \boldsymbol{q}_{\mathrm{DI}}\right) = \operatorname{div}\left(\frac{1}{\vartheta}\left(\boldsymbol{q}_e + \boldsymbol{q}_{\mathrm{DI}}\right)\right) + \frac{1}{\vartheta^2}\left(\boldsymbol{q}_e + \boldsymbol{q}_{\mathrm{DI}}\right)\cdot\nabla\vartheta$ to obtain the evolution equation for the entropy in the form

$$\varrho\frac{\mathrm{d}\eta}{\mathrm{d}t} = \frac{1}{\vartheta}\left[\left(\mathbb{T} + \mathbb{T}_{\mathrm{DI}}\right)^{\delta} : \mathbb{D}^{\delta} + \left(m + m_{\mathrm{DI}} + p_{\mathrm{th}}\right)\operatorname{div}\boldsymbol{v} - \sum_{i=1}^{N-1}\boldsymbol{\jmath}_i \cdot \nabla\mu_i - \left(\frac{\boldsymbol{q}_e + \boldsymbol{q}_{\mathrm{DI}}}{\vartheta}\right)\cdot\nabla\vartheta\right] - \operatorname{div}\left(\frac{\boldsymbol{q}_e + \boldsymbol{q}_{\mathrm{DI}}}{\vartheta}\right). \quad (3.39)$$

Now, if we compare (2.93f) and (3.39), we immediately see that the entropy flux corresponds to

$$\boldsymbol{q}_\eta = \frac{\boldsymbol{q}_e + \boldsymbol{q}_{\mathrm{DI}}}{\vartheta}, \quad (3.40)$$

and the entropy production $\xi = \frac{\zeta}{\vartheta}$ is given by

$$\zeta = \left(\mathbb{T} + \mathbb{T}_{\mathrm{DI}}\right)^{\delta} : \mathbb{D}^{\delta} + \left(m + m_{\mathrm{DI}} + p_{\mathrm{th}}\right)\operatorname{div}\boldsymbol{v} - \sum_{i=1}^{N-1}\boldsymbol{\jmath}_i \cdot \nabla\mu_i - \left(\frac{\boldsymbol{q}_e + \boldsymbol{q}_{\mathrm{DI}}}{\vartheta}\right)\cdot\nabla\vartheta. \quad (3.41)$$

3.2.2 Constitutive relations

We assume that each term on the right hand side of (3.41) represents an independent dissipation process described as a product of thermodynamic affinity and corresponding thermodynamic flux. This is a legitimate assumption as we have

eliminated one of the N diffusive fluxes at the very beginning of the derivation of (3.41). (Recall that the mass diffusive fluxes are not independent due to the first constraint in (2.20).)

Now we are ready to fix the constitutive relations. We simply postulate the entropy production to be piecewise quadratic function of its thermodynamic affinities in the form[4]

$$\xi = \frac{1}{\vartheta}\left[2\nu\left|\mathbb{D}^{\delta}\right|^2 + \tilde{\upsilon}\,(\operatorname{div}\boldsymbol{v})^2 + \sum_{i=1}^{N-1} M_i\,|\nabla\mu_i|^2 + \frac{\kappa}{\vartheta}\,|\nabla\vartheta|^2\right]. \tag{3.42}$$

Provided that the coefficients $\nu, \tilde{\upsilon}, M_i$ and κ are non-negative functions of the aspiring primitive quantities $\vartheta, \varrho, \boldsymbol{c}$ and possibly $\boldsymbol{v}$ (through its symmetric gradient), we obtain a material model which automatically satisfies the second law of thermodynamics due to non-negativity of the entropy production. By comparing (3.41) and (3.42) we obtain the constitutive relations

$$\left(\mathbb{T} + \mathbb{T}_{\mathrm{DI}}\right)^{\delta} = 2\nu\mathbb{D}^{\delta}, \tag{3.43a}$$

$$m + m_{\mathrm{DI}} + p_{\mathrm{th}} = \tilde{\upsilon}\operatorname{div}\boldsymbol{v}, \tag{3.43b}$$

$$\boldsymbol{\jmath}_i = -M_i\,\nabla\mu_i, \quad i = 1,\dots,N-1, \tag{3.43c}$$

$$\boldsymbol{q}_e + \boldsymbol{q}_{\mathrm{DI}} = -\kappa\,\nabla\vartheta. \tag{3.43d}$$

If we use a more traditional notation $\upsilon = \tilde{\upsilon} - 2\nu/3$, we can rewrite the above constitutive relations to take the form

$$\mathbb{T} = (-p_{\mathrm{th}} + \upsilon\operatorname{div}\boldsymbol{v})\,\mathbb{I} + 2\nu\mathbb{D} - \sum_{i=1}^{N-1}\widetilde{\boldsymbol{\varsigma}}_i^{c}\otimes\nabla c_i, \tag{3.44a}$$

$$\boldsymbol{\jmath}_i = -M_i\,\nabla\mu_i, \quad i = 1,\dots,N-1, \tag{3.44b}$$

$$\boldsymbol{q}_e = -\kappa\,\nabla\vartheta - \sum_{i=1}^{N}\left(\frac{1}{2}M_i\,\nabla\mu_i^2 + \frac{1}{\varrho}\operatorname{div}\left(M_i\,\nabla\mu_i\right)\widetilde{\boldsymbol{\varsigma}}_i^{c}\right). \tag{3.44c}$$

The remaining diffusive flux $\boldsymbol{\jmath}_N$ can be obtained, if needed, as $\boldsymbol{\jmath}_N = -\sum_{i=1}^{N-1}\boldsymbol{\jmath}_i$.

Remark 3.5. Heida et al. (2012b) in their work present the derivation of (3.44) based on the assumption of the maximization of the entropy production rate and on the alternative form of the entropy production *ansatz*

$$\xi = \frac{1}{\vartheta}\left[\frac{1}{2\nu}\left|\left(\mathbb{T} + \mathbb{T}_{\mathrm{DI}}\right)^{\delta}\right|^2 + \frac{1}{\tilde{\upsilon}}(m + m_{\mathrm{DI}} + p_{\mathrm{th}})^2 + \frac{1}{\kappa}\left|\boldsymbol{q}_e + \boldsymbol{q}_{\mathrm{DI}}\right|^2 + \sum_{i=1}^{N-1}\frac{1}{M_i}\left|\boldsymbol{\jmath}_i\right|^2\right], \tag{3.45}$$

where the coefficients $\nu, \tilde{\upsilon}, M_i$ and κ are considered to be strictly positive.

[4]The norm of an arbitrary second order tensor $\mathbb{A}$ is defined by $|\mathbb{A}|^2 = \mathbb{A} : \mathbb{A}$.

3.2.3 Evolution equation for the temperature

Having the expression for the entropy production in the form (3.42) we can return back to the evolution equation for the entropy. The aim is to rewrite this equation as an evolution equation for the temperature.

From the discussion in Section 2.4 we already know that the entropy can be expressed as a function of the temperature and other state variables, namely $\eta = \eta\left(\vartheta, \varrho, \boldsymbol{c}, \nabla \boldsymbol{c}\right)$. Using the chain rule we see that

$$\frac{\mathrm{d}\eta}{\mathrm{d}t} = \frac{\partial \eta}{\partial \vartheta}\frac{\mathrm{d}\vartheta}{\mathrm{d}t} + \frac{\partial \eta}{\partial \varrho}\frac{\mathrm{d}\varrho}{\mathrm{d}t} + \sum_{i=1}^{N-1}\left(\frac{\partial \eta}{\partial c_i}\frac{\mathrm{d}c_i}{\mathrm{d}t} + \frac{\partial \eta}{\partial \nabla c_i}\cdot\frac{\mathrm{d}\nabla c_i}{\mathrm{d}t}\right), \tag{3.46}$$

which can be further rewritten solely in terms of the Helmholtz free energy and its derivatives as

$$\frac{\mathrm{d}\eta}{\mathrm{d}t} = -\frac{\partial^2 \psi}{\partial \vartheta^2}\frac{\mathrm{d}\vartheta}{\mathrm{d}t} - \frac{\partial^2 \psi}{\partial \varrho \partial \vartheta}\frac{\mathrm{d}\varrho}{\mathrm{d}t} - \sum_{i=1}^{N-1}\left(\frac{\partial^2 \psi}{\partial c_i \partial \vartheta}\frac{\mathrm{d}c_i}{\mathrm{d}t} + \frac{\partial^2 \psi}{\partial \nabla c_i \partial \vartheta}\cdot\frac{\mathrm{d}\nabla c_i}{\mathrm{d}t}\right). \tag{3.47}$$

(Recall that $\eta = -\frac{\partial \psi}{\partial \vartheta}$, see (2.89).)

Using the interchangeability of the second derivatives it is possible to rewrite the last formula as

$$\frac{\mathrm{d}\eta}{\mathrm{d}t} = \frac{\mathrm{c_v}}{\vartheta}\frac{\mathrm{d}\vartheta}{\mathrm{d}t} - \frac{1}{\varrho^2}\frac{\partial p_{\mathrm{th}}}{\partial \vartheta}\frac{\mathrm{d}\varrho}{\mathrm{d}t} - \sum_{i=1}^{N-1}\left(\frac{\partial \mu_i^c}{\partial \vartheta}\frac{\mathrm{d}c_i}{\mathrm{d}t} + \frac{1}{\varrho}\frac{\partial \widetilde{\boldsymbol{\varsigma}}_i^c}{\partial \vartheta}\cdot\frac{\mathrm{d}\nabla c_i}{\mathrm{d}t}\right). \tag{3.48}$$

Next, we multiply (3.48) by $\varrho\vartheta$ and we substitute there once again from the system of governing equations (2.93). After some algebraic manipulations, we obtain

$$\begin{aligned}\varrho\vartheta\frac{\mathrm{d}\eta}{\mathrm{d}t} = \varrho \mathrm{c_v}\frac{\mathrm{d}\vartheta}{\mathrm{d}t} + \vartheta\frac{\partial p_{\mathrm{th}}}{\partial \vartheta}\operatorname{div}\boldsymbol{v} + \mathbb{T}_{\mathrm{DI},\vartheta} : \nabla \boldsymbol{v}^{\top} \\ + \sum_{i=1}^{N-1}\mu_{i,\vartheta}\operatorname{div}\boldsymbol{\jmath}_i + \operatorname{div}\left(\frac{\vartheta}{\varrho}\sum_{i=1}^{N-1}\left(\operatorname{div}\boldsymbol{\jmath}_i\right)\frac{\partial \widetilde{\boldsymbol{\varsigma}}_i^c}{\partial \vartheta}\right),\end{aligned} \tag{3.49}$$

where we have introduced the notation

$$\mu_{i,\vartheta} \overset{\mathrm{def}}{=} \vartheta\frac{\partial \mu_i^c}{\partial \vartheta} - \frac{1}{\varrho}\operatorname{div}\left(\vartheta\frac{\partial \widetilde{\boldsymbol{\varsigma}}_i^c}{\partial \vartheta}\right), \qquad \mathbb{T}_{\mathrm{DI},\vartheta} \overset{\mathrm{def}}{=} \sum_{i=1}^{N-1}\vartheta\frac{\partial \widetilde{\boldsymbol{\varsigma}}_i^c}{\partial \vartheta}\otimes\nabla c_i. \tag{3.50}$$

Now we are ready to put all the pieces together. In Section 3.2.2 we have derived the evolution equation for the entropy in the form

$$\varrho\frac{\mathrm{d}\eta}{\mathrm{d}t} = \operatorname{div}\left(\frac{\kappa\nabla\vartheta}{\vartheta}\right) + \xi, \tag{3.51}$$

where ξ is given by (3.42). Combining (3.49) with (3.43c) and (3.51), we arrive to the evolution equation

$$\begin{aligned}\varrho \mathrm{c_v}\frac{\mathrm{d}\vartheta}{\mathrm{d}t} = 2\nu\mathbb{D}^\delta : \mathbb{D}^\delta + \tilde{\upsilon}(\operatorname{div}\boldsymbol{v})^2 + \sum_{i=1}^{N-1} M_i \left|\nabla\mu_i\right|^2 \\ - \vartheta\frac{\partial p_{\mathrm{th}}}{\partial\vartheta}\operatorname{div}\boldsymbol{v} - \mathbb{T}_{\mathrm{DI},\vartheta} : \nabla\boldsymbol{v}^\top + \sum_{i=1}^{N-1}\mu_{i,\vartheta}\operatorname{div}\left(M_i\,\nabla\mu_i\right) \\ + \operatorname{div}\left(\kappa\,\nabla\vartheta + \frac{\vartheta}{\varrho}\sum_{i=1}^{N-1}\frac{\partial\widetilde{\boldsymbol{\varsigma}}_i^c}{\partial\vartheta}\operatorname{div}\left(M_i\,\nabla\mu_i\right)\right). \quad (3.52)\end{aligned}$$

Since the tensor $\mathbb{T}_{\mathrm{DI},\vartheta}$ is symmetric, see (3.23), we can manipulate the last equation into its final form

$$\begin{aligned}\varrho \mathrm{c_v}\frac{\mathrm{d}\vartheta}{\mathrm{d}t} = (2\nu\mathbb{D} - \mathbb{T}_{\mathrm{DI},\vartheta}) : \mathbb{D} + \sum_{i=1}^{N-1} M_i \left|\nabla\mu_i\right|^2 \\ + \left(\upsilon\operatorname{div}\boldsymbol{v} - \vartheta\frac{\partial p_{\mathrm{th}}}{\partial\vartheta}\right)\operatorname{div}\boldsymbol{v} + \sum_{i=1}^{N-1}\mu_{i,\vartheta}\operatorname{div}\left(M_i\,\nabla\mu_i\right) \\ + \operatorname{div}\left(\kappa\,\nabla\vartheta + \frac{\vartheta}{\varrho}\sum_{i=1}^{N-1}\operatorname{div}\left(M_i\,\nabla\mu_i\right)\frac{\partial\widetilde{\boldsymbol{\varsigma}}_i^c}{\partial\vartheta}\right). \quad (3.53)\end{aligned}$$

3.2.4 Summary: FC-CHNSF model

Let us recapitulate the full system of governing equations for a compressible heat conducting fluid-like mixture consisting of N components. The specific Helmholtz free energy of such physical system is assumed to take the form

$$\psi\left(\vartheta,\varrho,\boldsymbol{c},\nabla\boldsymbol{c}\right) = \frac{\hat{\varepsilon}}{4}\sum_{i,j=1}^{N-1}\lambda_{ij}(\vartheta)\,\nabla c_i\cdot\nabla c_j + \psi_{\mathrm{th}}(\vartheta,\varrho,\boldsymbol{c}), \quad (3.54)$$

where $\boldsymbol{c} = [c_1,\ldots,c_{N-1}]^\top$, $\hat{\varepsilon}$ is a constant parameter, ψ_{th} is a given function, and λ_{ij} are given mixing surface energy coefficients such that the matrix $\boldsymbol{\Lambda} = [\lambda_{ij}]_{(N-1)\times(N-1)}$ is SPD. Let

$$\nu = \nu(\vartheta,\varrho,\boldsymbol{c},\mathbb{D}),\quad \tilde{\upsilon} = \tilde{\upsilon}(\vartheta,\varrho,\boldsymbol{c},\mathbb{D}),\quad \kappa = \kappa(\vartheta,\varrho,\boldsymbol{c},\mathbb{D}),\quad M_i = M_i(\vartheta,\varrho,\boldsymbol{c},\mathbb{D}) \quad (3.55)$$

are given non-negative functions that characterize the entropy production $\xi = \frac{\zeta}{\vartheta}$,

$$\zeta = 2\nu\left|\mathbb{D}^\delta\right|^2 + \tilde{\upsilon}\left(\operatorname{div}\boldsymbol{v}\right)^2 + \sum_{i=1}^{N-1} M_i\left|\nabla\mu_i\right|^2 + \frac{\kappa}{\vartheta}\left|\nabla\vartheta\right|^2. \quad (3.56)$$

Summary 8: Governing equations for FC-CHNSF model

The system of governing equations for the primitive quantities $\vartheta, \varrho, \boldsymbol{c}$ and $\boldsymbol{v}$ reads

$$\varrho \frac{\mathrm{d}c_i}{\mathrm{d}t} = \operatorname{div}(M_i \nabla \mu_i), \quad i = 1, \dots, N-1, \tag{3.57a}$$

$$\mu_i = \mu_i^c - \frac{1}{\varrho} \operatorname{div} \widetilde{\boldsymbol{\varsigma}}_i^c, \quad i = 1, \dots, N-1, \tag{3.57b}$$

$$\frac{\mathrm{d}\varrho}{\mathrm{d}t} = -\varrho \operatorname{div} \boldsymbol{v}, \tag{3.57c}$$

$$\varrho \frac{\mathrm{d}\boldsymbol{v}}{\mathrm{d}t} = \operatorname{div} \mathbb{T} + \varrho \boldsymbol{g}, \tag{3.57d}$$

and

$$\begin{aligned} \varrho \mathrm{c_v} \frac{\mathrm{d}\vartheta}{\mathrm{d}t} = {} & \left(2\nu \mathbb{D} - \sum_{i=1}^{N-1} \vartheta \frac{\partial \widetilde{\boldsymbol{\varsigma}}_i^c}{\partial \vartheta} \otimes \nabla c_i \right) : \mathbb{D} + \sum_{i=1}^{N-1} M_i \left| \nabla \mu_i \right|^2 \\ & + \left(\upsilon \operatorname{div} \boldsymbol{v} - \vartheta \frac{\partial p_{\mathrm{th}}}{\partial \vartheta} \right) \operatorname{div} \boldsymbol{v} + \sum_{i=1}^{N-1} \mu_{i,\vartheta} \operatorname{div}(M_i \nabla \mu_i) \\ & + \operatorname{div} \left(\kappa \nabla \vartheta + \frac{\vartheta}{\varrho} \sum_{i=1}^{N-1} \operatorname{div}(M_i \nabla \mu_i) \frac{\partial \widetilde{\boldsymbol{\varsigma}}_i^c}{\partial \vartheta} \right), \end{aligned} \tag{3.57e}$$

where

$$\mathbb{T} = (-p_{\mathrm{th}} + \upsilon \operatorname{div} \boldsymbol{v}) \mathbb{I} + 2\nu \mathbb{D} - \sum_{i=1}^{N-1} \widetilde{\boldsymbol{\varsigma}}_i^c \otimes \nabla c_i, \quad \upsilon = \tilde{\upsilon} - \frac{2\nu}{3}, \tag{3.57f}$$

$$\mu_{i,\vartheta} = \vartheta \frac{\partial \mu_i^c}{\partial \vartheta} - \frac{1}{\varrho} \operatorname{div} \left(\vartheta \frac{\partial \widetilde{\boldsymbol{\varsigma}}_i^c}{\partial \vartheta} \right), \tag{3.57g}$$

and, finally,

$$\mu_i^c = \frac{\partial \psi_{\mathrm{th}}}{\partial c_i}, \tag{3.57h}$$

$$\widetilde{\boldsymbol{\varsigma}}_i^c = \frac{1}{2} \varrho \hat{\varepsilon} \sum_{j=1}^{N-1} \lambda_{ij}(\vartheta) \nabla c_j, \tag{3.57i}$$

$$\mathrm{c_v} = -\vartheta \frac{\partial^2 \psi_{\mathrm{th}}}{\partial \vartheta^2} - \vartheta \frac{\hat{\varepsilon}}{4} \sum_{i,j=1}^{N-1} \lambda_{ij}''(\vartheta) \nabla c_i \cdot \nabla c_j, \tag{3.57j}$$

$$p_{\mathrm{th}} = \varrho^2 \frac{\partial \psi_{\mathrm{th}}}{\partial \varrho}. \tag{3.57k}$$

where λ_{ij}'' denotes the second derivative of λ_{ij} with respect to ϑ.

3.3 Quasi-incompressible model

3.3.1 Identification of the entropy production

Identification of the entropy producing processes is merely the same as in Section 3.2.1, hence we shall proceed a little bit faster. Applying the material time derivative to $\psi = \psi(\vartheta, \varrho, \boldsymbol{\phi}, \nabla\boldsymbol{\phi})$, see (3.25), we get

$$\frac{\mathrm{d}\psi}{\mathrm{d}t} = -\eta\frac{\mathrm{d}\vartheta}{\mathrm{d}t} + \frac{p_{\mathrm{th}}}{\varrho^2}\frac{\mathrm{d}\varrho}{\mathrm{d}t} + \frac{1}{\varrho}\sum_{i=1}^{N-1}\left(\widetilde{\mu}_i^{\,\phi}\frac{\mathrm{d}\phi_i}{\mathrm{d}t} + \widetilde{\boldsymbol{\varsigma}}_i^{\,\phi}\cdot\frac{\mathrm{d}\nabla\phi_i}{\mathrm{d}t}\right), \tag{3.58}$$

Next, we apply the material time derivative also to (2.87) and we substitute the result to the left hand side of (3.58). Upon multiplication of the resulting equation by ϱ, and after rearranging the terms, we arrive to the identity

$$\varrho\vartheta\frac{\mathrm{d}\eta}{\mathrm{d}t} = \varrho\frac{\mathrm{d}e}{\mathrm{d}t} - \frac{p_{\mathrm{th}}}{\varrho}\frac{\mathrm{d}\varrho}{\mathrm{d}t} - \sum_{i=1}^{N-1}\left(\widetilde{\mu}_i^{\,\phi}\frac{\mathrm{d}\phi_i}{\mathrm{d}t} + \widetilde{\boldsymbol{\varsigma}}_i^{\,\phi}\cdot\frac{\mathrm{d}\nabla\phi_i}{\mathrm{d}t}\right). \tag{3.59}$$

Now, we use the equations from (2.94) to substitute into the right hand side of the previous formula. After some algebraic manipulation we obtain

$$\begin{aligned}\varrho\vartheta\frac{\mathrm{d}\eta}{\mathrm{d}t} = (\mathbb{T}+\mathbb{T}_{\mathrm{DI}})^{\delta} : \mathbb{D}^{\delta} + \left(m + m_{\mathrm{DI}} + p_{\mathrm{th}} + \sum_{i=1}^{N-1}\phi_i\widetilde{\mu}_i\right)\operatorname{div}\boldsymbol{v} \\ + \sum_{i=1}^{N-1}\widetilde{\mu}_i\operatorname{div}\widetilde{\boldsymbol{\jmath}}_i - \operatorname{div}\left(\boldsymbol{q}_e - \sum_{i=1}^{N-1}\left(\phi_i\operatorname{div}\boldsymbol{v} + \operatorname{div}\widetilde{\boldsymbol{\jmath}}_i\right)\widetilde{\boldsymbol{\varsigma}}_i^{\,\phi}\right),\end{aligned} \tag{3.60}$$

where we have defined, by analogy with the definitions in the preceding section,

$$\widetilde{\mu}_i \stackrel{\mathrm{def}}{=} \widetilde{\mu}_i^{\,\phi} - \operatorname{div}\widetilde{\boldsymbol{\varsigma}}_i^{\,\phi} \tag{3.61}$$

and

$$\mathbb{T}_{\mathrm{DI}} \stackrel{\mathrm{def}}{=} \sum_{i=1}^{N-1}\widetilde{\boldsymbol{\varsigma}}_i^{\,\phi}\otimes\nabla\phi_i. \tag{3.62}$$

The complementary stress tensor $\mathbb{T}_{\mathrm{DI}}$ is symmetric due to our specific choice of the constitutive assumption (3.26) with symmetric matrix $\boldsymbol{\Lambda} = [\lambda_{ij}]_{(N-1)\times(N-1)}$. The decomposition $\mathbb{T}_{\mathrm{DI}} = m_{\mathrm{DI}}\mathbb{I} + \mathbb{T}_{\mathrm{DI}}^{\delta}$ gives us the spherical part in the form $m_{\mathrm{DI}} = \frac{1}{3}\sum_{i=1}^{N-1}\widetilde{\boldsymbol{\varsigma}}_i^{\,\phi}\cdot\nabla\phi_i$.

We are almost ready to exploit the constraint (2.94b). Before doing so, let us briefly discuss its role regarding the stress exerted in the material. Let us assume that the mean normal stress can be decomposed following the relation

$$m = m_0 + m_{\mathrm{eff}}. \tag{3.63}$$

The stress contribution associated with the first part, that is $m_0\mathbb{I}$, is supposed to be responsible for maintaining the constraint (2.94b) without any contribution to the entropy production. It means that m_0 cannot be determined constitutively and becomes an unknown field variable. The second term in (3.63) accounts for "effective" stress contributions and will be determined from constitutive relations.

Definition 3.6 (Augmented pressure)**.** *Let the mean normal stress consist of the two separable contributions introduced in* (3.63)*. The quantity*

$$p_{\mathrm{a}} \stackrel{\mathrm{def}}{=} -m_0 \tag{3.64}$$

is called the augmented pressure*.*

In the next step, we modify (3.60) by exploiting the constraint (2.94b) in the term $p_{\mathrm{a}} \operatorname{div} \boldsymbol{v}$, which appears if we use (3.63)–(3.64). The resulting equation reads

$$\begin{aligned}\varrho\vartheta\frac{\mathrm{d}\eta}{\mathrm{d}t} = (\mathbb{T}+\mathbb{T}_{\mathrm{DI}})^{\delta} : \mathbb{D}^{\delta} + \left(m_{\mathrm{eff}} + m_{\mathrm{DI}} - \widetilde{\psi} + \sum_{i=1}^{N-1}\phi_i\widetilde{\mu}_i\right)\operatorname{div}\boldsymbol{v} \\ + \sum_{i=1}^{N-1}(\widetilde{\mu}_i + \hat{r}_i p_{\mathrm{a}})\operatorname{div}\widetilde{\boldsymbol{\jmath}}_i - \operatorname{div}\left(\boldsymbol{q}_e - \sum_{i=1}^{N-1}(\phi_i\operatorname{div}\boldsymbol{v} + \operatorname{div}\widetilde{\boldsymbol{\jmath}}_i)\,\widetilde{\boldsymbol{\varsigma}}_i^{\phi}\right).\end{aligned} \tag{3.65}$$

(Recall that according to (3.29) we have $p_{\mathrm{th}} = -\widetilde{\psi}$.) In order to abbreviate subsequent manipulations, we introduce the auxiliary notation

$$\widetilde{\mu}_i^p \stackrel{\mathrm{def}}{=} \widetilde{\mu}_i + \hat{r}_i p_{\mathrm{a}}, \qquad \tilde{m}_{\mathrm{eff}} \stackrel{\mathrm{def}}{=} m_{\mathrm{eff}} + m_{\mathrm{DI}} - \widetilde{\psi} + \sum_{i=1}^{N-1}\phi_i\widetilde{\mu}_i. \tag{3.66}$$

The identification of the entropy producing processes in equation (3.65) is now quite straightforward. We manipulate the first sum on the second line to obtain

$$\begin{aligned}\varrho\vartheta\frac{\mathrm{d}\eta}{\mathrm{d}t} = (\mathbb{T}+\mathbb{T}_{\mathrm{DI}})^{\delta} : \mathbb{D}^{\delta} + \tilde{m}_{\mathrm{eff}}\operatorname{div}\boldsymbol{v} - \sum_{i=1}^{N-1}\widetilde{\boldsymbol{\jmath}}_i\cdot\nabla\widetilde{\mu}_i^p \\ - \operatorname{div}\left[\boldsymbol{q}_e - \sum_{i=1}^{N}\left(\widetilde{\mu}_i^p\widetilde{\boldsymbol{\jmath}}_i + (\phi_i\operatorname{div}\boldsymbol{v} + \operatorname{div}\widetilde{\boldsymbol{\jmath}}_i)\,\widetilde{\boldsymbol{\varsigma}}_i^{\phi}\right)\right],\end{aligned} \tag{3.67}$$

We see that another useful shorthand is

$$\boldsymbol{q}_{\mathrm{DI}} \stackrel{\mathrm{def}}{=} -\sum_{i=1}^{N}\left(\widetilde{\mu}_i^p\widetilde{\boldsymbol{\jmath}}_i + (\phi_i\operatorname{div}\boldsymbol{v} + \operatorname{div}\widetilde{\boldsymbol{\jmath}}_i)\,\widetilde{\boldsymbol{\varsigma}}_i^{\phi}\right), \tag{3.68}$$

which, when divided by ϑ, can be seen as the extra component of the entropy flux. Indeed, by repeating the manipulation from Section 3.2.1, we end up with

$$\begin{aligned}\varrho\frac{\mathrm{d}\eta}{\mathrm{d}t} = \frac{1}{\vartheta}\Bigg[(\mathbb{T}+\mathbb{T}_{\mathrm{DI}})^{\delta} : \mathbb{D}^{\delta} + \tilde{m}_{\mathrm{eff}}\operatorname{div}\boldsymbol{v} - \sum_{i=1}^{N-1}\widetilde{\boldsymbol{\jmath}}_i\cdot\nabla\widetilde{\mu}_i^p \\ - \left(\frac{\boldsymbol{q}_e + \boldsymbol{q}_{\mathrm{DI}}}{\vartheta}\right)\cdot\nabla\vartheta\Bigg] - \operatorname{div}\left(\frac{\boldsymbol{q}_e + \boldsymbol{q}_{\mathrm{DI}}}{\vartheta}\right).\end{aligned} \tag{3.69}$$

The entropy production $\xi = \frac{\zeta}{\vartheta}$ then reads

$$\zeta = (\mathbb{T}+\mathbb{T}_{\mathrm{DI}})^{\delta} : \mathbb{D}^{\delta} + \tilde{m}_{\mathrm{eff}}\operatorname{div}\boldsymbol{v} - \sum_{i=1}^{N-1}\widetilde{\boldsymbol{\jmath}}_i\cdot\nabla\widetilde{\mu}_i^p - \left(\frac{\boldsymbol{q}_e + \boldsymbol{q}_{\mathrm{DI}}}{\vartheta}\right)\cdot\nabla\vartheta. \tag{3.70}$$

3.3.2 Constitutive relations

Following the discussion in Section 3.2.2 we shall directly deduce the appropriate form of the constitutive relations for the quasi-incompressible model. From (3.70) we see that if we put

$$(\mathbb{T} + \mathbb{T}_{\mathrm{DI}})^{\delta} = 2\nu\mathbb{D}^{\delta}, \tag{3.71a}$$

$$\tilde{m}_{\mathrm{eff}} = \tilde{v}\,\mathrm{div}\,\boldsymbol{v}, \tag{3.71b}$$

$$\widetilde{\boldsymbol{\jmath}}_i = -M_i\,\nabla\widetilde{\mu}_i^p, \quad i = 1, \dots, N-1, \tag{3.71c}$$

$$\boldsymbol{q}_e + \boldsymbol{q}_{\mathrm{DI}} = -\kappa\,\nabla\vartheta, \tag{3.71d}$$

where $\nu, \tilde{v}, \kappa$ and M_i are given non-negative functions of $\vartheta, \boldsymbol{\phi}$ and possibly $\mathbb{D}$, we will again obtain a material model which automatically satisfies the second law of thermodynamics due to non-negativity of the entropy production.

Note that the augmented pressure p_{a} enters the equation for the diffusive volume fluxes $\widetilde{\boldsymbol{\jmath}}_i$ via $\widetilde{\mu}_i^p$, see (3.66). However, the diffusive fluxes are naturally supposed to vanish in pure components away from mixed interfacial regions. But since p_{a} is an unknown variable, we cannot a priori ensure that its gradient will vanish in pure components. Equally, the k-th diffusive flux $\widetilde{\boldsymbol{\jmath}}_k$ is expected to completely vanish if the k-th component is not present in the considered system. Otherwise, we cannot assure that the system of governing equations for the N-component model—with the k-th component being omitted—will properly reduce to the corresponding $(N-1)$-component model. We postpone further discussion concerning these issues to Chapter 4. Nevertheless, we shall slightly generalize the constitutive relations in (3.71c) for the purpose of that discussion.

Let the constitutive relations for the diffusive fluxes take the form

$$\widetilde{\boldsymbol{\jmath}}_i = -\sum_{j=1}^{N-1} M_{ij}\,\nabla\widetilde{\mu}_j^p, \quad i = 1, \dots, N-1, \tag{3.72}$$

where M_{ij} denote entries of a SPD matrix $\mathbf{M} \in \mathbb{R}^{(N-1)\times(N-1)}$, which will be called the matrix of mobility coefficients or, simply, the *mobility matrix*. The required properties of $\mathbf{M}$ ensures non-negativity (even positivity) of the second term in (3.70).

Using the above definitions and the more traditional notation $\upsilon = \tilde{v} - 2\nu/3$, we can rewrite the constitutive relations to take the form

$$\mathbb{T} = -\left(p_{\mathrm{a}} - \widetilde{\psi} + \sum_{i=1}^{N-1}\phi_i\widetilde{\mu}_i\right)\mathbb{I} + \upsilon(\mathrm{div}\,\boldsymbol{v})\mathbb{I} + 2\nu\mathbb{D} - \sum_{i=1}^{N-1}\widetilde{\boldsymbol{\varsigma}}_i^{\phi}\otimes\nabla\phi_i, \tag{3.73a}$$

$$\widetilde{\boldsymbol{\jmath}}_i = -\sum_{j=1}^{N-1} M_{ij}\,\nabla\widetilde{\mu}_j^p, \quad i = 1, \dots, N-1, \tag{3.73b}$$

$$\boldsymbol{q}_e = -\kappa\,\nabla\vartheta + \sum_{i=1}^{N}\left(\widetilde{\mu}_i^p\widetilde{\boldsymbol{\jmath}}_i + (\phi_i\,\mathrm{div}\,\boldsymbol{v} + \mathrm{div}\,\widetilde{\boldsymbol{\jmath}}_i)\,\widetilde{\boldsymbol{\varsigma}}_i^{\phi}\right). \tag{3.73c}$$

If we substitute the derived constitutive relations into the formula for the entropy production (3.70), we observe that

$$\xi = \frac{1}{\vartheta}\left[2\nu\left|\mathbb{D}^{\delta}\right|^2 + \tilde{\upsilon}(\operatorname{div}\boldsymbol{v})^2 + \sum_{i,j=1}^{N-1} M_{ij}\,\nabla\widetilde{\mu}_j^p\cdot\nabla\widetilde{\mu}_i^p + \frac{\kappa}{\vartheta}\left|\nabla\vartheta\right|^2\right]. \tag{3.74}$$

Remark 3.7. Combining (3.63), (3.66) and (3.71b) we obtain

$$m = -p_{\mathrm{a}} - m_{\mathrm{DI}} + \widetilde{\psi} - \sum_{i=1}^{N-1}\phi_i\widetilde{\mu}_i + \tilde{\upsilon}\operatorname{div}\boldsymbol{v}. \tag{3.75}$$

3.3.3 Evolution equation for the temperature

In the current setting with (3.25) we assume that the entropy can be expressed as a function of $\vartheta, \varrho, \boldsymbol{\phi}$ and $\nabla\boldsymbol{\phi}$, where we still consider $\varrho = \varrho(\boldsymbol{\phi})$, see (2.10a), which is independent of the temperature. Repeating the procedure outlined in Section 3.2.3, we first obtain

$$\frac{\mathrm{d}\eta}{\mathrm{d}t} = -\frac{\partial^2\psi}{\partial\vartheta^2}\frac{\mathrm{d}\vartheta}{\mathrm{d}t} - \frac{\partial^2\psi}{\partial\varrho\partial\vartheta}\frac{\mathrm{d}\varrho}{\mathrm{d}t} - \sum_{i=1}^{N-1}\left(\frac{\partial^2\psi}{\partial\phi_i\partial\vartheta}\frac{\mathrm{d}\phi_i}{\mathrm{d}t} + \frac{\partial^2\psi}{\partial\nabla\phi_i\partial\vartheta}\cdot\frac{\mathrm{d}\nabla\phi_i}{\mathrm{d}t}\right). \tag{3.76}$$

(Recall that $\eta = -\frac{\partial\psi}{\partial\vartheta}$, see (2.89).)

Using the interchangeability of the second derivatives and the definition of the specific heat at constant volume, see (2.90), it is possible to rewrite the last formula as

$$\frac{\mathrm{d}\eta}{\mathrm{d}t} = \frac{\mathrm{c_v}}{\vartheta}\frac{\mathrm{d}\vartheta}{\mathrm{d}t} - \frac{1}{\varrho^2}\frac{\partial p_{\mathrm{th}}}{\partial\vartheta}\frac{\mathrm{d}\varrho}{\mathrm{d}t} - \frac{1}{\varrho}\sum_{i=1}^{N-1}\left(\frac{\partial\widetilde{\mu}_i^{\,\phi}}{\partial\vartheta}\frac{\mathrm{d}\phi_i}{\mathrm{d}t} + \frac{\partial\widetilde{\boldsymbol{\varsigma}}_i^{\phi}}{\partial\vartheta}\cdot\frac{\mathrm{d}\nabla\phi_i}{\mathrm{d}t}\right). \tag{3.77}$$

If we further multiply (3.77) by $\varrho\vartheta$ and if we use evolution equations (2.94e) and (2.94f), we obtain

$$\begin{aligned}\varrho\vartheta\frac{\mathrm{d}\eta}{\mathrm{d}t} = \varrho\mathrm{c_v}\frac{\mathrm{d}\vartheta}{\mathrm{d}t} + \vartheta\frac{\partial p_{\mathrm{th}}}{\partial\vartheta}\operatorname{div}\boldsymbol{v} - \sum_{i=1}^{N-1}\left(\vartheta\frac{\partial\widetilde{\mu}_i^{\,\phi}}{\partial\vartheta} - \operatorname{div}\left(\vartheta\frac{\partial\widetilde{\boldsymbol{\varsigma}}_i^{\phi}}{\partial\vartheta}\right)\right)\frac{\mathrm{d}\phi_i}{\mathrm{d}t}\\ - \operatorname{div}\left(\sum_{i=1}^{N-1}\vartheta\frac{\partial\widetilde{\boldsymbol{\varsigma}}_i^{\phi}}{\partial\vartheta}\frac{\mathrm{d}\phi_i}{\mathrm{d}t}\right) + \sum_{i=1}^{N-1}\left(\vartheta\frac{\partial\widetilde{\boldsymbol{\varsigma}}_i^{\phi}}{\partial\vartheta}\otimes\nabla\phi_i\right) : \nabla\boldsymbol{v}^{\top}.\end{aligned} \tag{3.78}$$

By analogy with (3.50) we introduce the notation

$$\widetilde{\mu}_{i,\vartheta} \overset{\mathrm{def}}{=} \vartheta\frac{\partial\widetilde{\mu}_i^{\,\phi}}{\partial\vartheta} - \operatorname{div}\left(\vartheta\frac{\partial\widetilde{\boldsymbol{\varsigma}}_i^{\phi}}{\partial\vartheta}\right), \qquad \mathbb{T}_{\mathrm{DI},\vartheta} \overset{\mathrm{def}}{=} \sum_{i=1}^{N-1}\vartheta\frac{\partial\widetilde{\boldsymbol{\varsigma}}_i^{\phi}}{\partial\vartheta}\otimes\nabla\phi_i. \tag{3.79}$$

Based on the argumentation below (3.62), we see that $\mathbb{T}_{\mathrm{DI},\vartheta}$ is a symmetric tensor. We proceed by comparing (3.78) and (3.51), where into the former equation we

substitute from (2.94a) and (3.72), and from (3.74) into the latter. The resulting equation reads

$$\begin{aligned}\varrho \mathrm{c_v}\frac{\mathrm{d}\vartheta}{\mathrm{d}t} &= (2\nu\mathbb{D}-\mathbb{T}_{\mathrm{DI},\vartheta}):\mathbb{D}+\sum_{i,j=1}^{N-1}M_{ij}\,\nabla\widetilde{\mu}_j^p\cdot\nabla\widetilde{\mu}_i^p\\ &\quad+\left(\upsilon\,\mathrm{div}\,\boldsymbol{v}+\vartheta\frac{\partial\widetilde{\psi}}{\partial\vartheta}-\sum_{i=1}^{N-1}\phi_i\widetilde{\mu}_{i,\vartheta}\right)\mathrm{div}\,\boldsymbol{v}+\sum_{i,j=1}^{N-1}\widetilde{\mu}_{i,\vartheta}\,\mathrm{div}\left(M_{ij}\,\nabla\widetilde{\mu}_j^p\right)\\ &\quad+\mathrm{div}\left(\kappa\,\nabla\vartheta+\vartheta\sum_{i,j=1}^{N-1}\left[\mathrm{div}\left(M_{ij}\,\nabla\widetilde{\mu}_j^p\right)-\phi_i\,\mathrm{div}\,\boldsymbol{v}\right]\frac{\partial\widetilde{\boldsymbol{\varsigma}}_i^{\phi}}{\partial\vartheta}\right).\end{aligned}\tag{3.80}$$

(Recall that $p_{\mathrm{th}}=-\widetilde{\psi}$.)

3.3.4 Summary: QI-CHNSF model

Let us recapitulate the system of governing equations for a quasi-incompressible heat conducting fluid-like mixture consisting of N incommpressible components. The specific Helmholtz free energy of such physical system is assumed to take the form

$$\psi(\vartheta,\varrho,\boldsymbol{\phi},\nabla\boldsymbol{\phi})=\frac{1}{\varrho}\left(\frac{a\varepsilon}{4}\sum_{i,j=1}^{N-1}\lambda_{ij}(\vartheta)\,\nabla\phi_i\cdot\nabla\phi_j+\widetilde{\psi}_0(\vartheta,\boldsymbol{\phi})\right),\tag{3.81a}$$

where $\boldsymbol{\phi}=[\phi_1,\dots,\phi_{N-1}]^\top$, $\varrho=\sum_{i=1}^{N-1}(\hat{\varrho}_i-\hat{\varrho}_N)\phi_i+\hat{\varrho}_N$, λ_{ij} are given mixing surface energy coefficients such that the matrix $\boldsymbol{\Lambda}=[\lambda_{ij}]_{(N-1)\times(N-1)}$ is SPD, and a,ε are given constants. The function $\widetilde{\psi}_0$ is given by

$$\widetilde{\psi}_0(\vartheta,\boldsymbol{\phi})=\frac{b}{\varepsilon}F(\boldsymbol{\phi})+\sum_{i=1}^{N-1}(\widetilde{\psi}_i(\vartheta)-\widetilde{\psi}_N(\vartheta))\phi_i+\widetilde{\psi}_N(\vartheta),\tag{3.81b}$$

where F is a given multi-well potential, b is another constant, and

$$\widetilde{\psi}_i(\vartheta)=-\hat{\varrho}_i\hat{\mathrm{c}}_{\mathrm{v},i}\left[\ln\left(\frac{\vartheta}{\hat{\vartheta}_{\mathrm{iso}}}\right)-\frac{\vartheta-\hat{\vartheta}_{\mathrm{iso}}}{\vartheta}\right]\vartheta,\tag{3.81c}$$

for $i\in\{1,\dots,N\}$. Let

$$M_{ij}=M_{ij}(\vartheta,\boldsymbol{\phi},\mathbb{D})\tag{3.82a}$$

are given functions such that the matrix $\mathbf{M}=[M_{ij}]_{(N-1)\times(N-1)}$ is SPD, and

$$\nu=\nu(\vartheta,\boldsymbol{\phi},\mathbb{D}),\qquad\tilde{\upsilon}=\tilde{\upsilon}(\vartheta,\boldsymbol{\phi},\mathbb{D}),\qquad\kappa=\kappa(\vartheta,\boldsymbol{\phi},\mathbb{D})\tag{3.82b}$$

are another given non-negative functions that all together characterize the entropy production $\xi=\frac{\zeta}{\vartheta}$,

$$\zeta=2\nu\left|\mathbb{D}^\delta\right|^2+\tilde{\upsilon}(\mathrm{div}\,\boldsymbol{v})^2+\sum_{i,j=1}^{N-1}M_{ij}\,\nabla\widetilde{\mu}_j^p\cdot\nabla\widetilde{\mu}_i^p+\frac{\kappa}{\vartheta}\left|\nabla\vartheta\right|^2.\tag{3.83}$$

Summary 9: Governing equations for QI-CHNSF model

The system of governing equations for the unknown quantities $\vartheta, \boldsymbol{\phi}, \boldsymbol{v}$ and p_a reads

$$\frac{\mathrm{d}\phi_i}{\mathrm{d}t} + \phi_i \operatorname{div} \boldsymbol{v} = \sum_{j=1}^{N-1} \operatorname{div}\left(M_{ij}\, \nabla \widetilde{\mu}_j^p\right), \quad i = 1, \dots, N-1, \tag{3.84a}$$

$$\widetilde{\mu}_i^p = \widetilde{\mu}_i^{\,\phi} - \operatorname{div} \widetilde{\boldsymbol{\varsigma}}_i^{\phi} + \hat{r}_i p_\mathrm{a}, \quad i = 1, \dots, N-1, \tag{3.84b}$$

$$\operatorname{div} \boldsymbol{v} = \sum_{i,j=1}^{N-1} \hat{r}_i \operatorname{div}\left(M_{ij}\, \nabla \widetilde{\mu}_j^p\right), \tag{3.84c}$$

$$\varrho \frac{\mathrm{d}\boldsymbol{v}}{\mathrm{d}t} = \operatorname{div} \mathbb{T} + \varrho \boldsymbol{g}, \tag{3.84d}$$

and

$$\begin{aligned} \varrho \mathrm{c_v} \frac{\mathrm{d}\vartheta}{\mathrm{d}t} = {} & \left(2\nu \mathbb{D} - \sum_{i=1}^{N-1} \vartheta \frac{\partial \widetilde{\boldsymbol{\varsigma}}_i^{\phi}}{\partial \vartheta} \otimes \nabla \phi_i \right) : \mathbb{D} + \sum_{i,j=1}^{N-1} M_{ij}\, \nabla \widetilde{\mu}_j^p \cdot \nabla \widetilde{\mu}_i^p \\ & + \left(\upsilon \operatorname{div} \boldsymbol{v} + \vartheta \frac{\partial \widetilde{\psi}}{\partial \vartheta} - \sum_{i=1}^{N-1} \phi_i \widetilde{\mu}_{i,\vartheta} \right) \operatorname{div} \boldsymbol{v} + \sum_{i,j=1}^{N-1} \widetilde{\mu}_{i,\vartheta} \operatorname{div}\left(M_{ij}\, \nabla \widetilde{\mu}_j^p\right) \\ & + \operatorname{div} \left(\kappa \nabla \vartheta + \vartheta \sum_{i,j=1}^{N-1} \left[\operatorname{div}\left(M_{ij}\, \nabla \widetilde{\mu}_j^p\right) - \phi_i \operatorname{div} \boldsymbol{v} \right] \frac{\partial \widetilde{\boldsymbol{\varsigma}}_i^{\phi}}{\partial \vartheta} \right), \end{aligned} \tag{3.84e}$$

where $\hat{r}_i = 1 - \frac{\hat{\varrho}_i}{\hat{\varrho}_N}$ are given constants,

$$\mathbb{T} = -\left(p_\mathrm{a} - \widetilde{\psi} + \sum_{i=1}^{N-1} \phi_i \widetilde{\mu}_i - \upsilon \operatorname{div} \boldsymbol{v} \right) \mathbb{I} + 2\nu \mathbb{D} - \sum_{i=1}^{N-1} \widetilde{\boldsymbol{\varsigma}}_i^{\phi} \otimes \nabla \phi_i, \quad \upsilon = \tilde{\upsilon} - \frac{2\nu}{3}, \tag{3.84f}$$

$$\widetilde{\mu}_i = \widetilde{\mu}_i^{\,\phi} - \operatorname{div} \widetilde{\boldsymbol{\varsigma}}_i^{\phi}, \qquad \widetilde{\mu}_{i,\vartheta} = \vartheta \frac{\partial \widetilde{\mu}_i^{\,\phi}}{\partial \vartheta} - \operatorname{div}\left(\vartheta \frac{\partial \widetilde{\boldsymbol{\varsigma}}_i^{\phi}}{\partial \vartheta} \right), \tag{3.84g}$$

and, finally,

$$\widetilde{\mu}_i^{\,\phi} = \frac{\partial \widetilde{\psi}_0}{\partial \phi_i}, \tag{3.84h}$$

$$\widetilde{\boldsymbol{\varsigma}}_i^{\phi} = \frac{a\varepsilon}{2} \sum_{j=1}^{N-1} \lambda_{ij}(\vartheta)\, \nabla \phi_j, \tag{3.84i}$$

$$\mathrm{c_v} = -\frac{\vartheta}{\varrho} \left(\frac{\partial^2 \widetilde{\psi}_0}{\partial \vartheta^2} + \frac{a\varepsilon}{4} \sum_{i,j=1}^{N-1} \lambda_{ij}''(\vartheta)\, \nabla \phi_i \cdot \nabla \phi_j \right), \tag{3.84j}$$

where λ_{ij}'' denotes the second derivative of λ_{ij} with respect to ϑ.

3.4 Fully-incompressible model

Let us introduce an auxiliary notation that will be useful in the forthcoming manipulation with the equations previously summarized in Section 2.5.3. In the current description we have $\varrho = \sum_{i=1}^{N-1} (\hat{\varrho}_i - \hat{\varrho}_N)\,\phi_i + \hat{\varrho}_N = \hat{\varrho}_N \left(1 - \sum_{i=1}^{N-1} \hat{r}_i \phi_i\right)$ and $\boldsymbol{J} = \sum_{i=1}^{N-1} (\hat{\varrho}_i - \hat{\varrho}_N)\,\widetilde{\boldsymbol{\jmath}}_i = -\hat{\varrho}_N \sum_{i=1}^{N-1} \hat{r}_i \widetilde{\boldsymbol{\jmath}}_i$. It follows that

$$\varrho^{-1}\boldsymbol{J} = -\sum_{i=1}^{N-1} z_i \widetilde{\boldsymbol{\jmath}}_i, \qquad z_i = z_i(\boldsymbol{\phi}) \stackrel{\text{def}}{=} \frac{\hat{r}_i}{1 - \sum_{j=1}^{N-1} \hat{r}_j \phi_j}. \tag{3.85}$$

3.4.1 Identification of the entropy production

We already know, see (3.59), that

$$\varrho\vartheta \frac{\mathrm{d}\eta}{\mathrm{d}t} = \varrho \frac{\mathrm{d}e}{\mathrm{d}t} - \frac{p_{\mathrm{th}}}{\varrho}\frac{\mathrm{d}\varrho}{\mathrm{d}t} - \sum_{i=1}^{N-1} \left(\widetilde{\mu}_i^{\phi} \frac{\mathrm{d}\phi_i}{\mathrm{d}t} + \widetilde{\boldsymbol{\varsigma}}_i^{\phi} \cdot \frac{\mathrm{d}\nabla\phi_i}{\mathrm{d}t} \right), \tag{3.86}$$

and we are ready to repeat the procedure outlined in Sections 3.2 and 3.3. We substitute into (3.86) from the system of equations (2.95) to obtain

$$\begin{aligned} \varrho\vartheta \frac{\mathrm{d}\eta}{\mathrm{d}t} &= \Theta_2 e \operatorname{div} \boldsymbol{J} + \mathbb{T}^{\delta} : \left(\mathbb{D} + \Theta_1 \nabla_{\mathrm{sym}} \left(\varrho^{-1}\boldsymbol{J}\right)\right)^{\delta} - \operatorname{div} \boldsymbol{q}_e \\ &\quad + \Theta_1 m \operatorname{div}\left(\varrho^{-1}\boldsymbol{J}\right) + \Theta_1 \varrho^{-1}\boldsymbol{J} \cdot \left([\nabla \boldsymbol{v}]\,\boldsymbol{J} + \Theta_0 \frac{\mathrm{d}\boldsymbol{J}}{\mathrm{d}t} \right) + \Theta_2 \varrho^{-1} p_{\mathrm{th}} \operatorname{div} \boldsymbol{J} \\ &\quad + \sum_{i=1}^{N-1} \widetilde{\mu}_i \operatorname{div} \widetilde{\boldsymbol{\jmath}}_i + \mathbb{T}_{\mathrm{DI}} : \mathbb{D} + \operatorname{div} \left(\sum_{i=1}^{N-1} (\operatorname{div} \widetilde{\boldsymbol{\jmath}}_i)\, \widetilde{\boldsymbol{\varsigma}}_i^{\phi} \right), \end{aligned} \tag{3.87}$$

where we have used the notation for $\widetilde{\mu}_i$ and $\mathbb{T}_{\mathrm{DI}}$ introduced in (3.61) and (3.62) respectively. We again decompose $\mathbb{T}_{\mathrm{DI}}$ into its spherical and deviatoric part. Since $\boldsymbol{v}$ is divergence-free in the current setting, we have $\mathbb{T}_{\mathrm{DI}} : \mathbb{D} = \mathbb{T}_{\mathrm{DI}}^{\delta} : \mathbb{D}^{\delta}$. Next, we reuse the formula (2.87) in the first term on the right hand side of (3.87). In doing so, we obtain the term $\eta \operatorname{div} \boldsymbol{J}$ which appears in the general form of the entropy balance (2.95g). Upon rearranging the terms, the previous equation reads

$$\begin{aligned} \vartheta \left(\varrho \frac{\mathrm{d}\eta}{\mathrm{d}t} - \Theta_2 \eta \operatorname{div} \boldsymbol{J} \right) &= \left(\mathbb{T} + \mathbb{T}_{\mathrm{DI}}\right)^{\delta} : \left(\mathbb{D} + \Theta_1 \nabla_{\mathrm{sym}} \left(\varrho^{-1}\boldsymbol{J}\right)\right)^{\delta} \\ &\quad + \Theta_2 \varrho^{-1} \left(\widetilde{\psi} + p_{\mathrm{th}}\right) \operatorname{div} \boldsymbol{J} + \Theta_1 \left(m + m_{\mathrm{DI}}\right) \operatorname{div}\left(\varrho^{-1}\boldsymbol{J}\right) - \Theta_1 \mathbb{T}_{\mathrm{DI}} : \nabla\left(\varrho^{-1}\boldsymbol{J}\right) \\ &\quad - \operatorname{div} \left(\boldsymbol{q}_e - \sum_{i=1}^{N-1} (\operatorname{div} \widetilde{\boldsymbol{\jmath}}_i)\, \widetilde{\boldsymbol{\varsigma}}_i^{\phi} \right) + \sum_{i=1}^{N-1} \widetilde{\mu}_i \operatorname{div} \widetilde{\boldsymbol{\jmath}}_i + \Theta_1 \varrho^{-1}\boldsymbol{J} \cdot \left([\nabla \boldsymbol{v}]\,\boldsymbol{J} + \Theta_0 \frac{\mathrm{d}\boldsymbol{J}}{\mathrm{d}t} \right). \end{aligned} \tag{3.88}$$

Note that the first term on the second line vanishes in virtue of (3.29). Using the manipulations of the type $\mathbb{T}_{\mathrm{DI}} : \nabla(\varrho^{-1}\boldsymbol{J}) = \operatorname{div}(\varrho^{-1}\mathbb{T}_{\mathrm{DI}}\boldsymbol{J}) - \varrho^{-1}\boldsymbol{J} \cdot \operatorname{div} \mathbb{T}_{\mathrm{DI}}$ and

$m \operatorname{div}(\varrho^{-1}\boldsymbol{J}) = \operatorname{div}(m\varrho^{-1}\boldsymbol{J}) - \varrho^{-1}\boldsymbol{J}\cdot\nabla m$, we can restate the previous equation in the form

$$\vartheta\left(\varrho\frac{\mathrm{d}\eta}{\mathrm{d}t} - \Theta_2\eta\operatorname{div}\boldsymbol{J}\right) = (\mathbb{T}+\mathbb{T}_{\mathrm{DI}})^{\delta} : \left(\mathbb{D} + \Theta_1\nabla_{\mathrm{sym}}\left(\varrho^{-1}\boldsymbol{J}\right)\right)^{\delta} - \operatorname{div}(\boldsymbol{q}_e + \boldsymbol{q}_{\mathrm{DI}})$$
$$-\sum_{i=1}^{N-1}\widetilde{\boldsymbol{\jmath}}_i\cdot\nabla\widetilde{\mu}_i + \Theta_1\varrho^{-1}\boldsymbol{J}\cdot\left(\operatorname{div}\mathbb{T}_{\mathrm{DI}} + [\nabla\boldsymbol{v}]\,\boldsymbol{J} - \nabla(m+m_{\mathrm{DI}}) + \Theta_0\frac{\mathrm{d}\boldsymbol{J}}{\mathrm{d}t}\right), \quad (3.89)$$

with the complementary energy flux

$$\boldsymbol{q}_{\mathrm{DI}} \overset{\mathrm{def}}{=} \Theta_1\varrho^{-1}\mathbb{T}_{\mathrm{DI}}\boldsymbol{J} - \Theta_1\,(m+m_{\mathrm{DI}})\,\varrho^{-1}\boldsymbol{J} - \sum_{i=1}^{N-1}\left(\widetilde{\mu}_i\widetilde{\boldsymbol{\jmath}}_i + (\operatorname{div}\widetilde{\boldsymbol{\jmath}}_i)\,\widetilde{\boldsymbol{\varsigma}}_i^{\phi}\right). \quad (3.90)$$

Finally, we put together the terms on the second line of (3.89) using the relation (3.85). Then it remains to divide the equation by the temperature and repeat the manipulation with the divergence of the entropy flux, just as it was done in the preceding sections. The resulting equation reads

$$\varrho\frac{\mathrm{d}\eta}{\mathrm{d}t} - \Theta_2\eta\operatorname{div}\boldsymbol{J} = -\operatorname{div}\left(\frac{\boldsymbol{q}_e+\boldsymbol{q}_{\mathrm{DI}}}{\vartheta}\right) + \xi, \quad (3.91)$$

where we have identified the entropy production $\xi = \frac{\zeta}{\vartheta}$ which is given by

$$\zeta = (\mathbb{T}+\mathbb{T}_{\mathrm{DI}})^{\delta} : \left(\mathbb{D} + \Theta_1\nabla_{\mathrm{sym}}\left(\varrho^{-1}\boldsymbol{J}\right)\right)^{\delta} - \left(\frac{\boldsymbol{q}_e+\boldsymbol{q}_{\mathrm{DI}}}{\vartheta}\right)\cdot\nabla\vartheta$$
$$-\sum_{i=1}^{N-1}\widetilde{\boldsymbol{\jmath}}_i\cdot\left(\nabla\widetilde{\mu}_i + \Theta_1 z_i\left([\nabla\boldsymbol{v}]\,\boldsymbol{J} + \operatorname{div}\mathbb{T}_{\mathrm{DI}} - \nabla(m+m_{\mathrm{DI}}) + \Theta_0\frac{\mathrm{d}\boldsymbol{J}}{\mathrm{d}t}\right)\right). \quad (3.92)$$

Recall that the equations that have been manipulated within this section were obtained as a result of the model reduction in the sense of transition from the detailed componentwise formulation of the balance equations towards their averaged formulation for the mixture as a whole. As an integral part of the model reduction, we have lost the detailed information about the structure of the diffusive fluxes $\widetilde{\boldsymbol{\jmath}}_i$ and it only remains to relate each of them to some other known quantities (via a constitutive relation). In the current setting, we see that in order to find such a relation, we would need to recover the information that had been previously lost. Otherwise, we cannot say anything about the last term in (3.92) describing the temporal changes of a weighted sum of the relevant diffusive fluxes, see (2.24). This issue has been already commented in Section 2.5.3. In order to proceed further we accept the zeroth level of approximation (2.96a).

3.4.2 Constitutive relations

In Section 2.5.3, we have introduced a set of "toggle coefficients" $\{\Theta_0, \Theta_1, \Theta_2\}$ which stand in front of the chosen terms in equations (2.95c)–(2.95e), and which are supposed to attain the values of either one or zero. These coefficients allow

us to reach three different levels of approximation in the derivation of the model for multi-component systems in FI description.

As in the previous two cases, we deduce the appropriate form of the constitutive relations directly from (3.92). On the zeroth level of approximation, with $\Theta_0 = 0$, we choose the constitutive relations of the form

$$(\mathbb{T} + \mathbb{T}_{\mathrm{DI}})^{\delta} = 2\nu\big(\mathbb{D} + \Theta_1 \nabla_{\mathrm{sym}}\left(\varrho^{-1}\boldsymbol{J}\right)\big)^{\delta}, \tag{3.93a}$$

$$\widetilde{\boldsymbol{\jmath}}_i = -\sum_{j=1}^{N-1} M_{ij}\left(\nabla\widetilde{\mu}_j + \Theta_1 z_j\left([\nabla\boldsymbol{v}]\,\boldsymbol{J} + \operatorname{div}\mathbb{T}_{\mathrm{DI}} + \nabla\tilde{p}_{\mathrm{a}}\right)\right), \quad i = 1,\dots,N-1, \tag{3.93b}$$

$$\boldsymbol{q}_e + \boldsymbol{q}_{\mathrm{DI}} = -\kappa\,\nabla\vartheta, \tag{3.93c}$$

with ν, κ and M_{ij} that were introduced in Section 3.3.2. The modified augmented pressure[5] $\tilde{p}_{\mathrm{a}}$, the gradient of which appears in (3.93b), is defined by

$$\tilde{p}_{\mathrm{a}} \stackrel{\mathrm{def}}{=} -(m + m_{\mathrm{DI}}). \tag{3.94}$$

As in the previous case of QI systems, we observe that the momentum balance is strongly coupled with the rest of the system due to the presence of the augmented pressure in the constitutive relations for diffusive fluxes. The situation on the current level of approximation is even more complicated due to the presence of the other terms in (3.93b). Note that $\mathbb{D} + \nabla_{\mathrm{sym}}\left(\varrho^{-1}\boldsymbol{J}\right) = \nabla_{\mathrm{sym}}\left(\boldsymbol{v} + \varrho^{-1}\boldsymbol{J}\right)$ corresponds to the symmetric gradient of the mass-averaged velocity by virtue of the first relation in (2.21). The "correction" term $\varrho^{-1}\boldsymbol{J}$ gives rise to some extra terms in the standard transcription of the Cauchy stress tensor,

$$\mathbb{T} = -\tilde{p}_{\mathrm{a}}\mathbb{I} + 2\nu\mathbb{D} - \sum_{i=1}^{N-1}\widetilde{\boldsymbol{\varsigma}}_i^{\phi}\otimes\nabla\phi_i + 2\Theta_1\nu\left(\nabla_{\mathrm{sym}}\left(\varrho^{-1}\boldsymbol{J}\right) - \frac{1}{3}\operatorname{div}\left(\varrho^{-1}\boldsymbol{J}\right)\mathbb{I}\right). \tag{3.95}$$

At this point, we proceed to the subsequent level of approximation and we put $\Theta_1 = 0$ everywhere in the previous expressions. In this way we will arrive to the class of models developed by Abels et al. (2012) for binary systems, and Dong (2014a) who provided extensions to general multi-component systems.

3.4.3 Evolution equation for the temperature

In what follows, we stay on the first level of approximation, with $\Theta_0 = \Theta_1 = 0$, and we shall derive the appropriate form of the evolution equation for the temperature. Repeating the steps from the beginning of Section 3.3.3, we obtain

$$\begin{aligned}\varrho\vartheta\frac{\mathrm{d}\eta}{\mathrm{d}t} = \varrho\mathrm{c}_{\mathrm{v}}\frac{\mathrm{d}\vartheta}{\mathrm{d}t} + \Theta_2\vartheta\frac{\partial p_{\mathrm{th}}}{\partial\vartheta}\operatorname{div}\boldsymbol{J} + \sum_{i=1}^{N-1}\left(\vartheta\frac{\partial\widetilde{\mu}_i^{\phi}}{\partial\vartheta} - \operatorname{div}\left(\vartheta\frac{\partial\widetilde{\boldsymbol{\varsigma}}_i^{\phi}}{\partial\vartheta}\right)\right)\operatorname{div}\widetilde{\boldsymbol{\jmath}}_i \\ + \operatorname{div}\left(\sum_{i=1}^{N-1}\vartheta\left(\operatorname{div}\widetilde{\boldsymbol{\jmath}}_i\right)\frac{\partial\widetilde{\boldsymbol{\varsigma}}_i^{\phi}}{\partial\vartheta}\right) + \sum_{i=1}^{N-1}\left(\vartheta\frac{\partial\widetilde{\boldsymbol{\varsigma}}_i^{\phi}}{\partial\vartheta}\otimes\nabla\phi_i\right) : \nabla\boldsymbol{v}^{\top}.\end{aligned} \tag{3.96}$$

[5]The rationale of the chosen terminology will be clarified in Section 3.6.3.

As a next step, we substitute $p_{\rm th} = -\varrho\psi$, see (3.29), into the second term on the right hand side of the previous equation. Since the density $\varrho = \varrho(\boldsymbol{\phi})$ is independent of the temperature, we have $\frac{\partial p_{\rm th}}{\partial \vartheta} = \varrho\eta$ by virtue of the fist formula in (2.89). Last but not least, we can reuse the notation introduced in (3.79), with $\mathbb{T}_{\mathrm{DI},\vartheta}$ being symmetric, to get

$$\vartheta\left(\varrho\frac{\mathrm{d}\eta}{\mathrm{d}t} - \Theta_2\eta\,\mathrm{div}\,\boldsymbol{J}\right) = \varrho\mathrm{c_v}\frac{\mathrm{d}\vartheta}{\mathrm{d}t} + \sum_{i=1}^{N-1}\widetilde{\mu}_{i,\vartheta}\,\mathrm{div}\,\widetilde{\boldsymbol{\jmath}}_i + \mathrm{div}\left(\sum_{i=1}^{N-1}\vartheta\,(\mathrm{div}\,\widetilde{\boldsymbol{\jmath}}_i)\,\frac{\partial\widetilde{\boldsymbol{\varsigma}}_i^{\phi}}{\partial\vartheta}\right) + \sum_{i=1}^{N-1}\left(\vartheta\frac{\partial\widetilde{\boldsymbol{\varsigma}}_i^{\phi}}{\partial\vartheta}\otimes\nabla\phi_i\right) : \mathbb{D}. \quad (3.97)$$

It remains to substitute into the previous equation from (3.89) and (3.93), where we put $\Theta_1 = 0$. The resulting evolution equation for the temperature reads

$$\varrho\mathrm{c_v}\frac{\mathrm{d}\vartheta}{\mathrm{d}t} = (2\nu\mathbb{D} - \mathbb{T}_{\mathrm{DI},\vartheta}) : \mathbb{D} + \sum_{i,j=1}^{N-1} M_{ij}\,\nabla\widetilde{\mu}_j\cdot\nabla\widetilde{\mu}_i + \sum_{i,j=1}^{N-1}\widetilde{\mu}_{i,\vartheta}\,\mathrm{div}\,(M_{ij}\,\nabla\widetilde{\mu}_j) + \mathrm{div}\left(\kappa\,\nabla\vartheta + \vartheta\sum_{i,j=1}^{N-1}\mathrm{div}\,(M_{ij}\,\nabla\widetilde{\mu}_j)\frac{\partial\widetilde{\boldsymbol{\varsigma}}_i^{\phi}}{\partial\vartheta}\right). \quad (3.98)$$

3.4.4 Summary: FI-CHNSF model

Let us recapitulate the system of governing equations for a quasi-incompressible heat conducting fluid-like mixture consisting of N incommpressible components. The specific Helmholtz free energy of such physical system is assumed to take the form

$$\psi(\vartheta,\varrho,\boldsymbol{\phi},\nabla\boldsymbol{\phi}) = \frac{1}{\varrho}\left(\frac{a\varepsilon}{4}\sum_{i,j=1}^{N-1}\lambda_{ij}(\vartheta)\,\nabla\phi_i\cdot\nabla\phi_j + \widetilde{\psi}_0(\vartheta,\boldsymbol{\phi})\right), \quad (3.99)$$

where $\boldsymbol{\phi} = [\phi_1,\dots,\phi_{N-1}]^\top$, $\varrho = \sum_{i=1}^{N-1}(\hat{\varrho}_i - \hat{\varrho}_N)\phi_i + \hat{\varrho}_N$, $\widetilde{\psi}_0$ is a given function of the form (3.27), λ_{ij} are given mixing surface energy coefficients such that the matrix $\boldsymbol{\Lambda} = [\lambda_{ij}]_{(N-1)\times(N-1)}$ is SPD, and a,ε are given constants. Let

$$M_{ij} = M_{ij}(\vartheta,\boldsymbol{\phi},\mathbb{D}) \quad (3.100a)$$

are given functions such that the matrix $\mathbf{M} = [M_{ij}]_{(N-1)\times(N-1)}$ is SPD, and

$$\nu = \nu(\vartheta,\boldsymbol{\phi},\mathbb{D}), \qquad \kappa = \kappa(\vartheta,\boldsymbol{\phi},\mathbb{D}) \quad (3.100b)$$

are another given non-negative functions that all together characterize the entropy production $\xi = \frac{\zeta}{\vartheta}$,

$$\zeta = 2\nu\left|\mathbb{D}^\delta\right|^2 + \sum_{i,j=1}^{N-1}M_{ij}\,\nabla\widetilde{\mu}_j\cdot\nabla\widetilde{\mu}_i + \frac{\kappa}{\vartheta}\left|\nabla\vartheta\right|^2. \quad (3.101)$$

Summary 10: Governing equations for FI-CHNSF model

The system of governing equations for the unknown quantities $\vartheta, \boldsymbol{\phi}, \boldsymbol{v}$ and $\tilde{p}_{\mathrm{a}}$ reads[a]

$$\frac{\mathrm{d}\phi_i}{\mathrm{d}t} = \sum_{j=1}^{N-1} \operatorname{div}\left(M_{ij}\,\nabla\widetilde{\mu}_j\right), \quad i = 1, \ldots, N-1, \tag{3.102a}$$

$$\widetilde{\mu}_i = \widetilde{\mu}_i^{\,\phi} - \operatorname{div}\widetilde{\boldsymbol{\varsigma}}_i^{\phi} \quad i = 1, \ldots, N-1, \tag{3.102b}$$

$$\operatorname{div}\boldsymbol{v} = 0, \tag{3.102c}$$

$$\varrho\frac{\mathrm{d}\boldsymbol{v}}{\mathrm{d}t} + \Theta_2\left[\nabla\boldsymbol{v}\right]\boldsymbol{J} = \operatorname{div}\mathbb{T} + \varrho\boldsymbol{g}, \quad \boldsymbol{J} = -\sum_{i,j=1}^{N-1} M_{ij}\left(\hat{\varrho}_i - \hat{\varrho}_N\right)\nabla\widetilde{\mu}_j, \tag{3.102d}$$

and

$$\varrho \mathrm{c_v}\frac{\mathrm{d}\vartheta}{\mathrm{d}t} = \left(2\nu\mathbb{D} - \sum_{i=1}^{N-1}\vartheta\frac{\partial\widetilde{\boldsymbol{\varsigma}}_i^{\phi}}{\partial\vartheta}\otimes\nabla\phi_i\right) : \mathbb{D} + \sum_{i,j=1}^{N-1} M_{ij}\,\nabla\widetilde{\mu}_j\cdot\nabla\widetilde{\mu}_i$$
$$+ \sum_{i,j=1}^{N-1}\widetilde{\mu}_{i,\vartheta}\operatorname{div}\left(M_{ij}\,\nabla\widetilde{\mu}_j\right) + \operatorname{div}\left(\kappa\,\nabla\vartheta + \vartheta\sum_{i,j=1}^{N-1}\operatorname{div}\left(M_{ij}\,\nabla\widetilde{\mu}_j\right)\frac{\partial\widetilde{\boldsymbol{\varsigma}}_i^{\phi}}{\partial\vartheta}\right), \tag{3.102e}$$

where

$$\mathbb{T} = -\tilde{p}_{\mathrm{a}}\mathbb{I} + 2\nu\mathbb{D} - \sum_{i=1}^{N-1}\widetilde{\boldsymbol{\varsigma}}_i^{\phi}\otimes\nabla\phi_i, \tag{3.102f}$$

$$\widetilde{\mu}_{i,\vartheta} = \vartheta\frac{\partial\widetilde{\mu}_i^{\,\phi}}{\partial\vartheta} - \operatorname{div}\left(\vartheta\frac{\partial\widetilde{\boldsymbol{\varsigma}}_i^{\phi}}{\partial\vartheta}\right), \tag{3.102g}$$

and, finally,

$$\widetilde{\mu}_i^{\,\phi} = \frac{\partial\widetilde{\psi}_0}{\partial\phi_i}, \tag{3.102h}$$

$$\widetilde{\boldsymbol{\varsigma}}_i^{\phi} = \frac{a\varepsilon}{2}\sum_{j=1}^{N-1}\lambda_{ij}(\vartheta)\,\nabla\phi_j, \tag{3.102i}$$

$$\mathrm{c_v} = -\frac{\vartheta}{\varrho}\left(\frac{\partial^2\widetilde{\psi}_0}{\partial\vartheta^2} + \frac{a\varepsilon}{4}\sum_{i,j=1}^{N-1}\lambda_{ij}''(\vartheta)\,\nabla\phi_i\cdot\nabla\phi_j\right), \tag{3.102j}$$

where λ_{ij}'' denotes the second derivative of λ_{ij} with respect to ϑ.

[a] The auxiliary coefficient Θ_2 in (3.102d) is by default equal to 1. If we put $\Theta_2 = 0$, we reach the final level of approximation in the FI description, see Summary 7. With this type of approximation we rederive models that are based on coupling of CH with incompressible NS equations through advective term and capillary force respectively. Models of this type, for $N = 3$, were considered for example in Boyer and Lapuerta (2006), Boyer et al. (2010).

3.5 Interpolation of material parameters

The coefficients introduced in the constitutive relations for the Cauchy stress tensor and the energy flux are well-known from the context of the single-component NSF model. Indeed, ν represents the shear viscosity, $\tilde{\upsilon}$ is known as the bulk viscosity and κ corresponds to the thermal conductivity. All these coefficients are naturally defined in the mixing region by interpolating the relevant material parameters associated with individual components, that is ν_i, $\tilde{\upsilon}_i$ and κ_i respectively. In order to emphasize the role of the evolution equation for the temperature in our non-isothermal models, we admit that the material parameters can significantly depend on the temperature.

Following the simple expression of the total density in terms of volume fractions, see (2.10a), we define

$$\nu(\vartheta, \boldsymbol{\phi}) \stackrel{\text{def}}{=} \sum_{i=1}^{N-1} \left(\nu_i(\vartheta) - \nu_N(\vartheta)\right) \phi_i + \nu_N(\vartheta), \tag{3.103}$$

$$\tilde{\upsilon}(\vartheta, \boldsymbol{\phi}) \stackrel{\text{def}}{=} \sum_{i=1}^{N-1} \left(\tilde{\upsilon}_i(\vartheta) - \tilde{\upsilon}_N(\vartheta)\right) \phi_i + \tilde{\upsilon}_N(\vartheta), \tag{3.104}$$

$$\kappa(\vartheta, \boldsymbol{\phi}) \stackrel{\text{def}}{=} \sum_{i=1}^{N-1} \left(\kappa_i(\vartheta) - \kappa_N(\vartheta)\right) \phi_i + \kappa_N(\vartheta). \tag{3.105}$$

Let us emphasize that while the expression for the total density was obtained as the consequence of Assumptions 1–3, the definitions in (3.103)–(3.105) are purely artificial. In principle, any other type of interpolation can be considered, bearing in mind that **computed results can be significantly impacted by a particular choice of the interpolation**. This is demonstrated in Sections 6.1 and 6.3.

In our previous algebraic manipulations we have also used the so-called second viscosity coefficient υ which in our current setting corresponds to[6]

$$\upsilon(\vartheta, \boldsymbol{\phi}) = \tilde{\upsilon}(\vartheta, \boldsymbol{\phi}) - \frac{2}{3}\nu(\vartheta, \boldsymbol{\phi}). \tag{3.106}$$

3.6 Generalizations of existing binary models

In the remainder of this chapter, we shall formulate reduced versions of the previously derived models, which are applicable for systems involving only two components. We shall point out what are the new features of these models when compared to some existing and well-known models which are available in the literature.

Let us make some remarks concerning the notation used in this section. Knowing that here we will always work with two components, we shall drop the superfluous subscripts, which have been used to associate the quantities with relevant

[6]Since the interpolation used in (3.103) and (3.104) is linear, we immediately see that υ is given as the same linear combination of the coefficients $\upsilon_i = \tilde{\upsilon}_i - 2\nu_i/3$.

components, whenever no confusion can arise. For example, we use the notation $c = c_1$, $\mu^c = \mu_1^c$, $\phi = \phi_1$, $\sigma = \sigma_{12}$, $\hat{r} = \hat{r}_1$ and so forth, but we keep the indices to differentiate between $\hat{\varrho}_1$ and $\hat{\varrho}_2$, or ϱ_1 and ϱ_2. Derivatives of functions with a single argument, like $\sigma(\vartheta)$ or $f(\phi)$, will be denoted by prime. (That is, σ' denotes the derivative of σ with respect to ϑ, while f' denotes the derivative of f with respect to ϕ.)

Sections 3.6.1–3.6.3 have the same structure. Each of them begins with the formulation of the generalized binary model in the chosen description, then we provide its reduction to the isothermal setting, and finally, we discuss its reduction to the setting with only one single-component fluid.

3.6.1 Binary FC-CHNSF model

In this section, we formulate the full system of governing equations for a compressible **heat conducting fluid-like mixture** consisting of two components with **temperature-dependent material parameters**. The model presented here generalizes its isothermal counterpart previously derived in Lowengrub and Truskinovsky (1998).

Non-isothermal model

Let us consider a binary mixture with the specific Helmholtz free energy ψ given by (3.13), that is

$$\psi(\vartheta, \varrho, c, \nabla c) = \frac{1}{2}\epsilon\sigma(\vartheta)\,|\nabla c|^2 + \psi_{\text{th}}(\vartheta, \varrho, c). \tag{3.107}$$

Note that (Lowengrub and Truskinovsky, 1998, Eq. (3.31)) used the same *ansatz* with the temperature-independent coefficient $\epsilon_{\text{LT}} \equiv \epsilon\sigma$ and ψ_{th} restricted to the isothermal setting. In what follows, we explicitly write $\sigma = \sigma(\vartheta)$ in order to emphasize the difference between the standard setting and the setting with a temperature-dependent surface tension. The system of governing equations for the primitive quantities ϑ, ϱ, c and $\boldsymbol{v}$ reads

$$\varrho\frac{\mathrm{d}c}{\mathrm{d}t} = \operatorname{div}(M\,\nabla\mu), \quad \mu = \mu^c - \frac{\epsilon}{\varrho}\operatorname{div}(\varrho\sigma(\vartheta)\,\nabla c) \tag{3.108a}$$

$$\frac{\mathrm{d}\varrho}{\mathrm{d}t} = -\varrho\operatorname{div}\boldsymbol{v}, \tag{3.108b}$$

$$\varrho\frac{\mathrm{d}\boldsymbol{v}}{\mathrm{d}t} = -\nabla p_{\text{th}}^{\text{NSF}} + \nabla(\upsilon\operatorname{div}\boldsymbol{v}) + \operatorname{div}(2\nu\mathbb{D} - \epsilon\sigma(\vartheta)\varrho\,\nabla c\otimes\nabla c) + \varrho\boldsymbol{g}, \tag{3.108c}$$

and

$$\begin{aligned}\varrho\left(\mathrm{c}_{\mathrm{v}}^{\text{NSF}} - \frac{\vartheta\epsilon}{2}\sigma''(\vartheta)\,|\nabla c|^2\right)\frac{\mathrm{d}\vartheta}{\mathrm{d}t} &= (2\nu\mathbb{D} - \varrho\vartheta\epsilon\sigma'(\vartheta)\,\nabla c\otimes\nabla c) : \mathbb{D}\\ &+ \left(\upsilon\operatorname{div}\boldsymbol{v} - \vartheta\frac{\partial p_{\text{th}}^{\text{NSF}}}{\partial\vartheta}\right)\operatorname{div}\boldsymbol{v} + \operatorname{div}(\kappa\,\nabla\vartheta + \vartheta\epsilon\sigma'(\vartheta)\operatorname{div}(M\,\nabla\mu)\,\nabla c)\\ &+ M\,|\nabla\mu|^2 + \left(\vartheta\frac{\partial\mu^c}{\partial\vartheta} - \frac{\epsilon}{\varrho}\operatorname{div}(\varrho\vartheta\sigma'(\vartheta)\,\nabla c)\right)\operatorname{div}(M\,\nabla\mu),\end{aligned} \tag{3.108d}$$

where[7]

$$\mu^c = \frac{\partial \psi_{\mathrm{th}}}{\partial c}, \qquad \mathrm{c_v^{NSF}} = \vartheta \frac{\partial^2 \psi_{\mathrm{th}}}{\partial \vartheta^2}, \qquad p_{\mathrm{th}}^{\mathrm{NSF}} = \varrho^2 \frac{\partial \psi_{\mathrm{th}}}{\partial \varrho}. \tag{3.108e}$$

Recall that the material parameters ν, υ, κ and M are—in a general case—some given functions of ϑ, ϱ, c and possibly $\mathbb{D}$.

If we can assume that σ is independent of the temperature, but we aim to work in the non-isothermal setting with variable temperature field and one or more temperature-dependent material parameters ν, υ, κ, or M, then the corresponding evolution equation for ϑ reads

$$\varrho \mathrm{c_v^{NSF}} \frac{\mathrm{d}\vartheta}{\mathrm{d}t} = 2\nu\mathbb{D} : \mathbb{D} + \left(\upsilon \operatorname{div} \boldsymbol{v} - \vartheta \frac{\partial p_{\mathrm{th}}^{\mathrm{NSF}}}{\partial \vartheta} \right) \operatorname{div} \boldsymbol{v} + \operatorname{div} (\kappa \nabla \vartheta) + M \left| \nabla \mu \right|^2 + \vartheta \frac{\partial \mu^c}{\partial \vartheta} \operatorname{div} (M \nabla \mu). \tag{3.109}$$

Reduction to the isothermal model

In the isothermal setting we are typically not concerned with the evolution equation for ϑ. If we suppress the temperature effects in equations (3.108a)–(3.108c), then the resulting model coincides with the one derived in (Lowengrub and Truskinovsky, 1998, Eq. (3.34)). We do not repeat the equations here for the sake of brevity.

Reduction to a single-component fluid

Finally, let us imagine that we want to apply the above model in the setting with a single-component fluid. In such a case we have $\varrho \equiv \varrho_1$ and thus we put $c \equiv 1$ everywhere in (3.108a)–(3.108d). If we can additionally assume that the diffusive flux $\boldsymbol{j} = -M \nabla \mu$ vanishes, then c does not evolve according to (3.108a). Moreover, the rest of the system coincides with the standard compressible NSF equations

$$\frac{\mathrm{d}\varrho}{\mathrm{d}t} = -\varrho \operatorname{div} \boldsymbol{v}, \tag{3.110a}$$

$$\varrho \frac{\mathrm{d}\boldsymbol{v}}{\mathrm{d}t} = -\nabla p_{\mathrm{th}}^{\mathrm{NSF}} + \nabla(\upsilon \operatorname{div} \boldsymbol{v}) + \operatorname{div} (2\nu\mathbb{D}) + \varrho \boldsymbol{g}, \tag{3.110b}$$

$$\varrho \mathrm{c_v^{NSF}} \frac{\mathrm{d}\vartheta}{\mathrm{d}t} = 2\nu\mathbb{D} : \mathbb{D} + \left(\upsilon \operatorname{div} \boldsymbol{v} - \vartheta \frac{\partial p_{\mathrm{th}}^{\mathrm{NSF}}}{\partial \vartheta} \right) \operatorname{div} \boldsymbol{v} + \operatorname{div} (\kappa \nabla \vartheta). \tag{3.110c}$$

The assumption of vanishing diffusive flux will be discussed in more detail later when we are dealing with incompressible mixtures.

[7] We use the notation with $^{\mathrm{NSF}}$ to emphasize that the relevant quantities coincide with their counterparts traditionally introduced in the context of NSF equations, provided that only one component is present in our considered physical system.

3.6.2 Binary QI-CHNSF model

In this section, we formulate the full system of governing equations for a quasi-incompressible **heat conducting fluid-like mixture** consisting of two components with **temperature-dependent material parameters**. It generalizes the isothermal binary model studied by Shen et al. (2013).

Non-isothermal model

Let us consider a binary mixture the components of which have constant material densities $\hat{\varrho}_1$ and $\hat{\varrho}_2$. The total density ϱ is given by (2.10a), that is

$$\varrho = \varrho(\phi) = (\hat{\varrho}_1 - \hat{\varrho}_2)\phi + \hat{\varrho}_2 = \hat{\varrho}_2 \left(1 - \hat{r}\phi\right), \tag{3.111}$$

where $\hat{r} = 1 - \hat{\varrho}_1/\hat{\varrho}_2$. We further assume that the coefficients ν, $\tilde{v}$ and κ are temperature-dependent, given by (3.103)–(3.105) for $N = 2$. On the other hand, from now on we assume that the influence of the temperature on the surface tension is negligible, so that $\sigma \equiv \hat{\sigma}$ is a given constant. (This assumption is made for the sake of brevity of the formulae that would otherwise involve extra terms with derivatives of σ.) Last but not least, the mobility coefficient M is supposed to degenerate in the pure components, meaning that

$$M|_{\phi=0} = M|_{\phi=1} = 0. \tag{3.112}$$

We will see that this assumption is crucial for the correct reduction of the model to the case with a single-component fluid in the current setting.

Let the specific Helmholtz free energy is given by (3.15) with

$$\widetilde{\psi}(\vartheta, \phi, \nabla\phi) = \frac{a}{2}\varepsilon\hat{\sigma}\,|\nabla\phi|^2 + b\frac{\hat{\sigma}}{\varepsilon}f(\phi) + (\widetilde{\psi}_1(\vartheta) - \widetilde{\psi}_2(\vartheta))\phi + \widetilde{\psi}_2(\vartheta), \tag{3.113}$$

see (3.17) and (3.19) respectively. The function $f(\phi) = \phi^2(1-\phi)^2$ represents the double-well potential for which we have $a = \frac{3}{2}$ and $b = 12$ as stated in (3.10b). The individual Helmholtz free energy densities are again assumed to be given by (3.22). Under these conditions we obtain the following identity for the specific heat at constant volume, namely

$$\varrho \mathrm{c_v} = (\hat{\varrho}_1\hat{\mathrm{c}}_{\mathrm{v},1} - \hat{\varrho}_2\hat{\mathrm{c}}_{\mathrm{v},2})\phi + \hat{\varrho}_2\hat{\mathrm{c}}_{\mathrm{v},2}, \tag{3.114}$$

cf. (3.28). (Note that if $\hat{\mathrm{c}}_{\mathrm{v},1} = \hat{\mathrm{c}}_{\mathrm{v},2} = \hat{\mathrm{c}}_{\mathrm{v}}$, then we have $\mathrm{c_v} \equiv \hat{\mathrm{c}}_{\mathrm{v}}$.) The quantities introduced in (3.30) correspond to

$$\widetilde{\mu}^{\,\phi} = 12\frac{\hat{\sigma}}{\varepsilon}f'(\phi) + \widetilde{\psi}_1(\vartheta) - \widetilde{\psi}_2(\vartheta), \qquad \widetilde{\boldsymbol{\varsigma}}^{\,\phi} = \frac{3}{2}\varepsilon\hat{\sigma}\,\nabla\phi. \tag{3.115}$$

The system of governing equations for the unknown quantities $\vartheta, \phi, \boldsymbol{v}$ and p_{a} reads

$$\frac{\mathrm{d}\phi}{\mathrm{d}t} = -\phi \operatorname{div} \boldsymbol{v} + \operatorname{div}(M \nabla \widetilde{\mu}_{\mathrm{a}}^{p}), \tag{3.116a}$$

$$\widetilde{\mu}_{\mathrm{a}}^{p} = \widetilde{\mu} + \hat{r} p_{\mathrm{a}}, \quad \widetilde{\mu} = -\frac{3}{2}\varepsilon\hat{\sigma}\Delta\phi + 12\frac{\hat{\sigma}}{\varepsilon} f'(\phi) + \widetilde{\psi}_1(\vartheta) - \widetilde{\psi}_2(\vartheta), \tag{3.116b}$$

$$\operatorname{div} \boldsymbol{v} = \hat{r} \operatorname{div}(M \nabla \widetilde{\mu}_{\mathrm{a}}^{p}), \tag{3.116c}$$

$$\varrho \frac{\mathrm{d}\boldsymbol{v}}{\mathrm{d}t} = -\nabla\Big(p_{\mathrm{a}} - \widetilde{\psi} + \phi\widetilde{\mu} - \upsilon \operatorname{div} \boldsymbol{v}\Big) + \operatorname{div}\left(2\nu\mathbb{D} - \frac{3}{2}\varepsilon\hat{\sigma}\, \nabla\phi \otimes \nabla\phi\right) + \varrho \boldsymbol{g}, \tag{3.116d}$$

and

$$\varrho \mathrm{c}_{\mathrm{v}} \frac{\mathrm{d}\vartheta}{\mathrm{d}t} = 2\nu\mathbb{D} : \mathbb{D} + \left(\upsilon \operatorname{div} \boldsymbol{v} + \vartheta \frac{\partial \widetilde{\psi}}{\partial \vartheta}\right) \operatorname{div} \boldsymbol{v} + \operatorname{div}(\kappa \nabla \vartheta) + M\,|\nabla \widetilde{\mu}_{\mathrm{a}}^{p}|^2 + (1 - \hat{r}\phi)\vartheta \Big(\widetilde{\psi}_1'(\vartheta) - \widetilde{\psi}_2'(\vartheta)\Big) \operatorname{div}(M \nabla \widetilde{\mu}_{\mathrm{a}}^{p}). \tag{3.116e}$$

The tensor product under the divergence in (3.116d) can be manipulated using the sequence of identities

$$\operatorname{div}\left(\frac{3}{2}\varepsilon\hat{\sigma}\, \nabla\phi \otimes \nabla\phi\right) = \frac{3}{2}\varepsilon\hat{\sigma}\left(\Delta\phi\, \nabla\phi + \frac{1}{2}\nabla\big(|\nabla\phi|^2\big)\right) = \frac{3}{4}\varepsilon\hat{\sigma}\, \nabla\big(|\nabla\phi|^2\big) + \left(12\frac{\hat{\sigma}}{\varepsilon} f'(\phi) + \widetilde{\psi}_1(\vartheta) - \widetilde{\psi}_2(\vartheta) - \widetilde{\mu}\right) \nabla\phi = \nabla\widetilde{\psi} - \frac{\partial \widetilde{\psi}}{\partial \vartheta} \nabla\vartheta - \widetilde{\mu} \nabla\phi.$$

Equation (3.116d) then reduces to

$$\varrho \frac{\mathrm{d}\boldsymbol{v}}{\mathrm{d}t} = -\nabla p_{\mathrm{a}} + \operatorname{div}(2\nu\mathbb{D} + \upsilon(\operatorname{div} \boldsymbol{v})\mathbb{I}) - \phi \nabla\widetilde{\mu} + \frac{\partial \widetilde{\psi}}{\partial \vartheta} \nabla\vartheta + \varrho \boldsymbol{g}. \tag{3.117}$$

Reduction to the isothermal model

Let us consider the standard isothermal setting with the temperature being fixed at $\hat{\vartheta}_{\mathrm{iso}}$. In such a case we are not concerned with the evolution equation for ϑ and equations (3.116a)–(3.116d) take the reduced form

$$\frac{\mathrm{d}\phi}{\mathrm{d}t} = -\phi \operatorname{div} \boldsymbol{v} + \operatorname{div}(M \nabla \widetilde{\mu}_{\mathrm{a}}^{p}), \tag{3.118a}$$

$$\widetilde{\mu}_{\mathrm{a}}^{p} = \widetilde{\mu} + \hat{r} p_{\mathrm{a}}, \quad \widetilde{\mu} = -\frac{3}{2}\varepsilon\hat{\sigma}\Delta\phi + 12\frac{\hat{\sigma}}{\varepsilon} f'(\phi), \tag{3.118b}$$

$$\operatorname{div} \boldsymbol{v} = \hat{r} \operatorname{div}(M \nabla \widetilde{\mu}_{\mathrm{a}}^{p}), \tag{3.118c}$$

$$\varrho \frac{\mathrm{d}\boldsymbol{v}}{\mathrm{d}t} = -\nabla p_{\mathrm{a}} + \operatorname{div}(2\nu\mathbb{D} + \upsilon(\operatorname{div} \boldsymbol{v})\mathbb{I}) - \phi \nabla\widetilde{\mu} + \varrho \boldsymbol{g}. \tag{3.118d}$$

The above system of equations represents the isothermal model previously derived by (Shen et al., 2013, Eq. (2.13)). Moreover, it can be shown that the model (3.118) can be obtained as a special case (without phase transitions) of the generalized model developed by Aki et al. (2014).

Remark 3.8. A slightly different, isothermal formulation of the binary quasi-incompressible model in terms of mass fractions can be found in (Lowengrub and Truskinovsky, 1998, Sect. 4), where the authors gave a theoretical reasoning for the derivation of the model based on the thermodynamic description in terms of the Gibbs free energy. The approach applied within this thesis, however, leads to the qualitatively same model.

Reduction to a single-component fluid

The couple of conditions in (3.112) ensures that $\widetilde{\boldsymbol{\jmath}} = -M\,\nabla\widetilde{\mu}_{\mathrm{a}}^{p}$ vanishes (degenerates) in pure components. If we put $\phi \equiv 1$ in (3.116), which corresponds to the setting with a single incompressible fluid, then $\operatorname{div}\boldsymbol{v} = 0$ according to (3.116c) and the right hand side of (3.116a) is also equal to zero. Consequently, ϕ does not evolve in time and remains identically equal to 1. (The analogous observation can be made with $\phi \equiv 0$.)

Remark 3.9. If M was constant, it would not be ensured that ϕ does not evolve due to the presence of p_{a} and $\widetilde{\psi}_1(\vartheta) - \widetilde{\psi}_2(\vartheta)$ in (3.116b). The latter term vanishes in the isothermal setting as a consequence of (3.21). In Appendix B, we propose an alternative non-isothermal extension of the double-well potential which ensures that $\widetilde{\mu} \equiv 0$ if either $\phi \equiv 1$ or $\phi \equiv 0$. The pressure term, however, remains "active" even in the isothermal setting. Shen et al. (2013) numerically compared the full model against its approximated version with $\widetilde{\mu}_{\mathrm{a}}^{p} \approx \widetilde{\mu}$. The predictions made by the two models were consistent in their numerical examples.

Provided that we are dealing with a single incompressible fluid, taking into account the degenerate mobility (3.112), we see that the model given by (3.116) reduces to the standard system of incompressible NSF equations for the unknowns $\vartheta, \boldsymbol{v}$ and p, namely

$$\operatorname{div}\boldsymbol{v} = 0, \tag{3.119a}$$

$$\varrho\frac{\mathrm{d}\boldsymbol{v}}{\mathrm{d}t} = -\nabla p + \operatorname{div}(2\nu\mathbb{D}) + \varrho\boldsymbol{g}, \tag{3.119b}$$

$$\varrho c_{\mathrm{v}}\frac{\mathrm{d}\vartheta}{\mathrm{d}t} = 2\nu\mathbb{D} : \mathbb{D} + \operatorname{div}(\kappa\,\nabla\vartheta). \tag{3.119c}$$

Here, the augmented pressure p corresponds to $p_{\mathrm{a}} - \widetilde{\psi}_2$, where the correction comes from the free energy density appearing under the gradient in (3.116d).

3.6.3 Binary FI-CHNSF model

In this section, we formulate the full system of governing equations for a fully-incompressible **heat conducting fluid-like mixture** consisting of two components with **temperature-dependent material parameters**. Technically it is the same material as in the previous case, but its behaviour is described differently from the modelling point of view. It generalizes the isothermal binary model originally developed by Abels et al. (2012).

Non-isothermal model

In the current setting we use the same *ansatz* for the specific Helmholtz free energy as in the previous section, see (3.113), hence we shall also use the notation introduced therein. The system of governing equations for the unknown quantities $\vartheta, \phi, \boldsymbol{v}$ and $\tilde{p}_{\mathrm{a}}$ reads

$$\frac{\mathrm{d}\phi}{\mathrm{d}t} = \operatorname{div}(M\,\nabla\widetilde{\mu}), \tag{3.120a}$$

$$\widetilde{\mu} = -\frac{3}{2}\varepsilon\hat{\sigma}\Delta\phi + 12\frac{\hat{\sigma}}{\varepsilon}f'(\phi) + \widetilde{\psi}_1(\vartheta) - \widetilde{\psi}_2(\vartheta), \tag{3.120b}$$

$$\operatorname{div}\boldsymbol{v} = 0, \tag{3.120c}$$

$$\varrho\frac{\mathrm{d}\boldsymbol{v}}{\mathrm{d}t} + \Theta_2\,[\nabla\boldsymbol{v}]\,\boldsymbol{J} = -\nabla\tilde{p}_{\mathrm{a}} + \operatorname{div}\left(2\nu\mathbb{D} - \frac{3}{2}\varepsilon\hat{\sigma}\,\nabla\phi\otimes\nabla\phi\right) + \varrho\boldsymbol{g}, \tag{3.120d}$$

and

$$\varrho c_{\mathrm{v}}\frac{\mathrm{d}\vartheta}{\mathrm{d}t} = 2\nu\mathbb{D}:\mathbb{D} + \operatorname{div}(\kappa\,\nabla\vartheta) + M\,|\nabla\widetilde{\mu}|^2 + \vartheta\left(\widetilde{\psi}_1'(\vartheta) - \widetilde{\psi}_2'(\vartheta)\right)\operatorname{div}(M\,\nabla\widetilde{\mu}), \tag{3.120e}$$

with $\boldsymbol{J} = -M(\hat{\varrho}_1 - \hat{\varrho}_2)\,\nabla\widetilde{\mu}$. Recall that Θ_2 is the constant toggle coefficient which is by default equal to 1. Equation (3.120d) can be manipulated exactly as in the previous case of (3.116d) to take the form

$$\varrho\frac{\mathrm{d}\boldsymbol{v}}{\mathrm{d}t} + \Theta_2\,[\nabla\boldsymbol{v}]\,\boldsymbol{J} = -\nabla p_{\mathrm{a}} + \operatorname{div}(2\nu\mathbb{D}) - \phi\,\nabla\widetilde{\mu} + \frac{\partial\widetilde{\psi}}{\partial\vartheta}\,\nabla\vartheta + \varrho\boldsymbol{g}, \tag{3.121}$$

where $p_{\mathrm{a}} = \tilde{p}_{\mathrm{a}} + \widetilde{\psi} - \phi\widetilde{\mu}$ formally coincides with the augmented pressure defined in (3.64). Indeed, the same relation between the two quantities can be obtained by comparing (3.75) and (3.94), provided that we take into account the constraint $\operatorname{div}\boldsymbol{v} = 0$ in the former relation.

Reduction to the isothermal model

Let us consider the standard isothermal setting with the temperature being fixed at $\hat{\vartheta}_{\mathrm{iso}}$. In such a case we are not concerned with the evolution equation for ϑ and equations (3.120a)–(3.120d) take the reduced form

$$\frac{\mathrm{d}\phi}{\mathrm{d}t} = \operatorname{div}(M\,\nabla\widetilde{\mu}), \tag{3.122a}$$

$$\widetilde{\mu} = -\frac{3}{2}\varepsilon\hat{\sigma}\Delta\phi + 12\frac{\hat{\sigma}}{\varepsilon}f'(\phi), \tag{3.122b}$$

$$\operatorname{div}\boldsymbol{v} = 0, \tag{3.122c}$$

$$\varrho\frac{\mathrm{d}\boldsymbol{v}}{\mathrm{d}t} + \Theta_2\,[\nabla\boldsymbol{v}]\,\boldsymbol{J} = -\nabla p_{\mathrm{a}} + \operatorname{div}(2\nu\mathbb{D}) - \phi\,\nabla\widetilde{\mu} + \varrho\boldsymbol{g}. \tag{3.122d}$$

If $\Theta_2 = 1$, then the above system of equations corresponds to the model originally developed by Abels et al. (2012). The equations with $\Theta_2 = 0$ were previously used for example by Ding et al. (2007) and Shen and Yang (2010); see also Aland and Voigt (2012).

Reduction to a single-component fluid

Provided that we are dealing with a single incompressible fluid, which can be again achieved by considering $\phi \equiv 1$ in the governing equations, we observe that the model given by (3.120) reduces to the standard system of incompressible NSF equations (3.119) for the primitive variables ϑ, $\boldsymbol{v}$ and p.

Let us emphasize that in the isothermal setting it is not necessary to consider degenerate mobility (3.112) to enforce zero diffusive flux in pure components. Indeed, we see that $\widetilde{\mu}$ in (3.122b) is identically zero if either $\phi \equiv 1$ or $\phi \equiv 0$. As a consequence, the diffusive flux $\widetilde{\boldsymbol{j}} = -M\,\nabla\widetilde{\mu}$ also vanishes in pure components.

3.6.4 Proposal of a simple study case

Let us consider two incompressible fluids of equal density ($\hat{\varrho} = \hat{\varrho}_1 = \hat{\varrho}_2$). We can immediately observe that the two models (3.116) and (3.120) coincide in this special case, as the assumption on matching densities yields $\hat{r} = 1 - \hat{\varrho}_1/\hat{\varrho}_2 = 0$ and $\boldsymbol{J} = -M(\hat{\varrho}_1 - \hat{\varrho}_2)\,\nabla\widetilde{\mu} = \boldsymbol{0}$. The degenerate mobility M is considered to take the simple form

$$M(\phi) = M_0(1-\phi)^2\phi^2, \tag{3.123}$$

where M_0 is a positive constant.

The two fluids are supposed to have the same constant viscosity ($\hat{\nu} = \hat{\nu}_1 = \hat{\nu}_2$), but the coefficients of specific heat at constant volume are assumed to be different for each material ($\hat{\mathrm{c}}_{\mathrm{v},1} \neq \hat{\mathrm{c}}_{\mathrm{v},2}$). The last assumption applies also for the constant coefficients of thermal conductivity ($\hat{\kappa}_1 \neq \hat{\kappa}_2$). The corresponding system of governing equations for the unknown variables ϑ, ϕ, $\boldsymbol{v}$ and p_{a} reads

$$\frac{\mathrm{d}\phi}{\mathrm{d}t} = \operatorname{div}(M\,\nabla\widetilde{\mu}), \tag{3.124a}$$

$$\widetilde{\mu} = -\frac{3}{2}\varepsilon\hat{\sigma}\Delta\phi + 12\frac{\hat{\sigma}}{\varepsilon}f'(\phi) + \widetilde{\psi}_1(\vartheta) - \widetilde{\psi}_2(\vartheta), \tag{3.124b}$$

$$\operatorname{div}\boldsymbol{v} = 0, \tag{3.124c}$$

$$\hat{\varrho}\frac{\mathrm{d}\boldsymbol{v}}{\mathrm{d}t} = -\nabla p_{\mathrm{a}} + \hat{\nu}\Delta\boldsymbol{v} - \phi\,\nabla\widetilde{\mu} + \frac{\partial\widetilde{\psi}}{\partial\vartheta}\nabla\vartheta + \hat{\varrho}\boldsymbol{g}, \tag{3.124d}$$

and

$$\hat{\varrho}\mathrm{c}_{\mathrm{v}}\frac{\mathrm{d}\vartheta}{\mathrm{d}t} = 2\hat{\nu}\mathbb{D}:\mathbb{D} + \operatorname{div}(\kappa\,\nabla\vartheta) + M\,|\nabla\widetilde{\mu}|^2 + \vartheta\left(\widetilde{\psi}_1'(\vartheta) - \widetilde{\psi}_2'(\vartheta)\right)\operatorname{div}(M\,\nabla\widetilde{\mu}). \tag{3.124e}$$

The first dissipation term on the right hand side of the temperature equation is often neglected in practical applications. On the other hand, the last two terms in the same equation are non-standard and their influence on the dynamics of the moving interfaces should be subject to a deeper numerical study in an appropriate geometrical setting. Dimensionless analysis of the presented model will be carried out as a part of our upcoming research.

Chapter 4

Isothermal Flows of Immiscible Incompressible Fluids

Despite the fact that our target application described in Section 1.1 is clearly non-isothermal, and in fact the temperature effects play the essential role in the float glass forming process, its initial stage is considered to be isothermal in our first modelling approach[1]. Proper handling of numerical simulations in such approximated setting is a prerequisite for further research regarding the applicability of CHNSF models in a similar type of problems.

Recall that all fluids involved in our target application are modelled as being incompressible. Hence, in the remainder of the thesis we shall restrict our attention to models developed for incompressible multi-component systems, see Figure 1.7. Shen et al. (2013) in their numerical study compared binary CHNS models that in our terminology correspond to QI and FI variants presented in Sections 3.6.2 and 3.6.3 respectively. According to the observations made in that study, the deviation between the predictions by both type of models depends on the size of the mixing zone. In particular, when the size of the mixing zone is small compared to the entire fluid domain, exactly like in our case of thin interfacial layers separating the immiscible fluids, both model predictions agree qualitatively[2].

One of the characteristic features of the QI model is the non-solenoidal mass-averaged velocity field. Different sophisticated solution strategies have been recently developed for this type of model (or its approximations), see for example Shen et al. (2013), Guo et al. (2014) or Roudbari et al. (2018), yet we prefer to work with the FI model which incorporates the incompressible NS equations with the divergence-free velocity. The latter variant thus offers the possibility to directly exploit efficient preconditioning strategies that have been developed in the context of incompressible fluid flows for recent decades; see the review paper by Benzi et al. (2005). One of the strategies will be discussed later in Section 5.4.

In this chapter, in particular in Section 4.1, we first formulate a set of con-

[1]The temperature variations in the close proximity of the spout lip are expected to occur only at moderate scales (compared to variations observed in the full manufacturing process).

[2]In the thesis we are not interested in simulations with large mixing zones, like in the phase separation process described in Section 3.1.1, for which the numerical tests carried out by Shen et al. (2013) showed different dynamics with respect to the chosen variant of the model.

sistency conditions that are expected to be satisfied by the N-component model with $N \geq 3$. Based on the consistency conditions, we obtain the appropriate form of the mixing surface energy coefficients, the mobility matrix, and also the appropriate form of the nonlinear potential function with the multi-well structure. The same approach was originally used by Boyer and Minjeaud (2014), and it was applied also in the recent studies by Dong (2017) or Wu and Xu (2017). The complete description of the final version of the model, including boundary and initial conditions, is given in Section 4.2.

4.1 Consequences of consistency conditions

In this section, we formulate a set of four consistency conditions for incompressible multi-component systems with more than two components. These conditions play the crucial role regarding the choice of the mixing surface energy coefficients λ_{ij}, the mobility coefficients M_{ij} and the multi-well potential F; see (3.99), (3.100a), and (3.27) respectively.

The conditions adopted in the thesis are based on the concept of algebraic consistency as it was first formalized by Boyer and Lapuerta (2006), who used it to derive a suitable form of the free energy functional for ternary CH models. This concept was later generalized and discussed in the context of N-component CH models in the distinguished work by Boyer and Minjeaud (2014). The idea is based on the requirement of proper reduction of the N-component models to the K-component ones ($2 \leq K \leq N-1$) whenever $L = N - K$ components are absent in the system. Recently, Dong (2017) extended the basic set of consistency conditions and used them in the context of CHNS models.

Let us formulate the consistency conditions for the general non-isothermal models from Sections 3.3.4 and 3.4.4. We shall use the term "N-component free energy density" as the equivalent of (3.26), and "N-component governing equations" as the reference for either (3.84) or (3.102). Inspired by Dong (2017), we consider the following set of consistency conditions:

($\mathcal{C}1$) The N-component free energy density is required to coincide with (3.17) if $N = 2$.

($\mathcal{C}2$) The N-component free energy density is required to reduce to the K-component free energy density if only K ($2 \leq K \leq N-1$) components are present in the physical system.

($\mathcal{C}3$) If L ($1 \leq L \leq N-2$) components are absent from the initial data, they are required to remain absent in the solution of the corresponding N-component problem.

($\mathcal{C}4$) The N-component governing equations are required to reduce to the K-component governing equations if only K ($2 \leq K \leq N-1$) components are present in the physical system.

The first two conditions determine the choice of the coefficients λ_{ij} in (3.26). Before we start to explore consequences of the other required properties, let us

restate the equations (3.84a) and (3.102a) in their vector form using the full vector of volume fractions $\boldsymbol{\phi}_\star = [\phi_1, \dots, \phi_N]^\top$. We begin with (3.84a), that is

$$\frac{\mathrm{d}\phi_i}{\mathrm{d}t} + \phi_i \operatorname{div} \boldsymbol{v} = \sum_{j=1}^{N-1} \operatorname{div} \left(M_{ij} \, \nabla(\widetilde{\mu}_j + \hat{r}_j p_\mathrm{a}) \right), \quad i = 1, \dots, N-1. \tag{4.1a}$$

The evolution equation for ϕ_N can be obtained as a consequence of (2.8), (3.84a) and (3.84c). It reads

$$\frac{\mathrm{d}\phi_N}{\mathrm{d}t} + \phi_N \operatorname{div} \boldsymbol{v} = \operatorname{div} \left(\sum_{i,j=1}^{N-1} (\hat{r}_i - 1) \, M_{ij} \, \nabla(\widetilde{\mu}_j + \hat{r}_j p_\mathrm{a}) \right). \tag{4.1b}$$

Let us introduce the following auxiliary notation

$$\mathbf{Z}_{\hat{\mathbf{r}}} = \begin{bmatrix} \mathbf{I}_{N-1} \\ (\hat{\mathbf{r}} - \mathbf{1}_{N-1})^\top \end{bmatrix}_{N \times (N-1)}, \tag{4.2}$$

where $\mathbf{I}_{N-1} = [\delta_{ij}]_{(N-1)\times(N-1)}$, $\hat{\mathbf{r}} = [\hat{r}_i]_{(N-1)\times 1}$ and $\mathbf{1}_{N-1} = [1]_{(N-1)\times 1}$. Further, let $\widetilde{\boldsymbol{\mu}} = [\widetilde{\mu}_i]_{(N-1)\times 1}$ denote the vector of generalized chemical potentials with entries given by (3.84b). The equations in (4.1) can be rewritten in the matrix form

$$\frac{\mathrm{d}\boldsymbol{\phi}_\star}{\mathrm{d}t} + \boldsymbol{\phi}_\star \operatorname{div} \boldsymbol{v} = \operatorname{div} \left(\mathbf{Z}_{\hat{\mathbf{r}}} \mathbf{M} \, \nabla(\widetilde{\boldsymbol{\mu}} + p_\mathrm{a} \hat{\mathbf{r}}) \right). \tag{4.3}$$

In the same way we deduce that (3.102a) expressed in the matrix form reads

$$\frac{\mathrm{d}\boldsymbol{\phi}_\star}{\mathrm{d}t} = \operatorname{div} \left(\mathbf{Z}_{\mathbf{0}} \mathbf{M} \, \nabla \widetilde{\boldsymbol{\mu}} \right). \tag{4.4}$$

Note that this equation formally coincides with (4.3) provided that $\hat{\mathbf{r}} = \mathbf{0}$, which further implies that $\operatorname{div} \boldsymbol{v} = 0$ by virtue of (3.84c). According to (3.81b), (3.84h) and (3.84i), we see that

$$\widetilde{\boldsymbol{\mu}} = -\frac{a\varepsilon}{2} \operatorname{div} \left(\boldsymbol{\Lambda} \, \nabla \boldsymbol{\phi} \right) + \frac{b}{\varepsilon} \mathbf{d}^F + \widetilde{\boldsymbol{\psi}}^{\mathrm{diff}}, \tag{4.5a}$$

where

$$\mathbf{d}^F = \left[\frac{\partial F}{\partial \phi_i} \right]_{(N-1)\times 1}, \qquad \widetilde{\boldsymbol{\psi}}^{\mathrm{diff}} = \left[\widetilde{\psi}_i(\vartheta) - \widetilde{\psi}_N(\vartheta) \right]_{(N-1)\times 1}. \tag{4.5b}$$

Substitution of the above formula into (4.3) yields

$$\frac{\mathrm{d}\boldsymbol{\phi}_\star}{\mathrm{d}t} + \boldsymbol{\phi}_\star \operatorname{div} \boldsymbol{v} = \operatorname{div} \left[\mathbf{Z}_{\hat{\mathbf{r}}} \mathbf{M} \, \nabla \left(-\frac{a\varepsilon}{2} \operatorname{div} \left(\boldsymbol{\Lambda} \, \nabla \boldsymbol{\phi} \right) + \frac{b}{\varepsilon} \mathbf{d}^F + \widetilde{\boldsymbol{\psi}}^{\mathrm{diff}} + p_\mathrm{a} \hat{\mathbf{r}} \right) \right]. \tag{4.6}$$

Obviously, to satisfy consistency conditions ($\mathcal{C}2$)–($\mathcal{C}4$) it suffices to consider the case with exactly one component that is absent in the physical system, meaning that we need to ensure the correct reduction of the N-component model to the

$(N-1)$-component model. Suppose that the fluid k is absent in our considered physical system, that is

$$\phi_k \equiv 0 \text{ for some } k \in \{1, \dots, N\}. \tag{4.7}$$

The consistency condition $(\mathcal{C}3)$ requires that the k-th component of the expression on the right hand side of (4.6) vanishes, so that ϕ_k is not generated in the system. Similarly, the consistency condition $(\mathcal{C}4)$ requires that the remaining governing equations, (3.84d)–(3.84e) and (3.102d)–(3.102e) respectively, are reduced accordingly.

For the purpose of further discussion, we restrict our our attention to the isothermal FI model in which case the equation (4.6) takes the simple form

$$\frac{\mathrm{d}\boldsymbol{\phi}_\star}{\mathrm{d}t} = \operatorname{div}\left[\mathbf{Z_0}\mathbf{M}\,\nabla\left(-\frac{a\varepsilon}{2}\boldsymbol{\Lambda}\Delta\boldsymbol{\phi} + \frac{b}{\varepsilon}\mathbf{d}^F\right)\right]. \tag{4.8}$$

Now the task is as follows. For the given constant SPD matrix $\boldsymbol{\Lambda}$, we need to construct $\mathbf{M}$ and F, such that the k-th component of the expression on the right hand side of (4.8) vanishes if (4.7) holds. Up to our best knowledge, this problem has not been entirely solved yet. In the following three sections, we shall briefly analyze an acceptable choice of $\boldsymbol{\Lambda}$, $\mathbf{M}$ and F which will be used in our numerical simulations.

4.1.1 Specification of mixing surface energy coefficients

Let σ_{ij} denote the pairwise surface tension coefficients between the individual fluids. As such, they are assumed to be symmetric ($\sigma_{ij} = \sigma_{ji}$) and strictly positive. In what follows, we use the convention

$$\sigma_{ii} \equiv 0, \quad i = 1, \dots, N, \tag{4.9}$$

and we introduce the surface tension matrix $\boldsymbol{\Sigma} = [\sigma_{ij}]_{N\times N}$. Let the N-component Helmholtz free energy density is given in the form $\widetilde{\psi} = \widetilde{\psi}_\star(\boldsymbol{\phi}_\star, \nabla\boldsymbol{\phi}_\star)$, where

$$\widetilde{\psi}_\star(\boldsymbol{\phi}_\star, \nabla\boldsymbol{\phi}_\star) = -\frac{a\varepsilon}{4}\sum_{\substack{i,j=1\\ i\neq j}}^{N}\sigma_{ij}\,\nabla\phi_i\cdot\nabla\phi_j + \frac{b}{\varepsilon}F_\star(\boldsymbol{\phi}_\star), \tag{4.10}$$

cf. (3.26). The central assumption in the construction and the analysis of the CH models proposed by Boyer and Minjeaud (2014) is the following statement[3],

$$\boldsymbol{y}_\star^\top\boldsymbol{\Sigma}\boldsymbol{y}_\star \le -C_{\boldsymbol{\Sigma}}\,|\boldsymbol{y}_\star|^2, \quad \forall \boldsymbol{y}_\star \in \mathbb{R}^N, \text{ s.t. } \boldsymbol{y}_\star\cdot\mathbf{1}_\star = 0, \text{ with } \mathbf{1}_\star = [1,\dots,1]^\top \in \mathbb{R}^N, \tag{4.11}$$

which is assumed to hold for some $C_{\boldsymbol{\Sigma}} > 0$, see (Boyer and Minjeaud, 2014, Eq. (2.6)) and the discussion therein. One can easily verify that the first term

[3]The coercivity assumption (4.11) ensures that the contribution of the first term in (4.10) is positive at the interfaces.

on the right hand side of (4.10) obeys the consistency conditions ($\mathcal{C}1$) and ($\mathcal{C}2$). Indeed, for $N = 2$ we have

$$-\frac{a\varepsilon}{4}\sum_{i,j=1}^{2}\sigma_{ij}\,\nabla\phi_i\cdot\nabla\phi_j = -\frac{a\varepsilon}{2}\sigma_{12}\,\nabla\phi_1\cdot\nabla(1-\phi_1) = \frac{a\varepsilon}{2}\sigma_{12}\,|\nabla\phi_1|^2\,,$$

which coincides with the first term on the right hand side of (3.17). Moreover, if (4.7) holds, then $\nabla\phi_k \equiv \mathbf{0}$ and the second condition is also satisfied.

The mixing surface energy coefficients λ_{ij} are obtained from (4.10) by eliminating ϕ_N using the constraint (2.8). In this sense we introduce

$$\widetilde{\psi}(\boldsymbol{\phi},\nabla\boldsymbol{\phi}) \stackrel{\text{def}}{=} \widetilde{\psi}_\star(\boldsymbol{\phi}_\star,\nabla\boldsymbol{\phi}_\star)\Big|_{\phi_N=1-\sum_{i=1}^{N-1}\phi_i}\,, \tag{4.12}$$

and

$$\lambda_{ij} \stackrel{\text{def}}{=} \sigma_{iN}+\sigma_{jN}-\sigma_{ij}. \tag{4.13}$$

We immediately see that $\boldsymbol{\Lambda} = [\lambda_{ij}]_{(N-1)\times(N-1)}$ is symmetric. According to the following proposition, it is also positive definite.

Proposition 4.1. *$\boldsymbol{\Sigma}$ satisfies the coercivity assumption* (4.11) *if and only if $\boldsymbol{\Lambda}$ defined by* (4.13) *is positive definite.*

Proof. We first show that $\boldsymbol{y}_\star^\top\boldsymbol{\Sigma}\boldsymbol{y}_\star = -\boldsymbol{y}^\top\boldsymbol{\Lambda}\boldsymbol{y}$ for $\boldsymbol{y}_\star = [y_1,\dots,y_N]^\top \in \mathbb{R}^N$ such that $\boldsymbol{y}_\star\cdot\mathbf{1} = 0$ and $\boldsymbol{y} = [y_1,\dots,y_{N-1}]^\top \in \mathbb{R}^{N-1}$. Let $\boldsymbol{\Sigma}_0 \in \mathbb{R}^{(N-1)\times(N-1)}$ corresponds to $\boldsymbol{\Sigma}$ in which we have removed the last row and the last column that both correspond to $\boldsymbol{\sigma}_N = [\sigma_{iN}]_{i=1}^{N-1} \in \mathbb{R}^{N-1}$. Then

$$\begin{aligned}\boldsymbol{y}_\star^\top\boldsymbol{\Sigma}\boldsymbol{y}_\star &= \boldsymbol{y}^\top\boldsymbol{\Sigma}_0\boldsymbol{y} + 2\,(\boldsymbol{\sigma}_N\cdot\boldsymbol{y})\,y_N = \boldsymbol{y}^\top\boldsymbol{\Sigma}_0\boldsymbol{y} - \sum_{j=1}^{N-1}(\boldsymbol{\sigma}_N\cdot\boldsymbol{y})\,y_j\\ &\quad - \sum_{i=1}^{N-1}(\boldsymbol{\sigma}_N\cdot\boldsymbol{y})\,y_i = \sum_{i,j=1}^{N-1} y_i\,(\sigma_{ij}-\sigma_{iN}-\sigma_{jN})\,y_j = -\sum_{i,j=1}^{N-1} y_i\lambda_{ij}y_j = -\boldsymbol{y}^\top\boldsymbol{\Lambda}\boldsymbol{y}.\end{aligned}$$

Let $\boldsymbol{\Sigma}$ satisfies (4.11). Let $\boldsymbol{y}\in\mathbb{R}^{N-1}$ is an arbitrary non-zero vector and let $\boldsymbol{y}_\star$ is chosen accordingly, that is with $y_N = -\sum_{i=1}^{N-1} y_i$. There exists $C_{\boldsymbol{\Sigma}} > 0$ such that $\boldsymbol{y}^\top\boldsymbol{\Lambda}\boldsymbol{y} = -\boldsymbol{y}_\star^\top\boldsymbol{\Sigma}\boldsymbol{y}_\star \geq C_{\boldsymbol{\Sigma}}\,|\boldsymbol{y}_\star|^2 \geq C_{\boldsymbol{\Sigma}}\,|\boldsymbol{y}|^2$, which proofs that $\boldsymbol{\Lambda}$ is SPD.

To prove the reverse implication, let $\boldsymbol{\Lambda}$ is SPD. There exists $C_{\boldsymbol{\Sigma}} > 0$ such that $\boldsymbol{y}^\top\boldsymbol{\Lambda}\boldsymbol{y} \geq NC_{\boldsymbol{\Sigma}}\,|\boldsymbol{y}|^2$. We observe that

$$\begin{aligned}NC_{\boldsymbol{\Sigma}}\,|\boldsymbol{y}|^2 = C_{\boldsymbol{\Sigma}}\left(|\boldsymbol{y}|^2+(N-1)\,|\boldsymbol{y}|^2\right) &\geq C_{\boldsymbol{\Sigma}}\,|\boldsymbol{y}|^2 + C_{\boldsymbol{\Sigma}}\left(\sum_{i=1}^{N-1} y_i\right)^2\\ &= C_{\boldsymbol{\Sigma}}\left(\sum_{i=1}^{N-1} y_i^2 + (-y_N)^2\right) = C_{\boldsymbol{\Sigma}}\,|\boldsymbol{y}_\star|^2\,,\end{aligned}$$

where we have used the Cauchy-Schwarz inequality. It immediately follows that $\boldsymbol{y}_\star^\top\boldsymbol{\Sigma}\boldsymbol{y}_\star = -\boldsymbol{y}^\top\boldsymbol{\Lambda}\boldsymbol{y} \leq -C_{\boldsymbol{\Sigma}}\,|\boldsymbol{y}_\star|^2$. □

4.1.2 Specification of mobility matrix

Let us assume that the mobility matrix takes the form of a constant matrix multiplied by a (not necessarily constant) mobility coefficient, namely $\mathbf{M} = M_0\bar{\mathbf{M}}$. In light of (4.8), the consistency condition ($\mathcal{C}3$) requires

$$\operatorname{div}\left[M_0\,\nabla\left(-\frac{a\varepsilon}{2}\left[\mathbf{Z_0}\bar{\mathbf{M}}\boldsymbol{\Lambda}\Delta\boldsymbol{\phi}\right]_k+\frac{b}{\varepsilon}\left[\mathbf{Z_0}\bar{\mathbf{M}}\boldsymbol{\Lambda}\mathbf{d}^F\right]_k\right)\right]\equiv 0 \tag{4.14}$$

if $\phi_k \equiv 0$ for some $k \in \{1,\dots,N\}$. Following the procedure outlined in (Dong, 2017, Sec. 2.3), we put

$$\bar{\mathbf{M}} = \boldsymbol{\Lambda}^{-1}, \tag{4.15}$$

which is SPD provided that the same holds true for $\boldsymbol{\Lambda}$. In order to ensure that $\mathbf{M}$ is also positive definite, we shall require $M_0 > 0$.

Remark 4.2. In practice, it is of course possible to work with a degenerate mobility coefficient $M_0 = M_0(\boldsymbol{\phi})$, provided that it is a non-negative function which is necessary to ensure non-negativity of the corresponding term in the entropy production (3.101). A commonly used degenerate mobility coefficient is given by

$$M_0(\boldsymbol{\phi}) \overset{\text{def}}{=} \hat{M}_0\prod_{i=1}^{N}(1-\phi_i)^2, \tag{4.16}$$

where $\hat{M}_0 > 0$ is a constant parameter.

Let us explore the consequences of the choice (4.15). First of all, for arbitrary $k \in \{1,\dots,N\}$ we have

$$\left[\mathbf{Z_0}\bar{\mathbf{M}}\boldsymbol{\Lambda}\Delta\boldsymbol{\phi}\right]_k = \Delta\phi_k. \tag{4.17}$$

(The above identity follows from (4.2) where we have put $\hat{\mathbf{r}} = \mathbf{0}$.) As a consequence, the condition in (4.14) is reduced to

$$\operatorname{div}\left(M_0\,\nabla\left[\mathbf{Z_0}\boldsymbol{\Lambda}^{-1}\mathbf{d}^F\right]_k\right)\equiv 0 \text{ if } \phi_k\equiv 0 \text{ for some } k\in\{1,\dots,N\}. \tag{4.18}$$

In theory, this should be ensured by an appropriate choice of the potential F.

4.1.3 Specification of multi-well potential function

The construction of a potential function with the multi-well structure which would satisfy all consistency conditions ($\mathcal{C}1$)–($\mathcal{C}4$) is a highly non-trivial and challenging problem. It has been completely answered only in the simple case of matching pairwise surface tensions ($\sigma_{ij} = \sigma$), see Boyer and Minjeaud (2014).

In the constitutive assumption (4.10), we have introduced $F_\star$ as the notation for a multi-well potential function in terms of the full vector of volume fractions. In the remainder of the thesis, we consider the potential function of the form

$$F_\star(\boldsymbol{\phi}_\star) = \sum_{i,j=1}^{N}\frac{\sigma_{ij}}{4}\left[f(\phi_i)+f(\phi_j)-f(\phi_i+\phi_j)\right]. \tag{4.19}$$

where f is given by (3.9). The choice of the above formula is in accordance with the consistency conditions ($\mathcal{C}1$) and ($\mathcal{C}2$). However, it does not comply with ($\mathcal{C}3$) and ($\mathcal{C}4$) in the general case.

It can be shown that (4.19) meets the requirements of ($\mathcal{C}3$) and ($\mathcal{C}4$) if only a pair of fluids is present in the physical system, that is, if $L = N - 2$ in ($\mathcal{C}3$) and $K = 2$ in ($\mathcal{C}4$). We refer to (Dong, 2017, App. C) for the proof of this statement, which basically says that the interfaces between exactly two components, excluding multiple points, are properly captured. Boyer and Minjeaud (2014) successfully constructed the multi-well potential which meets the condition ($\mathcal{C}3$) if $L \geq N - 3$. However, the construction of the fully consistent potential for N-component systems is still an open problem.

Remark 4.3. Boyer and Minjeaud (2014) also suggested to add a stabilization term in the form of a higher order polynomial to (4.19), see also Boyer and Lapuerta (2006). This kind of stabilization is of importance mainly in the context of *total spreading situations* which are not covered in the thesis.

In light of (4.12) and (4.19), we introduce the multi-well potential F as the function of the first $(N-1)$ volume fractions through

$$F(\boldsymbol{\phi}) = \sum_{i,j=1}^{N} \frac{\sigma_{ij}}{4} \left[f(\phi_i) + f(\phi_j) - f(\phi_i + \phi_j) \right] \Big|_{\phi_N = 1 - \sum_{i=1}^{N-1} \phi_i}. \tag{4.20}$$

Finally, components of the previously introduced vector $\mathbf{d}^F$, see (4.5b), are obtained in the form

$$\begin{aligned} \frac{\partial F}{\partial \phi_i} = \frac{\partial F_\star}{\partial \phi_i} - \frac{\partial F_\star}{\partial \phi_N} &= \sum_{j=1}^{N} \frac{\sigma_{ij}}{2} \left[f'(\phi_i) - f'(\phi_i + \phi_j) \right] \Big|_{\phi_N = 1 - \sum_{k=1}^{N-1} \phi_k} \\ &- \sum_{j=1}^{N} \frac{\sigma_{jN}}{2} \left[f'(\phi_N) - f'(\phi_N + \phi_j) \right] \Big|_{\phi_N = 1 - \sum_{k=1}^{N-1} \phi_k}, \quad i = 1, \ldots, N-1. \end{aligned} \tag{4.21}$$

4.2 Consistent formulation of FI-CHNS model

Now we are ready to put together all the information needed to develop a model suitable for the description of isothermal flows of immiscible incompressible fluids in a fixed flow domain. Our final model is based on the isothermal version of governing equations (3.102a)–(3.102d), which can be obtained by considering the Helmholtz free energy density (3.26) in the special form

$$\widetilde{\psi}(\boldsymbol{\phi}, \nabla \boldsymbol{\phi}) = \frac{a\varepsilon}{4} \sum_{i,j=1}^{N-1} \lambda_{ij} \nabla \phi_i \cdot \nabla \phi_j + \frac{b}{\varepsilon} F(\boldsymbol{\phi}). \tag{4.22}$$

The coefficients λ_{ij} have been specified in (4.13) and F is given by (4.20). With this particular choice of $\widetilde{\psi}$ we have

$$\widetilde{\mu}_i = \frac{b}{\varepsilon} \frac{\partial F}{\partial \phi_i} - \frac{a\varepsilon}{2} \sum_{j=1}^{N-1} \lambda_{ij} \Delta \phi_j, \tag{4.23}$$

cf. (3.102b). Our specific choice of the mobility matrix $\mathbf{M} = M_0\mathbf{\Lambda}^{-1}$ tempts us to introduce the notation

$$\chi_i \overset{\text{def}}{=} \sum_{j=1}^{N-1} \ell_{ij}\widetilde{\mu}_j, \tag{4.24}$$

where ℓ_{ij} denote entries of $\mathbf{\Lambda}^{-1}$. Using this notation we will transform the coupled equations (3.102a) and (3.102b) in our final model. The newly introduced variable χ_i will be referred to as the *combined chemical potential* associated with the i-th component in the system. Clearly, the inverse transformation to (4.24) reads

$$\widetilde{\mu}_i = \sum_{j=1}^{N-1} \lambda_{ij}\chi_j. \tag{4.25}$$

Looking at the balance of linear momentum (3.102d), we see that the choice of the approximation level through Θ_2, see Summary 7 in Section 2.5.3, offers the possibility to eliminate the effect of $\boldsymbol{J}$ in that equation. At this point, we let the auxiliary parameter to be absorbed by the flux variable in the sense of introducing a new notation, for instance $\boldsymbol{J}_\Theta \equiv \Theta_2\boldsymbol{J}$, but we shall continue to write $\boldsymbol{J}$ for the redefined flux. Hence, in the current setting with the alternative notation, we have

$$\boldsymbol{J} = -\Theta_2 \sum_{i=1}^{N-1} M_0(\hat{\varrho}_i - \hat{\varrho}_N)\,\nabla\chi_i, \qquad \Theta_2 = \begin{cases} 1 \rightsquigarrow & \text{FI-CHNS-L1,} \\ 0 \rightsquigarrow & \text{FI-CHNS-L2,} \end{cases} \tag{4.26}$$

and

$$\varrho\frac{\partial \boldsymbol{v}}{\partial t} + [\nabla \boldsymbol{v}](\varrho\boldsymbol{v} + \boldsymbol{J}) = -\nabla p + \operatorname{div}(2\nu\mathbb{D}) + \boldsymbol{f}_{\text{ca}} + \varrho\boldsymbol{g}. \tag{4.27}$$

Here, $\boldsymbol{f}_{\text{ca}} \overset{\text{def}}{=} -\frac{a\varepsilon}{2}\sum_{i,j=1}^{N-1}\lambda_{ij}\operatorname{div}(\nabla\phi_j \otimes \nabla\phi_i)$ represents the capillary force and p is the universal notation for the pressure field, which at the moment coincides with $\tilde{p}_{\text{a}}$. The capillary force can be rewritten using the simple identity

$$\operatorname{div}(\nabla\phi_i \otimes \nabla\phi_j) = (\Delta\phi_j)\,\nabla\phi_i + \frac{1}{2}\nabla(\nabla\phi_i \cdot \nabla\phi_j). \tag{4.28}$$

The contribution associated with the second term on the right hand side can be obviously added to the pressure gradient, while the first term can be further modified by substituting from (4.23). This gives us several possibilities of how to reformulate the equation (4.27). Table 4.1 summarizes the most commonly used equivalent formulations.

Note that once the effect of $\boldsymbol{J}$ is eliminated, by letting $\Theta_2 = 0$ in (4.26), it is correctly eliminated also in the balance of mass

$$\frac{\partial \varrho}{\partial t} + \operatorname{div}(\varrho\boldsymbol{v}) = -\operatorname{div}\boldsymbol{J}, \tag{4.29}$$

cf. (2.95e).

Table 4.1: Equivalent formulations of the balance of linear momentum (4.27) suitable for implementation of various discretization schemes for FI-CHNS model.

Variant	Equation	$\boldsymbol{f}_{\mathrm{ca}}$	p (ref. symbol)
(BLM0)	$\varrho\frac{\partial \boldsymbol{v}}{\partial t} + [\nabla \boldsymbol{v}](\varrho \boldsymbol{v} + \boldsymbol{J}) = -\nabla p + \operatorname{div}(2\nu\mathbb{D}) + \boldsymbol{f}_{\mathrm{ca}} + \varrho \boldsymbol{g}$	$-\frac{a\varepsilon}{2}\sum_{i,j=1}^{N-1}\lambda_{ij}\operatorname{div}(\nabla\phi_j \otimes \nabla\phi_i)$	$\tilde{p}_{\mathrm{a}}$ (P_0)
(BLM1)*	$\frac{\partial \boldsymbol{v}}{\partial t} + [\nabla \boldsymbol{v}]\,\boldsymbol{v} + \frac{1}{\varrho}[\nabla \boldsymbol{v}]\,\boldsymbol{J} = -\frac{1}{\varrho}\nabla p + \frac{\nu}{\varrho}\Delta \boldsymbol{v} + \frac{2}{\varrho}\mathbb{D}\nabla\nu + \frac{1}{\varrho}\boldsymbol{f}_{\mathrm{ca}} + \boldsymbol{g}$	$-\frac{a\varepsilon}{2}\sum_{i,j=1}^{N-1}\lambda_{ij}(\Delta\phi_j)\nabla\phi_i$	$P_0 + \frac{a\varepsilon}{4}\sum_{i,j=1}^{N-1}\lambda_{ij}\nabla\phi_i\cdot\nabla\phi_j$ (P_1)
(BLM2)†	$\varrho\frac{\partial \boldsymbol{v}}{\partial t} + [\nabla \boldsymbol{v}](\varrho \boldsymbol{v} + \boldsymbol{J}) = -\nabla p + \operatorname{div}(2\nu\mathbb{D}) + \boldsymbol{f}_{\mathrm{ca}} + \varrho \boldsymbol{g}$	$\sum_{i,j=1}^{N-1}\lambda_{ij}\chi_j\nabla\phi_i$	$P_1 + \frac{b}{\varepsilon}F(\boldsymbol{\phi})$ (P_2)
(BLM3)‡	$\sqrt{\varrho}\frac{\partial}{\partial t}(\sqrt{\varrho}\boldsymbol{v}) + [\nabla \boldsymbol{v}](\varrho \boldsymbol{v} + \boldsymbol{J}) + \frac{1}{2}\boldsymbol{v}\operatorname{div}(\varrho \boldsymbol{v} + \boldsymbol{J})$ $= -\nabla p + \operatorname{div}(2\nu\mathbb{D}) + \boldsymbol{f}_{\mathrm{ca}} + \varrho \boldsymbol{g}$	$-\sum_{i,j=1}^{N-1}\lambda_{ij}\phi_i\nabla\chi_j$	$P_2 - \sum_{i,j=1}^{N-1}\lambda_{ij}\phi_i\chi_j$ (P_3)

* [Dong (2017)] Manipulation based on using (4.28).
† [Boyer and Lapuerta (2006)] Manipulation based on using (4.28), (4.23) and (4.25).
‡ [Minjeaud (2013)] Manipulation based on using (4.29) and $\nabla(\phi_i\chi_i) = \phi_i\nabla\chi_i + \chi_i\nabla\phi_i$.

4.2.1 Final form of governing equations

The N-component FI-CHNS model, which we use to simulate mutual interaction of immiscible incompressible fluids in a thermally isolated fixed flow domain Ω, is composed of PDEs in the form

$$\frac{\partial \phi_i}{\partial t} + \operatorname{div}(\phi_i \boldsymbol{v}) = \operatorname{div}(M_0 \nabla \chi_i), \quad i = 1, \dots, N-1, \tag{4.30a}$$

$$\chi_i = \frac{b}{\varepsilon} \sum_{j=1}^{N-1} \ell_{ij} \frac{\partial F}{\partial \phi_j} - \frac{a\varepsilon}{2} \Delta \phi_i, \quad i = 1, \dots, N-1, \tag{4.30b}$$

$$\operatorname{div} \boldsymbol{v} = 0, \tag{4.30c}$$

$$\varrho \frac{\partial \boldsymbol{v}}{\partial t} + [\nabla \boldsymbol{v}](\varrho \boldsymbol{v} + \boldsymbol{J}) = -\nabla p + \operatorname{div}(2\nu \mathbb{D}) - \sum_{i,j=1}^{N-1} \lambda_{ij} \phi_i \nabla \chi_j + \varrho \boldsymbol{g}. \tag{4.30d}$$

Recall that $\boldsymbol{J} = -\Theta_2 \sum_{i=1}^{N-1} M_0(\hat{\varrho}_i - \hat{\varrho}_N) \nabla \chi_i$. The left hand side of the last equation can be further manipulated using (4.29) to fit (BLM3) presented in Table 4.1. This final form of the model will be particularly suitable for the derivation of the unconditionally energy-stable numerical scheme which is described in Chapter 5.

Model parameters and primitive variables are summarized in Table 4.2. Their brief description together with physical units can be found in the overview at the beginning of the thesis.

Table 4.2: Overview of field variables and parameters of different types used in the FI-CHNS model (4.30).

Variables to be solved	Input parameters	Derived parameters	(Eq.)
ϕ_i $(1 \le i \le N-1)$	$\hat{M}_0$	$M_0(\boldsymbol{\phi})$	(4.16)
$\boldsymbol{v}$	ε	a, b	(3.10b)*
p	σ_{ij} $(1 \le i < j \le N)$	λ_{ij}, ℓ_{ij} $(1 \le i, j \le N-1)$	(4.13)†
	$\hat{\varrho}_i$ $(1 \le i \le N)$	$\varrho(\boldsymbol{\phi})$	(2.10a)
	ν_i $(1 \le i \le N)$	$\nu(\boldsymbol{\phi})$	(3.103)
	Θ_2	$\boldsymbol{J}$	(4.26)
	$\boldsymbol{g}$	$F(\boldsymbol{\phi})$	(4.20)*

* Depends on the choice of f. Here we take $f(\phi) = \phi^2(1-\phi)^2$, see (3.9).
† $\boldsymbol{\Lambda} = [\lambda_{ij}]_{(N-1)\times(N-1)}$, $\boldsymbol{\Lambda}^{-1} = [\ell_{ij}]_{(N-1)\times(N-1)}$.

4.2.2 Example of boundary conditions

We assume that $\Omega \subset \mathbb{R}^3$ is a bounded domain with Lipschitz boundary $\partial\Omega$. Let $\boldsymbol{n}$ denote outer unit normal vector defined at (almost) all points of the boundary. We supplement the above system of PDEs with different types of boundary conditions depending on the particular problem we want to describe and simulate.

The typical flow domain inspired by our target application from Section 1.1 is schematically depicted in Figure 4.1. The domain boundary consists of several

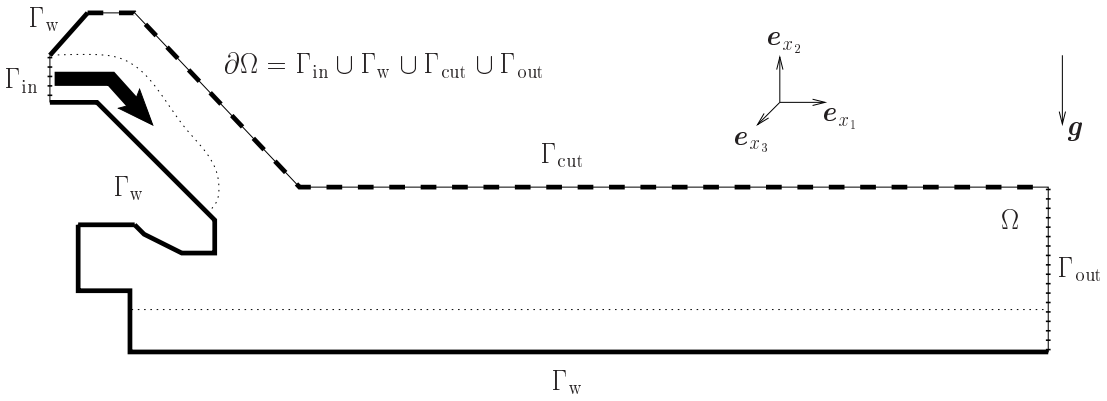

Figure 4.1: Sketch of the computational domain for the initial stage of the float glass forming process with different types of boundaries.

distinct parts, namely $\partial\Omega = \Gamma_{\mathrm{in}} \cup \Gamma_{\mathrm{w}} \cup \Gamma_{\mathrm{cut}} \cup \Gamma_{\mathrm{out}}$. At the inlet part of the boundary, Γ_{in}, we prescribe

$$\boldsymbol{v} = \boldsymbol{v}_{\mathrm{in}} \qquad \text{on } \Gamma_{\mathrm{in}}, \tag{4.31a}$$

$$\boldsymbol{\phi} = \boldsymbol{\phi}_{\mathrm{in}} \qquad \text{on } \Gamma_{\mathrm{in}}, \tag{4.31b}$$

$$\nabla\chi_i \cdot \boldsymbol{n} = 0, \quad i = 1, \ldots, N-1, \qquad \text{on } \Gamma_{\mathrm{in}}. \tag{4.31c}$$

The first condition prescribes the inlet velocity profile. The second condition is used to specify which fluid flows into the domain, typically[4] $\boldsymbol{\phi}_{\mathrm{in}} = \boldsymbol{e}_j$ for some $j \in \{1, \ldots, N-1\}$ or $\boldsymbol{\phi}_{\mathrm{in}} = \boldsymbol{0}$ if it is the N-th fluid which flows in. Finally, the third group of conditions says that there is no diffusive flux in the normal direction to Γ_{in}, so that the inflow is advective.

At solid walls of the domain, Γ_{w}, we prescribe

$$\boldsymbol{v} = \boldsymbol{v}_{\mathrm{w}} \qquad \text{on } \Gamma_{\mathrm{w}}, \tag{4.32a}$$

$$\nabla\phi_i \cdot \boldsymbol{n} = 0, \quad i = 1, \ldots, N-1, \qquad \text{on } \Gamma_{\mathrm{w}}, \tag{4.32b}$$

$$\nabla\chi_i \cdot \boldsymbol{n} = 0, \quad i = 1, \ldots, N-1, \qquad \text{on } \Gamma_{\mathrm{w}}. \tag{4.32c}$$

The first condition is typically chosen to be no-slip and no-penetration condition $\boldsymbol{v}_{\mathrm{w}} = \boldsymbol{0}$. The second group of conditions ensures that the interfaces in between the individual fluids are perpendicular to the boundary. The contact angle between any interface and the wall is thus always 90° in our case[5]. The group of conditions on the third line prevents any diffusion through the solid wall.

The dashed line labeled by Γ_{cut} in Figure 4.1 is an artificial boundary that can be interpreted as a cut across the domain through a pure fluid away from interfaces. Such a cut is done in order to decrease the size of the problem. The fluid in the vicinity of this artificial boundary must have the chance to freely

[4]The set of vectors $\{\boldsymbol{e}_i\}_{i=1}^{N-1}$ forms the standard (natural) basis of $\mathbb{R}^{N-1}$.

[5]In practice, it is possible to prescribe general contact angles at the boundaries (different from 90°), but we do not consider this option at the moment; see for example Jacqmin (2000), Ding and Spelt (2007), Khatavkar et al. (2007), Lee and Kim (2011) for two-component systems or Dong (2017) for N-component systems.

outflow from the domain as it is being "pushed out" by another fluid which flows into the domain through the inlet. We put

$$[-p\mathbb{I} + 2\nu\mathbb{D}]\boldsymbol{n} = -G\boldsymbol{n} \qquad \text{on } \Gamma_{\text{cut}}, \tag{4.33a}$$

where G is assumed to satisfy $\nabla G = \varrho\boldsymbol{g}$ on Γ_{cut}. This condition simply balances the hydrostatic contribution to the pressure in the sense that $p = G$ in the absence of flow. Let us suppose that *only the k-th fluid is present in the vicinity of* Γ_{cut}. Then we have $G = -\hat{\varrho}_k g_{\text{a}} x_2 + const.$, where $g_{\text{a}} = |\boldsymbol{g}|$, see Figure 4.1. Optionally, one can support the current assumption by enforcing redundant conditions

$$\boldsymbol{\phi} = \begin{cases} \boldsymbol{e}_k, & \text{if } k \in \{1, \ldots, N-1\}, \\ \boldsymbol{0}, & \text{if } k = N, \end{cases} \qquad \text{on } \Gamma_{\text{cut}}, \tag{4.33b}$$

and

$$\nabla\chi_i \cdot \boldsymbol{n} = 0, \quad i = 1, \ldots, N-1, \qquad \text{on } \Gamma_{\text{cut}}. \tag{4.33c}$$

The outlet part of the boundary, Γ_{out}, is of a similar nature as in the previous case. Nevertheless, this time the we want to enable simultaneous outflow of several fluids, meaning that the the interfaces in between them are expected to intersect/penetrate the boundary. Proper handling of a relevant outflow boundary condition is important from the point of view of our target application, however, it is out of scope of the thesis[6]. For testing purposes we have replaced Γ_{out} by a solid wall Γ_{w}.

4.2.3 Function spaces and initial conditions

We briefly introduce the function spaces needed in the text below. Let $L^2(\Omega)$ denote the standard Lebesgue space consisting of measurable functions $u : \Omega \to \mathbb{R}$ with finite norm

$$\|u\|_{L^2} \stackrel{\text{def}}{=} \left(\int_\Omega |u|^2 \, \mathrm{d}\boldsymbol{x} \right)^{\frac{1}{2}}.$$

Apparently, $L^2(\Omega)^d$ denotes the space of d-dimensional vector-valued functions whose all components are square integrable in the previous sense. The corresponding norm for $\boldsymbol{u} \in L^2(\Omega)^d$ is defined by

$$\|\boldsymbol{u}\|_{L^2} \stackrel{\text{def}}{=} \left(\int_\Omega \boldsymbol{u} \cdot \boldsymbol{u} \, \mathrm{d}\boldsymbol{x} \right)^{\frac{1}{2}} = \left(\int_\Omega |\boldsymbol{u}|^2 \, \mathrm{d}\boldsymbol{x} \right)^{\frac{1}{2}}.$$

The standard Sobolev space $H^1(\Omega) \stackrel{\text{def}}{=} \{u \in L^2(\Omega); \nabla u \in L^2(\Omega)^3\}$ is traditionally equipped with the norm

$$\|u\|_{H^1} \stackrel{\text{def}}{=} \left(\|u\|_{L^2}^2 + \|\nabla u\|_{L^2}^2 \right)^{\frac{1}{2}}.$$

[6]The implementation of the outflow boundary condition at Γ_{out} is planned to follow the ideas presented in Dong (2014b).

Another traditional spaces $H_0^1(\Omega)$ and $H_\Gamma^1(\Omega)$ can be characterized as spaces consisting of functions $u \in H^1(\Omega)$ with zero trace on the boundary or on its part $\Gamma \subset \partial\Omega$ respectively. In these spaces we work with the norm $\|u\|_{H_0^1} \stackrel{\text{def}}{=} \|\nabla u\|_{L^2}$. The space $H^{\frac{1}{2}}(\partial\Omega) \subset L^2(\partial\Omega)$ represents the image of the linear bounded trace operator that is defined on $H^1(\Omega)$. The corresponding spaces for d-dimensional vector-valued functions (i.e. $H^1(\Omega)^d, H_0^1(\Omega)^d$, etc.) are introduced similarly as in the case of $L^2(\Omega)^d$ mentioned above.

We further introduce the following notation for the function spaces related to the primitive variables, namely

$$\mathcal{V}^\phi \stackrel{\text{def}}{=} H^1(\Omega), \qquad \mathcal{V}^\phi_{\Gamma_{\text{CH}}} \stackrel{\text{def}}{=} \{\phi \in H^1(\Omega);\, \phi|_{\Gamma_{\text{CH}}} = 0\}, \tag{4.34a}$$

$$\boldsymbol{\mathcal{V}}^\phi \stackrel{\text{def}}{=} H^1(\Omega)^{N-1}, \qquad \boldsymbol{\mathcal{V}}^\phi_{\Gamma_{\text{CH}}} \stackrel{\text{def}}{=} \{\boldsymbol{\phi} \in H^1(\Omega)^{N-1};\, \boldsymbol{\phi}|_{\Gamma_{\text{CH}}} = \mathbf{0}\}, \tag{4.34b}$$

$$\mathcal{V}^\chi \stackrel{\text{def}}{=} H^1(\Omega), \qquad \boldsymbol{\mathcal{V}}^\chi \stackrel{\text{def}}{=} H^1(\Omega)^{N-1}, \tag{4.34c}$$

$$\boldsymbol{\mathcal{V}}^{\boldsymbol{v}} \stackrel{\text{def}}{=} H^1(\Omega)^3, \qquad \boldsymbol{\mathcal{V}}^{\boldsymbol{v}}_{\Gamma_{\text{NS}}} \stackrel{\text{def}}{=} \{\boldsymbol{v} \in H^1(\Omega)^3;\, \boldsymbol{v}|_{\Gamma_{\text{NS}}} = \mathbf{0}\}, \tag{4.34d}$$

$$\mathcal{V}^p \stackrel{\text{def}}{=} L^2(\Omega), \qquad \mathcal{V}^p_0 \stackrel{\text{def}}{=} \{p \in L^2(\Omega);\, \int_\Omega p \,\mathrm{d}\boldsymbol{x} = 0\}. \tag{4.34e}$$

Here, $\Gamma_{\text{CH}} \subseteq \partial\Omega$ and $\Gamma_{\text{NS}} \subseteq \partial\Omega$ are introduced to cover those parts of the boundary on which we specify Dirichlet boundary conditions $\boldsymbol{\phi}_D, \boldsymbol{v}_D$ for volume fractions and velocity respectively. For instance, the velocity boundary conditions prescribed in Section 4.2.2 correspond to the setting with $\Gamma_{\text{NS}} = \Gamma_{\text{in}} \cup \Gamma_{\text{w}}$ and

$$\boldsymbol{v}_D = \begin{cases} \boldsymbol{v}_{\text{in}} & \text{on } \Gamma_{\text{in}}, \\ \boldsymbol{v}_{\text{w}} & \text{on } \Gamma_{\text{w}}. \end{cases}$$

(If needed, the velocity function space $\boldsymbol{\mathcal{V}}^{\boldsymbol{v}}_{\Gamma_{\text{NS}}}$ can be adapted in a straightforward way to incorporate slip boundary conditions.)

Since we are interested in time-dependent problems, we need to supplement the system with appropriate initial conditions. We put

$$\boldsymbol{\phi}|_{t=0} = \boldsymbol{\phi}^0, \qquad \boldsymbol{v}|_{t=0} = \boldsymbol{v}^0, \tag{4.35}$$

where $\boldsymbol{\phi}^0 \in \boldsymbol{\mathcal{V}}^\phi$ and $\boldsymbol{v}^0 \in \boldsymbol{\mathcal{V}}^{\boldsymbol{v}}$ are given functions.

4.2.4 Dimensionless form of the model

Let us now briefly describe how to obtain dimensionless form of the model. Our aim is to provide a normalization of the variables and parameters such that the form of the governing equations and the boundary/initial conditions remains unchanged upon non-dimensionalization.

Basic characteristic quantities are listed in Table 4.3. The normalization constants for all variables and parameters that appear in the model are summarized in Table 4.4. For example, the dimensionless viscosity is defined by $\nu/(\varrho_{\text{ref}} V_{\text{ref}} L_{\text{ref}})$ based on this table. As such, it corresponds to the reciprocal value of the Reynolds number which varies in space according to ν. The other commonly introduced

dimensionless numbers are listed in Table 4.5. In what follows, all variables and parameters are considered to be in their dimensionless form unless otherwise stated[7].

Table 4.3: Characteristic quantities.

Quantity	Description	SI unit	Default value
L_{ref}	length scale	m	1
V_{ref}	velocity scale	$\text{m} \cdot \text{s}^{-1}$	1
ϱ_{ref}	density scale	$\text{kg} \cdot \text{m}^{-3}$	1

Table 4.4: Normalization constants.

Variable/parameter	Constant	Variable/parameter	Constant
$\boldsymbol{x}$	L_{ref}	ε	L_{ref}
$\boldsymbol{v}$	V_{ref}	$\mathbb{D}$	$V_{\text{ref}}/L_{\text{ref}}$
t	$L_{\text{ref}}/V_{\text{ref}}$	ϕ_i	1
$\widetilde{\mu}_i$	$\varrho_{\text{ref}} V_{\text{ref}}^2$	χ_i	$1/L_{\text{ref}}$
$\sigma_{ij}, \lambda_{ij}, F$	$\varrho_{\text{ref}} V_{\text{ref}}^2 L_{\text{ref}}$	ℓ_{ij}	$1/(\varrho_{\text{ref}} V_{\text{ref}}^2 L_{\text{ref}})$
M_0	$V_{\text{ref}} L_{\text{ref}}^2$	a, b, f	1
$\varrho, \varrho_i, \hat{\varrho}_i$	ϱ_{ref}	ν, ν_i	$\varrho_{\text{ref}} V_{\text{ref}} L_{\text{ref}}$
p	$\varrho_{\text{ref}} V_{\text{ref}}^2$	$\boldsymbol{f}_{\text{ca}}$	$\varrho_{\text{ref}} V_{\text{ref}}^2 / L_{\text{ref}}$
$\boldsymbol{J}$	$\varrho_{\text{ref}} V_{\text{ref}}$	$\Theta_0, \Theta_1, \Theta_2$	1
$\boldsymbol{g}, g_{\text{a}}$	$V_{\text{ref}}^2 / L_{\text{ref}}$	G	$\varrho_{\text{ref}} V_{\text{ref}}^2$

Table 4.5: Dimensionless numbers.

Name	Notation	Representation	Normalized quantity
Cahn number	Cn	$\varepsilon/L_{\text{ref}}$	ε^*
Froude number	Fr	$V_{\text{ref}}/\sqrt{g_{\text{a}} L_{\text{ref}}}$	$1/\sqrt{g_{\text{a}}^*}$
Péclet number	Pe	$V_{\text{ref}} L_{\text{ref}}^2 / M_0$	$1/M_0^*$
Reynolds number	Re	$\varrho_{\text{ref}} V_{\text{ref}} L_{\text{ref}}/\nu$	$1/\nu^*$

[7]The original dimensional setting can be recovered if we put the characteristic quantities equal to their default values, see Table 4.3.

Chapter 5

Numerical Discretization

Let us assume, for the moment, that the external forces vanish identically and $\partial\Omega = \Gamma_{\mathrm{w}}$, so that boundary conditions (4.32) apply to the whole boundary. Multiplying (4.30a)–(4.30d) by $\sum_{j=1}^{N-1} \lambda_{ij}\chi_j$, $\sum_{j=1}^{N-1} \lambda_{ij}\frac{\partial \phi_j}{\partial t}$, p and $\boldsymbol{v}$ respectively, integrating over Ω and adding up the resulting equations, one formally recovers the energy equality in the form[1]

$$\frac{\mathrm{d}}{\mathrm{d}t}\int_\Omega \left(\frac{1}{2}\varrho\,|\boldsymbol{v}|^2 + \frac{b}{\varepsilon}F(\boldsymbol{\phi}) + \frac{a\varepsilon}{4}\sum_{i,j=1}^{N-1}\lambda_{ij}\,\nabla\phi_i\cdot\nabla\phi_j\right) = -\int_\Omega 2\nu\mathbb{D}:\mathbb{D} - \int_\Omega M_0\sum_{i,j=1}^{N-1}\lambda_{ij}\chi_i\chi_j. \quad (5.1)$$

The term on the left hand side represents the change of the total kinetic and free energy associated with the fluid inside the domain Ω, that is, the change of $\mathcal{E}(t) = \mathcal{E}_{\mathrm{kin}}(t) + \Psi(t)$, where

$$\mathcal{E}_{\mathrm{kin}}(t) = \int_\Omega \frac{1}{2}\varrho\,|\boldsymbol{v}|^2, \qquad \Psi(t) = \int_\Omega \left(\frac{b}{\varepsilon}F(\boldsymbol{\phi}) + \frac{a\varepsilon}{4}\sum_{i,j=1}^{N-1}\lambda_{ij}\,\nabla\phi_i\cdot\nabla\phi_j\right). \quad (5.2)$$

Since the contribution of both terms on the right hand side of (5.1) to the change of the total energy is negative, the energy in the system is dissipated. (Recall that $\boldsymbol{\Lambda}$ is assumed to be SPD.)

The numerical scheme described in this chapter is discretely consistent with thermodynamics in the sense that the discrete counterpart of the total energy is decreasing in time in the absence of external forces, see Proposition 5.4. Numerical schemes with such a property are usually called *energy-stable*. The ideas presented here have been previously applied in the works by Minjeaud (2013) and Guillen-Gonzalez and Tierra (2014) for a ternary FI-CHNS model (with $\Theta_2 = 0$) in the first case and for a binary model of the same type (with $\Theta_2 = 1$) in the other case, cf. (3.122).

[1] For the sake of brevity, we shall henceforth drop the measures $\mathrm{d}\boldsymbol{x}$, $\mathrm{d}\boldsymbol{s}$ from integrals.

5.1 Time discretization

Let us consider the time interval $[0, t_{\text{end}}]$ divided into $N_{t.s.}$ subintervals $[t_n, t_{n+1}]$, $n = 0, \dots, N_{t.s} - 1$, of a uniform length $\Delta_t = t_{\text{end}}/N_{t.s.}$. Note that for a function $f : [0, t_{\text{end}}] \to \mathcal{X}$, where $\mathcal{X}$ is a general Banach space, we abbreviate $f^n \equiv f(t_n)$, $n = 0, \dots, N_{t.s.}$. We assume that $\boldsymbol{\phi}^n \in \boldsymbol{\mathcal{V}}^{\phi}_{\Gamma_{\text{CH}}}$ and $\boldsymbol{v}^n \in \boldsymbol{\mathcal{V}}^{\boldsymbol{v}}_{\Gamma_{\text{NS}}}$ are given functions at the time level $t_n = n\Delta_t$. The time level $n = 0$ thus corresponds to $t_0 = 0$ with the initial conditions $\boldsymbol{\phi}^0, \boldsymbol{v}^0$ from (4.35). The objective of the current and the following section is to formulate the system of equations that must be solved in order to compute an appropriate approximation of the unknown functions[2] $\boldsymbol{\phi}^{n+1} \in \boldsymbol{\mathcal{V}}^{\phi}_{\Gamma_{\text{CH}}}$, $\boldsymbol{\chi}^{n+1} \in \boldsymbol{\mathcal{V}}^{\chi}$, $\boldsymbol{v}^{n+1} \in \boldsymbol{\mathcal{V}}^{\boldsymbol{v}}_{\Gamma_{\text{NS}}}$ and $p^{n+1} \in \mathcal{V}^p$ at the subsequent time level t_{n+1}.

For the ease of presentation, we shall assume that M_0 is constant. Following the ideas presented in (Minjeaud, 2013, Sec. II.A), we propose the time discretization of FI-CHNS model (4.30) in the form

$$\frac{\phi_i^{n+1} - \phi_i^n}{\Delta_t} + \operatorname{div}\left((\phi_i^n - \alpha_i)\boldsymbol{v}^*\right) - \operatorname{div}\left(M_0 \nabla \chi_i^{n+1}\right) = 0, \quad i = 1, \dots, N-1, \tag{5.3a}$$

$$\chi_i^{n+1} - \frac{b}{\varepsilon}\sum_{j=1}^{N-1} \ell_{ij} d_j^F(\boldsymbol{\phi}^{n+1}, \boldsymbol{\phi}^n) + \frac{a\varepsilon}{2}\Delta\phi_i^{n+\theta} = 0, \quad i = 1, \dots, N-1, \tag{5.3b}$$

$$\operatorname{div} \boldsymbol{v}^{n+1} = 0, \tag{5.3c}$$

$$\begin{aligned} &\varrho^n \frac{\boldsymbol{v}^{n+1} - \boldsymbol{v}^n}{\Delta_t} + \frac{1}{2}\frac{\varrho^{n+1} - \varrho^n}{\Delta_t}\boldsymbol{v}^{n+1} \\ &\quad + \left[\nabla \boldsymbol{v}^{n+1}\right]\left(\varrho^{n+1}\boldsymbol{v}^n + \boldsymbol{J}^{n+1}\right) + \frac{1}{2}\boldsymbol{v}^{n+1}\operatorname{div}\left(\varrho^{n+1}\boldsymbol{v}^n + \boldsymbol{J}^{n+1}\right) \\ &\qquad + \nabla p^{n+1} - \operatorname{div}\left(2\nu^{n+1}\mathbb{D}^{n+1}\right) + \sum_{i,j=1}^{N-1} \lambda_{ij}(\phi_i^n - \alpha_i)\nabla\chi_j^{n+1} = \varrho^{n+1}\boldsymbol{g}, \end{aligned} \tag{5.3d}$$

where $\boldsymbol{J}^{n+1} = -\Theta_2 \sum_{i=1}^{N-1} M_0(\hat{\varrho}_i - \hat{\varrho}_N)\nabla\chi_i^{n+1}$, $\nu^{n+1} = \sum_{i=1}^{N-1}(\nu_i - \nu_N)\phi_i^{n+1} + \nu_N$, $\varrho^{n+\beta} = \sum_{i=1}^{N-1}(\hat{\varrho}_i - \hat{\varrho}_N)\phi_i^{n+\beta} + \hat{\varrho}_N$ (for $\beta \in \{0, 1\}$) and $\phi_i^{n+\theta} = (1-\theta)\phi_i^n + \theta\phi_i^{n+1}$ for $\theta \in [\frac{1}{2}, 1]$. Let us briefly summarize the basic ideas that were applied in order to derive the above time discretization scheme:

- The advective velocity in (4.30a) was discretized using the so-called intermediate (projected) velocity[3]

$$\boldsymbol{v}^* \overset{\text{def}}{=} \boldsymbol{v}^n - \frac{\Delta_t}{\varrho^n}\sum_{j,k=1}^{N-1} \lambda_{jk}(\phi_j^n - \alpha_j)\nabla\chi_k^{n+1}. \tag{5.4}$$

[2]Note that we do not require the explicit knowledge of $\boldsymbol{\chi}^n$ and p^n to update the unknown variables in this particular case.

[3]The formula for the intermediate velocity comes from the time discretization of the reduced balance of linear momentum $\varrho\frac{\partial \boldsymbol{v}}{\partial t} = -\sum_{i,j=1}^{N-1} \lambda_{ij}\phi_i \nabla\chi_j$, cf. (4.30d).

Note that $\boldsymbol{v}^* \cdot \boldsymbol{n} = 0$ provided that $\boldsymbol{v}^n \cdot \boldsymbol{n} = 0$ and $\nabla \chi_i^{n+1} \cdot \boldsymbol{n} = 0$. However, supposing that $\sum_{i=1}^N \phi_i^n = 1$, we see that

$$\sum_{i=1}^{N} \operatorname{div}(\phi_i^n \boldsymbol{v}^*) = \operatorname{div} \boldsymbol{v}^* \neq 0. \tag{5.5}$$

This is in contrast with the continuous case where $\sum_{i=1}^N \operatorname{div}(\phi_i \boldsymbol{v}) = 0$ due to (4.30c) and the sum of the volume fractions remains equal to one[4]. The role of the additional terms $-\alpha_i \operatorname{div} \boldsymbol{v}^*$ in each of the equations in (5.3a) is to "re-equilibriate" the values of discretized volume fractions to ensure that their sum remains equal to one. The constant coefficients α_i must be chosen in such a way that $\sum_{i=1}^N \alpha_i = 1$, so that $\sum_{i=1}^N \operatorname{div}((\phi_i^n - \alpha_i)\boldsymbol{v}^*) = 0$. Here we put

$$\alpha_i \overset{\text{def}}{=} \frac{1}{|\Omega|} \int_\Omega \phi_i^0 \, \mathrm{d}\boldsymbol{x}, \quad i = 1, \dots, N. \tag{5.6}$$

Note that $\alpha_j = 0$ if ϕ_j is absent from the initial data and the above choice is therefore in accordance with the consistency condition ($\mathcal{C}3$).

- For the time discretization of the nonlinear terms $\frac{\partial F}{\partial \phi_j}$ in (4.30b) we use the semi-implicit formula described in Wu and Xu (2017); see also Boyer and Minjeaud (2011). Recall that in (4.21) we have noted the relation $\frac{\partial F}{\partial \phi_i} = \frac{\partial F_\star}{\partial \phi_i} - \frac{\partial F_\star}{\partial \phi_N}$ (for $i = 1, \dots, N-1$). The semi-implicit formula for the discretization of $\frac{\partial F_\star}{\partial \phi_i}$ (for $i = 1, \dots, N$) is given by[5]

$$d_i^{F_\star}(\boldsymbol{\phi}_\star^{n+1}, \boldsymbol{\phi}_\star^n) \overset{\text{def}}{=} \sum_{j=1}^{N} \frac{\sigma_{ij}}{2} \left[d^f(\phi_i^{n+1}, \phi_i^n) - d^f(\phi_i^{n+1} + \phi_j^{n+1}, \phi_i^n + \phi_j^n) \right], \tag{5.7a}$$

$$d^f(x, y) \overset{\text{def}}{=} \begin{cases} \dfrac{f(x) - f(y)}{x - y}, & x \neq y, \\ f'(x), & x = y. \end{cases} \tag{5.7b}$$

For f given by (3.9) we get $d^f(x, y) = (x + y)(1 + x^2 + y^2) - 2(x^2 + xy + y^2)$. Finally, in accordance with (4.21) we put

$$d_j^F(\boldsymbol{\phi}^{n+1}, \boldsymbol{\phi}^n) = \left(d_j^{F_\star}(\boldsymbol{\phi}_\star^{n+1}, \boldsymbol{\phi}_\star^n) - d_N^{F_\star}(\boldsymbol{\phi}_\star^{n+1}, \boldsymbol{\phi}_\star^n) \right) \Big|_{\substack{\phi_N^{n+\beta} = 1 - \sum_{k=1}^{N-1} \phi_k^{n+\beta} \\ \text{for } \beta \in \{0,1\}}}, \tag{5.8}$$

for $j = 1, \dots, N-1$. It is straightforward to verify that

$$F(\boldsymbol{\phi}^{n+1}) - F(\boldsymbol{\phi}^n) = \boldsymbol{d}^F(\boldsymbol{\phi}^{n+1}, \boldsymbol{\phi}^n) \cdot (\boldsymbol{\phi}^{n+1} - \boldsymbol{\phi}^n), \tag{5.9}$$

where $\boldsymbol{d}^F(\boldsymbol{\phi}^{n+1}, \boldsymbol{\phi}^n) = [d_1^F(\boldsymbol{\phi}^{n+1}, \boldsymbol{\phi}^n), \dots, d_{N-1}^F(\boldsymbol{\phi}^{n+1}, \boldsymbol{\phi}^n)]^\top$. As we will see, this property is crucial from the point of view of energy-stability of the scheme.

[4] Recall that the evolution equation for ϕ_N reads $\frac{\partial \phi_N}{\partial t} + \operatorname{div}(\phi_N \boldsymbol{v}) = -\operatorname{div}(M_0 \sum_{j=1}^{N-1} \nabla \chi_j)$, cf. (4.1b). With this, we formally retrieve the fundamental property $\frac{\partial}{\partial t} \sum_{i=1}^N \phi_i = 0$.

[5] See (Wu and Xu, 2017, Eq. (3.11)).

- The time discretization of (4.30d) is based on its equivalent form (BLM3) from Table 4.1. The first term on the left hand side was discretized following the identity $\sqrt{\varrho}\frac{\partial}{\partial t}\left(\sqrt{\varrho}\boldsymbol{v}\right) = \varrho\frac{\partial \boldsymbol{v}}{\partial t} + \frac{1}{2}\frac{\partial \varrho}{\partial t}\boldsymbol{v}$ and using the backward difference formula for the time derivatives. In the remaining two terms on the left hand side, the velocity from the previous time step was used as the advective velocity. Last but not least, the term corresponding to capillary force was adjusted to reflect the modification of the advection term in (5.3a). The energy contributions coming from advection of the volume fractions and from the capillary force thus remain counterbalanced on the discrete level, exactly as in the continuous case.

5.2 Space discretization

We assume that the computational domain Ω is polygonal/polyhedral (depending on its geometrical dimension). Let $\mathcal{T}_h$ be an admissible and regular partition of Ω using triangular or tetrahedral elements[6], parametrized by the maximum diameter of the elements h. The different parts of the boundary, which were introduced in Section 4.2.2, are supposed to be resolved by the mesh.

We use the Galerkin FEM to discretize (5.3) in space. The corresponding variational formulation will be given on finite dimensional spaces (denoted using the subscript h) consisting of piecewise polynomials[7], which approximate the original function spaces from (4.34). We further assume that the chosen approximations are *conforming*, meaning that $\boldsymbol{\mathcal{V}}_h^{\phi} \subset \boldsymbol{\mathcal{V}}^{\phi}$, $\boldsymbol{\mathcal{V}}_{h,\Gamma_{\mathrm{CH}}}^{\phi} \subset \boldsymbol{\mathcal{V}}_{\Gamma_{\mathrm{CH}}}^{\phi}$, $\boldsymbol{\mathcal{V}}_h^{\chi} \subset \boldsymbol{\mathcal{V}}^{\chi}$, $\boldsymbol{\mathcal{V}}_h^{\boldsymbol{v}} \subset \boldsymbol{\mathcal{V}}^{\boldsymbol{v}}$, $\boldsymbol{\mathcal{V}}_{h,\Gamma_{\mathrm{NS}}}^{\boldsymbol{v}} \subset \boldsymbol{\mathcal{V}}_{\Gamma_{\mathrm{NS}}}^{\boldsymbol{v}}$ and $\mathcal{V}_h^p \subset \mathcal{V}^p$. Moreover, the finite element spaces used for approximations of the velocity and the pressure are assumed to satisfy the well-known Babuška-Brezzi stability condition (discrete inf-sup condition).

Let us make a default choice of finite element spaces that will be used in numerical simulations covered by Chapter 6. Unless otherwise stated, we consider

$$\left.\begin{array}{c} \mathbb{P}_k \text{ elements for spaces associated with } \boldsymbol{\phi} \text{ and } \boldsymbol{\chi}, \\ \text{(Taylor-Hood) } \mathbb{P}_{k+1}/\mathbb{P}_k \text{ elements for spaces associated with } \boldsymbol{v} \text{ and } p, \end{array}\right\} \tag{5.10}$$

with $k = 1$. Now we are ready to formulate the Galerkin system which will be later used to derive a discrete counterpart of the energy equality (5.1).

Let $\boldsymbol{\phi}_h^n, \widetilde{\boldsymbol{\phi}}_h^{n+1} \in \boldsymbol{\mathcal{V}}_h^{\phi}$ and $\boldsymbol{v}_h^n, \widetilde{\boldsymbol{v}}_h^{n+1} \in \boldsymbol{\mathcal{V}}_h^{\boldsymbol{v}}$ are given functions which attain prescribed values on the Dirichlet parts of the boundary Γ_{CH} and Γ_{NS} respectively[8].

[6] We assume that $\bar{\Omega} = \cup_{T\in\mathcal{T}_h}\bar{T}$ and any two elements are either disjoint or share one common face/edge/vertex. Moreover, for each $T \in \mathcal{T}_h$ there is an inscribed sphere in T such that the ratio of the diameter of this sphere and the diameter of T is bounded from below, independently of T and h.

[7] By $\mathbb{P}_k$ we denote the space of *globally continuous* scalar-valued piecewise polynomials of order not exceeding k that are defined on $\mathcal{T}_h$, the boldface notation $\mathbb{P}_k$ is reserved for vector-valued polynomials, and finally $\mathbb{P}_k^{\mathrm{disc}}, \mathbb{P}_k^{\mathrm{disc}}$ is used if the global continuity is not required.

[8] See the discussion below (4.34).

The problem is to find $(\boldsymbol{\phi}_h^{n+1}, \boldsymbol{\chi}_h^{n+1}, \boldsymbol{v}_h^{n+1}, p_h^{n+1})$ such that

$$\boldsymbol{\phi}_h^{n+1} - \widetilde{\boldsymbol{\phi}}_h^{n+1} \in \boldsymbol{\mathcal{V}}_{h,\Gamma_{\mathrm{CH}}}^{\phi}, \quad \boldsymbol{\chi}_h^{n+1} \in \boldsymbol{\mathcal{V}}_h^{\chi}, \quad \boldsymbol{v}_h^{n+1} - \widetilde{\boldsymbol{v}}_h^{n+1} \in \boldsymbol{\mathcal{V}}_{h,\Gamma_{\mathrm{NS}}}^{\boldsymbol{v}}, \quad p_h^{n+1} \in \mathcal{V}_h^{p}, \tag{5.11}$$

and $\forall \chi_h^{\mathrm{te}} \in \mathcal{V}^{\chi}$, $\forall \phi_h^{\mathrm{te}} \in \mathcal{V}_{h,\Gamma_{\mathrm{CH}}}^{\phi}$, $\forall p_h^{\mathrm{te}} \in \mathcal{V}_h^{p}$, $\forall \boldsymbol{v}_h^{\mathrm{te}} \in \boldsymbol{\mathcal{V}}_{h,\Gamma_{\mathrm{NS}}}^{\boldsymbol{v}}$, we have

$$\begin{aligned}
&\int_\Omega \frac{\phi_{i,h}^{n+1} - \phi_{i,h}^{n}}{\Delta_t} \chi_h^{\mathrm{te}} + \int_{\Gamma_{\mathrm{in}} \cup \Gamma_{\mathrm{cut}}} (\boldsymbol{v}_h^* \cdot \boldsymbol{n})(\phi_{i,h}^n - \alpha_{i,h}) \chi_h^{\mathrm{te}} - \int_\Omega (\phi_{i,h}^n - \alpha_{i,h}) \boldsymbol{v}_h^* \cdot \nabla \chi_h^{\mathrm{te}} \\
&\qquad - \int_{\Gamma_{\mathrm{cut}}} M_0 (\nabla \chi_{i,h}^{n+1} \cdot \boldsymbol{n}) \chi_h^{\mathrm{te}} + \int_\Omega M_0 \nabla \chi_{i,h}^{n+1} \cdot \nabla \chi_h^{\mathrm{te}} = 0, \quad i = 1, \dots, N-1,
\end{aligned} \tag{5.12a}$$

$$\begin{aligned}
&\int_\Omega \chi_{i,h}^{n+1} \phi_h^{\mathrm{te}} - \int_\Omega \frac{b}{\varepsilon} \sum_{j=1}^{N-1} \ell_{ij} d_j^F(\boldsymbol{\phi}_h^{n+1}, \boldsymbol{\phi}_h^n) \phi_h^{\mathrm{te}} \\
&\qquad + \int_{\Gamma_{\mathrm{cut}}} \frac{a\varepsilon}{2} (\nabla \phi_{i,h}^{n+\theta} \cdot \boldsymbol{n}) \phi_h^{\mathrm{te}} - \int_\Omega \frac{a\varepsilon}{2} \nabla \phi_{i,h}^{n+\theta} \cdot \nabla \phi_h^{\mathrm{te}} = 0, \quad i = 1, \dots, N-1,
\end{aligned} \tag{5.12b}$$

$$\int_\Omega p_h^{\mathrm{te}} \operatorname{div} \boldsymbol{v}_h^{n+1} = 0, \tag{5.12c}$$

$$\begin{aligned}
&\int_\Omega \frac{1}{2} \frac{\varrho_h^{n+1} + \varrho_h^n}{\Delta_t} \boldsymbol{v}_h^{n+1} \cdot \boldsymbol{v}_h^{\mathrm{te}} + \int_{\Gamma_{\mathrm{cut}}} \frac{1}{2} \left((\varrho_h^{n+1} \boldsymbol{v}_h^n + \boldsymbol{J}_h^{n+1}) \cdot \boldsymbol{n} \right) \boldsymbol{v}_h^{n+1} \cdot \boldsymbol{v}_h^{\mathrm{te}} \\
&\qquad + \int_\Omega \frac{1}{2} \boldsymbol{v}_h^{\mathrm{te}} \cdot \left([\nabla \boldsymbol{v}_h^{n+1}] (\varrho_h^{n+1} \boldsymbol{v}_h^n + \boldsymbol{J}_h^{n+1}) \right) - \int_\Omega \frac{1}{2} \boldsymbol{v}_h^{n+1} \cdot \left([\nabla \boldsymbol{v}_h^{\mathrm{te}}] (\varrho_h^{n+1} \boldsymbol{v}_h^n + \boldsymbol{J}_h^{n+1}) \right) \\
&\qquad\qquad + \int_\Omega 2\nu_h^{n+1} \mathbb{D}_h^{n+1} : \nabla \boldsymbol{v}_h^{\mathrm{te}} - \int_\Omega p_h^{n+1} \operatorname{div} \boldsymbol{v}_h^{\mathrm{te}} \\
&= \int_\Omega \frac{\varrho_h^n}{\Delta_t} \boldsymbol{v}_h^n \cdot \boldsymbol{v}_h^{\mathrm{te}} - \int_\Omega \sum_{i,j=1}^{N-1} \lambda_{ij} (\phi_{i,h}^n - \alpha_{i,h}) \nabla \chi_{j,h}^{n+1} \cdot \boldsymbol{v}_h^{\mathrm{te}} + \int_\Omega \varrho_h^{n+1} \boldsymbol{g} \cdot \boldsymbol{v}_h^{\mathrm{te}} - \int_{\Gamma_{\mathrm{cut}}} G \boldsymbol{n} \cdot \boldsymbol{v}_h^{\mathrm{te}},
\end{aligned} \tag{5.12d}$$

where

$$\boldsymbol{v}_h^* = \boldsymbol{v}_h^n - \frac{\Delta_t}{\varrho_h^n} \sum_{i,j=1}^{N-1} \lambda_{ij} (\phi_{i,h}^n - \alpha_{i,h}) \nabla \chi_{j,h}^{n+1}, \qquad \alpha_{i,h} = \frac{1}{|\Omega|} \int_\Omega \phi_{i,h}^0,$$

$\boldsymbol{J}_h^{n+1} = -\Theta_2 \sum_{i=1}^{N-1} M_0 (\hat{\varrho}_i - \hat{\varrho}_N) \nabla \chi_{i,h}^{n+1}$, $\nu_h^{n+1} = \sum_{i=1}^{N-1} (\nu_i - \nu_N) \phi_{i,h}^{n+1} + \nu_N$ and $\varrho_h^{n+\beta} = \sum_{i=1}^{N-1} (\hat{\varrho}_i - \hat{\varrho}_N) \phi_{i,h}^{n+\beta} + \hat{\varrho}_N$ (for $\beta \in \{0, 1\}$). The nonlinear terms d_j^F appearing in (5.12b) are given by (5.8).

Remark 5.1. To be more precise, we should have written $\phi_{i,h}^{n+1} = \widetilde{\phi}_{i,h}^{n+1} + \varphi_{i,h}^{n+1}$ and $\boldsymbol{v}_h^{n+1} = \widetilde{\boldsymbol{v}}_h^{n+1} + \boldsymbol{u}_h^{n+1}$ everywhere in (5.12). The functions $\widetilde{\phi}_{i,h}^{n+1}$, $\widetilde{\boldsymbol{v}}_h^{n+1}$ introduced in (5.11) represent extensions of given Dirichlet boundary data, while $\varphi_{i,h}^{n+1}$, $\boldsymbol{u}_h^{n+1}$ are functions sought in the constrained spaces $\mathcal{V}_{h,\Gamma_{\mathrm{CH}}}^{\phi}$ and $\boldsymbol{\mathcal{V}}_{h,\Gamma_{\mathrm{NS}}}^{\boldsymbol{v}}$ respectively.

Remark 5.2. The discrete functions $\boldsymbol{\phi}_h^0 \in \boldsymbol{\mathcal{V}}_h^{\phi}$ and $\boldsymbol{v}_h^0 \in \boldsymbol{\mathcal{V}}_h^{\boldsymbol{v}}$ can be obtained from the initial conditions (4.35), typically by nodal interpolation or by appropriate projection method.

Remark 5.3. If $\Gamma_{\mathrm{cut}} = \emptyset$, then we change our definition of $\mathcal{V}_h^p$ in the sense of inclusion $\mathcal{V}_h^p \subset \mathcal{V}_0^p$, see (4.34e), in order to fix the pressure.

In order to show the energy-stability of the scheme, let us assume for the moment that $\boldsymbol{g} = \boldsymbol{0}$, $\Gamma_{\text{in}} = \Gamma_{\text{cut}} = \emptyset$ so that $\partial\Omega = \Gamma_{\text{w}}$, and $\boldsymbol{v}_{\text{w}} = \boldsymbol{0}$. Proposition 5.4 formulated below generalizes Proposition 3.1 from (Minjeaud, 2013, p. 595) to N-component model. The proof follows the arguments given therein.

Proposition 5.4 (Discrete energy equality)**.** *Let $\boldsymbol{\phi}_h^n \in \boldsymbol{\mathcal{V}}_h^\phi, \boldsymbol{v}_h^n \in \boldsymbol{\mathcal{V}}_{h,\partial\Omega}^{\boldsymbol{v}}$ are given functions. Assume that $(\boldsymbol{\phi}_h^{n+1}, \boldsymbol{\chi}_h^{n+1}, \boldsymbol{v}_h^{n+1}, p_h^{n+1}) \in \boldsymbol{\mathcal{V}}_h^\phi \times \boldsymbol{\mathcal{V}}_h^\chi \times \boldsymbol{\mathcal{V}}_{h,\partial\Omega}^{\boldsymbol{v}} \times \mathcal{V}_h^p$ solve the problem given by* (5.12) *with $\boldsymbol{g} = \boldsymbol{0}$. Then we have the equality*

$$\begin{aligned}\mathcal{E}^{n+1} - \mathcal{E}^n = &-\Delta_t M_0 \left\| \boldsymbol{\Lambda}^{\frac{1}{2}} \boldsymbol{\chi}_h^{n+1} \right\|_{H_0^1}^2 - \Delta_t \int_\Omega 2\nu_h^{n+1} \mathbb{D}_h^{n+1} : \mathbb{D}_h^{n+1} \\ &- (2\theta - 1) \frac{a\varepsilon}{2} \left\| \boldsymbol{\Lambda}^{\frac{1}{2}} (\boldsymbol{\phi}_h^{n+1} - \boldsymbol{\phi}_h^{n+1}) \right\|_{H_0^1}^2 - \int_\Omega \frac{1}{2} \varrho_h^n \left(\left| \boldsymbol{v}_h^{n+1} - \boldsymbol{v}_h^* \right|^2 + |\boldsymbol{v}_h^* - \boldsymbol{v}_h^n|^2 \right). \end{aligned} \tag{5.13}$$

Proof. Recall that $\boldsymbol{\Lambda}$ is a constant matrix here. If we take $\chi_h^{\text{te}} = \sum_{j=1}^{N-1} \lambda_{ij} \chi_{j,h}^{n+1}$ and $\phi_h^{\text{te}} = \frac{1}{\Delta_t} \sum_{j=1}^{N-1} \lambda_{ij} (\phi_{j,h}^{n+1} - \phi_{j,h}^n)$ as test functions in (5.12a)–(5.12b) and if we sum up the equations over $i = 1, \dots, N-1$, we get

$$\begin{aligned}\frac{1}{\Delta_t} \int_\Omega \sum_{i,j=1}^{N-1} (\phi_{i,h}^{n+1} - \phi_{i,h}^n) \lambda_{ij} \chi_{j,h}^{n+1} + \int_\Omega \sum_{i,j=1}^{N-1} M_0 \lambda_{ij} \nabla \chi_{i,h}^{n+1} \cdot \nabla \chi_{j,h}^{n+1} \\ - \int_\Omega \sum_{i,j=1}^{N-1} \lambda_{ij} (\phi_{i,h}^n - \alpha_{i,h}) \boldsymbol{v}_h^* \cdot \nabla \chi_{j,h}^{n+1} = 0, \end{aligned} \tag{5.14a}$$

$$\begin{aligned}\frac{1}{\Delta_t} \int_\Omega \sum_{i,j=1}^{N-1} \chi_{i,h}^{n+1} \lambda_{ij} (\phi_{j,h}^{n+1} - \phi_{j,h}^n) - \frac{1}{\Delta_t} \int_\Omega \frac{b}{\varepsilon} \boldsymbol{d}^F(\boldsymbol{\phi}_h^{n+1}, \boldsymbol{\phi}_h^n) \cdot (\boldsymbol{\phi}_h^{n+1} - \boldsymbol{\phi}_h^n) \\ - \frac{1}{\Delta_t} \int_\Omega \frac{a\varepsilon}{2} \sum_{i,j=1}^{N-1} \lambda_{ij} \nabla \phi_{i,h}^{n+\theta} \cdot \nabla (\phi_{j,h}^{n+1} - \phi_{j,h}^n) = 0, \end{aligned} \tag{5.14b}$$

As a next step, we modify integrands in (5.14b). We apply the symmetry of λ_{ij} to interchange i and j in the first term, we use (5.9) in the second one, and in the third one we apply the simple formula

$$\begin{aligned}\nabla \phi_{i,h}^{n+\theta} \cdot \nabla (\phi_{j,h}^{n+1} - \phi_{j,h}^n) = \frac{1}{2} \big(&\nabla \phi_{i,h}^{n+1} \cdot \nabla \phi_{j,h}^{n+1} - \nabla \phi_{i,h}^n \cdot \nabla \phi_{j,h}^n \\ &+ (2\theta - 1) (\nabla \phi_{i,h}^{n+1} - \nabla \phi_{i,h}^n) \cdot (\nabla \phi_{j,h}^{n+1} - \nabla \phi_{j,h}^n) \big). \end{aligned} \tag{5.15}$$

(Recall that $\phi_{i,h}^{n+\theta} = (1-\theta)\phi_{i,h}^n + \theta \phi_{i,h}^{n+1}$.) Upon subtracting the resulting equation from (5.14a) and multiplying the result by Δ_t, we obtain

$$\begin{aligned}\Psi^{n+1} - \Psi^n + \Delta_t M_0 \left\| \boldsymbol{\Lambda}^{\frac{1}{2}} \boldsymbol{\chi}_h^{n+1} \right\|_{H_0^1}^2 + (2\theta - 1) \frac{a\varepsilon}{2} \left\| \boldsymbol{\Lambda}^{\frac{1}{2}} (\boldsymbol{\phi}_h^{n+1} - \boldsymbol{\phi}_h^{n+1}) \right\|_{H_0^1}^2 \\ = \Delta_t \int_\Omega \sum_{i,j=1}^{N-1} \lambda_{ij} (\phi_{i,h}^n - \alpha_{i,h}) \boldsymbol{v}_h^* \cdot \nabla \chi_{j,h}^{n+1}. \end{aligned} \tag{5.16}$$

The term on the right hand side can be rewritten using the identity[9]

$$\Delta_t \sum_{i,j=1}^{N-1} \lambda_{ij}(\phi_{i,h}^n - \alpha_{i,h}) \boldsymbol{v}_h^* \cdot \nabla \chi_{j,h}^{n+1} = \frac{1}{2}\varrho_h^n \left|\boldsymbol{v}_h^n\right|^2 - \frac{1}{2}\varrho_h^n \left|\boldsymbol{v}_h^*\right|^2 - \frac{1}{2}\varrho_h^n \left|\boldsymbol{v}_h^n - \boldsymbol{v}_h^*\right|^2 .$$

In light of this manipulation we obtain

$$\begin{aligned} \Psi^{n+1} - \Psi^n + \int_\Omega \frac{1}{2}\varrho_h^n \left|\boldsymbol{v}_h^*\right|^2 - \int_\Omega \frac{1}{2}\varrho_h^n \left|\boldsymbol{v}_h^n\right|^2 + \Delta_t M_0 \left\|\boldsymbol{\Lambda}^{\frac{1}{2}} \boldsymbol{\chi}_h^{n+1}\right\|_{H_0^1}^2 \\ + (2\theta - 1)\frac{a\varepsilon}{2} \left\|\boldsymbol{\Lambda}^{\frac{1}{2}}(\boldsymbol{\phi}_h^{n+1} - \boldsymbol{\phi}_h^{n+1})\right\|_{H_0^1}^2 = -\int_\Omega \frac{1}{2}\varrho_h^n \left|\boldsymbol{v}_h^n - \boldsymbol{v}_h^*\right|^2 . \quad (5.17) \end{aligned}$$

It remains to put $p_h^{\mathrm{te}} = p_h^{n+1}$ and $\boldsymbol{v}_h^{\mathrm{te}} = \boldsymbol{v}_h^{n+1}$ in (5.12c)–(5.12d). Upon some algebraic manipulations, one arrives at

$$\begin{aligned} \int_\Omega \frac{1}{2}\varrho_h^{n+1} \left|\boldsymbol{v}_h^{n+1}\right|^2 - \int_\Omega \frac{1}{2}\varrho_h^n \left|\boldsymbol{v}_h^*\right|^2 + \Delta_t \int_\Omega 2\nu_h^{n+1} \mathbb{D}_h^{n+1} : \mathbb{D}_h^{n+1} \\ = -\int_\Omega \frac{1}{2}\varrho_h^n \left|\boldsymbol{v}_h^{n+1} - \boldsymbol{v}_h^*\right|^2 , \quad (5.18) \end{aligned}$$

Finally, the discrete energy equality (5.13) is obtained by summing up equations (5.17) and (5.18). □

The terms on the second line in (5.13) represent the numerical dissipation introduced by the time discretization error. Provided that $\theta \in [\frac{1}{2}, 1]$, we see that the contribution of all terms on the right hand side of the discrete energy equality are non-positive. This means that the discretized values of $\mathcal{E}(t) = \mathcal{E}_{\mathrm{kin}}(t) + \Psi(t)$ are decreasing in time independently of the size of Δ_t. We say that the numerical scheme is *unconditionally stable*.

Remark 5.5. It is often the case that the computed values of the individual components of $\boldsymbol{\phi}^{n+1}$ exceed marginal values of the interval $[0, 1]$ due to finite precision arithmetic used in practical computations. In order to prevent from unrealistic values of the density and the viscosity, we follow (Dong, 2017, Eq. (130)) and—in case of large density ratios—we further clamp the values of $\varrho_h^{n+\beta}$, for $\beta \in \{0, 1\}$, and ν_h^{n+1} in the sense of piecewise definitions

$$\underline{\varrho}_h^{n+\beta} \overset{\mathrm{def}}{=} \begin{cases} \varrho_h^{n+\beta}, & \text{if } \varrho_h^{n+\beta} \in [\hat{\varrho}_{\min}, \hat{\varrho}_{\max}], \\ \hat{\varrho}_{\max}, & \text{if } \varrho_h^{n+\beta} > \hat{\varrho}_{\max}, \\ \hat{\varrho}_{\min}, & \text{if } \varrho_h^{n+\beta} < \hat{\varrho}_{\min}, \end{cases} \qquad \underline{\nu}_h^{n+1} \overset{\mathrm{def}}{=} \begin{cases} \nu_h^{n+1}, & \text{if } \nu_h^{n+1} \in [\nu_{\min}, \nu_{\max}], \\ \nu_{\max}, & \text{if } \nu_h^{n+1} > \nu_{\max}, \\ \nu_{\min}, & \text{if } \nu_h^{n+1} < \nu_{\min}, \end{cases} \quad (5.19)$$

where $\hat{\varrho}_{\max} = \max(\hat{\varrho}_1, \ldots, \hat{\varrho}_N)$, $\hat{\varrho}_{\min} = \min(\hat{\varrho}_1, \ldots, \hat{\varrho}_N)$, $\nu_{\max} = \max(\nu_1, \ldots, \nu_N)$ and $\nu_{\min} = \min(\nu_1, \ldots, \nu_N)$.

[9] Take the inner product of the definition $\boldsymbol{v}_h^* = \boldsymbol{v}_h^n - \frac{\Delta_t}{\varrho_h^n} \sum_{i,j=1}^{N-1} \lambda_{ij}(\phi_{i,h}^n - \alpha_{i,h}) \nabla \chi_{j,h}^{n+1}$ with $\varrho_h^n \boldsymbol{v}_h^*$, rearrange the terms and finally use $2\boldsymbol{v}^n \cdot \boldsymbol{v}^* = \left|\boldsymbol{v}^n\right|^2 + \left|\boldsymbol{v}^*\right|^2 - \left|\boldsymbol{v}^n - \boldsymbol{v}^*\right|^2$.

5.3 Implementation

One of the most important advantages of the time discretization scheme proposed in (5.3) is the fact that it allows for splitting of the original coupled problem. Indeed, the sought solution of (5.12) can be obtained in a decoupled fashion following the steps highlighted in Algorithm 1.

Algorithm 1 Semi-decoupled scheme based on (5.12)

Require:
Input parameters [Table 4.2]
Mesh and boundary data $[(\Gamma_{\mathrm{CH}}, \boldsymbol{\phi}_D), (\Gamma_{\mathrm{NS}}, \boldsymbol{v}_D)]$
Initial conditions $[\boldsymbol{\phi}_h^0, \boldsymbol{v}_h^0]$
Time domain specification $[t_{\mathrm{end}}, N_{t.s.}, \Delta_t]$
Ensure:
... ▷ initialization of variables and derived coefficients [Table 4.2]

for $n = 0, 1, \ldots, N_{t.s.} - 1$ **do**
Step 1: solve (5.12a)–(5.12b) for $\boldsymbol{\phi}_h^{n+1}, \boldsymbol{\chi}_h^{n+1}$ ▷ CH part, nonlinear solve
Step 2: solve (5.12c)–(5.12d) for $\boldsymbol{v}_h^{n+1}, p_h^{n+1}$ ▷ NS part, linear solve
end for

The system of nonlinear algebraic equations arising in the CH part of the problem is solved using the standard Newton-Raphson method. The NS part of the problem leads to a linear system of algebraic equations due to the fact that the velocity from the previous time step has been used as the advective velocity in (5.3d), which corresponds to the so-called *Oseen type linearization*. It turns out to be very important to have an efficient numerical solution strategy for this linearized system in order to properly handle large three-dimensional simulations based on the current model. Further discussion of the development of robust and effective solvers for the subproblems arising in Algorithm 1 is postponed until Section 5.4.

5.3.1 MUFLON software library

The above numerical scheme has been implemented as part of the MUFLON software library developed alongside the thesis, see Řehoř (2017). The library is built on top of the FEniCS Project which is a collection of free software with an extensive list of features for automated, efficient solution of differential equations. FEniCS incorporates C++/Python problem solving environment DOLFIN, see Logg et al. (2012), and the form language UFL, see Alnæs et al. (2014). More details about the FEniCS Project can be found, for example, in Logg et al. (2012) or Alnæs et al. (2015).

The general purpose of the MUFLON library is twofold. In a broad scope, it is designed with the perspective to *enable straightforward implementation and comparison of different diffuse interface models* the development of which is covered in Chapters 2–4 of the present thesis. Note that such concept includes

the possibility to test different designs of double-well/multi-well potentials and other subtle details characterizing the individual models. In a narrow scope, the MUFLON library *provides an automated framework for testing of different FEM-based schemes* developed for numerical discretization of diffuse interface models. In particular, it allows to alter the choice of finite element spaces, recall our default choice (5.10), as well as to implement different time-stepping algorithms, see Section 5.3.2.

In Figure 5.1, we show a simplified code snippet introducing the Python interface for a multi-phase flow simulation using FEniCS with the MUFLON library. The ease with which it is possible implement variational forms (5.12a) and (5.12b) using FEniCS is illustrated in Figure 5.2.

Python code

```
# Suppose that FEniCS is imported and we have the following at our disposal:
#   - mesh 'mesh'
#   - boundary markers 'bndry_markers'
#   - linear and quadratic finite elements 'P1', 'P2'
#   - time step 'dt' and final time 't_end'
import muflon

# --- Create discretization scheme ---
scheme = "SemiDecoupled" # alt. "FullyDecoupled"
DS = muflon.DiscretizationFactory.create(scheme, mesh, P1, P1, P2, P1)
DS.parameters["N"] = 3   # number of components (phases)
DS.parameters["PTL"] = 1 # number of Previous Time Levels for time stepping
DS.setup()               # finishes the initialization process

# --- Access to solution functions ---
sol_ctl = DS.solution_ctl()        # Current Time Level t^(n+1)
sol_ptl = DS.solution_ptl(level=0) # Previous Time Level t^(n-level)

# --- Create and load initial conditions ---
ic = muflon.SimpleCppIC() # collects init. conds. for primitive variables
ic.add("phi", "sin(a0*x[0])", a0=pi) # adds 1st component of vector phi
# ... etc.
DS.load_ic_from_simple_cpp(ic) # sol_ptl <-- ic

# --- Create Dirichlet boundary conditions ---
bcs = {"v": DirichletBC(DS.subspace("v", 0), Constant(0.0), bndry_markers, 0)}
# ... etc.

# --- Create model ---
mtype = "Incompressible" # alt. "Quasi-incompressible" (not yet implemented)
model = muflon.ModelFactory.create(mtype, dt, DS)
forms = model.create_forms()
# ... space for updating forms, e.g. by adding boundary integrals
#     (DS provides access to primitive variables + test and trial functions)

# --- Create solver ---
solver = mufon.SolverFactory.create(scheme, sol_ctl, forms, bcs)

# --- Run time-stepping algorithm ---
TS = muflon.TimeSteppingFactory.create(
        "ConstantTimeStep", mesh.mpi_comm(), dt, t_end, solver, sol_ptl)
result = TS.run()
```

Figure 5.1: Illustration of MUFLON's application programming interface.

Python code

```python
# Suppose that FEniCS is imported and we have the following at our disposal:
#   - dictionaries 'pv', 'pv0' containing primitive variables
#       at new and old time levels as 'Function' objects from FEniCS
#       (prepared by muflon.DiscretizationFactory)
#   - dictionary 'test' containing 'TestFunction' objects from FEniCS
#       (prepared by muflon.DiscretizationFactory)
#   - dictionary 'cc' containing constant coefficients including
#       + matrix of surface tensions "S"
#       + matrix of mixing energy coefficients "LA" and its inverse "iLA"
#       + interface thickness "eps"
#       + ...
#   - mobility 'Mo', time step 'dt', density 'rho0'
from muflon.models.potentials import DoublewellFactory, multiwell
from muflon.models.varcoeffs import capillary_force

# --- Unwrap primitive variables ---
phi, chi, v, p = pv["phi"], pv["chi"], pv["v"], pv["p"]
phi0, v0 = pv0["phi"], pv0["v"]

# --- Get double-well potential ---
dw = DoublewellFactory.create("Poly4")
cc["a"], cc["b"] = dw.free_energy_coefficents()

# --- Compute derivative of multi-well potential ---
_phi = variable(phi)
F  = multiwell(dw, _phi, cc["S"])
dF = diff(F, _phi)

# --- Get capillary force ---
domain_size = assemble(1.0*dx)
alpha = [assemble(phi0[i]*dx)/domain_size for i in range(len(phi0))]
ca = as_vector([phi0[i] - Constant(alpha[i]) for i in range(len(phi0))])
f_cap = capillary_force(phi0, chi, cc["LA"])

# --- Define intermediate velocity ---
v_star = v0 + dt*f_cap/rho0

# --- Define nonlinear CH system (linear form in test functions) ---
eqn_phi = (
      (1.0/dt)*inner(phi - phi0, test["chi"])
    - inner(ca, dot(grad(test["chi"]), v_star))
    + Mo*inner(grad(chi), grad(test["chi"]))
)*dx

phi_star = cc["theta"]*phi + (1.0 - cc["theta"])*fact_ptl*phi0
eqn_chi = (
      inner(chi, test["phi"])
    - 0.5*cc["a"]*cc["eps"]*inner(grad(phi_star), grad(test["phi"]))
    - (cc["b"]/cc["eps"])*inner(dot(cc["iLA"], dF), test["phi"])
)*dx

system_ch = eqn_phi + eqn_chi
# NOTE:
#   The above variational form contains only volume integrals.
#   Application-dependent boundary integrals must be added elsewhere.
```

Figure 5.2: Implementation of (5.12a)–(5.12b) as part of the MUFLON library.

5.3.2 A short note on alternative numerical schemes

Different numerical schemes for models of FI-CHNS type (4.30) are available in the literature. The MUFLON library currently provides implementation of the semi-decoupled scheme described in Algorithm 1 and another splitting scheme developed by Dong (2017), who has used continuous high-order spectral elements for the implementation; see also Dong (2014a, 2015). This scheme is briefly described in Appendix C. One of its main advantages—at least with respect to the computational efficiency—is the fact that the scheme is designed in a way which further decouples the equations both in CH and NS parts of the original problem (see Algorithm 1). Moreover, the linear algebraic systems resulting from the proposed discretization involve only constant and time-independent coefficient matrices.

To name a few more alternatives, let us mention promising numerical schemes that were recently developed for binary FI-CHNS models by Grün and Klingbeil (2014) or Bosch et al. (2018). These schemes could be integrated into the MUFLON library at some point in the future.

5.4 Solution techniques

Algorithm 1 requires successive solution of the two subproblems at each time step. As already mentioned, these subproblems lead to the nonlinear system of algebraic CH equations and the linearized system of algebraic NS equations. Such systems are typically very large as a sufficiently fine mesh is needed close to interfacial regions in order to properly capture the interface dynamics. This naturally leads to the need to use high performance computers, and to the need to fully exploit the parallelization approach in the associated matrix computations.

For smaller (two-dimensional) problems, we use parallel *direct solvers* for all intermediate linear systems in the CH part as well as for the linearized system in the NS part of the problem. In particular, we use FEniCS compiled with PETSc library, see Balay et al. (2014a,b, 1997), which provides us, among others, with linear algebra data structures and bindings to the parallel[10] sparse direct solver MUMPS, see Amestoy et al. (2001, 2006).

For larger (three-dimensional) problems, the straightforward implementation described in the previous paragraph needs to be improved using the *iterative Krylov subspace solvers* with a good preconditioning strategy. Up to now, the main effort has been invested in the implementation of the framework that would be suitable for the development of efficient (fast and robust) solvers exclusively for the NS part of the problem. The intermediate linear algebraic systems encountered in the CH part are solved using the GMRES algorithm, see Saad and Schultz (1986), with point block Jacobi preconditioner from PETSc.

The preconditioning strategy for the NS part is built on the idea of modifying the pressure convection–diffusion (PCD) preconditioner which was developed and successfully used for solving incompressible NS equations, see Elman et al. (2014)

[10]For parallelelization, MPI framework is used by both FEniCS and PETSc.

and references therein. Our motivation for choosing this particular approach originates in the work by Kay and Welford (2007), where it was applied directly in the context of a particular CHNS model for two incompressible fluids with matching viscosities. The main issue in the design of the preconditioner is the need to handle NS system with very large density and viscosity variations.

Current state of the efforts for efficient implementation of the PCD preconditioner in FEniCS is available in the FENaPack software package, see Blechta and Řehoř (2017). The package mirrors our recent improvements achieved by revisiting the key ideas of the PCD strategy from the point of view of the *operator preconditioning theory*, cf. Málek and Strakoš (2015). The new theoretical results will appear in Blechta (2018).

In the remainder of this section we shall discuss a heuristic derivation of a variant of PCD preconditioner which has been tailored to the needs of the current discretization scheme. The aim here is to demonstrate capabilities of the recently implemented framework for the development of similar type of preconditioners, rather than to provide a rigorous analysis for this specific numerical approach. The performance of the suggested preconditioner will be illustrated in Section 6.3.

5.4.1 Preconditioning of incompressible Navier–Stokes equations with variable coefficients

At each time step of Algorithm 1, we need to solve the problem

$$\begin{aligned}
&\int_\Omega \frac{1}{2}\frac{\varrho_h^{n+1}+\varrho_h^n}{\Delta_t}\boldsymbol{v}_h^{n+1}\cdot\boldsymbol{v}_h^{\mathrm{te}} + \int_{\Gamma_{\mathrm{cut}}}\frac{1}{2}\left((\varrho_h^{n+1}\boldsymbol{v}_h^n+\boldsymbol{J}_h^{n+1})\cdot\boldsymbol{n}\right)\boldsymbol{v}_h^{n+1}\cdot\boldsymbol{v}_h^{\mathrm{te}} \\
&\quad+\int_\Omega\frac{1}{2}\boldsymbol{v}_h^{\mathrm{te}}\cdot\left([\nabla\boldsymbol{v}_h^{n+1}](\varrho_h^{n+1}\boldsymbol{v}_h^n+\boldsymbol{J}_h^{n+1})\right)-\int_\Omega\frac{1}{2}\boldsymbol{v}_h^{n+1}\cdot\left([\nabla\boldsymbol{v}_h^{\mathrm{te}}](\varrho_h^{n+1}\boldsymbol{v}_h^n+\boldsymbol{J}_h^{n+1})\right) \\
&\qquad+\int_\Omega 2\nu_h^{n+1}\mathbb{D}_h^{n+1}:\nabla\boldsymbol{v}_h^{\mathrm{te}}-\int_\Omega p_h^{n+1}\operatorname{div}\boldsymbol{v}_h^{\mathrm{te}}=\int_\Omega\widetilde{\boldsymbol{f}}\cdot\boldsymbol{v}_h^{\mathrm{te}}-\int_{\Gamma_{\mathrm{cut}}}G\boldsymbol{n}\cdot\boldsymbol{v}_h^{\mathrm{te}}, \qquad (5.20a)\\
&\qquad\qquad-\int_\Omega p_h^{\mathrm{te}}\operatorname{div}\boldsymbol{v}_h^{n+1}=0, \qquad (5.20b)
\end{aligned}$$

where we have used the shorthand notation

$$\widetilde{\boldsymbol{f}}\overset{\mathrm{def}}{=}\frac{\varrho_h^n}{\Delta_t}\boldsymbol{v}_h^n-\sum_{i,j=1}^{N-1}\lambda_{ij}(\phi_{i,h}^n-\alpha_{i,h})\nabla\chi_{j,h}^{n+1}+\varrho_h^{n+1}\boldsymbol{g}, \qquad (5.21)$$

cf. (5.12c)–(5.12d). To identify the corresponding linear algebra problem, we introduce a set of vector-valued functions $\{\boldsymbol{\varphi}_\iota^{\boldsymbol{v}}\}_{\iota=1}^{\omega^{\boldsymbol{v}}}$ which forms a basis of the constrained space $\boldsymbol{\mathcal{V}}_{h,\Gamma_{\mathrm{NS}}}^{\boldsymbol{v}}$. Then we can express the sought velocity in the form

$$\boldsymbol{v}_h^{n+1}=\widetilde{\boldsymbol{v}}_h^{n+1}+\sum_{\iota=1}^{\omega^{\boldsymbol{v}}}\mathrm{v}_\iota\boldsymbol{\varphi}_\iota^{\boldsymbol{v}}, \qquad (5.22)$$

cf. Remark 5.1. Similarly, let $\{\varphi_\iota^p\}_{\iota=1}^{\omega^p}$ denote a set of pressure basis functions such that

$$p_h^{n+1}=\sum_{\iota=1}^{\omega^p}\mathrm{p}_\iota\varphi_\iota^p. \qquad (5.23)$$

The discrete formulation (5.20) can be expressed as a system of linear equations

$$\underbrace{\begin{bmatrix}\mathbf{F} & \mathbf{B}^\top \\ \mathbf{B} & \mathbf{0}\end{bmatrix}}_{\bar{\mathbf{A}}} \underbrace{\begin{bmatrix}\mathbf{v} \\ \mathbf{p}\end{bmatrix}}_{\bar{\mathbf{x}}} = \underbrace{\begin{bmatrix}\mathbf{f} \\ \mathbf{g}\end{bmatrix}}_{\bar{\mathbf{b}}}. \tag{5.24}$$

The matrix $\mathbf{F} = [\mathrm{F}_{\iota\kappa}]_{\omega^{\boldsymbol{v}}\times\omega^{\boldsymbol{v}}}$ can be understood as a *convection-diffusion-reaction operator* given by $\mathrm{F}_{\iota\kappa} = \frac{1}{\Delta_t}\mathrm{M}_{\iota\kappa} + \frac{1}{2}\mathrm{M}^{\Gamma_{\mathrm{cut}}}_{\iota\kappa} + \frac{1}{2}\left(\mathrm{K}_{\iota\kappa} - \mathrm{K}_{\kappa\iota}\right) + \mathrm{A}_{\iota\kappa} + \mathrm{A}^{\mathrm{off}}_{\iota\kappa}$, where

$$\mathrm{M}_{\iota\kappa} = \int_\Omega \frac{\varrho_h^{n+1} + \varrho_h^n}{2} \boldsymbol{\varphi}^{\boldsymbol{v}}_\kappa \cdot \boldsymbol{\varphi}^{\boldsymbol{v}}_\iota, \quad \mathrm{M}^{\Gamma_{\mathrm{cut}}}_{\iota\kappa} = \int_{\Gamma_{\mathrm{cut}}} \left((\varrho_h^{n+1}\boldsymbol{v}_h^n + \boldsymbol{J}_h^{n+1})\cdot\boldsymbol{n}\right) \boldsymbol{\varphi}^{\boldsymbol{v}}_\kappa \cdot \boldsymbol{\varphi}^{\boldsymbol{v}}_\iota, \tag{5.25}$$

$$\mathrm{K}_{\iota\kappa} = \int_\Omega \boldsymbol{\varphi}^{\boldsymbol{v}}_\iota \cdot \left([\nabla\boldsymbol{\varphi}^{\boldsymbol{v}}_\kappa](\varrho_h^{n+1}\boldsymbol{v}_h^n + \boldsymbol{J}_h^{n+1})\right), \tag{5.26}$$

$$\mathrm{A}_{\iota\kappa} = \int_\Omega \nu_h^{n+1}\, \nabla\boldsymbol{\varphi}^{\boldsymbol{v}}_\kappa : \nabla\boldsymbol{\varphi}^{\boldsymbol{v}}_\iota, \tag{5.27}$$

$$\mathrm{A}^{\mathrm{off}}_{\iota\kappa} = \int_\Omega \frac{1}{2}\nu_h^{n+1} \left((\nabla\boldsymbol{\varphi}^{\boldsymbol{v}}_\kappa)^\top : \nabla\boldsymbol{\varphi}^{\boldsymbol{v}}_\iota + \nabla\boldsymbol{\varphi}^{\boldsymbol{v}}_\kappa : (\nabla\boldsymbol{\varphi}^{\boldsymbol{v}}_\iota)^\top\right). \tag{5.28}$$

The matrix $\mathbf{B} = [\mathrm{B}_{\iota\kappa}]_{\omega^p\times\omega^{\boldsymbol{v}}}$ then corresponds to

$$\mathrm{B}_{\iota\kappa} = -\int_\Omega \varphi^p_\iota \operatorname{div} \boldsymbol{\varphi}^{\boldsymbol{v}}_\kappa. \tag{5.29}$$

Both $\mathbf{F}$ and $\mathbf{B}$ have a block structure determined by spatial directions. In practice, the velocity components are approximated using a single finite element space. Using the natural componentwise splitting we make simple observations concerning the individual matrices contributing to $\mathbf{F}$, see Table 5.1. Finally, the entries of the vectors $\mathbf{f} = [\mathrm{f}]_{\omega^{\boldsymbol{v}}\times 1}$ and $\mathbf{g} = [\mathrm{g}]_{\omega^p\times 1}$ on the right hand side of (5.24) are

$$\begin{aligned}\mathrm{f}_\iota = {} & \int_\Omega \widetilde{\boldsymbol{f}}\cdot\boldsymbol{\varphi}^{\boldsymbol{v}}_\iota - \int_{\Gamma_{\mathrm{cut}}} G\boldsymbol{n}\cdot\boldsymbol{\varphi}^{\boldsymbol{v}}_\iota - \int_{\Gamma_{\mathrm{cut}}} \frac{1}{2}\left((\varrho_h^{n+1}\boldsymbol{v}_h^n + \boldsymbol{J}_h^{n+1})\cdot\boldsymbol{n}\right)\widetilde{\boldsymbol{v}}_h^{n+1}\cdot\boldsymbol{\varphi}^{\boldsymbol{v}}_\iota \\ & - \int_\Omega \frac{1}{2}\frac{\varrho_h^{n+1}+\varrho_h^n}{\Delta_t}\widetilde{\boldsymbol{v}}_h^{n+1}\cdot\boldsymbol{\varphi}^{\boldsymbol{v}}_\iota - \int_\Omega \frac{1}{2}\boldsymbol{\varphi}^{\boldsymbol{v}}_\iota\cdot\left([\nabla\widetilde{\boldsymbol{v}}_h^{n+1}](\varrho_h^{n+1}\boldsymbol{v}_h^n + \boldsymbol{J}_h^{n+1})\right) \\ & + \int_\Omega \frac{1}{2}\widetilde{\boldsymbol{v}}_h^{n+1}\cdot\left([\nabla\boldsymbol{\varphi}^{\boldsymbol{v}}_\iota](\varrho_h^{n+1}\boldsymbol{v}_h^n + \boldsymbol{J}_h^{n+1})\right) - \int_\Omega \nu_h^{n+1}\left(\nabla\widetilde{\boldsymbol{v}}_h^{n+1} + (\nabla\widetilde{\boldsymbol{v}}_h^{n+1})^\top\right) : \nabla\boldsymbol{\varphi}^{\boldsymbol{v}}_\iota,\end{aligned} \tag{5.30}$$

$$\mathrm{g}_\iota = \int_\Omega \varphi^p_\iota \operatorname{div}\widetilde{\boldsymbol{v}}_h^{n+1}. \tag{5.31}$$

Table 5.1: Properties of the matrices contributing to discrete convection–diffusion–reaction operator $\mathbf{F}$.

Matrix	Symmetric	Diagonal blocks	Off-diagonal blocks	Entries
$\mathbf{M}, \mathbf{M}^{\Gamma_{\mathrm{cut}}}$	✓	✓	✗	(5.25)
$\mathbf{K}$	✗	✓	✗	(5.26)
$\mathbf{A}$	✓	✓	✗	(5.27)
$\mathbf{A}^{\mathrm{off}}$	✓	✓	✓	(5.28)

The function pair $(\boldsymbol{v}_h^{n+1}, p_h^{n+1})$, which is obtained upon substituting the solution vectors $\mathbf{v} \in \mathbb{R}^{\omega^{\boldsymbol{v}}}$ and $\mathbf{p} \in \mathbb{R}^{\omega^p}$ into (5.22) and (5.23) respectively, is the mixed finite element solution of the NS part of the original problem. The system (5.24)–(5.31) is henceforth referred to as the *discrete Oseen problem*.

Ideal version of the preconditioner

The discrete Oseen problem is difficult to solve as it leads to a large non-symmetric indefinite system. One possible approach, that is suitable for dealing with this type of problems, is the application of the GMRES algorithm with right preconditioning. The preconditioned version of the problem (5.24) reads

$$\bar{\mathbf{A}}\bar{\mathbf{P}}^{-1}\bar{\mathbf{y}} = \bar{\mathbf{b}}, \qquad \bar{\mathbf{P}}\bar{\mathbf{x}} = \bar{\mathbf{y}}, \tag{5.32}$$

where $\bar{\mathbf{P}}$ represents a preconditioning operator. The optimal choice of $\bar{\mathbf{P}}$ in the current setting is given by the upper triangular approximation of the Schur complement factorization of $\bar{\mathbf{A}}$, namely

$$\bar{\mathbf{P}} = \begin{bmatrix} \mathbf{F} & \mathbf{B}^\top \\ \mathbf{0} & -\mathbf{S} \end{bmatrix}, \tag{5.33}$$

where $\mathbf{S} = \mathbf{B}\mathbf{F}^{-1}\mathbf{B}^\top$ denotes the *Schur complement operator*. The above choice yields

$$\bar{\mathbf{A}}\bar{\mathbf{P}}^{-1} = \begin{bmatrix} \mathbf{F} & \mathbf{B}^\top \\ \mathbf{B} & \mathbf{0} \end{bmatrix} \begin{bmatrix} \mathbf{F}^{-1} & \mathbf{F}^{-1}\mathbf{B}^\top\mathbf{S}^{-1} \\ \mathbf{0} & -\mathbf{S}^{-1} \end{bmatrix} = \begin{bmatrix} \mathbf{I} & \mathbf{0} \\ \mathbf{B}\mathbf{F}^{-1} & \mathbf{I} \end{bmatrix}. \tag{5.34}$$

We see that all eigenvalues of the preconditioned system matrix are equal to one and GMRES converges in at most two iterations, cf. Murphy et al. (2000).

At each step of the algorithm we need to compute the action of $\bar{\mathbf{P}}^{-1}$, that is, for given $\mathbf{w} \in \mathbb{R}^{\omega^{\boldsymbol{v}}}$ and $\mathbf{r} \in \mathbb{R}^{\omega^p}$ we need to evaluate

$$\begin{bmatrix} \mathbf{u} \\ \mathbf{q} \end{bmatrix} = \begin{bmatrix} \mathbf{F}^{-1} & \mathbf{F}^{-1}\mathbf{B}^\top\mathbf{S}^{-1} \\ \mathbf{0} & -\mathbf{S}^{-1} \end{bmatrix} \begin{bmatrix} \mathbf{w} \\ \mathbf{r} \end{bmatrix}. \tag{5.35}$$

This is a two stage process. First, $\mathbf{q} \in \mathbb{R}^{\omega^p}$ is obtained by solving $\mathbf{S}\mathbf{q} = -\mathbf{r}$. Second, $\mathbf{u} \in \mathbb{R}^{\omega^{\boldsymbol{v}}}$ is obtained as a solution of $\mathbf{F}\mathbf{u} = \mathbf{w} - \mathbf{B}^\top\mathbf{q}$. However, there is one important issue. The Schur complement $\mathbf{S}$ is non-local in the sense that the matrix $\mathbf{F}^{-1}$ appearing in its definition is dense. As a consequence, the first stage corresponding to the action of $\mathbf{S}^{-1}$ would be computationally costly, as well as the computation of the action of $\mathbf{F}^{-1}$ itself. Therefore, in practice we replace $\mathbf{S}$ and $\mathbf{F}$ in (5.33) with some suitable approximations $\mathbf{S}_*$ and $\mathbf{F}_*$.

Towards the choice of $\mathbf{S}_*$

We begin with the observation that the Schur complement $\mathbf{S}$ formally corresponds to the composition of the triplet of operators on the original (non-discretized) function spaces, namely

$$\mathcal{S} \equiv -\operatorname{div} \circ \mathcal{F}^{-1} \circ \nabla, \tag{5.36}$$

where $\operatorname{div} : \boldsymbol{\mathcal{V}}^{\boldsymbol{v}}_{\Gamma_{\mathrm{NS}}} \to \mathcal{V}^p$ is bounded, $\nabla = -\operatorname{div}^{\#} : (\mathcal{V}^p)^{\#} \to (\boldsymbol{\mathcal{V}}^{\boldsymbol{v}}_{\Gamma_{\mathrm{NS}}})^{\#}$ (recall that $\mathcal{V}^p = L^2(\Omega)$) and $\mathcal{F} : \boldsymbol{\mathcal{V}}^{\boldsymbol{v}}_{\Gamma_{\mathrm{NS}}} \to (\boldsymbol{\mathcal{V}}^{\boldsymbol{v}}_{\Gamma_{\mathrm{NS}}})^{\#}$ is given by the duality mapping

$$\begin{aligned}\langle \mathcal{F}\boldsymbol{v}, \boldsymbol{u}\rangle = \int_\Omega \frac{1}{2}\frac{\varrho_h^{n+1}+\varrho_h^n}{\Delta_t}\boldsymbol{v}\cdot\boldsymbol{u} + \int_{\Gamma_{\mathrm{cut}}} \frac{1}{2}\left((\varrho_h^{n+1}\boldsymbol{v}_h^n + \boldsymbol{J}_h^{n+1})\cdot\boldsymbol{n}\right)\boldsymbol{v}\cdot\boldsymbol{u} \\ + \int_\Omega \frac{1}{2}\boldsymbol{u}\cdot\left([\nabla\boldsymbol{v}](\varrho_h^{n+1}\boldsymbol{v}_h^n + \boldsymbol{J}_h^{n+1})\right) - \int_\Omega \frac{1}{2}\boldsymbol{v}\cdot\left([\nabla\boldsymbol{u}](\varrho_h^{n+1}\boldsymbol{v}_h^n + \boldsymbol{J}_h^{n+1})\right) \\ + \int_\Omega \nu_h^{n+1}\,\nabla\boldsymbol{v} : \nabla\boldsymbol{u} + \int_\Omega \nu_h^{n+1}(\nabla\boldsymbol{v})^\top : \nabla\boldsymbol{u}, \quad \forall \boldsymbol{u}\in\boldsymbol{\mathcal{V}}^{\boldsymbol{v}}_{\Gamma_{\mathrm{NS}}}, \quad (5.37)\end{aligned}$$

cf. (5.20a). To better understand the mutual correspondence between $\mathcal{S}$ and $\mathbf{S}$, we shall discuss discrete counterparts of the above operators and their matrix representations.

The discrete divergence operator $\operatorname{div}_h : \boldsymbol{\mathcal{V}}^{\boldsymbol{v}}_{h,\Gamma_{\mathrm{NS}}} \to \mathcal{V}^p_h$ is defined with the help of L^2-projection

$$\int_\Omega q_h \operatorname{div}_h \boldsymbol{u}_h = \int_\Omega q_h \operatorname{div}\boldsymbol{u}_h, \qquad \forall q_h \in \mathcal{V}^p_h. \tag{5.38}$$

For $\boldsymbol{v}_h$ given and $p_h \equiv \operatorname{div}_h \boldsymbol{v}_h$, let $\boldsymbol{v}_h = \sum_{\kappa=1}^{\omega^{\boldsymbol{v}}} \mathrm{v}_\kappa \boldsymbol{\varphi}^{\boldsymbol{v}}_\kappa$ and $p_h = \sum_{\kappa=1}^{\omega^p} \mathrm{p}_\kappa \varphi^p_\kappa$ be representations in terms of basis $\{\boldsymbol{\varphi}^{\boldsymbol{v}}_\kappa\}_{\kappa=1}^{\omega^{\boldsymbol{v}}}$ and $\{\varphi^p_\kappa\}_{\kappa=1}^{\omega^p}$ respectively. Further, let

$$\widehat{\mathrm{Q}}_{\iota\kappa} = \int_\Omega \boldsymbol{\varphi}^{\boldsymbol{v}}_\kappa \cdot \boldsymbol{\varphi}^{\boldsymbol{v}}_\iota, \qquad\qquad \widehat{\mathrm{Q}}_{p,\iota\kappa} = \int_\Omega \varphi^p_\kappa \varphi^p_\iota \tag{5.39}$$

denote entries of the velocity mass matrix $\widehat{\mathbf{Q}} = [\widehat{\mathrm{Q}}_{\iota\kappa}]_{\omega^{\boldsymbol{v}}\times\omega^{\boldsymbol{v}}}$ and the pressure mass matrix $\widehat{\mathbf{Q}}_p = [\widehat{\mathrm{Q}}_{p,\iota\kappa}]_{\omega^p\times\omega^p}$. (Both matrices are constant as the partition $\mathcal{T}_h$ is fixed.) According to (5.29), we immediately see that (5.38) leads to

$$\widehat{\mathbf{Q}}_p\mathbf{p} = -\mathbf{B}\mathbf{v}. \tag{5.40}$$

That is, the discrete negative divergence operator has the matrix representation $\widehat{\mathbf{Q}}_p^{-1}\mathbf{B}$. In an analogous fashion we reveal that $\widehat{\mathbf{Q}}^{-1}\mathbf{B}^\top$ and $\widehat{\mathbf{Q}}^{-1}\mathbf{F}$ are the matrix representations of the discrete counterparts of ∇ and $\mathcal{F}$ respectively. Altogether, we obtain

$$(\widehat{\mathbf{Q}}_p^{-1}\mathbf{B})(\widehat{\mathbf{Q}}^{-1}\mathbf{F})^{-1}(\widehat{\mathbf{Q}}^{-1}\mathbf{B}^\top) = \widehat{\mathbf{Q}}_p^{-1}\mathbf{B}\mathbf{F}^{-1}\mathbf{B}^\top = \widehat{\mathbf{Q}}_p^{-1}\mathbf{S} \tag{5.41}$$

as the matrix representation of $\mathcal{S}$, cf. (5.36).

Roughly speaking, the basic idea used in the construction of a practical approximation $\mathbf{S}_*$ is to formally swap the order of operators in (5.36) and simultaneously replace $\mathcal{F}$ by an appropriate operator $\mathcal{F}_p$ reduced to the pressure space, see Silvester et al. (2001) and Kay et al. (2002). On the discrete level it means to swap the order of the terms on the left hand side of (5.41) and simultaneously replace $\widehat{\mathbf{Q}}^{-1}\mathbf{F}$ by $\widehat{\mathbf{Q}}_p^{-1}\mathbf{F}_p$, that is, by a matrix representation of $\mathcal{F}_p$ that will be determined later. The two possibilities are

$$\widehat{\mathbf{Q}}_p^{-1}\mathbf{S} \approx \widehat{\mathbf{Q}}_p^{-1}\mathbf{B}\widehat{\mathbf{Q}}^{-1}\mathbf{B}^\top\mathbf{F}_p^{-1}\widehat{\mathbf{Q}}_p \quad \text{or} \quad \widehat{\mathbf{Q}}_p^{-1}\mathbf{S} \approx \mathbf{F}_p^{-1}\mathbf{B}\widehat{\mathbf{Q}}^{-1}\mathbf{B}^\top.$$

The matrix $\mathbf{B}\widehat{\mathbf{Q}}^{-1}\mathbf{B}^\top$, appearing as a factor in the swapped Schur complement, is singular for enclosed flow boundary conditions ($\Gamma_{\text{in}} = \Gamma_{\text{cut}} = \Gamma_{\text{out}} = \emptyset$ in our notation, see Section 4.2.2), but nonsingular otherwise. In general, this matrix will be dense. For a way to address this, some kind of *sparse* discrete Laplacian on the pressure space can be used instead of this matrix. For stable mixed finite element approximations, it is plausible to use

$$\widehat{\mathbf{A}}_p = [\widehat{\mathrm{A}}_{p,\iota\kappa}]_{\omega^p\times\omega^p}, \qquad \widehat{\mathrm{A}}_{p,\iota\kappa} = \int_\Omega \nabla\varphi^p_\kappa \cdot \nabla\varphi^p_\iota, \tag{5.42}$$

see (Elman et al., 2014, Sec. 3.5.1, Sec. 9.2.1). Note that the above matrix is singular, regardless of whether the flow is enclosed or not, as the associated null space contains the vector $\mathbf{1} \in \mathbb{R}^{\omega^p}$. In case of nonenclosed flow problems, it will be necessary to specify additional artificial boundary conditions for the operator in (5.42); see the discussion on the next page.

A more direct way to get a sparse discrete Laplacian is to replace $\widehat{\mathbf{Q}}$ by its diagonal $\widehat{\mathbf{D}}_{\mathrm{Q}} \overset{\text{def}}{=} \operatorname{diag}(\widehat{\mathbf{Q}})$, so that $\mathbf{B}\widehat{\mathbf{Q}}^{-1}\mathbf{B}^\top$ is replaced by the sparse matrix

$$\widehat{\mathbf{A}}_p = \mathbf{B}\widehat{\mathbf{D}}_{\mathrm{Q}}^{-1}\mathbf{B}^\top. \tag{5.43}$$

For nonenclosed flow problems the matrices $\mathbf{B}\widehat{\mathbf{Q}}^{-1}\mathbf{B}^\top$ and $\mathbf{B}\widehat{\mathbf{D}}_{\mathrm{Q}}^{-1}\mathbf{B}^\top$ are both nonsingular, as is the coefficient matrix $\bar{\mathbf{A}}$ in (5.24).

In any case, the above discussion brings us to the following pair of the approximate discrete Schur complement operator

$$\mathbf{S}_{*\ell} = \widehat{\mathbf{A}}_p\mathbf{F}_p^{-1}\widehat{\mathbf{Q}}_p \qquad \text{or} \qquad \mathbf{S}_{*r} = \widehat{\mathbf{Q}}_p\mathbf{F}_p^{-1}\widehat{\mathbf{A}}_p, \tag{5.44}$$

where $\widehat{\mathbf{A}}_p$ is given either by (5.42) or by (5.43). It remains to specify $\mathbf{F}_p$. Before doing so, let us emphasize that the action of the inverse of the approximated Schur complement corresponds to

$$\mathbf{S}_{*\ell}^{-1} = \widehat{\mathbf{Q}}_p^{-1}\mathbf{F}_p\widehat{\mathbf{A}}_p^{-1} \sim \mathcal{F}_p \circ (-\Delta)^{-1}, \tag{5.45}$$

$$\mathbf{S}_{*r}^{-1} = \widehat{\mathbf{A}}_p^{-1}\mathbf{F}_p\widehat{\mathbf{Q}}_p^{-1} \sim (-\Delta)^{-1} \circ \mathcal{F}_p. \tag{5.46}$$

When we trace back the origin of the operator $\mathcal{F}$ defined by (5.37), we reveal that $\mathcal{F}\boldsymbol{v}$ roughly corresponds to $\varrho\partial_t\boldsymbol{v} + \varrho(\boldsymbol{w}\cdot\nabla)\boldsymbol{v} - \operatorname{div}(2\nu\mathbb{D})$, where $\boldsymbol{w}$ denotes a fixed wind. Motivated by this, we choose $\mathbf{F}_p$ which roughly corresponds to $\varrho\partial_t p + \varrho\boldsymbol{w}\cdot\nabla p - \operatorname{div}(\nu\nabla p)$, namely

$$\mathbf{F}_p = \frac{1}{\Delta_t}\mathbf{M}_p + \mathbf{K}_p + \mathbf{A}_p. \tag{5.47}$$

The matrices on the right hand side are given by the relations (5.25)–(5.27) with the velocity basis functions replaced by the pressure basis functions, so that $\mathbf{A}_p = [\mathrm{A}_{p,\iota\kappa}]_{\omega^p\times\omega^p}$ is given by[11] $\mathrm{A}_{p,\iota\kappa} = \int_\Omega \nu_h^{n+1}\nabla\varphi^p_\kappa\cdot\nabla\varphi^p_\iota$ and so forth.

[11]Note the difference between $\mathbf{A}_p$ and $\widehat{\mathbf{A}}_p$ given by (5.42).

On the choice of artificial boundary conditions

Once again, we see that additional artificial boundary conditions for the Laplace solve $(-\Delta)^{-1}$ might be needed to perform the action of the preconditioner given by (5.45) or (5.46). Let us consider a nonenclosed flow problem with naturally defined inflow and outflow parts of the boundary, see Section 4.2.2. If the discrete Laplacian is represented by $\widehat{\mathbf{A}}_p$ from (5.42), then for given $\mathbf{r} \in \mathbb{R}^{\omega^p}$ we need to supplement the problem corresponding to $\widehat{\mathbf{A}}_p\mathbf{q} = \mathbf{r}$ with appropriate boundary conditions that must be satisfied by the function associated with the coefficient vector $\mathbf{q} \in \mathbb{R}^{\omega^p}$. This issue has been discussed many times in the literature mostly in the context of steady NS equations; see for example Howle et al. (2006), Elman and Tuminaro (2009), Olshanskii and Vassilevski (2007) or (Elman et al., 2014, Sec. 9.3.2).

At this point, we fix our choice of the approximate discrete Schur complement,

$$\mathbf{S}_* \equiv \mathbf{S}_{*\ell}, \tag{5.48}$$

for which the Laplace solve in (5.45) will be supplemented by the homogeneous Dirichlet condition on Γ_{in} and the homogeneous Neumann condition otherwise.

Remark 5.6. A different choice of boundary conditions is required for the variant (5.46), see (Elman et al., 2014, Sec. 9.2.2) and Blechta (2018).

Remark 5.7. In case of an enclosed flow problem, where $\Gamma_{\mathrm{in}} = \emptyset$, use of either version of $\mathbf{S}_*^{-1}$ requires the application of the inverse of singular, rank 1 deficient matrices (5.42) and/or (5.43). As discussed in (Elman et al., 2014, Sec. 9.3.5), this issue is handled by iterative solvers and a straightforward implementation of the above preconditioning approach is applicable also in that case.

Scaling of PCD operators

First of all, let us assume that the density and the viscosity are constants, that is, $\varrho_h^n = \varrho_h^{n+1} = \varrho_*$ and $\nu_h^{n+1} = \nu_*$. Then we have the simple relations $\mathbf{M}_p = \varrho_*\widehat{\mathbf{Q}}_p$ for the pressure mass matrix, $\mathbf{A}_p = \nu_*\widehat{\mathbf{A}}_p$ for the discrete Laplacian given by (5.42), and finally

$$\varrho_*^{-1}\widehat{\mathbf{A}}_p = \mathbf{B}\mathbf{D}_{\mathrm{M}}^{-1}\mathbf{B}^\top, \quad \mathbf{D}_{\mathrm{M}} \stackrel{\mathrm{def}}{=} \mathrm{diag}(\mathbf{M}), \tag{5.49}$$

for the discrete Laplacian given by (5.43). Using $\mathbf{F}_p$ given by (5.47) together with the above relations for $\mathbf{M}_p$ and $\mathbf{A}_p$ in (5.45), one obtains

$$\mathbf{S}_*^{-1} = \widehat{\mathbf{Q}}_p^{-1}\left(\frac{1}{\Delta_t}\varrho_*\widehat{\mathbf{Q}}_p + \mathbf{K}_p + \nu_*\widehat{\mathbf{A}}_p\right)\widehat{\mathbf{A}}_p^{-1}. \tag{5.50}$$

For the purpose of practical implementation, we rewrite the above formula in the expanded form

$$\mathbf{S}_*^{-1} = \frac{1}{\Delta_t}\varrho_*\widehat{\mathbf{A}}_p^{-1} + \nu_*\widehat{\mathbf{Q}}_p^{-1}\left(\nu_*^{-1}\mathbf{K}_p\widehat{\mathbf{A}}_p^{-1} + \mathbf{I}\right), \tag{5.51}$$

where $\mathbf{I}$ denotes the identity matrix. It immediately follows that (5.49) can be substituted into the first term on the right hand side of (5.51).

Based on the previous observations, we suggest to implement the action of the approximated Schur complement with variable coefficients in the form

$$\mathbf{S}_*^{-1} = \frac{1}{\Delta_t}\widetilde{\mathbf{A}}_p^{-1} + \widetilde{\mathbf{Q}}_p^{-1}\left(\widetilde{\mathbf{K}}_p\widehat{\mathbf{A}}_p^{-1} + \mathbf{I}\right), \tag{5.52}$$

where

$$\widetilde{\mathbf{Q}}_p = [\widetilde{\mathrm{Q}}_{p,\iota\kappa}]_{\omega^p\times\omega^p} \qquad \widetilde{\mathrm{Q}}_{p,\iota\kappa} = \int_\Omega \left(\nu_h^{n+1}\right)^{-1}\varphi_\kappa^p\varphi_\iota^p, \tag{5.53}$$

$$\widetilde{\mathbf{K}}_p = [\widetilde{\mathrm{K}}_{p,\iota\kappa}]_{\omega^p\times\omega^p}, \qquad \widetilde{\mathrm{K}}_{p,\iota\kappa} = \int_\Omega \left(\nu_h^{n+1}\right)^{-1}\varphi_\iota^p(\varrho_h^{n+1}\boldsymbol{v}_h^n + \boldsymbol{J}_h^{n+1})\cdot\nabla\varphi_\kappa^p, \tag{5.54}$$

and

$$\widetilde{\mathbf{A}}_p = \mathbf{B}\mathbf{D}_{\mathrm{M}}^{-1}\mathbf{B}^\top. \tag{5.55}$$

Remark 5.8. The choice of $\widetilde{\mathbf{A}}_p$ can be justified in the case of $\Delta_t \to 0_+$, for which $\mathbf{S}^{-1} = (\mathbf{B}\mathbf{F}^{-1}\mathbf{B}^\top)^{-1} \approx \frac{1}{\Delta_t}(\mathbf{B}\mathbf{M}^{-1}\mathbf{B}^\top)^{-1}$ and simultaneously $\mathbf{S}_*^{-1} \approx \frac{1}{\Delta_t}\widetilde{\mathbf{A}}_p^{-1}$. Thus, choosing $\widetilde{\mathbf{A}}_p$ as in (5.55) means that the Schur complement is consistently approximated in the small time-step limit.

Remark 5.9. It is worth noting that the inverse of the approximate Schur complement given by (5.52) reduces to $\widetilde{\mathbf{Q}}_p^{-1}$ in the absence of convection and reaction terms. The pressure mass matrix scaled by the reciprocal of viscosity is known to be a good approximation to the Schur complement in the context of stationary Stokes problems.

Remark 5.10. Practical evidence shows that the presence of the identity matrix in (5.51) and (5.52) can be critical for the performance of the preconditioner, especially for stationary problems. In fact, one should avoid implementing the action of $\mathbf{S}_*^{-1}$ in the form (5.50) which is thought to collect the terms inside parentheses into a single matrix $\mathbf{F}_p$. Let us briefly explain why. First of all, recall that the action of $\widehat{\mathbf{A}}_p^{-1}$ is implemented by solving the linear system $\widehat{\mathbf{A}}_p\mathbf{q} = \mathbf{r}$ for a given $\mathbf{r} \in \mathbb{R}^{\omega^p}$, with possible application of Dirichlet boundary conditions on part of the boundary. Note that $\mathbf{F}_p\widehat{\mathbf{A}}_p^{-1}$ includes the multiplication $\widehat{\mathbf{A}}_p\widehat{\mathbf{A}}_p^{-1}$. The problem is that the identity

$$\widehat{\mathbf{A}}_p\widehat{\mathbf{A}}_p^{-1} = \mathbf{I}$$

might be lost due to inexact solve of $\widehat{\mathbf{A}}_p\mathbf{q} = \mathbf{r}$ and/or, more importantly, due to application of the associated artificial boundary conditions. This problem was formerly encountered in the literature, even though it has not been put into the same context. For instance, Olshanskii and Vassilevski (2007) imposed the same artificial boundary conditions using a fictitious external layer of cells/nodes adjacent to the inlet part of the boundary. Their motivation was based on the seemingly different argument, see (Olshanskii and Vassilevski, 2007, p. 2700): *"Dirichlet boundary conditions may not be imposed on the boundary nodes, since these nodes contribute to the set of pressure degrees of freedom."*

Towards the choice of $\mathbf{F}_*$

Recall that in the practical use of the preconditioned GMRES algorithm we aim to approximate the action of $\mathbf{F}^{-1}$. For moderate velocities, the system of algebraic equations corresponding to the velocity convection–diffusion(–reaction) operator can be treated with algebraic multigrid (AMG) methods. Typically, we use a fixed number of AMG iterations to generate only approximate (inexact) solution of the corresponding subsidiary problem. It means that the computed action of $\mathbf{F}^{-1}$ is inexact and corresponds to the action of $\mathbf{F}_*^{-1}$ for some theoretical $\mathbf{F}_*$.

From this point of view, it is equally possible to apply the limited number of AMG iterations not directly to $\mathbf{F}$, but to its suitable approximation/modification for which we will also use the notation $\mathbf{F}_*$. In particular, we put

$$\mathbf{F}_* = \frac{1}{\Delta_t}\mathbf{M} + \mathbf{K} + \mathbf{A}, \tag{5.56}$$

cf. (5.47). Inverting $\mathbf{F}_*$ by AMG has shown to be more practical than inverting $\mathbf{F}$ with the non-standard terms arising from the multi-component background of the model and its energy-stable discretization[12].

Concluding remarks

We have seen that there are plenty of possibilities concerning the final subtle design of PCD preconditioners for NS equations with variable coefficients. Remember that the variant suggested above was derived in a heuristic manner and further analysis is necessary to provide some of the ideas with better theoretical support. For instance, the scaling arguments used to reformulate the expression (5.45) into its final form (5.52) need to be clarified. Better performance of the scaled version is currently justified only by the experimental evidence. Also note that the current version of the Schur complement approximation requires ceaseless updates of the matrices (5.53)–(5.55) due to the presence of time-dependent coefficients. A proper numerical analysis could give us the clue if there is a possibility to make the preconditioners more efficient by avoiding unnecessary re-assembling.

We have experimentally tested several possible modifications of PCD preconditioners following the heuristic ideas presented here. In the following section, we summarize the so-called

"expanded pressure convection–diffusion–reaction (PCDR) preconditioner"

which is the above-described variant suitable for the application in Algorithm 1.

5.4.2 Summary: Expanded PCDR preconditioner

The discrete Oseen problem

$$\begin{bmatrix} \mathbf{F} & \mathbf{B}^\top \\ \mathbf{B} & \mathbf{0} \end{bmatrix} \begin{bmatrix} \mathbf{v} \\ \mathbf{p} \end{bmatrix} = \begin{bmatrix} \mathbf{f} \\ \mathbf{g} \end{bmatrix}, \tag{5.57}$$

[12] We have observed worsened mesh-dependent behaviour of the preconditioner with $\mathbf{F}$ in the example from Section 6.3.2.

where $\mathbf{F} = \frac{1}{\Delta_t}\mathbf{M} + \frac{1}{2}\mathbf{M}^{\Gamma_{\text{cut}}} + \frac{1}{2}(\mathbf{K} - \mathbf{K}^\top) + \mathbf{A} + \mathbf{A}^{\text{off}}$, $\mathbf{B}, \mathbf{f}$ and $\mathbf{g}$ were defined in (5.25)–(5.31), is solved using the right preconditioned GMRES algorithm with the upper triangular block preconditioner $\bar{\mathbf{P}}$ of the form

$$\bar{\mathbf{P}} = \begin{bmatrix} \mathbf{F}_* & \mathbf{B}^\top \\ \mathbf{0} & -\mathbf{S}_* \end{bmatrix}. \tag{5.58}$$

The action of $\mathbf{F}_*^{-1}$ is determined by applying a single V-cycle of AMG[13]. Our preferred choice of $\mathbf{S}_*$ corresponds to

$$\mathbf{S}_*^{-1} = \frac{1}{\Delta_t}\left(\mathbf{B}\mathbf{D}_{\text{M}}^{-1}\mathbf{B}^\top\right)^{-1} + \widetilde{\mathbf{Q}}_p^{-1}\left(\widetilde{\mathbf{K}}_p\widehat{\mathbf{A}}_p^{-1} + \mathbf{I}\right), \tag{5.59}$$

where $\mathbf{D}_{\text{M}} = \text{diag}(\mathbf{M})$, the discrete Laplacian $\widehat{\mathbf{A}}_p$ is assembled once using (5.42) and the remaining scaled matrices $\widetilde{\mathbf{Q}}_p$ and $\widetilde{\mathbf{K}}_p$, requiring an update per time step, are given by (5.53) and (5.54) respectively. The subsidiary solves involving $\mathbf{B}\mathbf{D}_{\text{M}}^{-1}\mathbf{B}^\top$ and $\widehat{\mathbf{A}}_p$ in (5.59) are replaced by a fixed number of AMG iterations[14], similarly as in the case of $\mathbf{F}_*^{-1}$. We impose the homogeneous Dirichlet boundary condition on Γ_{in} in each solve with $\widehat{\mathbf{A}}_p$ for nonenclosed flow problems, and we apply the homogeneous Neumann condition otherwise. Finally, $\widetilde{\mathbf{Q}}_p$ is inverted by five Chebyshev iterations, cf. Wathen and Rees (2008).

Summary 11: Key features of expanded PCDR preconditioner

The following list highlights the key features of the preconditioner (5.58):

- $\mathbf{F}_*$ is based on (5.56) to mimic the standard structure of the velocity convection–diffusion–reaction block.
- $\mathbf{S}_*^{-1}$ is implemented in the expanded form (5.59) with separately treated contributions from convection, diffusion and reaction terms of the leading PCDR operator $\mathbf{F}_p$ given by (5.47).
- The reaction contribution is designed to ensure the consistency between $\mathbf{S}_*$ and the full Schur complement in the small time-step limit, see Remark 5.8.
- Operators in the combined convection-diffusion contribution are scaled in a way ensuring the proper reduction of $\mathbf{S}_*$ in the Stokes limit, see Remark 5.9.
- The *a priori* enforcement of the identity $\widehat{\mathbf{A}}_p\widehat{\mathbf{A}}_p^{-1} = \mathbf{I}$ in the diffusion contribution prevents from losing it due to inconsistent imposition of Dirichlet boundary conditions associated with $\widehat{\mathbf{A}}_p^{-1}$, see Remark 5.10.
- Numerical results in Section 6.3.2 suggest that the preconditioner is not very sensitive to material parameters and indicates only a mild deterioration of convergence rates with respect to mesh refinement (at least for problems with moderate velocities), see Figure 6.17.

[13] We use hypre's BoomerAMG algebraic multigrid implementation, see Falgout et al. (2006).

[14] We again use a single V-cycle to determine $\left(\mathbf{B}\mathbf{D}_{\text{M}}^{-1}\mathbf{B}^\top\right)_*^{-1}$ and $\widehat{\mathbf{A}}_{p*}^{-1}$ respectively.

Chapter 6

Numerical Experiments

In this chapter we present a series of numerical experiments with the FI-CHNS model formulated in Chapter 4. We begin with a simple shear flow modified for two incompressible fluids of non-matching viscosities. The problem is described in Section 6.1 where we discuss the influence of interpolation of material parameters across the interface. In Section 6.2, we first verify the implementation of Algorithm 1 (Section 5.3) and Algorithm 2 (Appendix C) respectively by examining their convergence properties. Both algorithms are subsequently compared head-to-head with the aid of the classical rising bubble benchmark in Section 6.3. The same example is used to get an idea about the performance/robustness of the preconditioning strategy developed in Section 5.4.2. In the last Section 6.4, we clarify the presence of artificial numerical velocities which typically occur in numerical simulations involving low viscosity materials with density contrasts. We demonstrate this on a simple "no-flow" problem with a single interface and a stationary solution that is expected to balance hydrostatic conditions. We shall address particular methods with the capability to suppress numerical artifacts of this type, although further exploration is required and the methods have not been fully integrated into our simulation software yet.

Finite element triangular meshes in our numerical simulations were generated using either the built-in mesh generator of FEniCS, or using the finite element mesh generator Gmsh, see Geuzaine and Remacle (2009). Matplotlib and ParaView, see Hunter (2007) and Ahrens et al. (2005) respectively, were used as the tools for visualization of numerical results.

Before we start with the presentation of the results, let us make a short note on the choice of the parameter ε in our numerical simulations, cf. Table 4.2.

On the choice of interface thickness

The numerical parameter $\varepsilon > 0$, introduced in (3.10a) as being proportional to the thickness of the interfacial regions, will be chosen based on the following heuristics. Using the double-well potential (3.9), the interfacial equilibrium profile in one space dimension is given by

$$\phi_{\mathrm{eq}}(x) = \frac{1}{2}\left(1 + \tanh\left(\frac{2x}{\varepsilon}\right)\right), \tag{6.1}$$

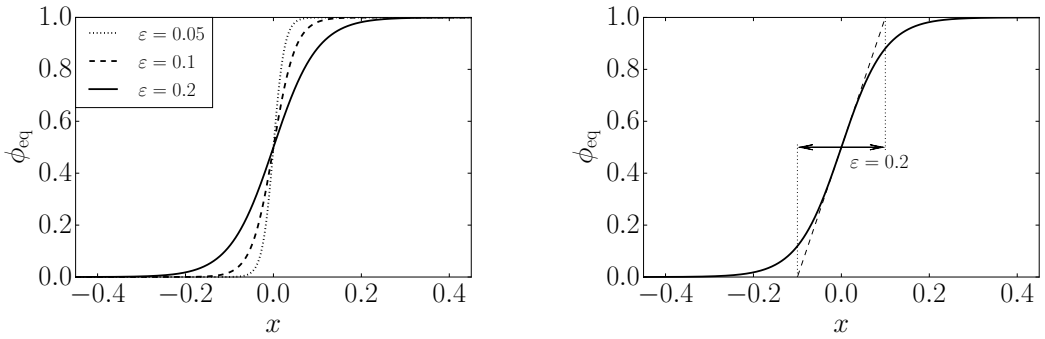

(a) Profiles for varying parameter ε.

(b) Illustration of the role of ε.

Figure 6.1: One-dimensional equilibrium interface profile (6.1) for the polynomial double-well potential (3.9) and the role of the length scale ε.

see (Boyer and Lapuerta, 2006, Sec. 1). This profile is shown in Figure 6.1a for different values of ε. As illustrated by Figure 6.1b, we see that ε does not precisely match the real interface width. Therefore, let us describe the interface thickness as the length of the interval $[-x_w, x_w]$ with $\phi_{\mathrm{eq}}(x_w) = 0.975$. Then, we can express the equilibrium thickness via ε by

$$0.975 = \frac{1}{2}\left(1 + \tanh\left(\frac{2x_w}{\varepsilon}\right)\right),$$

which is equivalent to $x_w = 0.5\,\mathrm{arctanh}(0.95)\varepsilon$. Hence, the equilibrium thickness corresponds to $\mathrm{arctanh}(0.95)\varepsilon$. Following Bosch (2016), we want to ensure that at least nine mesh points lie on the interface. This requirement leads to an indicative upper bound for the mesh element size, namely

$$h \leq \frac{\mathrm{arctanh}(0.95)\varepsilon}{8} k \approx 0.229\,\varepsilon k, \tag{6.2}$$

where k was introduced in (5.10).

6.1 Simple shear flow

According to our previous discussion in Section 3.5, let us recall that the formula (2.10a) for the density is physically motivated, while the choice of the analogous formula (3.103) for the viscosity is rather artificial. A logical suggestion is to obey the former in numerical simulations and experiment with the latter to see whether it influences the computed results. To highlight the possible effects, we will first reduce our complicated model to a simpler setting.

Let us consider the following thought experiment with two incompressible fluids of equal densities ($\hat{\varrho}_\star = \hat{\varrho}_1 = \hat{\varrho}_2$) and different viscosities ($\hat{\nu}_1 \neq \hat{\nu}_2$). We assume that the fluids can be stratified to form two horizontal layers, separated

by a flat and sharp interface, between two parallel plates in a unit square domain[1], see Figure 6.2. The bottom plate is fixed, while the top plate is loaded by a constant shear stress $\boldsymbol{\tau} = [\tau, 0]^\top$. (Recall that all quantities are assumed to be dimensionless, see Section 4.2.4.)

We further assume that each of the two fluids sticks to the corresponding plate, and also that the velocity and the shear stress are continuous at the interface. Supposing that the pressure is uniform in the plane perpendicular to $\boldsymbol{e}_{x_2}$, the velocity field $\boldsymbol{v}(\boldsymbol{x}, t) = [v_1(x_2), 0]^\top$, given by

$$v_1(x_2) = \begin{cases} \frac{\tau}{\hat{\nu}_1} x_2, & 0 \le x_2 < \frac{1}{2}, \\ \frac{\tau}{\hat{\nu}_2} x_2 + \frac{\tau}{2}\left(\frac{1}{\hat{\nu}_1} - \frac{1}{\hat{\nu}_2}\right), & \frac{1}{2} \le x_2 \le 1, \end{cases}$$

describes a fully developed (stationary) simple shear flow induced between the two plates. More precisely, the above velocity field in combination with $p(\boldsymbol{x}, t) = \hat{\varrho}_\star g_\mathrm{a}(1 - x_2)$ solve the stationary Stokes problem

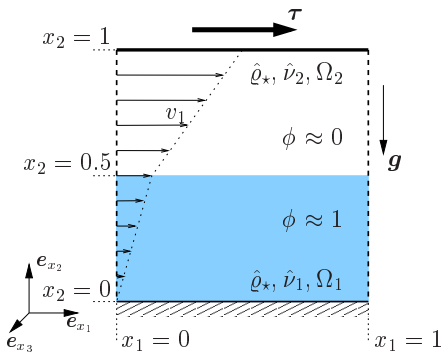

Figure 6.2: Simple shear flow of two stratified fluids between a fixed plate and a moving plate loaded by a constant force.

$$\operatorname{div} \boldsymbol{v} = 0, \qquad (\text{in } \Omega_1 \cup \Omega_2) \tag{6.3a}$$

$$-\operatorname{div}(2\nu\mathbb{D}) + \nabla p = \hat{\varrho}_\star \boldsymbol{g}, \qquad (\text{in } \Omega_1 \cup \Omega_2) \tag{6.3b}$$

supplemented by the following list of boundary conditions,

$$v_2|_{x_1=0} = v_2|_{x_1=1} = 0, \tag{6.3c}$$

$$v_1|_{x_2=0} = v_2|_{x_2=0} = 0, \tag{6.3d}$$

$$(2\nu D_{12})|_{x_2=1} = \tau, \tag{6.3e}$$

$$p|_{x_1=0} = p|_{x_1=1} = \hat{\varrho}_\star g_\mathrm{a}(1 - x_2), \tag{6.3f}$$

and the two conditions ensuring continuity of the velocity and the shear stress at the interface. The viscosity $\nu(\boldsymbol{x}, t) = \nu(x_2)$ in the above expressions should be understood as a piecewise constant function satisfying

$$\nu(x_2) = \begin{cases} \hat{\nu}_1, & 0 < x_2 < \frac{1}{2}, \\ \hat{\nu}_2, & \frac{1}{2} < x_2 < 1. \end{cases} \tag{6.4}$$

As a next step we reformulate the above problem using the diffuse interface approach explained in preceding chapters. We assume that the interface separating the fluids is captured by a fixed volume fraction

$$\phi(\boldsymbol{x}, t) = \frac{1}{2}\left(1 - \tanh\left(\frac{2x_2 - 1}{\varepsilon}\right)\right), \tag{6.5}$$

[1]The remaining spatial dimension is suppressed simply by assuming that the domain occupied by the two fluids is infinite in the direction of $\boldsymbol{e}_{x_3}$.

which mimics the equilibrium profile (6.1) and ensures that $\chi = \frac{b}{2\varepsilon} f'(\phi) - \frac{a\varepsilon}{2}\Delta\phi$, with f given by (3.9), identically vanishes in the whole domain. Let ν be given by an arbitrary expression from Table 6.1. Boundary value problem (6.3) can now be identified as a simplified version of a general problem associated with governing equations (4.30). As such, it will be solved numerically using the discretization techniques described in Section 5.2.

Parameter values used in our numerical experiments are listed in Table 6.2. The computational mesh is fixed with (6.2) fulfilled in the direction perpendicular to the interface. Let us emphasize that our choice of the applied shear stress is such that the top plate moves with a unit (reference) velocity. We shall briefly discuss the interpolation effects for different viscosity contrasts, supposing that $\hat{\nu}_1 > \hat{\nu}_2$. (Similar effects would be observed also in the opposite case.)

Table 6.1: Examples of interpolated viscosity for binary systems.

Type of interpolation	Expression
linear	$\nu = \hat{\nu}_1\phi + \hat{\nu}_2(1-\phi)$
harmonic	$\nu = \left(\hat{\nu}_1^{-1}\phi + \hat{\nu}_2^{-1}(1-\phi)\right)^{-1}$
exponential	$\nu = \hat{\nu}_1^{\phi}\hat{\nu}_2^{(1-\phi)}$
discontinuous	$\nu = \begin{cases} \hat{\nu}_1, & \phi > 0.975 \\ \frac{1}{2}\left(\hat{\nu}_1 + \hat{\nu}_2\right), & 0.025 \le \phi \le 0.975 \\ \hat{\nu}_2, & \phi < 0.025 \end{cases}$

Table 6.2: Parameter values for a simple shear flow with two stratified fluids.

Parameter	Value	Parameter	Value	Parameter	Value
$\hat{\varrho}_\star$	1.0	$\hat{\nu}_1$	1.0	$\hat{\nu}_2$	varied
g_a	1.0	ε	0.05	τ	$2\hat{\nu}_1\hat{\nu}_2/(\hat{\nu}_1+\hat{\nu}_2)$

In Figure 6.3, we observe that the exact (sharp interface) solution of (6.3) is well approximated using the diffuse interface approach for small viscosity contrasts (we put $\hat{\nu}_2 = 0.5\hat{\nu}_1$). The influence of different types of interpolation for similar viscosity values seems to be almost negligible. However, for larger viscosity contrasts the situation is different. For illustration see Figure 6.4, where we put $\hat{\nu}_2 = 10^{-3}\hat{\nu}_1$.

From our tested variants, only the harmonic interpolation yields the expected result, while the other interpolations end up with an undervalued velocity in the upper fluid. It is related to the fact that the position of the interface—should it be determined solely from the interpolated viscosity—seems to be different for different types of interpolation, cf. Figure 6.4a. The velocity error grows systematically as the order of viscosity ratio increases.

We can postpone the onset of these effects by considering a smaller value of ε which results in less significant differences among individual interpolants and

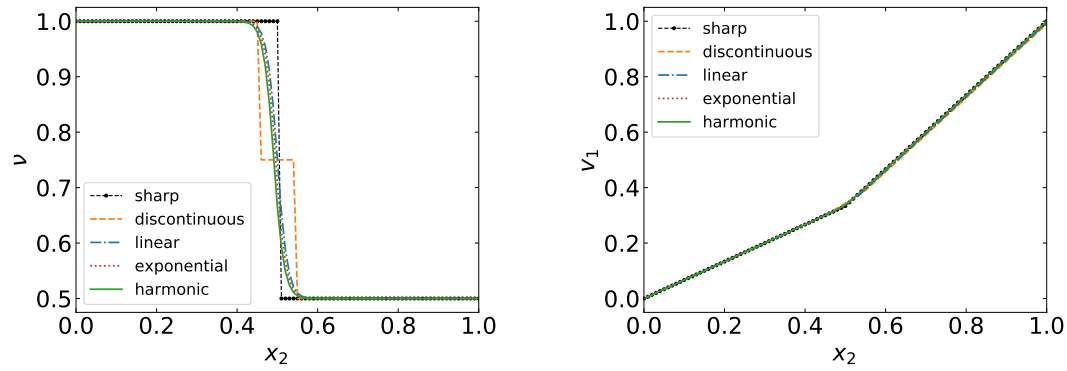

(a) Viscosity profiles from Table 6.1. (b) Computed velocity profiles.

Figure 6.3: Simple shear flow with $\varepsilon = 0.05$ and $\hat{\nu}_2 = 0.5\hat{\nu}_1$.

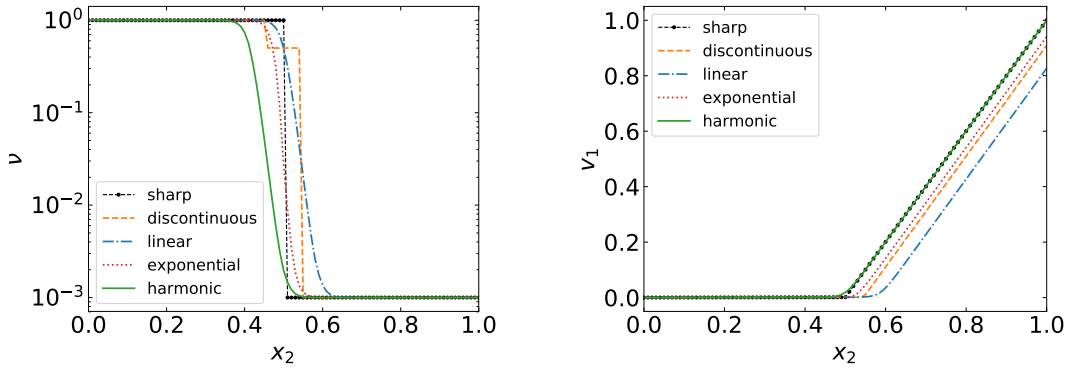

(a) Viscosity profiles from Table 6.1. (b) Computed velocity profiles.

Figure 6.4: Simple shear flow with $\varepsilon = 0.05$ and $\hat{\nu}_2 = 10^{-3}\hat{\nu}_1$.

brings us closer to the situation depicted in Figure 6.3a. Nevertheless, keep in mind that realistic values of ε, which would prevent to observe such effects at all, remain unachievable from the point of view of affordable computational costs.

On this rather toy example we have demonstrated that interpolation of material parameters across the interface can potentially influence numerical simulations based on diffuse interface models. Another proof of evidence, supporting this observation, will be given in Section 6.3.2.

6.2 Convergence tests

The goal of this section is to verify our implementation of the methods described in Chapter 5 and Appendix C, and illustrate their convergence rates. To achieve this we will use the well-known method of manufactured solutions, see Salari and Knupp (2000), which in our case involves construction of contrived terms appearing in governing equations (4.30a) and (4.30d).

We use the same test case as Dong (2015, 2017) with a four-component fluid mixture in the flow domain $\Omega = \{(x_1, x_2); 0 \leq x_1 \leq 2, -1 \leq x_2 \leq 1\}$. We take

the following *ansatz*,

$$v_1 = \hat{A}_0 \sin(\hat{a}_0 x_1) \cos(\hat{b}_0 x_2) \sin(\hat{\omega}_0 t), \tag{6.6a}$$

$$v_2 = -\frac{\hat{A}_0 \hat{a}_0}{\hat{b}_0} \cos(\hat{a}_0 x_1) \sin(\hat{b}_0 x_2) \sin(\hat{\omega}_0 t), \tag{6.6b}$$

$$p = \hat{A}_0 \sin(\hat{a}_0 x_1) \sin(\hat{b}_0 x_2) \cos(\hat{\omega}_0 t), \tag{6.6c}$$

$$\phi_1 = \frac{1}{6}\left[1 + \hat{A}_1 \cos(\hat{a}_1 x_1) \cos(\hat{b}_1 x_2) \sin(\hat{\omega}_1 t)\right], \tag{6.6d}$$

$$\phi_2 = \frac{1}{6}\left[1 + \hat{A}_2 \cos(\hat{a}_2 x_1) \cos(\hat{b}_2 x_2) \sin(\hat{\omega}_2 t)\right], \tag{6.6e}$$

$$\phi_3 = \frac{1}{6}\left[1 + \hat{A}_3 \cos(\hat{a}_3 x_1) \cos(\hat{b}_3 x_2) \sin(\hat{\omega}_3 t)\right], \tag{6.6f}$$

where v_1 and v_2 denote the components of the velocity vector $\boldsymbol{v}$ and $\hat{A}_i, \hat{a}_i, \hat{b}_i, \hat{\omega}_i$ for $i = 0, \ldots, 3$ are constant parameters specified in Table 6.3. (Recall that the remaining volume fraction is given by $\phi_4 = 1 - \sum_{i=1}^{3} \phi_i$.)

Let us explore some properties of the above *ansatz*. We immediately see that $\operatorname{div} \boldsymbol{v} = 0$. We further assume that $\partial\Omega = \Gamma_{\mathrm{w}}$. The boundary velocity $\boldsymbol{v}_{\mathrm{w}}$ in (4.32a) is chosen according to (6.6a) and (6.6b). It is straightforward to verify validity of boundary conditions in (4.32b) and (4.32c)[2]. We use additional Dirichlet boundary condition to fix the pressure in the lower left corner whenever we wish to solve the problem with the aid of direct solvers based on LU factorization. Moreover, the pressure is adjusted by subtracting the mean value within a postprocessing step, hereafter called "pressure calibration". The analytic expressions from (6.6) are further used to contrive the source terms that must be taken into consideration in (4.30a) and (4.30d). The derived term in the latter case is used in place of $\boldsymbol{g}$. Its precise form is based on (BLM1) or (BLM3) from Table 4.1 depending on the chosen algorithm[3]. The initial conditions for the velocity and volume fractions are obtained from (6.6) by setting $t = 0$. The velocity and pressure fields at $t = 0.1$ are visualized in Figure 6.5a.

Table 6.3: Parameter values for convergence tests.

Parameter	Value	Parameter	Value	Parameter	Value
$\hat{\omega}_0, \hat{\omega}_1$	1.0	$\hat{\omega}_2$	1.2	$\hat{\omega}_3$	0.8
$\hat{A}_0$	2.0	$\hat{A}_1, \hat{A}_2, \hat{A}_3$	1.0	$\hat{a}_0, \hat{a}_1, \hat{a}_2, \hat{a}_3$	π
$\hat{M}_0$	1.0E−05	Θ_2	1.0	$\hat{b}_0, \hat{b}_1, \hat{b}_2, \hat{b}_3$	π
$\hat{\varrho}_1$	1.0	ν_1	0.01	σ_{12}	6.236E−03
$\hat{\varrho}_2$	3.0	ν_2	0.02	σ_{13}	7.265E−03
$\hat{\varrho}_3$	2.0	ν_3	0.03	σ_{14}	3.727E−03
$\hat{\varrho}_4$	4.0	ν_4	0.04	σ_{23}	8.165E−03
ε	$0.2 \cdot \sqrt{2}$	h	varied	σ_{24}	5.270E−03
t_{end}	0.1 or 1.0	Δ_t	varied	σ_{34}	6.455E−03

[2]It can be seen from the structure of ϕ_i given by (6.6d)–(6.6f), from (4.30b) and (4.21).
[3]Note that (4.29), used to derive (BLM3) from (4.30d), is not satisfied by (6.6).

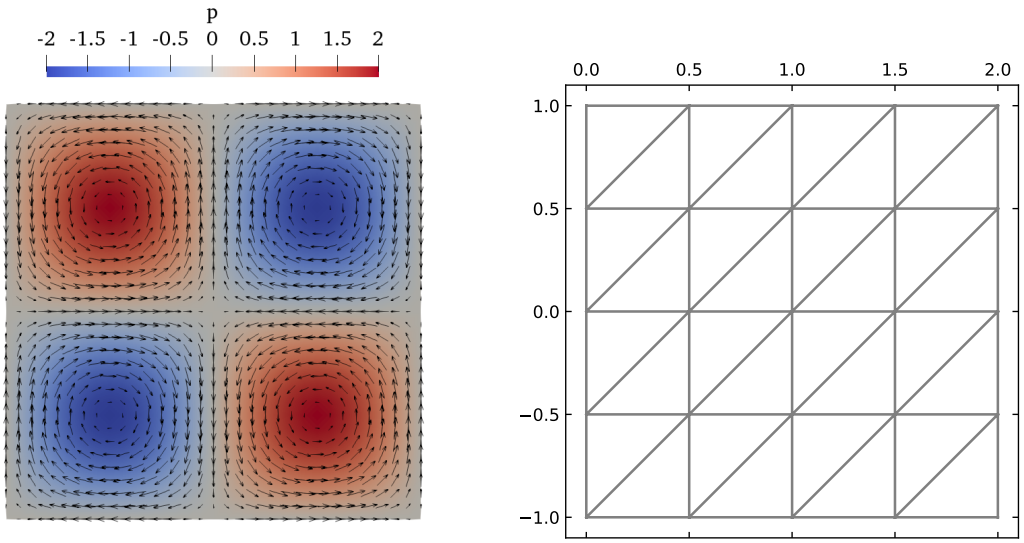

(a) Velocity vector field (6.6a)–(6.6b) and pressure field (6.6c) visualized at $t = 0.1$.

(b) The coarsest computational mesh used in convergence tests ($h = 2^{-1} \cdot \sqrt{2}$).

Figure 6.5: Geometry $\Omega = \{(x_1, x_2); 0 \leq x_1 \leq 2, -1 \leq x_2 \leq 1\}$ used in convergence tests and visualization of the analytic solution.

To simulate the problem we partition the domain Ω using the triangular mesh shown in Figure 6.5b. We employ Algorithms 1 and 2 respectively to solve the system of equations (4.30) with the modifications and boundary conditions described in the previous paragraph. The algorithms are stopped at $t = t_{\text{end}}$ where we make comparisons of the numerical solution with the exact solution from (6.6) by computing the L^2–norm of their difference. Following Dong (2015, 2017), we perform two groups of tests.

The first group is designed to illustrate spatial convergence of the developed numerical schemes. To this aim, we fix the time step size at $\Delta_t = 10^{-3}$ and we systematically decrease h by performing global refinements of the mesh[4]. With the fixed value of ε listed in Table 6.3, we start at $h = 2^{-1} \cdot \sqrt{2}$ and we gradually decrease it down to $h = 2^{-7} \cdot \sqrt{2}$. The results are compared after 100 time steps, that is, at $t_{\text{end}} = 0.1$. Figure 6.6 shows the corresponding numerical errors for different field variables, each of them plotted as a function of the mesh element size. In both cases it can be observed that, as the mesh element size decreases, the numerical errors decrease almost with optimal convergence rates. However, once the element size reaches a certain threshold, the error curves level off with further mesh refinements due to the saturation by the temporal truncation error. This is fairly visible in Figure 6.6a, where the threshold roughly corresponds to $h = 2^{-5} \cdot \sqrt{2}$. Note that the time discretization employed in the semi-decoupled scheme is less accurate than in the case of fully-decoupled variant[5], for which the similar effect occurs much later, cf. Figure 6.6b.

[4]Unlike Dong (2015, 2017) who uses C^0–continuous spectral elements for space discretization and systematically varies the element order on the fixed mesh.

[5]In this particular test we put $\theta = 1$ in (5.3b) and $\mathfrak{T} = 2$ in (C.3).

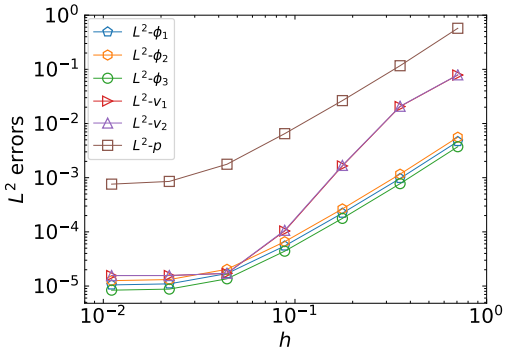

(a) Semi-decoupled scheme (5.12) with $\theta = 1$, direct solvers and pressure calibration applied.

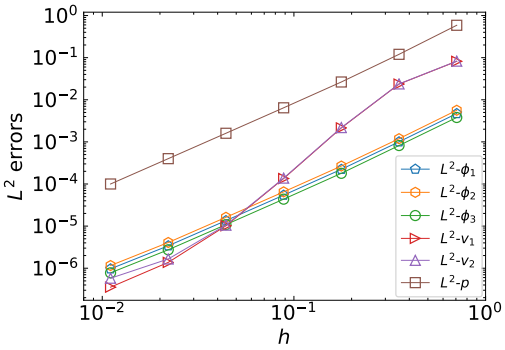

(b) Fully-decoupled scheme (C.18) with $\mathfrak{T} = 2$, direct solvers and pressure calibration applied.

Figure 6.6: Numerical errors as functions of the mesh element size (fixed Δ_t) with polynomial approximation orders given by $k = 1$ in (5.10).

The second group of tests is designed to support our previous notice concerning the temporal accuracy of the individual discretization schemes. In order to get some information about time convergence rates of the proposed methods, we systematically vary the time step size between $\Delta_t = 0.1 \cdot 2^{-5}$ and $\Delta_t = 0.1$. We fix the mesh size at $h = 2^{-5} \cdot \sqrt{2}$ and we put $k = 3$ in (5.10) to effectively suppress propagation of space discretization errors into the results. Figure 6.7 shows the numerical errors at $t_{\text{end}} = 1.0$ for different variables plotted against the time step size. As expected, the obtained results indicate first-order temporal accuracy of the semi-decoupled scheme and second-order temporal accuracy of the fully decoupled scheme. Let us remark that the semi-decoupled scheme indicates the first-order accuracy also for $\theta = \frac{1}{2}$, which is to be expected as long as the time discretization scheme for the NS subproblem remains unchanged.

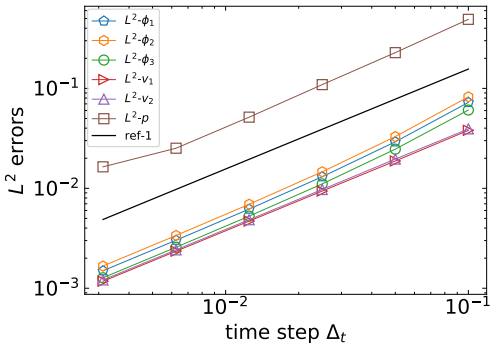

(a) Semi-decoupled scheme (5.12) with $\theta = 1$, direct solvers and pressure calibration applied.

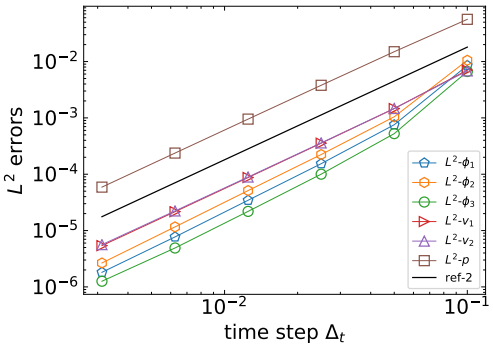

(b) Fully-decoupled scheme (C.18) with $\mathfrak{T} = 2$, direct solvers and pressure calibration applied.

Figure 6.7: Numerical errors as functions of the time step size (fixed mesh element size h) with polynomial approximation orders given by $k = 3$ in (5.10).

6.3 Rising bubble benchmark

Our next validation step consists in performing simulations following the numerical benchmark configuration proposed by Hysing et al. (2009) for two-dimensional bubble dynamics. While the original study compares numerical results obtained by various sharp interface techniques, the same configuration was later used by Aland and Voigt (2012) to compare several diffuse interface models.

The initial configuration of the benchmark is depicted in Figure 6.8. The domain $\Omega = \{(x_1, x_2); 0 \leq x_1 \leq 1, 0 \leq x_2 \leq 2\}$ is occupied by a fluid with an immersed bubble. The bubble rises as its density is smaller than the density of the surrounding fluid. The task is to track its evolution for the two test cases specified in Table 6.4. The first test with small density and viscosity contrasts is characterized by moderate shape deformations, while the larger contrasts in the second test lead to larger deformations and topological changes.

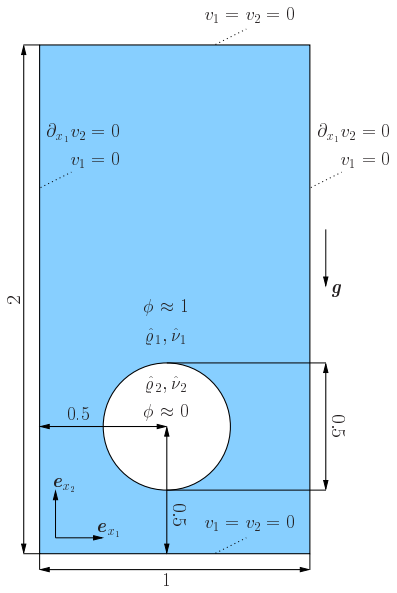

Figure 6.8: Initial configuration for the rising bubble benchmark.

Table 6.4: Test case setup for the rising bubble benchmark.

	$\hat{\varrho}_1$	$\hat{\varrho}_2$	$\hat{\nu}_1$	$\hat{\nu}_2$	σ_{12}	$\boldsymbol{g}$
Test case 1	1000	100	10	1	24.5	$[0, -0.98]^\top$
Test case 2	1000	1	10	0.1	1.96	$[0, -0.98]^\top$

The bubble is initially at rest, described by a single volume fraction following the heuristics based on the equilibrium profile (6.1). Our default choice of finite element spaces from (5.10) does not apply in this particular example. We continue to use the classical $\mathbb{P}_2/\mathbb{P}_1$ element for the velocity/pressure pair, but this time we combine it with $\mathbb{P}_2$ elements for ϕ and χ (instead of $\mathbb{P}_1$). The same combination was considered also by Aland and Voigt (2012). The computational mesh is similar to that one in Figure 6.5b, but here we use the cross-diagonal pattern. The individual computations are carried out on a sequence of uniformly refined meshes with numerical parameters listed in Table 6.5. Let us remark that the bound in (6.2) is not satisfied by $h_{\max}$ (edges in vertical/horizontal directions), but it is at least satisfied by $h_{\min}$ (edges in diagonal directions).

The evolution of the bubble is tracked for three time units during which the defined benchmark quantities are measured. For the sake of brevity, we only report the position of the center of mass and the rise velocity. Results are visually compared with the reference solution corresponding to the data of group 3 from Hysing et al. (2009).

Table 6.5: Numerical parameters for the rising bubble benchmark.

$h_{\max}$	$h_{\min}$	ε	Δ_t	$\gamma^\dagger$
$1/16$	$\sqrt{2}/32$	$0.08 \cdot \sqrt{2}$	0.008	4.0E−07
$1/32$	$\sqrt{2}/64$	$0.04 \cdot \sqrt{2}$	0.004	2.0E−07
$1/64$	$\sqrt{2}/128$	$0.02 \cdot \sqrt{2}$	0.002	1.0E−07
$1/128$	$\sqrt{2}/256$	$0.01 \cdot \sqrt{2}$	0.001	5.0E−08

† γ is used to compute the constant mobility coefficient $\hat{M}_0 = 8\sigma_{12}\gamma$

6.3.1 Comparison of discretization schemes

First of all we shall qualitatively compare results of the benchmark computations conducted with the two discretization schemes previously discussed in Section 6.2. The model with constant mobility and linear type of viscosity interpolation was used in the simulations, and only direct solvers were applied.

The first-order semi-decoupled scheme with the above parameters worked as expected in both test cases, although we had to apply the truncation from (5.19) in the computationally demanding test case 2. The same trick was used for the second-order fully-decoupled scheme, for which it was furthermore necessary to use the half time step size for successful simulation of test case 2.

Remark 6.1 (Degenerate mobility)**.** Semi-decoupled scheme with degenerate mobility $M_0(\phi) = 10^2\hat{M}_0\phi^2(1-\phi)^2$ was also tested. The non-linear dependence on ϕ was treated explicitly using values from the previous time step. The results were found indistinguishable from those for the constant mobility case.

Figure 6.9 shows the bubble shapes, captured via a single contour $\phi = 0.5$, at the final time ($t = 3$) on the finest computational mesh. The bubble shapes differ for the two discretization schemes considered. The individual plots capturing the rise velocity and the center of mass are presented in Figures 6.10–6.13 together with the 'ref' line representing the reference sharp interface results. Our results qualitatively agree with the observations made by Aland and Voigt (2012).

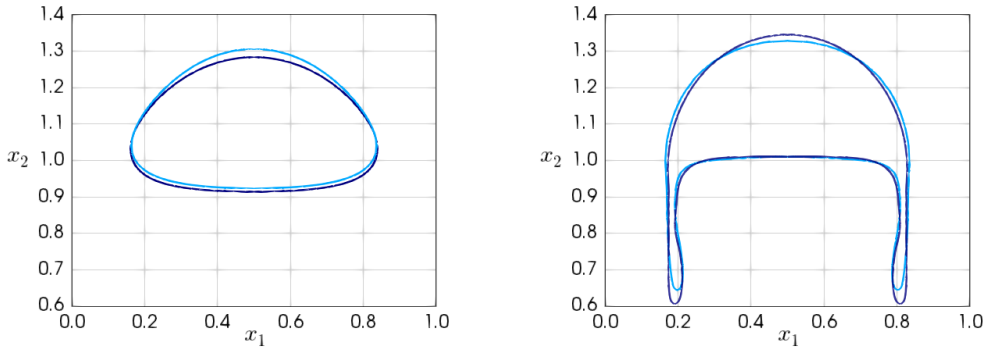

(a) Test case 1. (b) Test case 2.

Figure 6.9: Bubble shapes at $t = 3$ computed with semi-decoupled (dark blue) scheme (5.12) and fully-decoupled (light blue) scheme (C.18).

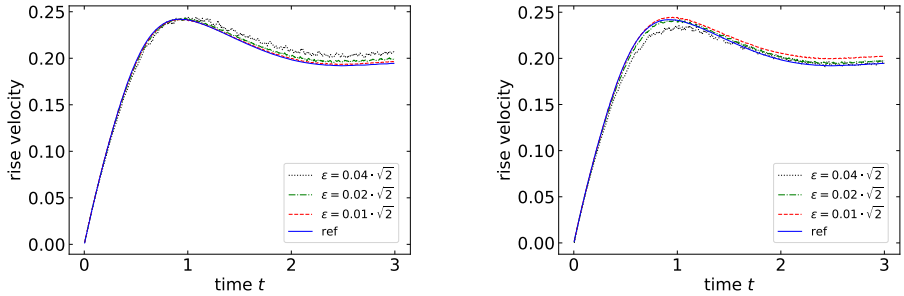

Figure 6.10: Rise velocity over time for test case 1 with semi-decoupled (left) and fully-decoupled (right) schemes (5.12) and (C.18) respectively.

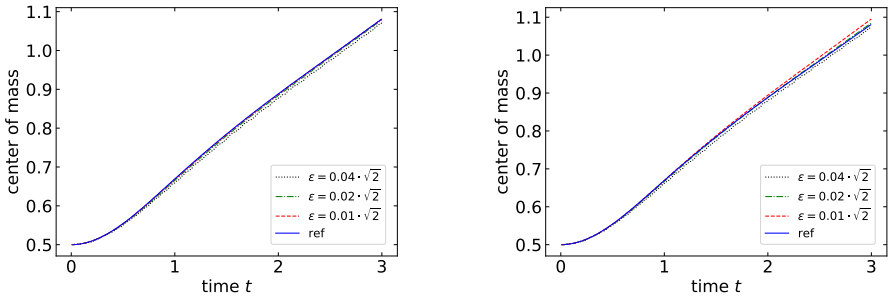

Figure 6.11: Center of mass over time for test case 1 with semi-decoupled (left) and fully-decoupled (right) schemes (5.12) and (C.18) respectively.

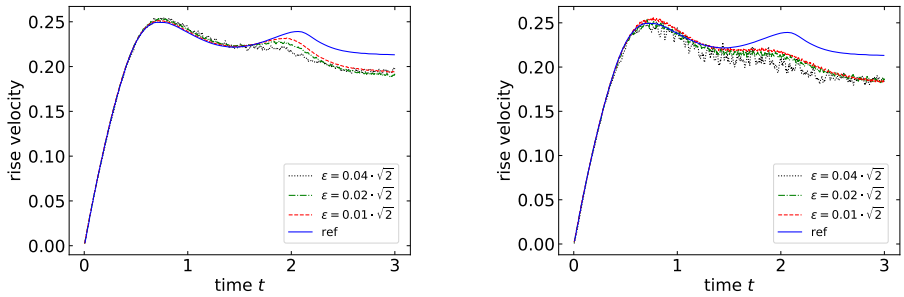

Figure 6.12: Rise velocity over time for test case 2 with semi-decoupled (left) and fully-decoupled (right) schemes (5.12) and (C.18) respectively.

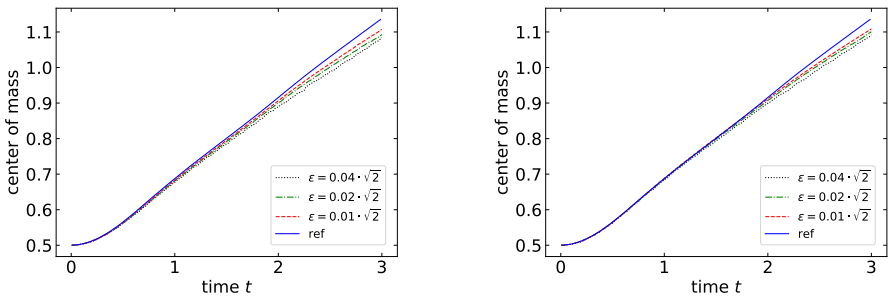

Figure 6.13: Center of mass over time for test case 2 with semi-decoupled (left) and fully-decoupled (right) schemes (5.12) and (C.18) respectively.

In test case 1 with semi-decoupled scheme, we observe that the computed benchmark quantities converge to their reference values. On the other hand, the results obtained in the same test case with the fully-decoupled scheme indicate that the bubble rises a little bit faster. In test case 2, the bubble develops a more non-convex shape together with thin filaments. The solutions given in Hysing et al. (2009) are not identical and it is hard to tell which one, if any, is really correct. In some cases, the thin filaments tend to break off, although it is unclear if such a phenomenon should be observed in the current two-dimensional setting. The benchmark quantities seem to converge, but deviations from the chosen reference solution remain visible even on the finest computational mesh with $\varepsilon = 0.01 \cdot \sqrt{2}$. The filaments become thinner with decreasing ε, see Figure 6.14a, but the splitting does not occur in the current setting. The last statement is no longer valid if a different type of viscosity interpolation is considered, see the following Section 6.3.2.

Remark 6.2 (Comparison of models)**.** The reported results were obtained with the model *FI-CHNS-L1*, see (4.26). Almost no visual differences were recognized, especially on finer meshes, when the other variant *FI-CHNS-L2* was used.

6.3.2 Interpolation effects and iterative solver performance

In this section, we again compute test case 2 on a sequence of refined meshes with decreasing ε (see Table 6.5), but this time we restrict our attention to semi-decoupled scheme (5.12) with degenerate mobility (see Remark 6.1) and **harmonic interpolation** for the viscosity (see Table 6.1). Furthermore, the linear systems arising in Algorithm 1 are solved using the iterative approach described in Section 5.4.

Figure 6.14 shows that the bubble shapes qualitatively differ from the previously computed solutions. On coarser meshes, we observe formation of small trailing bubbles as the thin filaments break off. The trailing bubbles get smaller with decreasing ε and they are not formed on the finest mesh with $\varepsilon = 0.01 \cdot \sqrt{2}$, which

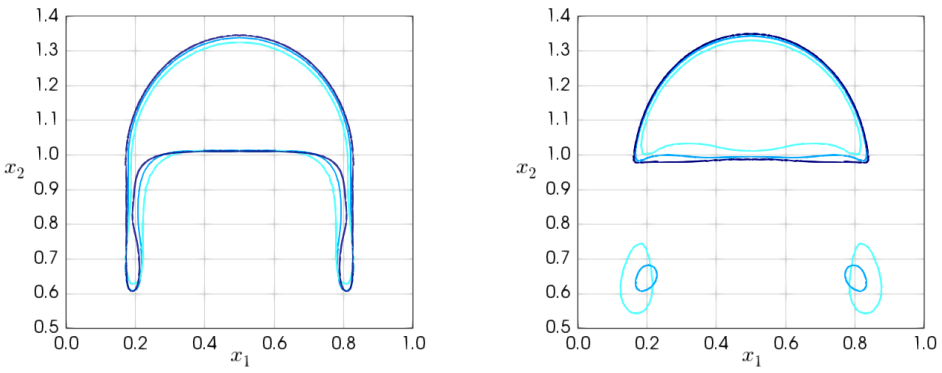

(a) Linear interpolation. (b) Harmonic interpolation.

Figure 6.14: Bubble shapes at $t = 3$ for $\varepsilon = 0.04 \cdot \sqrt{2}$ (light blue), $\varepsilon = 0.02 \cdot \sqrt{2}$ (blue) and $\varepsilon = 0.01 \cdot \sqrt{2}$ (dark blue), computed with semi-decoupled scheme (5.12) using two different viscosity interpolations from Table 6.1.

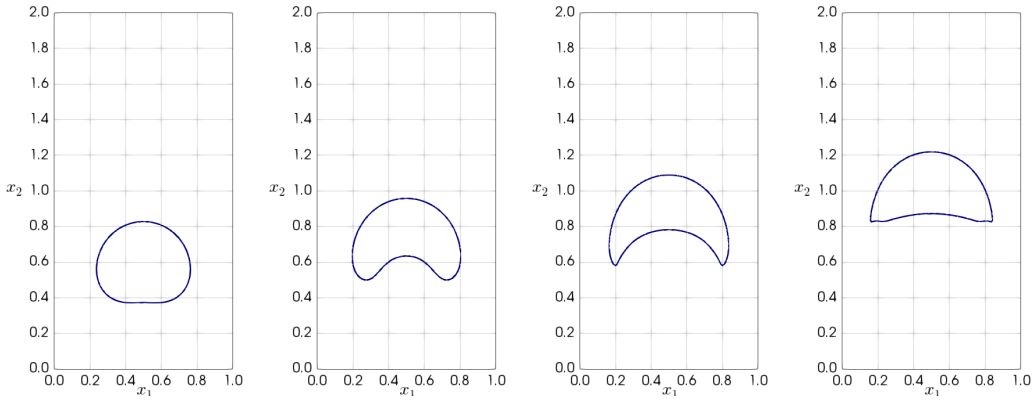

(a) $t = 0.6$ (b) $t = 1.2$ (c) $t = 1.8$ (d) $t = 2.4$

Figure 6.15: Time evolution of the interface for test case 2 with harmonic viscosity interpolation, computed on the finest mesh with $\varepsilon = 0.01 \cdot \sqrt{2}$.

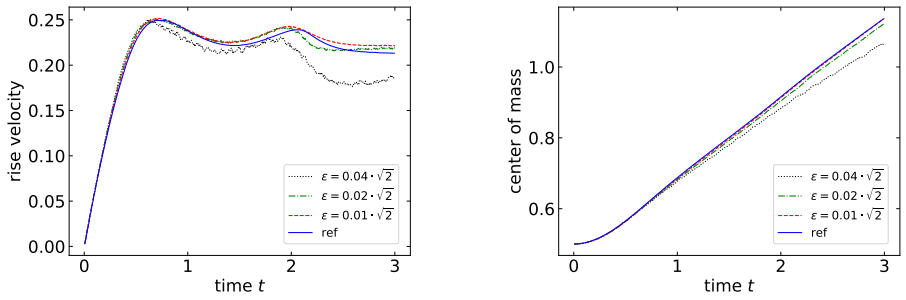

Figure 6.16: Rise velocity and center of mass over time for test case 2 with semi-decoupled schemes (5.12) and harmonic viscosity interpolation from Table 6.1.

is demonstrated in Figure 6.15. Looking at the computed benchmark quantities in Figure 6.16 indicates that we are getting closer to the chosen reference solution. In fact, our solution on the finest mesh appears similar to the solution from group 1 in (Hysing et al., 2009, cf. Figure 27).

Let us remark that the solutions obtained using harmonic viscosity interpolation in test case 1 are indistinguishable from those computed with linear viscosity interpolation. One of the most important features of an optimally preconditioned iterative solver is its convergence in a constant number of iterations independently of the problem parameters. Having a reliable solver for the NS part of the problem seems to be critical in our solution approach. The iterative solver described in Section 5.4.2 performs reasonably well regarding the expected iteration counts. Indeed, in Figure 6.17, we observe only a mild increase of the

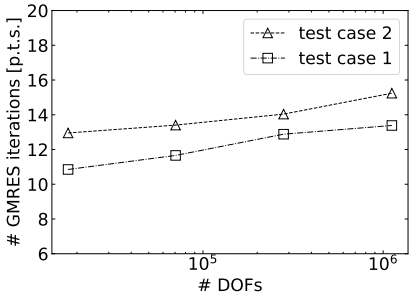

Figure 6.17: Performance of iterative solver from Section 5.4.2. The average number of GMRES iterations needed to resolve NS subproblem per time step is plotted for the sequence of computational meshes from Table 6.2.

average (per time step) number of outer GMRES iterations with increasing number of degrees of freedom (DOFs), due to successive mesh refinement, as well as with the transition from the test case 1 to the computationally challenging test case 2. In order to verify algorithmic and parallel scalability of our iterative scheme, more extensive tests are required. A series of relevant tests will be carried out as part of our future research.

6.4 No-flow problem with flat interface

In what follows, we show that the choice of finite elements made in (5.10) may not be optimal from the point of view of many practical applications. Recently, John et al. (2017) revisited the divergence constraint of the incompressible NS equations in the mixed finite element framework, explaining that many standard (stable and convergent) methods introduce a pressure-dependent consistency error which can potentially pollute the computed velocity. The lack of the so-called "pressure-robustness" is typical also for the Taylor-Hood elements, which have been used in our numerical simulations so far.

To illustrate the effects related to the choice of "non-robust" finite elements in numerical simulation of flows of immiscible incompressible fluids, we again reduce our complicated model to the simplest possible setting. Following the configuration from Section 6.1, we consider a unit square domain with two stratified fluids as in Figure 6.18. Here we assume that the walls are fixed, with no-slip and no-penetration boundary conditions. The two fluids have generally different densities ($\hat{\varrho}_1 \geq \hat{\varrho}_2$) and the same viscosity ($\hat{\nu}_1 = \hat{\nu}_2 = \hat{\nu}_\star$). The latter assumption is made in order to suppress the effects already discussed in Section 6.1. The only external source is the gravitational force which is balanced by the hydrostatic pressure. No flow is thus effectively induced inside the domain. The problem can be described by the stationary Stokes equations

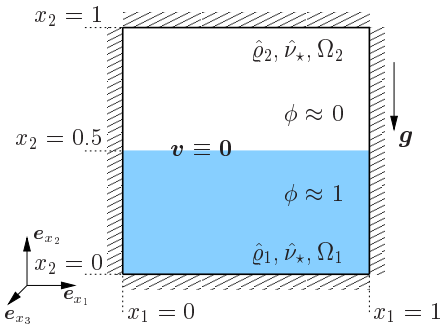

Figure 6.18: No-flow problem with flat interface between two fluids in a fixed domain.

$$\operatorname{div} \boldsymbol{v} = 0, \tag{6.7a}$$

$$-\hat{\nu}_\star \Delta \boldsymbol{v} + \nabla p = \varrho \boldsymbol{g}, \tag{6.7b}$$

supplemented by the boundary condition $\boldsymbol{v}|_{\partial\Omega} = \boldsymbol{0}$. The density on the right hand side of (6.7b) is understood in the diffuse interface sense, that is

$$\varrho(\phi) = \hat{\varrho}_1 \phi + \hat{\varrho}_2 (1 - \phi), \tag{6.8}$$

where ϕ is again fixed, given by the equilibrium profile (6.5). One finds that

$$\boldsymbol{v}(\boldsymbol{x}, t) = \boldsymbol{0}, \qquad p(\boldsymbol{x}, t) = g_{\mathrm{a}} \int_{x_2}^{1} \varrho(\phi(y)) \mathrm{d}y \tag{6.9}$$

is the solution of the above boundary value problem. More precisely, we have

$$p(\boldsymbol{x},t) = \frac{1}{4}(\hat{\varrho}_1 - \hat{\varrho}_2)\left[\varepsilon \ln\left(\cosh\left(\frac{2x_2-1}{\varepsilon}\right)\right) - 2x_2\right] g_\mathrm{a} + (1-x_2)\hat{\varrho}_2 g_\mathrm{a} + K, \quad (6.10)$$

where K is a constant.

The problem can be normalized by considering $L_\mathrm{ref} = 1, V_\mathrm{ref} = 1$ and $\varrho_\mathrm{ref} = \hat{\varrho}_1$ (see Section 4.2.4). Recall that $\mathrm{Re} = \varrho_\mathrm{ref} V_\mathrm{ref} L_\mathrm{ref}/\hat{\nu}_\star$. Applying the discretization introduced in Section 5.2, we perform a series of computations using the parameter values from Table 6.6. Here, we consider a mesh of the same type as in Figure 6.5b, with the element size given by $h = 2^{-l}\sqrt{2}/11$, $l \in \{1,\dots,5\}$. The two cases with distinct dimensionless density difference are studied. In each case we change the Reynolds number from 1 to 10^6 by changing the viscosity of the fluids.

Table 6.6: Parameter values for no-flow problem with flat interface.

Parameter	Value	Parameter	Value
$\hat{\varrho}_1$	1.0	$\hat{\varrho}_2$	0.99 or 0.01
g_a	1.0	$\hat{\nu}_\star$	varied
ε	0.05	h	varied

In Figure 6.19, we observe the well-known phenomenon that the velocity error grows with the increasing Reynolds number. In addition to that, it scales with the density difference which influences the forcing term on the right hand side of (6.7b). In particular, we see that the error can become large for low viscosity fluids ($\hat{\nu}_\star \ll 1$) with a mild density contrast. As already mentioned, all these effects are related to the choice of finite elements that lack a certain type of robustness. We shall clarify this in the next paragraph by interpreting the explanation given in (John et al., 2017, p. 505).

For the Taylor-Hood finite element pairs, as well as for some other inf-sup stable combinations, we have the following classical a priori error estimate for the

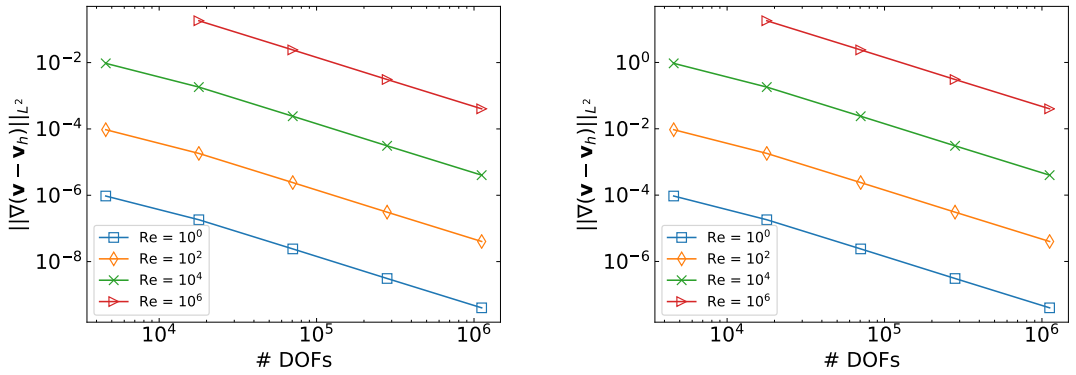

(a) $\hat{\varrho}_1 = 1.0$, $\hat{\varrho}_2 = 0.99$ (b) $\hat{\varrho}_1 = 1.0$, $\hat{\varrho}_2 = 0.01$

Figure 6.19: Velocity errors in the no-flow problem with flat interface between two fluids of different densities (results for the Taylor-Hood pair $\mathbb{P}_2/\mathbb{P}_1$).

velocity error,

$$\|\nabla(\boldsymbol{v}-\boldsymbol{v}_h)\|_{L^2} \leq C \inf_{\boldsymbol{u}_h \in \boldsymbol{\mathcal{V}}_{h,\partial\Omega}^{\boldsymbol{v}}} \|\nabla(\boldsymbol{v}-\boldsymbol{u}_h)\|_{L^2} + \hat{\nu}_\star^{-1} \inf_{q_h \in \mathcal{V}_h^p} \|p-q_h\|_{L^2}\,, \tag{6.11}$$

with a constant $C > 0$; see, for example, Girault and Raviart (1986). The above error estimate shows that the bound for the velocity error depends on the best approximation error of the pressure, which is scaled with the inverse of the viscosity. This term becomes large if $\hat{\nu}_\star$ is small or if the best approximation error is large.

The pressure given by (6.10) is linear if $\hat{\varrho}_1 = \hat{\varrho}_2$. As it is approximated by continuous piecewise linear polynomials, the best approximation error is small enough not to significantly contribute to the error bound in (6.11). On the other hand, the non-linear term in (6.10) is activated whenever the fluids have different densities. This term apparently yields larger approximation errors of the pressure, which inherently increase the error bound in (6.11). This behaviour is illustrated in Figure 6.20a, where we plot the actual pressure errors.

The presence of the pressure in the a priori estimate for the velocity error is closely related to the fact that—using the actual discretization method—the divergence constraint is enforced only discretely[6], see Figure 6.20b. More details are discussed in John et al. (2017), together with state-of-the-art techniques that improve, or even fix, standard mixed methods. The popular ones are *grad-div stabilization* and *appropriate modification of test functions*. The former reduces the lack of pressure-robustness, but does not remove it, while the latter leads to pressure-robust discretizations. None of the suggested techniques has been fully integrated into our simulation software so far. A straighforward extension of our actual computing environment could make use of the pressure-robust discretizations developed by Lederer et al. (2017).

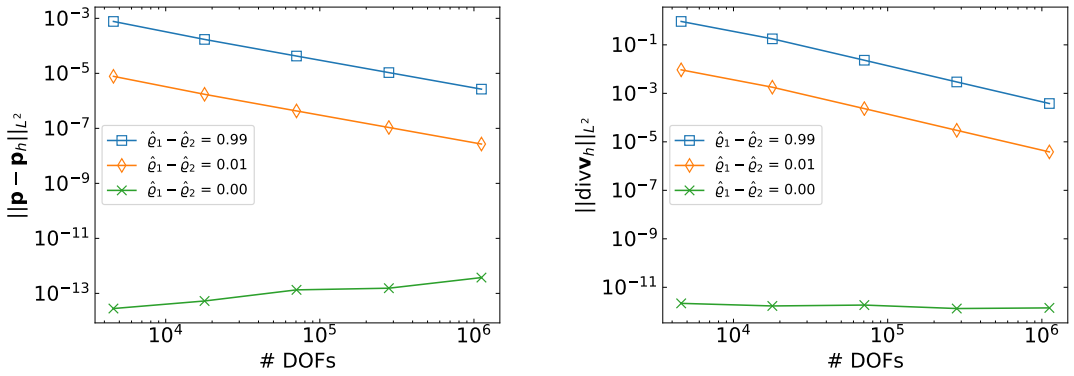

(a) Pressure error. (b) Divergence error.

Figure 6.20: Errors in the no-flow problem with flat interface between two fluids of equal/different densities for $\mathrm{Re} = 10^4$ (results for the Taylor-Hood pair $\mathbb{P}_2/\mathbb{P}_1$).

[6]This issue is sometimes called *poor mass conservation* in the literature.

Chapter 7

Conclusion

The following objectives were accomplished in the thesis:

- We provided a comprehensive thermodynamic analysis of diffuse interface models in a non-isothermal setting.
- We developed a numerical solver specifically suited to computer simulations of simultaneous transient flow of several immiscible fluids in a fixed domain.

Research conducted within the thesis was motivated by the need to address some practical issues concerning the applicability of diffuse interface models in simulations of the *float glass forming process*. We addressed the associated numerical challenges—previously discussed by Řehoř et al. (2017)—in the context of a general class of CHNSF models which combine the multi-component Cahn–Hilliard model and the generalized Navier–Stokes–Fourier model in the thermodynamically consistent way. The former model ensures separation of fluids, while the latter model describes flow of a heat conducting mixture.

The newly formulated models are promising candidates for the description of interfacial dynamics of immiscible fluids in a general non-isothermal setting. In particular, the models take into account both capillary and thermal effects.

The numerical solver developed in the thesis is applicable only in the isothermal setting, however, it *handles general N-component systems* and *allows for systematic use of scalable iterative solvers in the proposed numerical scheme*.

7.1 Development of diffuse interface models

The derivation of diffuse interface models for the given physical system was based on the concept of multi-component continuous medium. The system was treated as *a mixture of a given number of fluid-like components that are allowed to mix within thin interfacial regions*. This standard approach allowed us to describe the system in terms of conventional order parameters such as mass or volume fractions. Such a description is convenient from the numerical point of view since there is no need to explicitly track the interfaces between the components.

Taking into account some basic properties of individual fluids, we introduced three different levels of mathematical description of the kinematics of the given

multi-component system, see Figure 1.7. Each level represents a reduced model associated with the particular choice of order parameters and averaged velocity, see Section 2.5. The mechanical response of the system was supplied into the model by the identification of constitutive relations, see Chapter 3.

The derivation of constitutive relations was based on the specific forms of the Helmholtz free energy and the entropy production. These have been chosen in such a way that the resulting models describe simultaneous flows of either compressible or incompressible *Newtonian fluids*. The choice of the Helmholtz free energy enforces the components to mix only within thin interfacial layers. This brought us to the non-trivial question of extending the standard Ginzburg–Landau form of the Helmholtz free energy into the non-isothermal setting with the emphasis to keep the observed *multi-phase structure* of the system, see Section 3.1 and Assumption 4 therein.

The generalized Helmholtz free energy was used to explicitly formulate the evolution equation for the temperature, separately for *fully-compressible*, *quasi-incompressible* and *fully-incompressible* CHNSF models. The main advantage of the proposed thermodynamical analysis resides in the offered possibility to consistently incorporate thermal effects into diffuse interface models, for instance, through temperature-dependent coefficients of surface tension.

The wide class of CHNSF models includes the majority of standard isothermal models as its own subclass. All models presented in the thesis were developed in a unified way, which makes their mutual comparison on the theoretical level quite straightforward. We have observed that fully-incompressible models with solenoidal velocity field, for example those developed by Boyer et al. (2010) or Abels et al. (2012), can be obtained only by accepting some additional levels of approximation when compared to other models in the same class, see Summary 7 in Section 2.5.

While considering *isothermal* flows of immiscible fluids a special attention was paid to quasi-incompressible and fully-incompressible models. Based on the set of consistency/reduction conditions we elaborated a *consistent formulation* of the *fully-incompressible Cahn–Hilliard–Navier–Stokes* (FI-CHNS) model, see Chapter 4. A similar consistent formulation for the quasi-incompressible model with three or more components, as well as for the non-isothermal extension of both variants, remains an open problem.

7.2 Development of numerical solvers

In the remaining part of the thesis we addressed issues regarding the implementation of *efficient* and *robust* numerical solvers for the continuous FI-CHNS model from Chapter 4. The efficiency has been achieved, in the first instance, with the aid of appropriate splitting mechanism which either partially or fully decouples the system of governing equations on the level of time discretization. To ensure a reliable solution, we incorporated and tested two discretization schemes:

- *semi-decoupled* – inspired by Minjeaud (2013), see Chapter 5;
- *fully-decoupled* – inspired by Dong (2017), see Appendix C.

Both schemes were based on the use of finite element method. The semi-decoupled variant, which treats Cahn–Hilliard and Navier–Stokes subproblems in the model separately, gained more attention since it has shown better results in the standard two-dimensional rising bubble benchmark, see Section 6.3. We proved that the proposed scheme is *unconditionally energy-stable*. Moreover, we elaborated numerical solution of the underlying subproblems in Section 5.4 with the aim to improve the overall efficiency of the computational method.

The intermediate linear algebraic systems encountered in the Cahn–Hilliard subproblem have been solved using GMRES with *point block Jacobi preconditioning*. The more challenging Navier–Stokes subproblem has been tackled by the same outer algorithm, but this time with the sophisticated preconditioner based on the so-called *pressure convection–diffusion* (PCD) strategy. This strategy is known to work well in preconditioning of standard incompressible Navier–Stokes equations, see Elman et al. (2014). Our modified version of the preconditioner has been designed to handle variable coefficients in the model which can suffer from high density and viscosity contrasts.

The numerical methods have been implemented in the newly developed library MUFLON, see Section 5.3, which is based on the FEniCS Project and on our preconditioning package FENaPack. The code is capable of running *parallel* computer simulations of *three-dimensional* flows out of the box. The implementation was tested in the last chapter in simple configurations which allowed us to assess:

- influence of various choices of the interpolation for material parameters in the interfacial regions,
- convergence rates of implemented discretization schemes,
- causes of the occurrence of spurious velocity oscillations in steady problem with flat interface between two stratified fluids.

The earlier version of the code was applied in computer simulations of the float glass forming process, see Section 1.1.

7.3 Final remarks and further research

The numerical solver developed herein provides an efficient tool for simulating flows of multi-component systems consisting of an arbitrary (reasonable) number of immiscible incompressible fluids in fixed domains. It is applicable in different fields including microfluidics, materials science or even glass industry which was explicitly discussed in this work.

However, there are some limitations which prevent the current version of the numerical solver from being used to simulate challenging *processes involving low viscosity fluids with high density contrasts*. For illustration, Table 1.1 shows parameter values for the glass/tin/nitrogen system encountered in the float glass forming process. Although the adopted numerical scheme enabled us to successfully compute with much higher density/viscosity contrasts than in the case of

naive straightforward numerical schemes, we have not yet reached the density and viscosity values met in the applications. Simulations with real parameter values for float glass forming still have produced solutions polluted by numerical errors, see Figure 1.5a. Nevertheless, we have obtained satisfactory results for a wide range of model parameters with a slightly increased viscosity of the problematic components (tin, nitrogen). Moreover, thanks to the applied preconditioning strategy, we have been able to perform three-dimensional simulations in the same critical regimes efficiently.

Note that low viscosity fluids cause problems in numerical computations in general, even without the presence of interfaces. However, in the last chapter of the thesis, we have shown that the impact of small viscosity on the observed velocity error is intensified by density contrasts, see Figure 6.19. We discussed some particular methods with the capability to further improve our currently used discretization scheme in that respect. The methods should be implemented and tested in the follow-up research.

We have observed that numerical results depend on the chosen interpolation of material parameters, see Sections 6.1 and 6.3. Thus, the following question arises: *Can we make a "correct" choice of the interpolation based on some appropriate theoretical analysis?* Moreover, an analogous question could be formulated regarding the specific choice of the PCD preconditioner.

The developed computational framework is ready to assist in answering these and many other interesting questions. In particular, the interface provided by the newly developed MUFLON library is ready to incorporate:

- temperature equation for the non-isothermal extension of the model, see Section 3.6.4;
- boundary conditions including free outflow and general contact angles, see Section 4.2.2;
- other types of double-well potentials, see Remark 3.3;
- alternative discretization schemes, see Section 5.3.2.

On top of that, there are some modelling challenges. For instance, one possible direction for further research would be to develop models which take into account the evolution equation for diffusive fluxes, see Souček et al. (2014). Another possible direction is to apply the approach presented herein to develop diffuse interface models for multi-component systems involving *non-Newtonian* fluids. Such models would be capable to describe, for example, multi-phase flows of viscoelastic fluids that are encountered in rubber industry.

Appendix A

Balance of mass for mechanically incompressible components

Let us recall that material densities have been so far considered—in virtue of Assumption 2—to be positive constants. This corresponds to the fact that the individual components are incompressible (both mechanically and thermally).

In what follows, we shall slightly relax this requirement and we shall assume that the mixture we are dealing with is composed of components that are incompressible only mechanically. In such a case, there is a relation between the material density and the temperature. A detailed discussion of this class of materials from the point of view of single continuum mechanics can be found, for example, in Průša and Rajagopal (2013).

Assumption 2* (Mechanical incompressibility of components)**.** *We assume that components of any incompressible mixture are mechanically incompressible but thermally compressible/expansible in the sense that each material density is given as a positive invertible function of the temperature, that is*

$$\hat{\varrho}_i = \hat{\varrho}_i(\vartheta), \quad i = 1, \dots, N. \tag{A.1}$$

Following (Průša and Rajagopal, 2013, Sec. 2.2) we introduce α_i to be the coefficient of the thermal expansivity/compressibility for the i-th component which is defined in such a way that[1]

$$\frac{\partial \hat{\varrho}_i}{\partial \vartheta} = -\alpha_i \hat{\varrho}_i. \tag{A.2}$$

Note that the i-th component undergoes the thermal extension if α_i is positive, while in the case of negative α_i it undergoes the thermal compression. Clearly, if $\hat{\varrho}_i$ does not change with the temperature, then α_i is zero.

Remark A.1. The differential equation (A.2) can be obtained as a consequence of the balance of mass for the i-th component and the constitutive assumption that the determinant of the deformation gradient $\mathbb{F}_i$, see Remark 2.4, is a function of the temperature ϑ.

[1]We stick to use the notation for partial derivatives even though $\hat{\varrho}_i$ is a function of a single variable, so we should perhaps use the notation for ordinary derivatives. The reason is that we want to avoid possible confusion with the notation used for the material time derivative.

By differentiating (A.1) in the evolution equation (2.30) and using the formula given by (A.2), we get

$$\hat{\varrho}_i \frac{\mathrm{d}\phi_i}{\mathrm{d}t} + \phi_i \left(-\alpha_i \hat{\varrho}_i \frac{\mathrm{d}\vartheta}{\mathrm{d}t} + \hat{\varrho}_i \operatorname{div} \boldsymbol{v} \right) = - \operatorname{div} \boldsymbol{\jmath}_i. \tag{A.3}$$

This equation can be further divided by $\hat{\varrho}_i$. Upon rearranging the terms we can write

$$\frac{\mathrm{d}\phi_i}{\mathrm{d}t} + \phi_i \operatorname{div} \boldsymbol{v} = -\frac{1}{\hat{\varrho}_i} \operatorname{div} \boldsymbol{\jmath}_i + \alpha_i \phi_i \frac{\mathrm{d}\vartheta}{\mathrm{d}t}. \tag{A.4}$$

The first term on the right hand side of the last equation can be rewritten using the identity

$$\operatorname{div} \left(\frac{\boldsymbol{\jmath}_i}{\hat{\varrho}_i} \right) = \frac{1}{\hat{\varrho}_i} \operatorname{div} \boldsymbol{\jmath}_i + \alpha_i \frac{\boldsymbol{\jmath}_i}{\hat{\varrho}_i} \cdot \nabla \vartheta. \tag{A.5}$$

Recalling the relation (2.18), we finally write

$$\frac{\mathrm{d}\phi_i}{\mathrm{d}t} + \phi_i \operatorname{div} \boldsymbol{v} = - \operatorname{div} \widetilde{\boldsymbol{\jmath}}_i + \alpha_i \left(\phi_i \frac{\mathrm{d}\vartheta}{\mathrm{d}t} + \widetilde{\boldsymbol{\jmath}}_i \cdot \nabla \vartheta \right). \tag{A.6}$$

Note that the terms inside brackets on the right hand side correspond to material time derivative associated with the i-th component, that is $\frac{\mathrm{d}_i \vartheta}{\mathrm{d}t}$, multiplied by ϕ_i.

In order to obtain an analogy to constraint (2.29b) in the case of thermally compressible/expansible components, we add up (A.6) over the index i from 1 to N. Provided that the multicomponent system we are dealing with is volume additive, meaning that (2.8) holds, we conclude that

$$\operatorname{div} \boldsymbol{v} = - \operatorname{div} \widetilde{\boldsymbol{J}} + \sum_{i=1}^{N} \alpha_i \left(\phi_i \frac{\mathrm{d}\vartheta}{\mathrm{d}t} + \widetilde{\boldsymbol{\jmath}}_i \cdot \nabla \vartheta \right). \tag{A.7}$$

The first term on the right hand side appears due to the mechanical incompressibility of the components, while the rest is the consequence of their thermal compressibility/expansivity. As one would expect, equation (A.7) reduces to (2.29b) provided that each α_i is equal to zero.

It follows that the balance of mass for the considered class of multicomponent systems can be formulated in terms of volume fractions as

$$\frac{\mathrm{d}\phi_i}{\mathrm{d}t} + \phi_i \operatorname{div} \boldsymbol{v} = - \operatorname{div} \widetilde{\boldsymbol{\jmath}}_i + \alpha_i \left(\phi_i \frac{\mathrm{d}\vartheta}{\mathrm{d}t} + \widetilde{\boldsymbol{\jmath}}_i \cdot \nabla \vartheta \right), \ i = 1, \ldots, N-1, \tag{A.8a}$$

$$\operatorname{div} \boldsymbol{v} = - \operatorname{div} \widetilde{\boldsymbol{J}} + \sum_{i=1}^{N} \alpha_i \left(\phi_i \frac{\mathrm{d}\vartheta}{\mathrm{d}t} + \widetilde{\boldsymbol{\jmath}}_i \cdot \nabla \vartheta \right). \tag{A.8b}$$

(Compare equations in (A.8a) with the fourth row in Table 2.2.) The explicit expression for the total density as a function of volume fractions and material densities (2.10a) is still valid, and it can be shown that ϱ^{v} satisfies the balance of mass (2.28b) if the volume fractions satisfy the equations of (A.8).

Appendix B

Alternative non-isothermal extension of double-well potential

In Section 3.1.2, we suggested the nonlinear extension $\widetilde{\psi}_0$ of the double-well potential $f(\phi_1) = \phi_1^2(1-\phi_1)^2$ in the form (3.19). That extension was constructed with the aim to fulfill the consistency conditions given in (3.18). Here, we provide an alternative form of $\widetilde{\psi}_0$ which will satisfy

$$\left.\frac{\partial\widetilde{\psi}_0}{\partial\phi_1}\right|_{\phi_1=0} = \left.\frac{\partial\widetilde{\psi}_0}{\partial\phi_1}\right|_{\phi_1=1} = 0, \tag{B.1}$$

in addition to the aforementioned consistency conditions. In other words, the non-isothermal extension of f suggested here preserves the local minima at pure components. As we have already remarked in Section 3.6.3, this particular property might be helpful if we need to ensure that the diffusive flux will degenerate in pure components. The alternative form of (3.19) is given by

$$\widetilde{\psi}_0(\vartheta,\phi_1) = \frac{b}{\varepsilon}\sigma_{12}(\hat{\vartheta}_{\mathrm{iso}})f(\phi_1) + \widetilde{\psi}_{\mathrm{pw}}(\vartheta,\phi_1), \tag{B.2a}$$

with the following piecewise-defined function

$$\widetilde{\psi}_{\mathrm{pw}}(\vartheta,\phi_1) = \begin{cases} \widetilde{\psi}_1(\vartheta)(1-16f(\phi_1)), & \phi_1 \geq 0.5, \\ \widetilde{\psi}_2(\vartheta)(1-16f(\phi_1)), & \phi_1 < 0.5, \end{cases} \tag{B.2b}$$

and with partial free energy densities (3.22). This function is plotted in Figure B.1b for different values of ϑ. It can be easily verified that $\widetilde{\psi}_0$ in the above form satisfies the required conditions (3.18) and (B.1). The chemical potential $\widetilde{\mu}^{\,\phi} = \frac{\partial\widetilde{\psi}_0}{\partial\phi_1}$ is given by

$$\widetilde{\mu}^{\,\phi} = b\sigma(\hat{\vartheta}_{\mathrm{iso}})\varepsilon^{-1}f'(\phi_1) + \widetilde{\mu}^{\,\phi}_{\mathrm{pw}}(\vartheta,\phi_1),\ \widetilde{\mu}^{\,\phi}_{\mathrm{pw}}(\vartheta,\phi_1) = \begin{cases} -16\widetilde{\psi}_1(\vartheta)f'(\phi_1), & \phi_1 \geq 0.5, \\ -16\widetilde{\psi}_2(\vartheta)f'(\phi_1), & \phi_1 < 0.5, \end{cases} \tag{B.3}$$

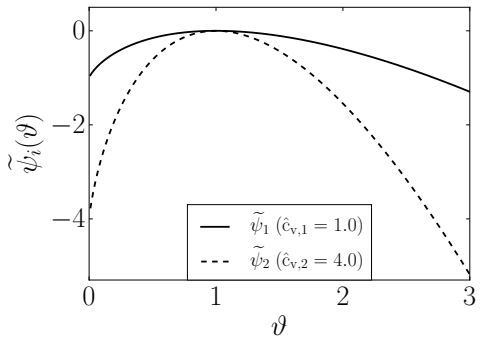

(a) The Helmholtz free energy density (3.22) for individual components with matching densities $\hat{\varrho}_1 = \hat{\varrho}_2 = 1$, but different values of the specific heat at constant volume.

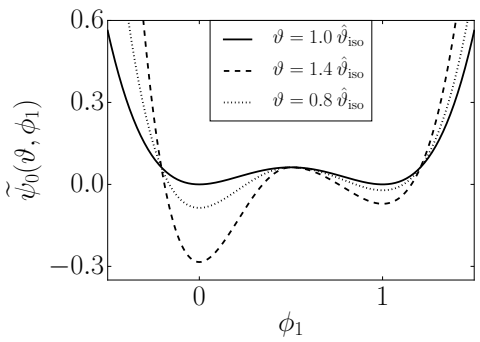

(b) The extended double-well potential (3.19) with $\widetilde{\psi}_1, \widetilde{\psi}_2$ depicted in (a) and $\varepsilon = \sigma_{12} = b = 1$. The full line corresponds to the double-well potential (3.9) which is often used in the isothermal setting.

Figure B.1: Alternative non-isothermal extension of the fourth-order polynomial double-well potential for an incompressible system consisting of two components with $\hat{\mathrm{c}}_{\mathrm{v},1} = 1$ and $\hat{\mathrm{c}}_{\mathrm{v},2} = 4$. The reference temperature is set to $\hat{\vartheta}_{\mathrm{iso}} = 1$.

which is zero at $\phi_1 = 0$ and $\phi_1 = 1$ irrespective of the actual value of ϑ. Note that the last statement does not hold for $\widetilde{\mu}^{\,\phi}$ previously derived in (3.115).

Let us assume that the surface tension is independent of the temperature. The specific heat at constant volume then corresponds to

$$\mathrm{c_v}(\phi_1) = -\frac{\vartheta}{\varrho(\phi_1)} \frac{\partial^2 \widetilde{\psi}_{\mathrm{pw}}}{\partial \vartheta^2} = \begin{cases} \hat{\varrho}_1 \hat{\mathrm{c}}_{\mathrm{v},1} (1 - 16 f(\phi_1))/\varrho(\phi_1), & \phi_1 \geq 0.5, \\ \hat{\varrho}_2 \hat{\mathrm{c}}_{\mathrm{v},2} (1 - 16 f(\phi_1))/\varrho(\phi_1), & \phi_1 < 0.5, \end{cases} \tag{B.4}$$

Note that the above function satisfies $\lim_{\phi \to 0.5_+} \mathrm{c_v}(\phi_1) = \lim_{\phi \to 0.5_-} \mathrm{c_v}(\phi_1) = 0$, thus it is effectively zero exactly in the middle of the interfacial layer independently of the temperature. It should be numerically verified if it is acceptable in the computer simulations. Finally, let us remark that we do not observe such behaviour with the originally suggested extension which leads to $\mathrm{c_v}$ given by (3.114).

Appendix C

Fully-decoupled numerical scheme for FI-CHNS model

In Chapter 5 we have developed the numerical algorithm for solving the system of equations (4.30). Although the equations are strongly coupled, the numerical solution of the corresponding discretized system is sought in a semi-decoupled fashion when one needs to succesively solve CH and NS subproblems to update the solution in time, see Algorithm 1 in Section 5.3. However, note that the equations in CH subproblem remain strongly coupled via the second term in (5.12b).

The MUFLON software library (see Section 5.3.1) implements alternative numerical algorithm which converts the coupled system of $(N-1)$ fourth-order PDEs (4.30a)–(4.30b) into $(N-1)$ computationally decoupled fourth-order equations, each of which is further reduced into two decoupled Helmholtz-type equations. Moreover, the algorithm employs a velocity correction-type projection scheme to computationally decouple the pressure and the velocity in the NS subproblem (4.30c)–(4.30d). This fully-decoupled numerical scheme was developed by Dong (2014a, 2015, 2017), where it is possible to find all the details. Here, we outline only the key steps that must be considered when restating the original scheme[1] in the current setting, using the notation from the thesis.

The derivation of the scheme is based on the formulation of FI-CHNS model with the momentum equation in the form (BLM1), see Table 4.1, and equations (4.30a)–(4.30b) written in the form[2]

$$\frac{\partial \phi_i}{\partial t} + \operatorname{div}(\phi_i \boldsymbol{v}) = \hat{M}_0 \Delta \left(-\frac{a\varepsilon}{2}\Delta\phi_i + \frac{b}{\varepsilon}\sum_{j=1}^{N-1} \ell_{ij} \frac{\partial F}{\partial \phi_j} \right), \quad i = 1, \dots, N-1. \tag{C.1}$$

Each of the above equations is discretized in the following sense,

$$\frac{\gamma_0 \phi_i^{n+1} - \phi_i^{\ddagger}}{\Delta_t} + \operatorname{div}(\phi_i^* \boldsymbol{v}^*) = \hat{M}_0 \Delta \left(-\frac{a\varepsilon}{2}\Delta\phi_i^{n+1} + \frac{S}{\varepsilon}(\phi_i^{n+1} - \phi_i^*) + \frac{b}{\varepsilon}\sum_{j=1}^{N-1} \ell_{ij} d_j^F(\boldsymbol{\phi}^*) \right), \tag{C.2}$$

[1] The scheme was originally developed in a *non-conservative* form for a general set of order parameters with a modified length scale for the interface thickness.

[2] Here we assume that the mobility coefficient is constant.

where d_j^F are given by (4.21) and we have added the stabilization term with a constant parameter S which will be determined below. The above notation is used for the simultaneous treatment of time discretization schemes which are either first or second-order accurate. Let $\mathfrak{T}$ denote the order of temporal accuracy. If Ξ is an arbitrary variable, then

$$\Xi^* = \begin{cases} \Xi^n, & \mathfrak{T} = 1, \\ 2\Xi^n - \Xi^{n-1}, & \mathfrak{T} = 2, \end{cases} \qquad \Xi^\ddagger = \begin{cases} \Xi^n, & \mathfrak{T} = 1, \\ 2\Xi^n - \frac{1}{2}\Xi^{n-1}, & \mathfrak{T} = 2. \end{cases} \tag{C.3a}$$

and

$$\gamma_0 = \begin{cases} 1, & \mathfrak{T} = 1, \\ \frac{3}{2}, & \mathfrak{T} = 2. \end{cases} \tag{C.3b}$$

When we rearrange the terms in (C.2), it can be written in the form

$$\Delta\left(\Delta\phi_i^{n+1} - \frac{2S}{a\varepsilon^2}\phi_i^{n+1}\right) + \frac{2\gamma_0}{a\varepsilon\hat{M}_0\Delta_t}\phi_i^{n+1} = Q_i^{n+1} + \operatorname{div}\left(\nabla R_i^{n+1} + \boldsymbol{Z}_i^{n+1}\right), \tag{C.4}$$

where

$$Q_i^{n+1} = \frac{2\phi_i^\ddagger}{a\varepsilon\hat{M}_0\Delta_t}, \quad R_i^{n+1} = \frac{2}{a\varepsilon}\left(\frac{b}{\varepsilon}\sum_{j=1}^{N-1}\ell_{ij}d_j^F(\boldsymbol{\phi}^*) - \frac{S}{\varepsilon}\phi_i^*\right), \quad \boldsymbol{Z}_i^{n+1} = -\frac{2\phi_i^*\boldsymbol{v}^*}{a\varepsilon\hat{M}_0}. \tag{C.5}$$

Let us further introduce $\varphi_i^{n+1} \overset{\text{def}}{=} \Delta\phi_i^{n+1} + \frac{2\alpha}{a\varepsilon^2}\phi_i^{n+1}$ to be an auxiliary variable with another constant parameter α. Then, we have

$$\begin{aligned} \Delta\varphi_i^{n+1} - \frac{2}{a\varepsilon^2}(\alpha+S)\varphi_i^{n+1} &= \Delta\left(\Delta\phi_i^{n+1} + \frac{2\alpha}{a\varepsilon^2}\phi_i^{n+1}\right) \\ - \frac{2}{a\varepsilon^2}(\alpha+S)\left(\Delta\phi_i^{n+1} + \frac{2\alpha}{a\varepsilon^2}\phi_i^{n+1}\right) &= \Delta\left(\Delta\phi_i^{n+1} - \frac{2S}{a\varepsilon^2}\phi_i^{n+1}\right) - \frac{4\alpha}{a^2\varepsilon^4}(\alpha+S)\phi_i^{n+1} \\ &= Q_i^{n+1} + \operatorname{div}\left(\nabla R_i^{n+1} + \boldsymbol{Z}_i^{n+1}\right) - \frac{2}{a\varepsilon}\left(\frac{\gamma_0}{\hat{M}_0\Delta_t} + \frac{2\alpha}{a\varepsilon^3}(\alpha+S)\right)\phi_i^{n+1}. \end{aligned}$$

Supposing that $\frac{\gamma_0}{\hat{M}_0\Delta_t} + \frac{2\alpha}{a\varepsilon^3}(\alpha+S) = 0$, we obtain the system of decoupled equations

$$\Delta\varphi_i^{n+1} - \frac{2(\alpha+S)}{a\varepsilon^2}\varphi_i^{n+1} = Q_i^{n+1} + \operatorname{div}\left(\nabla R_i^{n+1} + \boldsymbol{Z}_i^{n+1}\right), \qquad i = 1, \dots, N-1, \tag{C.6a}$$

$$\Delta\phi_i^{n+1} + \frac{2\alpha}{a\varepsilon^2}\phi_i^{n+1} = \varphi_i^{n+1}, \qquad i = 1, \dots, N-1, \tag{C.6b}$$

where α is chosen as one of the two possible roots of the aforementioned quadratic equation,

$$\alpha = \frac{S}{2}\left(-1 \pm \sqrt{1 - \frac{2a\varepsilon^3\gamma_0}{\hat{M}_0 S^2\Delta_t}}\right), \tag{C.7}$$

the existence of which is ensured by the additional assumption

$$S \geq \varepsilon\sqrt{\frac{2a\varepsilon\gamma_0}{\hat{M}_0\Delta_t}}. \tag{C.8}$$

Remark C.1. In the implementation, we take $S = \varepsilon\hat{S}\sqrt{\frac{2a\varepsilon\gamma_0}{\hat{M}_0\Delta_t}}$, with $\hat{S} \geq 1$, and we express the coefficients on the left hand side of (C.6a), (C.6b) in the form

$$\frac{2\alpha}{a\varepsilon^2} = \left(\sqrt{\hat{S}^2-1} - \hat{S}\right)\sqrt{\frac{2\gamma_0}{a\varepsilon\hat{M}_0\Delta_t}}, \qquad \frac{2(\alpha+S)}{a\varepsilon^2} = \left(\sqrt{\hat{S}^2-1} + \hat{S}\right)\sqrt{\frac{2\gamma_0}{a\varepsilon\hat{M}_0\Delta_t}}.$$

We choose $\hat{S} = 1$ as the default value.

According to (C.2) and (4.30b), we see that the value of χ_i at $t = t_{n+1}$ is approximated by $\chi_i^{n+1} = -\frac{a\varepsilon}{2}\Delta\phi_i^{n+1} + \frac{S}{\varepsilon}(\phi_i^{n+1} - \phi_i^*) + \frac{b}{\varepsilon}\sum_{j=1}^{N-1}\ell_{ij}d_j^F(\boldsymbol{\phi}^*)$, which can be rewritten as

$$\chi_i^{n+1} = -\frac{a\varepsilon}{2}\varphi_i^{n+1} + \frac{\alpha+S}{\varepsilon}\phi_i^{n+1} + \frac{a\varepsilon}{2}R_i^{n+1}. \tag{C.9}$$

The homogeneous Neumann boundary condition (4.32c) can be transformed into $\nabla\varphi_i^{n+1}\cdot\boldsymbol{n} = \frac{2(\alpha+S)}{a\varepsilon^2}\nabla\phi_i^{n+1}\cdot\boldsymbol{n} + \nabla R_i^{n+1}\cdot\boldsymbol{n}$. In virtue of (4.32b) we obtain

$$\nabla\varphi_i^{n+1}\cdot\boldsymbol{n} = \nabla R_i^{n+1}\cdot\boldsymbol{n},\ i = 1,\dots,N-1, \qquad \text{on } \Gamma_{\mathrm{w}}. \tag{C.10}$$

Let us assume that $\partial\Omega = \Gamma_{\mathrm{w}}$. This restrictive assumption prevents the scheme from its straightforward application in nonenclosed flow problems like the one described in Section 1.1. A special treatment of the inflow/outflow boundary conditions is required to provide a compatible scheme for this type of problems. We shall continue with the description of the fully-decoupled scheme for enclosed flow problems.

The above reformulation of the CH subproblem gives us the idea of how to get the updates $\boldsymbol{\phi}^{n+1}$ and $\boldsymbol{\chi}^{n+1}$, together with the derived quantities ϱ^{n+1}, ν^{n+1} and $\boldsymbol{J}^{n+1}$ respectively; see the relations below (5.3). It remains to compute the velocity and the pressure in the NS subproblem. For the pressure we consider the system of equations

$$\operatorname{div}\bar{\boldsymbol{v}}^{n+1} = 0, \tag{C.11a}$$

$$\frac{\gamma_0\bar{\boldsymbol{v}}^{n+1} - \boldsymbol{v}^{\ddagger}}{\Delta_t} + [\nabla\boldsymbol{v}^*]\left(\boldsymbol{v}^* + \frac{\boldsymbol{J}^{n+1}}{\varrho^{n+1}}\right) + \frac{1}{\hat{\varrho}_0}\nabla p^{n+1} = \left(\frac{1}{\hat{\varrho}_0} - \frac{1}{\varrho^{n+1}}\right)\nabla p^* \tag{C.11b}$$
$$- \frac{\nu^{n+1}}{\varrho^{n+1}}\operatorname{rot}(\operatorname{rot}\boldsymbol{v}^*) + \frac{2}{\varrho^{n+1}}\mathbb{D}^*\nabla\nu^{n+1} + \frac{1}{\varrho^{n+1}}\sum_{i,j=1}^{N-1}\lambda_{ij}\left(\frac{\alpha}{\varepsilon}\phi_j^{n+1} - \frac{a\varepsilon}{2}\varphi_j^{n+1}\right)\nabla\phi_i^{n+1} + \boldsymbol{g},$$

supplemented with the boundary condition $\bar{\boldsymbol{v}}^{n+1}\cdot\boldsymbol{n} = \boldsymbol{v}_{\mathrm{w}}^{n+1}\cdot\boldsymbol{n}$ on Γ_{w}. An auxiliary velocity $\bar{\boldsymbol{v}}^{n+1}$ in the above equations approximates $\boldsymbol{v}^{n+1}$, and $\hat{\varrho}_0$ is a chosen constant that must satisfy the condition

$$0 < \hat{\varrho}_0 \leq \min(\hat{\varrho}_1,\dots,\hat{\varrho}_N). \tag{C.12}$$

The shorthand notation

$$\boldsymbol{q}^{n+1} = \frac{\boldsymbol{v}^{\ddagger}}{\Delta_t} - [\nabla\boldsymbol{v}^*]\left(\boldsymbol{v}^* + \frac{\boldsymbol{J}^{n+1}}{\varrho^{n+1}}\right) + \left(\frac{1}{\hat{\varrho}_0} - \frac{1}{\varrho^{n+1}}\right)\nabla p^* + \nabla\left(\frac{\nu^{n+1}}{\varrho^{n+1}}\right)\times\operatorname{rot}\boldsymbol{v}^*$$
$$+ \frac{2}{\varrho^{n+1}}\mathbb{D}^*\nabla\nu^{n+1} + \frac{1}{\varrho^{n+1}}\sum_{i,j=1}^{N-1}\lambda_{ij}\left(\frac{\alpha}{\varepsilon}\phi_j^{n+1} - \frac{a\varepsilon}{2}\varphi_j^{n+1}\right)\nabla\phi_i^{n+1} + \boldsymbol{g} \tag{C.13}$$

will come in handy in the forthcoming manipulations. The corrected velocity is obtained by solving

$$\frac{\gamma_0 \boldsymbol{v}^{n+1} - \gamma_0 \bar{\boldsymbol{v}}^{n+1}}{\Delta_t} - \nu_0^{\mathrm{kin}} \Delta \boldsymbol{v}^{n+1} = \nu_0^{\mathrm{kin}} \operatorname{rot}(\operatorname{rot} \boldsymbol{v}^*), \tag{C.14}$$

where ν_0^{kin} is a chosen positive constant satisfying

$$\nu_0^{\mathrm{kin}} \geq \max\left(\frac{\nu_1}{\hat{\varrho}_1}, \dots, \frac{\nu_N}{\hat{\varrho}_N}\right). \tag{C.15}$$

Recall that $\boldsymbol{v}^{n+1}$ is required to satisfy the boundary condition (4.32a), that is, $\boldsymbol{v}^{n+1} = \boldsymbol{v}_{\mathrm{w}}^{n+1}$ on Γ_{w}. Adding together the equations (C.11b) and (C.14), we get

$$\frac{\gamma_0}{\Delta_t} \boldsymbol{v}^{n+1} - \nu_0^{\mathrm{kin}} \Delta \boldsymbol{v}^{n+1} = \boldsymbol{q}^{n+1} - \nabla\left(\frac{\nu^{n+1}}{\varrho^{n+1}}\right) \times \operatorname{rot} \boldsymbol{v}^* - \frac{1}{\hat{\varrho}_0} \nabla p^{n+1} - \left(\frac{\nu^{n+1}}{\varrho^{n+1}} - \nu_0^{\mathrm{kin}}\right) \operatorname{rot}(\operatorname{rot} \boldsymbol{v}^*). \tag{C.16}$$

Now we are ready to formulate the corresponding Galerkin system using the notation introduced in Section 5.2 together with the manipulations[3] that were considered by Dong (2017). Let $\boldsymbol{\phi}_h^n \in \boldsymbol{\mathcal{V}}_h^\phi$ and $\boldsymbol{v}_h^n, \widetilde{\boldsymbol{v}}_h^{n+1} \in \boldsymbol{\mathcal{V}}_h^{\boldsymbol{v}}$ are given functions which attain prescribed boundary values. Let $\mathcal{V}_h^p \subset H^1(\Omega)$, cf. (4.34e). The problem is to find $(\boldsymbol{\varphi}_h^{n+1}, \boldsymbol{\phi}_h^{n+1}, \boldsymbol{v}_h^{n+1}, p_h^{n+1})$ such that

$$\boldsymbol{\varphi}_h^{n+1} \in \boldsymbol{\mathcal{V}}_h^\chi, \qquad \boldsymbol{\phi}_h^{n+1} \in \boldsymbol{\mathcal{V}}_h^\phi, \qquad \boldsymbol{v}_h^{n+1} - \widetilde{\boldsymbol{v}}_h^{n+1} \in \boldsymbol{\mathcal{V}}_{h,\partial\Omega}^{\boldsymbol{v}}, \qquad p_h^{n+1} \in \mathcal{V}_h^p, \tag{C.17}$$

and $\forall \varphi_h^{\mathrm{te}} \in \mathcal{V}^\chi$, $\forall \phi_h^{\mathrm{te}} \in \mathcal{V}_h^\phi$, $\forall p_h^{\mathrm{te}} \in \mathcal{V}_h^p$, $\forall \boldsymbol{v}_h^{\mathrm{te}} \in \boldsymbol{\mathcal{V}}_{h,\partial\Omega}^{\boldsymbol{v}}$, we have

$$\begin{aligned}\int_\Omega \nabla \varphi_{i,h}^{n+1} \cdot \nabla \varphi_h^{\mathrm{te}} + \int_\Omega \frac{2(\alpha+S)}{a\varepsilon^2} \varphi_{i,h}^{n+1} \varphi_h^{\mathrm{te}} &= -\int_\Omega Q_{i,h}^{n+1} \varphi_h^{\mathrm{te}} \\ &\quad - \int_{\partial\Omega} \left(\boldsymbol{Z}_{i,h}^{n+1} \cdot \boldsymbol{n}\right) \varphi_h^{\mathrm{te}} + \int_\Omega \left(\nabla R_{i,h}^{n+1} + \boldsymbol{Z}_{i,h}^{n+1}\right) \cdot \nabla \varphi_h^{\mathrm{te}}, \quad i = 1, \dots, N-1,\end{aligned} \tag{C.18a}$$

$$\int_\Omega \nabla \phi_{i,h}^{n+1} \cdot \nabla \phi_h^{\mathrm{te}} - \int_\Omega \frac{2\alpha}{a\varepsilon^2} \phi_{i,h}^{n+1} \phi_h^{\mathrm{te}} = -\int_\Omega \varphi_{i,h}^{n+1} \phi_h^{\mathrm{te}}, \qquad i = 1, \dots, N-1, \tag{C.18b}$$

$$\begin{aligned}\int_\Omega \nabla p_h^{n+1} \cdot \nabla p_h^{\mathrm{te}} = \hat{\varrho}_0 \int_\Omega \boldsymbol{q}_h^{n+1} \cdot \nabla p_h^{\mathrm{te}} - \frac{\hat{\varrho}_0 \gamma_0}{\Delta_t} \int_{\partial\Omega} (\boldsymbol{v}_{\mathrm{w},h}^{n+1} \cdot \boldsymbol{n}) p_h^{\mathrm{te}} \\ - \hat{\varrho}_0 \int_{\partial\Omega} \frac{\nu_h^{n+1}}{\varrho_h^{n+1}} (\boldsymbol{n} \times \operatorname{rot} \boldsymbol{v}_h^*) \cdot \nabla p_h^{\mathrm{te}},\end{aligned} \tag{C.18c}$$

$$\begin{aligned}\int_\Omega \nabla \boldsymbol{v}_h^{n+1} : \nabla \boldsymbol{v}_h^{\mathrm{te}} + \frac{\gamma_0}{\nu_0^{\mathrm{kin}} \Delta_t} \int_\Omega \boldsymbol{v}_h^{n+1} \cdot \boldsymbol{v}_h^{\mathrm{te}} &= \frac{1}{\nu_0^{\mathrm{kin}}} \int_\Omega \left(\boldsymbol{q}_h^{n+1} - \frac{1}{\hat{\varrho}_0} \nabla p_h^{n+1}\right) \cdot \boldsymbol{v}_h^{\mathrm{te}} \\ &\quad - \frac{1}{\nu_0^{\mathrm{kin}}} \int_\Omega \left(\frac{\nu_h^{n+1}}{\varrho_h^{n+1}} - \nu_0^{\mathrm{kin}}\right) \operatorname{rot} \boldsymbol{v}_h^* \cdot \operatorname{rot} \boldsymbol{v}_h^{\mathrm{te}}.\end{aligned} \tag{C.18d}$$

[3]The equations (C.6a), (C.6b), (C.11a), (C.11b) and (C.16) formally coincide with (Dong, 2017, Eqs. (120a), (120b), (176a), (176b) and (182)).

The constants $\alpha, S, \hat{\varrho}_0$ and ν_0^{kin} in the above equations must be chosen according to (C.7), (C.8), (C.12) and (C.15) respectively. The terms $Q_{i,h}^{n+1}, R_{i,h}^{n+1}, \boldsymbol{Z}_{i,h}^{n+1}$ and $\boldsymbol{q}_h^{n+1}$ are given by the relations in (C.5) and (C.13). Finally, recall that

$$\varrho_h^{n+1} = \sum_{i=1}^{N-1} (\hat{\varrho}_i - \hat{\varrho}_N)\phi_{i,h}^{n+1} + \hat{\varrho}_N, \qquad \nu_h^{n+1} = \sum_{i=1}^{N-1} (\nu_i - \nu_N)\phi_{i,h}^{n+1} + \nu_N, \tag{C.19}$$

and

$$\boldsymbol{J}_h^{n+1} = -\Theta_2 \sum_{i=1}^{N-1} M_0(\hat{\varrho}_i - \hat{\varrho}_N)\, \nabla \chi_{i,h}^{n+1}, \tag{C.20}$$

where $\chi_{i,h}^{n+1}$ is given by (C.9). The discrete functions $\boldsymbol{\phi}_h^0 \in \boldsymbol{\mathcal{V}}_h^\phi$ and $\boldsymbol{v}_h^0 \in \boldsymbol{\mathcal{V}}_h^{\boldsymbol{v}}$ at the initial time level are chosen to approximate the initial conditions (4.35), see Remark 5.2. To initialize the variables required by the two-step second-order scheme with $\mathfrak{T} = 2$, we perform the first iteration of Algorithm 2 with $\mathfrak{T} = 1$.

Remark C.2. Let us emphasize that the scheme proposed by Dong (2017) is based on the equivalent form of (C.1) with the second term replaced by $\boldsymbol{v} \cdot \nabla \phi_i$. The resulting scheme, however, does not conserve order parameters on the discrete level (for enclosed flows) unlike the updated scheme presented here.

Algorithm 2 Fully-decoupled scheme based on (C.18)

Require:
Input parameters [Table 4.2]
Mesh and boundary data [$(\Gamma_{\text{w}} = \partial\Omega, \boldsymbol{v}_{\text{w}})$]
Initial conditions [$\boldsymbol{\phi}_h^0, \boldsymbol{v}_h^0$]
Time domain specification [$t_{\text{end}}, N_{t.s.}, \Delta_t$]
Specification of temporal accuracy [$\mathfrak{T}, \gamma_0$]
Ensure:
Initialization of a, b, λ_{ij}, ℓ_{ij} [Table 4.2]
Initialization of $\alpha, S, \hat{\varrho}_0, \nu_0^{\text{kin}}$ [(C.8), (C.7), (C.12), (C.15)]

for $n = 0, 1, \ldots, N_{t.s.} - 1$ **do**
Advance-Phase procedure: ▷ CH part
1. compute $Q_{i,h}^{n+1}, R_{i,h}^{n+1}, \boldsymbol{Z}_{i,h}^{n+1}$ based on (C.5)
2. solve (C.18a) for $\boldsymbol{\varphi}_h^{n+1}$ ▷ linear solve
3. solve (C.18b) for $\boldsymbol{\phi}_h^{n+1}$ ▷ linear solve

Advance-Flow procedure: ▷ NS part
4. compute $\boldsymbol{J}_h^{n+1}$ based on (C.20) and (C.9)
5. compute $\varrho_h^{n+1}, \nu_h^{n+1}$ based on (C.19)
6. compute $\boldsymbol{q}_h^{n+1}$ based on (C.13)
7. solve (C.18c) for p_h^{n+1} ▷ linear solve
8. solve (C.18d) for $\boldsymbol{v}_h^{n+1}$ ▷ linear solve

end for

Bibliography

Abels, H., H. Garcke, and G. Grün (2012). Thermodynamically consistent, frame indifferent diffuse interface models for incompressible two-phase flows with different densities. *Math. Models Methods Appl. Sci. 22*(3), 1150013, 40.

Adam, N. K. (1941). *The Physics And Chemistry Of Surfaces* (3rd ed.). Oxford University Press.

Ahrens, J., B. Geveci, and C. Law (2005). Paraview: An end-user tool for large-data visualization. In C. D. Hansen and C. R. Johnson (Eds.), *Visualization Handbook*, pp. 717 – 731. Burlington: Butterworth-Heinemann.

Aki, G. L., W. Dreyer, J. Giesselmann, and C. Kraus (2014). A quasi-incompressible diffuse interface model with phase transition. *Mathematical Models and Methods in Applied Sciences 24*(05), 827–861.

Aland, S. and A. Voigt (2012). Benchmark computations of diffuse interface models for two-dimensional bubble dynamics. *International Journal for Numerical Methods in Fluids 69*(3), 747–761.

Alnæs, M., J. Blechta, J. Hake, A. Johansson, B. Kehlet, A. Logg, C. Richardson, J. Ring, M. Rognes, and G. Wells (2015). The FEniCS Project Version 1.5. *Archive of Numerical Software 3*(100), 9–23.

Alnæs, M. S., A. Logg, K. B. Ølgaard, M. E. Rognes, and G. N. Wells (2014, March). Unified form language: A domain-specific language for weak formulations of partial differential equations. *ACM Trans. Math. Softw. 40*(2), 9:1–9:37.

Amestoy, P. R., I. S. Duff, J.-Y. L'Excellent, and J. Koster (2001). A fully asynchronous multifrontal solver using distributed dynamic scheduling. *SIAM Journal on Matrix Analysis and Applications 23*(1), 15–41.

Amestoy, P. R., A. Guermouche, J.-Y. L'Excellent, and S. Pralet (2006). Hybrid scheduling for the parallel solution of linear systems. *Parallel Computing 32*(2), 136 – 156. Parallel Matrix Algorithms and Applications (PMAA'04).

Anderson, D. M., G. B. McFadden, and A. A. Wheeler (1998). Diffuse-interface methods in fluid mechanics. *Annual Review of Fluid Mechanics 30*(1), 139–165.

Atkin, R. J. and R. E. Craine (1976a). Continuum theories of mixtures: Applications. *IMA J. Appl. Math. 17*(2), 153–207.

Atkin, R. J. and R. E. Craine (1976b). Continuum theories of mixtures: Basic theory and historical development. *Q. J. Mech. Appl. Math. 29*(2), 209–244.

Balay, S., S. Abhyankar, M. F. Adams, J. Brown, P. Brune, K. Buschelman, V. Eijkhout, W. D. Gropp, D. Kaushik, M. G. Knepley, L. C. McInnes, K. Rupp, B. F. Smith, and H. Zhang (2014b). PETSc users manual. Technical Report ANL-95/11 - Revision 3.5, Argonne National Laboratory.

Balay, S., S. Abhyankar, M. F. Adams, J. Brown, P. Brune, K. Buschelman, V. Eijkhout, W. D. Gropp, D. Kaushik, M. G. Knepley, L. C. McInnes, K. Rupp, B. F. Smith, and H. Zhang (2014a). PETSc Web page.

Balay, S., W. D. Gropp, L. C. McInnes, and B. F. Smith (1997). Efficient management of parallelism in object oriented numerical software libraries. In E. Arge, A. M. Bruaset, and H. P. Langtangen (Eds.), *Modern Software Tools in Scientific Computing*, Boston, MA, pp. 163–202. Birkhäuser Boston.

Benzi, M., G. H. Golub, and J. Liesen (2005). Numerical solution of saddle point problems. *Acta Numer. 14*, 1–137.

Blechta, J. (2018). Ph. D. thesis, Charles University, Prague, Czech Republic. In preparation.

Blechta, J. and M. Řehoř (2017). FENaPack 2017.2.0 (FEniCS Navier-Stokes preconditioning package). `https://github.com/blechta/fenapack`.

Blowey, J. F. and C. M. Elliott (1991). The Cahn-Hilliard gradient theory for phase separation with non-smooth free energy part i: Mathematical analysis. *European Journal of Applied Mathematics 2*(3), 233–280.

Bosch, J. (2016). *Fast Iterative Solvers for Cahn-Hilliard Problems*. Ph. D. thesis, Otto-von-Guericke Universität Magdeburg, Germany.

Bosch, J., C. Kahle, and M. Stoll (2018). Preconditioning of a coupled Cahn–Hilliard Navier–Stokes system. *Commun. Comput. Phys. 23*(2), 603–628.

Bowen, R. M. (1976). *Continuum physics*, Volume 3, Chapter Theory of mixtures, pp. 1–127. New York: Academic Press.

Boyer, F. (2002). A theoretical and numerical model for the study of incompressible mixture flows. *Computers & Fluids 31*(1), 41 – 68.

Boyer, F. and C. Lapuerta (2006, 7). Study of a three component Cahn-Hilliard flow model. *ESAIM: Mathematical Modelling and Numerical Analysis 40*, 653–687.

Boyer, F., C. Lapuerta, S. Minjeaud, B. Piar, and M. Quintard (2010). Cahn-Hilliard/Navier-Stokes model for the simulation of three-phase flows. *Transport in Porous Media 82*(3), 463–483.

Boyer, F. and S. Minjeaud (2011, 7). Numerical schemes for a three component cahn-hilliard model. *ESAIM: Mathematical Modelling and Numerical Analysis 45*, 697–738.

Boyer, F. and S. Minjeaud (2014). Hierarchy of consistent n-component cahn–hilliard systems. *Mathematical Models and Methods in Applied Sciences 24*(14), 2885–2928.

Brackbill, J., D. Kothe, and C. Zemach (1992). A continuum method for modeling surface tension. *Journal of Computational Physics 100*(2), 335 – 354.

Cahn, J. W. (1959). Free energy of a nonuniform system. ii. thermodynamic basis. *The Journal of Chemical Physics 30*(5), 1121–1124.

Cahn, J. W. and J. E. Hilliard (1958). Free Energy of a Nonuniform System. I. Interfacial Free Energy. *J. Chem. Phys. 28*(2), 258–267.

Callen, H. (1985). *Thermodynamics and an Introduction to Thermostatistics*. Wiley.

Chella, R. and J. Viñals (1996, Apr). Mixing of a two-phase fluid by cavity flow. *Phys. Rev. E 53*, 3832–3840.

Copetti, M. I. M. and C. M. Elliott (1990). Kinetics of phase decomposition processes: numerical solutions to Cahn-Hilliard equation. *Materials Science and Technology 6*(3), 273–284.

Copetti, M. I. M. and C. M. Elliott (1992, Dec). Numerical analysis of the cahn-hilliard equation with a logarithmic free energy. *Numerische Mathematik 63*(1), 39–65.

de Groot, S. R. and P. Mazur (1984). *Non-equilibrium thermodynamics*. New York: Dover Publications. Reprint of the 1962 original.

Ding, H., P. D. Spelt, and C. Shu (2007). Diffuse interface model for incompressible two-phase flows with large density ratios. *Journal of Computational Physics 226*(2), 2078 – 2095.

Ding, H. and P. D. M. Spelt (2007). Wetting condition in diffuse interface simulations of contact line motion. *Phys. Rev. E 75*, 046708.

Dong, S. (2014a). An efficient algorithm for incompressible N-phase flows. *Journal of Computational Physics 276*, 691–728.

Dong, S. (2014b). An outflow boundary condition and algorithm for incompressible two-phase flows with phase field approach. *Journal of Computational Physics 266*(Supplement C), 47 – 73.

Dong, S. (2015). Physical formulation and numerical algorithm for simulating N immiscible incompressible fluids involving general order parameters. *Journal of Computational Physics 283*, 98–128.

Dong, S. (2017). Wall-bounded multiphase flows of n immiscible incompressible fluids: Consistency and contact-angle boundary condition. *Journal of Computational Physics 338*, 21 – 67.

Eckart, C. (1940, Aug). The Thermodynamics of Irreversible Processes: II. Fluid Mixtures. *Phys. Rev. 58*, 269–275.

Eleuteri, M., E. Rocca, and G. Schimperna (2015). On a non-isothermal diffuse interface model for two-phase flows of incompressible fluids. *Discrete and Continuous Dynamical Systems 35*(6), 2497–2522.

Eleuteri, M., E. Rocca, and G. Schimperna (2016). Existence of solutions to a two-dimensional model for nonisothermal two-phase flows of incompressible fluids. *Annales de l'Institut Henri Poincare (C) Non Linear Analysis 33*(6), 1431 – 1454.

Elliott, C. M. (1989). The Cahn-Hilliard model for the kinetics of phase separation. In J. F. Rodrigues (Ed.), *Mathematical Models for Phase Change Problems*, Volume 88 of *International Series of Numerical Mathematics*, Basel, pp. 35–73. Birkhäuser Verlag.

Elman, H. C., D. J. Silvester, and A. J. Wathen (2014). *Finite elements and fast iterative solvers: with applications in incompressible fluid dynamics* (2nd ed.). Numerical Mathematics and Scientific Computation. Oxford University Press.

Elman, H. C. and R. S. Tuminaro (2009). Boundary conditions in approximate commutator preconditioners for the Navier-Stokes equations. *Electronic Transactions on Numerical Analysis 35*, 257–280.

Falgout, R. D., J. E. Jones, and U. M. Yang (2006). The design and implementation of hypre, a library of parallel high performance preconditioners. In A. M. Bruaset and A. Tveito (Eds.), *Numerical Solution of Partial Differential Equations on Parallel Computers*, Berlin, Heidelberg, pp. 267–294. Springer Berlin Heidelberg.

Fernández Oro, J. M., K. M. Argüelles Díaz, C. Santolaria Morros, A. F. Cobo Hedilla, and M. Lemaille (2008). Multiphase modelling of pouring glass over the spout lip of an industrial float in the flat glass forming process. *International Journal for Numerical Methods in Fluids 58*(10), 1147–1177.

Freistühler, H. and M. Kotschote (2017, Apr). Phase-field and korteweg-type models for the time-dependent flow of compressible two-phase fluids. *Archive for Rational Mechanics and Analysis 224*(1), 1–20.

Geuzaine, C. and J.-F. Remacle (2009). Gmsh: A 3-d finite element mesh generator with built-in pre- and post-processing facilities. *International Journal for Numerical Methods in Engineering 79*(11), 1309–1331.

Girault, V. and P. Raviart (1986). *Finite element methods for Navier-Stokes equations: theory and algorithms*. Springer series in computational mathematics. Springer-Verlag.

Grün, G. and F. Klingbeil (2014). Two-phase flow with mass density contrast: Stable schemes for a thermodynamic consistent and frame-indifferent diffuse-interface model. *Journal of Computational Physics 257*(Part A), 708 – 725.

Gueyffier, D., J. Li, A. Nadim, R. Scardovelli, and S. Zaleski (1999). Volume-of-fluid interface tracking with smoothed surface stress methods for three-dimensional flows. *Journal of Computational Physics 152*(2), 423 – 456.

Guillen-Gonzalez, F. and G. Tierra (2014, 12). Splitting schemes for a navier-stokes-cahn-hilliard model for two fluids with different densities. *Journal of Computational Mathematics 32*, 643–664.

Guo, Z., P. Lin, and J. S. Lowengrub (2014). A numerical method for the quasi-incompressible Cahn-Hilliard-Navier-Stokes equations for variable density flows with a discrete energy law. *J. Comput. Phys. 276*, 486–507.

Gurtin, M. E., E. Fried, and L. Anand (2010). *The mechanics and thermodynamics of continua*. Cambridge: Cambridge University Press.

Gurtin, M. E., D. Polignone, and J. Viñals (1996). Two-phase binary fluids and immiscible fluids described by an order parameter. *Mathematical Models and Methods in Applied Sciences 06*(06), 815–831.

Heida, M., J. Málek, and K. R. Rajagopal (2012a). On the development and generalizations of Allen-Cahn and Stefan equations within a thermodynamic framework. *Z. Angew. Math. Phys. 63*(4), 759–776.

Heida, M., J. Málek, and K. R. Rajagopal (2012b). On the development and generalizations of Cahn-Hilliard equations within a thermodynamic framework. *Z. Angew. Math. Phys. 63*(1), 145–169.

Hirt, C. and B. Nichols (1981). Volume of fluid (VOF) method for the dynamics of free boundaries. *Journal of Computational Physics 39*(1), 201 – 225.

Hohenberg, P. C. and B. I. Halperin (1977, Jul). Theory of dynamic critical phenomena. *Rev. Mod. Phys. 49*, 435–479.

Howle, V. E., J. Schroder, and R. Tuminaro (2006). The effect of boundary conditions within pressure convection-diffusion preconditioners. Technical report, Sandia Nationa Laboratories.

Hunter, J. D. (2007). Matplotlib: A 2d graphics environment. *Computing In Science & Engineering 9*(3), 90–95.

Hutter, K. and K. Jöhnk (2004). *Continuum methods of physical modeling*. Berlin: Springer-Verlag.

Hysing, S., S. Turek, D. Kuzmin, N. Parolini, E. Burman, S. Ganesan, and L. Tobiska (2009). Quantitative benchmark computations of two-dimensional bubble dynamics. *International Journal for Numerical Methods in Fluids 60*(11), 1259–1288.

Jacqmin, D. (2000). Contact-line dynamics of a diffuse fluid interface. *Journal of Fluid Mechanics 402*, 57–88.

Jasnow, D. and J. Viñals (1996). Coarse-grained description of thermo-capillary flow. *Physics of Fluids 8*(3), 660–669.

John, V., A. Linke, C. Merdon, M. Neilan, and L. G. Rebholz (2017). On the divergence constraint in mixed finite element methods for incompressible flows. *SIAM Review 59*(3), 492–544.

Kay, D., D. Loghin, and A. Wathen (2002). A preconditioner for the steady-state Navier-Stokes equations. *SIAM J. Sci. Comput. 24*(1), 237–256.

Kay, D. and R. Welford (2007). Efficient numerical solution of Cahn-Hilliard-Navier-Stokes fluids in 2D. *SIAM J. Sci. Comput. 29*(6), 2241–2257 (electronic).

Khatavkar, V. V., P. D. Anderson, and H. E. H. Meijer (2007). Capillary spreading of a droplet in the partially wetting regime using a diffuse-interface model. *Journal of Fluid Mechanics 572*, 367–387.

Kim, J. (2012). Phase-field models for multi-component fluid flows. *Commun. Comput. Phys. 12*(3), 613–661.

Lederer, P. L., A. Linke, C. Merdon, and J. Schöberl (2017). Divergence-free reconstruction operators for pressure-robust stokes discretizations with continuous pressure finite elements. *SIAM Journal on Numerical Analysis 55*(3), 1291–1314.

Lee, D., J.-Y. Huh, D. Jeong, J. Shin, A. Yun, and J. Kim (2014). Physical, mathematical, and numerical derivations of the cahn–hilliard equation. *Computational Materials Science 81*, 216–225.

Lee, H. G. and J. Kim (2011). Accurate contact angle boundary conditions for the cahn–hilliard equations. *Computers & Fluids 44*(1), 178–186.

Logg, A., K.-A. Mardal, G. N. Wells, et al. (2012). *Automated solution of differential equations by the finite element method*, Volume 84 of *Lecture Notes in Computational Science and Engineering*. Springer, Heidelberg. The FEniCS book.

Logg, A., G. N. Wells, and J. Hake (2012). *DOLFIN: a C++/Python finite element library*, pp. 173–225. Berlin, Heidelberg: Springer Berlin Heidelberg.

Lowengrub, J. and L. Truskinovsky (1998). Quasi-incompressible Cahn-Hilliard fluids and topological transitions. *R. Soc. Lond. Proc. Ser. A Math. Phys. Eng. Sci. 454*(1978), 2617–2654.

Málek, J. and Z. Strakoš (2015). *Preconditioning and the Conjugate Gradient Method in the Context of Solving PDEs*. SIAM Spotlight Series. Philadelphia: SIAM.

Minjeaud, S. (2013). An unconditionally stable uncoupled scheme for a triphasic Cahn-Hilliard/Navier-Stokes model. *Numerical Methods for Partial Differential Equations 29*(2), 584–618.

Murphy, M. F., G. H. Golub, and A. J. Wathen (2000). A note on preconditioning for indefinite linear systems. *SIAM Journal on Scientific Computing 21*(6), 1969–1972.

Narayanaswamy, O. S. (1977). A one-dimensional model of stretching float glass. *J. Amer. Ceram. Soc. 60*(1-2), 1–5.

Narayanaswamy, O. S. (1981). Computer simulation of float glass stretching. *J. Amer. Ceram. Soc. 64*(11), 666–670.

Noll, W. (1959). The foundations of classical mechanics in the light of recent advances in continuum mechanics. In *The axiomatic method. With special reference to geometry and physics. Proceedings of an International Symposium held at the Univ. of Calif., Berkeley, Dec. 26, 1957-Jan. 4, 1958 (edited by L. Henkin, P. Suppes and A. Tarski)*, Studies in Logic and the Foundations of Mathematics, pp. 266–281. North-Holland Publishing Co., Amsterdam.

Novick-Cohen, A. and L. A. Segel (1984, 03). Nonlinear aspects of the Cahn-Hilliard equation. *Physica D: Nonlinear Phenomena 10*, 277–298.

Olshanskii, M. A. and Y. V. Vassilevski (2007). Pressure Schur complement preconditioners for the discrete Oseen problem. *SIAM Journal on Scientific Computing 29*(6), 2686–2704.

Oono, Y. and S. Puri (1988). Study of phase-separation dynamics by use of cell dynamical systems. i. modeling. *Physical Review A - Atomic, Molecular, and Optical Physics 38*(1), 434–453.

Osher, S. and J. A. Sethian (1988). Fronts propagating with curvature-dependent speed: Algorithms based on hamilton-jacobi formulations. *Journal of Computational Physics 79*(1), 12 – 49.

Pilkington, L. A. B. (1969). Review lecture. The float glass process. *Proceedings of the Royal Society of London. Series A, Mathematical and Physical Sciences 314*(1516), 1–25.

Popov, V. (1982). Flow of a viscous film over the surface of an inviscid fluid. *Journal of Applied Mechanics and Technical Physics 23*, 188–194.

Popov, V. V. (1983). Flow of a viscous film with free boundaries in the one-dimensional approximation. *Journal of Applied Mechanics and Technical Physics 24*, 507–509.

Prieto, M., J. Díaz, and E. Egusquiza (2002). Analysis of the fluid-dynamic and thermal behaviour of a tin bath in float glass manufacturing. *International Journal of Thermal Sciences 41*(4), 348 – 359.

Průša, V. and K. R. Rajagopal (2013). On models for viscoelastic materials that are mechanically incompressible and thermally compressible or expansible and their Oberbeck–Boussinesq type approximations. *Math. Models Meth. Appl. Sci. 23*(10), 1761–1794.

Rajagopal, K. R. and L. Tao (1995). *Mechanics of mixtures*, Volume 35 of *Series on Advances in Mathematics for Applied Sciences*. River Edge, NJ: World Scientific Publishing Co. Inc.

Řehoř, M. (2017). MUFLON 2017.2.0 (MUlti-phase FLow simulatiON software library). `https://github.com/mrehor/muflon`.

Řehoř, M., J. Blechta, and O. Souček (2017). On some practical issues concerning the implementation of Cahn–Hilliard–Navier–Stokes type models. *International Journal of Advances in Engineering Sciences and Applied Mathematics 9*(1), 30–39.

Roudbari, M. S., G. Şimşek, E. H. van Brummelen, and K. G. van der Zee (2018). Diffuse-interface two-phase flow models with different densities: A new quasi-incompressible form and a linear energy-stable method. *Mathematical Models and Methods in Applied Sciences 28*(04), 733–770.

Saad, Y. and M. H. Schultz (1986). Gmres: A generalized minimal residual algorithm for solving nonsymmetric linear systems. *SIAM Journal on Scientific and Statistical Computing 7*(3), 856–869.

Salari, K. and P. Knupp (2000). Code verification by the method of manufactured solutions. Technical Report SAND2000-1444, Sandia Nationa Laboratories, Albuquerque, NM 87185-0825.

Samohýl, I. (1987). *Thermodynamics of irreversible processes in fluid mixtures*, Volume 12 of *Teubner-Texte zur Physik [Teubner Texts in Physics]*. Leipzig: Teubner.

Shen, J. and X. Yang (2010). A phase-field model and its numerical approximation for two-phase incompressible flows with different densities and viscosities. *SIAM Journal on Scientific Computing 32*(3), 1159–1179.

Shen, J., X. Yang, and Q. Wang (2013). Mass and volume conservation in phase field models for binary fluids. *Communications in Computational Physics 13*, 1045–1065.

Silvester, D., H. Elman, D. Kay, and A. Wathen (2001). Efficient preconditioning of the linearized Navier–Stokes equations for incompressible flow. *Journal of Computational and Applied Mathematics 128*(1–2), 261 – 279. Numerical Analysis 2000. Vol. VII: Partial Differential Equations.

Souček, O., V. Průša, J. Málek, and K. R. Rajagopal (2014). On the natural structure of thermodynamic potentials and fluxes in the theory of chemically non-reacting binary mixtures. *Acta Mech. 225*(11), 3157–3186.

Sun, P., C. Liu, and J. Xu (2009). Phase field model of thermo-induced Marangoni effects in the mixtures and its numerical simulations with mixed finite element method. *Commun. Comput. Phys. 6*(5), 1095–1117.

Sussman, M., P. Smereka, and S. Osher (1994). A level set approach for computing solutions to incompressible two-phase flow. *Journal of Computational Physics 114*(1), 146 – 159.

Truesdell, C. (1957a). Sulle basi della termomeccanica, I. *Rend. Lincei 8*(22), 33–38.

Truesdell, C. (1957b). Sulle basi della termomeccanica, II. *Rend. Lincei 8*(22), 158–166.

Truesdell, C. (1984). *Rational thermodynamics* (Second ed.). New York: Springer-Verlag. With an appendix by C. C. Wang, With additional appendices by 23 contributors.

Truesdell, C. and R. A. Toupin (1960). The classical field theories. In S. Flüge (Ed.), *Handbuch der Physik*, Volume III/1, pp. 226–793. Berlin-Heidelberg-New York: Springer-Verlag.

van der Waals, J. D. (1893). Thermodynamische theorie der capillariteit in de onderstelling van continue dichtheidsverandering. *Verhandel. Konink. Akad. Weten. Amsterdam Sect. 1*(8), 200–244. [in Dutch; English translation in J. Stat. Phys., 1979, 20:197].

Wathen, A. and T. Rees (2008). Chebyshev semi-iteration in preconditioning for problems including the mass matrix. *ETNA. Electronic Transactions on Numerical Analysis [electronic only] 34*, 125–135.

Wu, S. and J. Xu (2017). Multiphase Allen–Cahn and Cahn–Hilliard models and their discretizations with the effect of pairwise surface tensions. *Journal of Computational Physics 343*, 10 – 32.